Particle Breakage of Granular Soils: Evolution Laws and Constitutive Modelling

By

Chenxi Tong

BEng, MEng

A thesis submitted in partial fulfilment of the requirements for the degree of

Doctor of Philosophy

School of Civil and Environmental Engineering

Faculty of Engineering of Information Technology

University of Technology Sydney, Australia

April 2020

Certificate of original authorship

I, Chenxi Tong declare that this thesis is submitted in fulfilment of the requirements for the award of Doctor of Philosophy, in the Faculty of Engineering and Information Technology at the University of Technology Sydney.

This thesis is wholly my own work unless otherwise reference or acknowledged. In addition, I certify that all information sources and literature used are indicated in the thesis.

This document has not been submitted for qualifications at any other academic institution.

This research is supported by the Australian Government Research Training Program.

Production Note:
Signature: Chenxi Tong Signature removed prior to publication.
Date: 13/04/2020

Acknowledgements

I have thought about all kinds of acknowledgements when finishing my PhD thesis. However, there is not an easy way to start a word when the day comes. My PhD journey is full of challenges to living abroad alone, frustration after the failure of experiment, and joys after the acceptation of papers. I would like to express my sincere thanks to those who made this thesis possible.

I started the research presented in this PhD thesis when I studied my Master degree at Central South University (CSU, China) with supervisors of Prof Daichao Sheng and Prof Sheng Zhang. After that, I continued the same project with Prof Daichao Sheng at the University of Newcastle, Australia. Then I moved to the University of Technology Sydney (UTS) with my principal supervisor Prof Daichao Sheng.

First of all, I would like to express my gratitude to my principal supervisor, Professor Daichao Sheng, for his professional guidance, unrivalled support, critical suggestions, and continuous encouragement from the beginning of my research career.

I am grateful to Professor Sheng Zhang (CSU, China), who introduced me into the research field of particle breakage of granular soils. Sincere appreciation also goes to Dr Glen Burton, Dr Jubert Pineda who were the co-supervisors when I was in the UoN. They helped me a lot in my experiment and paper revision.

I would like to thank Mr Lachlan Bates, Mr. Ross Gibson, Mr. Mick Goodwin, Ms. Kirstin Dunncliff from the Faculty of Engineering and Built Environment of the UoN, and Ms. Van Le from the School of Civil and Environmental Engineering of the UTS for their kind help.

I would like to thank the friends that I have met in Australia, for their company, without whom my life in Australia will not be so colourful and wonderful.

This research was funded by the China Scholarship Council (CSC) and the UoN Top Up scholarship when I studied at UoN, and CSC-UTS scholarship and Faculty of Engineering and Information Technology Top Up Scholarship during my stay at the UTS. I would like to thank all the scholarship that I received during my study in Australia.

Finally, yet most importantly, I would like to thank my family, my parents Shougen Tong and Minxian Yu, my younger brother Huan Tong, my grandparents Qinggui Yu and Shuifeng Zhang. I owe my deepest gratitude to my fiancée Mrs Huihui Wan. This thesis is dedicated to her for her constant and unconditional support and encouragement.

Thesis Format

This thesis for the degree of Doctor of Philosophy is in the format of thesis by compilation.

List of Publications

Journal papers

(1). **Tong, C. X**., Burton, G. J., Zhang, S., & Sheng, D. (2018a). A simple particle-size distribution model for granular materials. ***Canadian Geotechnical Journal***, 55(2), 246-257.

(2). **Tong, C. X**., Zhang, K. F., Zhang, S., & Sheng, D. (2019a). A stochastic particle breakage model for granular soils subjected to one-dimensional compression with emphasis on the evolution of coordination number. ***Computers and Geotechnics***, 112, 72-80.

(3). **Tong, C. X**., Burton, G. J., Zhang, S., & Sheng, D. (2020a). Particle breakage of uniformly graded carbonate sands in dry/wet condition subjected to compression/shear tests. ***Acta Geotechnica***. https://doi.org/10.1007/s11440-020-00931-x.

(4). **Tong, C. X**., Sheng, D., & Zhang, S. (2020b). A critical state framework for granular soils experiencing particle breakage. ***Computers and Geotechnics***, under review. (Manuscript Number: COGE-D-20-00037).

Conference papers

(1). **Tong, C. X**., Zhang, S., & Sheng, D. (2018b). A Breakage Matrix Model for Calcareous Sands Subjected to One-Dimensional Compression. In GeoShanghai International Conference (pp. 17-24), Shanghai, China.

(2). **Tong, C. X**., Zhang, S., & Sheng, D. (2020c). Particle breakage observed in both transitional and non-transitional carbonate sands. The 4th International Conference on Transportation Geotechnics. Chicago, USA.(Abstract accept, full paper under review)

In additions to the above papers, there are three journal papers (one in English, and two in Chinese) published during my MSc study in Central South University (CSU, China). These papers have served as the foundation of my PhD research.

(1). Zhang, S., **Tong, C. X**., Li, X., & Sheng, D. (2015a). A new method for studying the evolution of particle breakage. ***Géotechnique***, 65(11), 911-922.

(2). **Tong, C. X**., Zhang, S., Li, X., & Sheng, D. (2015b). Evolution of geotechnical materials based on Markov chain considering particle crushing. Chinese Journal of Geotechnical Engineering, 37(5), 870-877. (In Chinese).

(3). **Tong, C. X**., Zhang, S., Li, X., & Sheng, D. (2015c). Evolution and ultimate state of breakage for uniformly graded granular materials. Rock and Soil Mechanics, 36(s1), 260-264. (In Chinese).

Table of Contents

List of Figures

List of Tables

Abstract

Granular soils are widely encountered in the construction of civil infrastructure. Particle breakage of granular soils results in changes in the particle size distribution (PSD), affects the stress-strain behaviour, and consequently reduces the serviceability of the infrastructure. It is of great importance to understand how the PSD of granular soils evolves under various loading conditions, and how the changes in the PSD affect the mechanical and deformational behaviour of soils. This PhD thesis-by-compilation provides a framework for studying the particle breakage of granular soils with specific attention on the quantification of PSD, breakage evolution law, and constitutive modelling.

The following primary contributions to the understanding of particle breakage of granular soils have been made through the doctoral research:

(1). The appropriate breakage indices for granular soils with different initial PSDs are proposed and discussed.

(2). The evolution of particle breakage in terms of the whole PSD, or in terms of a single breakage index is investigated via both experimental and mathematical approaches.

(3). The influence of PSD on the compression and shearing behaviour of the soils are discussed.

(4). A state-dependent constitutive model of granular soils experiencing particle breakage is developed based on a new state parameter and a dynamic evolution law of the critical state line and reference compression line.

This PhD thesis, which elaborates the work carried out during the course of the research, comprises four journal papers and two conference paper.

Chapter 1 Introduction

1.1 Background

Particle breakage is of great interest to several engineering fields, such as chemical manufacturing, mineral processing, food processing, pharmaceuticals industry, and geotechnical engineering. Granular soils, such as rockfill materials, ballast, and sand are widely used in the construction of civil infrastructures. In recent times, particle breakage of granular soils has attracted significant attention, owing largely to the emergence of larger earth-rockfill dams, increased number of offshore structures, higher embankments, and high-speed and heavy haul rail infrastructure. Particle breakage occurs in both weak and strong soil particles. Examples for the former include carbonate sands, weak rock fragments used in earth backfills, expansive clay pellets used in waste containments, and aggregates in compacted soils. On the other hand, some examples for the latter include track ballast subjected to repeated wheel loading, and rockfill materials of large earth dams subjected to self-weight. Particle breakage of soils underneath an infrastructure leads to accelerated degradation of materials and reduces the serviceability of the infrastructure, which in turn, increases maintenance costs and even causes eventual failure of the infrastructure.

The distribution of offshore structures that are constructed on carbonate sands worldwide is as shown in red colour in Figure 1.1. It was reported that when a pile was driven into a carbonate sand deposit in the Bass Strait off Australia (denoted by a blue star in the figure), the axial capacity of the sand reduced by up to 90%. This deterioration was attributed to particle breakage and a loss of lateral stress as a result of the volume change of the sand (Angemeer *et al.*, 1973).

Figure 1.1: Offshore occurrence of carbonate sand reported in the literature (modified after Murff, 1987)

In Australia, the annual cost of rehabilitating ballasted rail tracks owing to ballast degradation is quite large. Figure 1.2 shows a typical degradation of ballast that has occurred at the railway crossing at Thirroul in New South Wales, Australia. In December 2011, the Australian Rail Track Corporation (ARTC) announced a five-year reconstruction program of A$ 134 million in the Sydney - Melbourne rail corridor to clean-up or replace the ballast, and improve the drainage around the track (https://www.artc.com.au/projects/brp/).

(i) Crossing at Thirroul (ii) Enlarged view showing ballast breakage

Figure 1.2: Particle breakage of ballast at the railway crossing at Thirroul in New South Wales, Australia (after Nimbalkar *et al.*, 2012)

In Brazil, the Campos Novos concrete-faced rockfill dam (CFRD), with a height of 202 m and a crest length of 590 m, suffered damage during an impoundment in 2005, after the reservoir bed was lowered, which resulted in the cracking of the face slab on the bottom part of the dam as shown in Figure 1.3. The main reason for these cracks could be the compressibility of the rockfill material, in which particle breakage occurred as suggested by Gamboa (2011) and Yin *et al.* (2012).

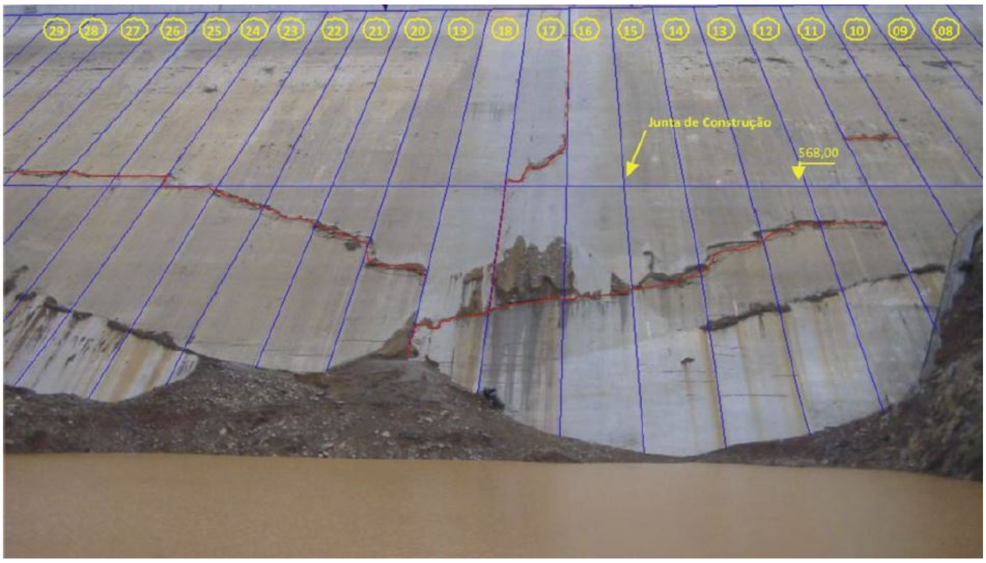

Figure 1.3: Cracks of Campos Novos dam
(http://www.cbdb.org.br/documentos/mbdiii/CamposNovos.pdf.)

These examples clearly illustrate the importance of understanding how particle breakage influences the mechanical and deformational behaviour of granular materials. This helps in assessing and quantifying the potential hazards caused by particle breakage more accurately, and possibly optimising the maintenance costs involved.

The most obvious impact of particle breakage is the change in Particle Size Distribution (PSD). Traditionally, PSD is treated as a soil constant that identifies one soil from other soils. Soil parameters such as void ratio, density, water content, degree of saturation, initial structure can all vary with stress and hydraulic paths, and hence are often regarded as variables in a constitutive model. However, when particle breakage does occur, the PSD is not necessarily a soil constant and should be treated as a constitutive variable. At present, only a few constitutive models take into account the change in PSD when the granular soils are compressed or sheared (Einav, 2007a). Thus, it is important to relate the change in PSD and the mechanical and deformational response of granular soil.

1.2 Objectives of the research

To tackle the issue of particle breakage, the following three key questions need to be considered and answered (Muir Wood, 2007; Muir Wood & Maeda, 2008; Muir Wood *et al.*, 2010, Zhang *et al.*, 2015):

(1). How can the PSD be reasonably represented by a simple variable that can be used in a constitutive model (PSD quantification)?

(2). How does this PSD variable evolve during particle breakage (breakage evolution law)?

(3). How does this PSD variable influence the mechanical and deformational behaviour of the material (constitutive law)?

To some extent, the issue of particle breakage is similar to the hardening law in plasticity theory, wherein we define a hardening parameter, establish a hardening law, and correlate the hardening parameter with other mechanical properties.

The aim of this doctoral research is to study the particle breakage of granular soils considering the three key questions mentioned above. The primary objective here is to provide a deeper understanding of particle breakage of granular soils ranging from the evolution laws to the constitutive modelling. The more specific objectives of this study are to:

(1). Propose a PSD model that is suitable for crushable granular soils, and that has a great potential for PSD quantification.

(2). Explore the evolution of PSD induced by particle breakage via experimental and mathematical modelling approaches.

(3). Investigate the influence of PSD on the mechanical behaviour of granular soils.

(4). Develop a constitutive model of granular soils considering the evolution of PSD induced by particle breakage.

1.3 Thesis outline

The dissertation is presented as a thesis-by-compilation with nine chapters, which are organised as follows:

(1). **Chapter 1** introduces the research background, research ideas, and objectives of this research.

(2). **Chapter 2** provides an extensive literature review on particle breakage of granular soils with specific focus on PSD quantification, evolution of PSD, effect of PSD on the mechanical behaviour of granular soils, and constitutive models of granular soils considering particle breakage.

(3). **Chapter 3** is based on journal paper #1, which proposes a simple and continuous PSD model for the granular soils involving particle breakage. The model has only two parameters. The determination of these two parameters is discussed first. The performance of the proposed model is then compared with other PSD models in the literature via a database of 53 granular soils with 154 varying PSD curves. Some potential applications of the proposed PSD model are also discussed.

(4). **Chapter 4** is based on conference paper #1, which proposes a straightforward method, named the 'breakage matrix model' for describing the particle size degradation of granular materials subjected to one-dimensional compression. The breakage matrix is obtained directly by experimental results on carbonate sands subjected to one-dimensional compression. The limitations of this model are also discussed.

(5). **Chapter 5** is based on journal paper #2, which presents a stochastic approach, namely the 'Markov chain model', for simulating the evolution of PSD of granular soils during one-dimensional compression, considering the evolution of the coordination number. The model highlights the importance of the coupling effect of the particle size and coordination number in calculating the breakage probability of particles in a particle assembly.

(6). **Chapter 6** is based on journal paper #3, which reports a series of ring shear tests and one-dimensional compression tests on carbonate sands with different uniformly-graded PSDs, in both dry and saturated conditions. The effect of saturation condition and initial PSD on particle breakage during compression and shearing is analysed. The evolution of the two PSD parameters proposed in Chapter 3 is also discussed.

(7). **Chapter 7** is based on conference paper #2, which presents the experimental results on the compression behaviour of carbonate sands with different fractal-graded PSDs and initial void ratios. The effect of PSD and void ratio on the compression behaviour of carbonate sand in terms of compression index, tangent-constrained modulus, and particle breakage is presented with both qualitative and quantitative approaches.

(8). **Chapter 8** is based on journal paper #4, which presents an improved state-dependent constitutive model for granular soils experiencing particle breakage. A modified state parameter is proposed based on a newly defined reference compression line (RCL). A simple dynamic evolution law of RCL incorporating particle breakage effect is suggested.

(9). **Chapter 9** contains concluding remarks and future work.

Chapter 2 . Literature review

2.1 Introduction

Particle breakage of granular soils has long been neglected because the high stresses required for particle breakage are not likely to be encountered *in situ* on a regular basis. With the boom of civil infrastructures, such as the emergence of larger earth-rockfill dams, higher embankments, more offshore structures, and faster and heavier rail networks, interest in particle breakage has been reawakened within the last few decades. This chapter provides a review of the literature on particle breakage of granular soils, mainly in the following four areas: (i) PSD quantification including the breakage indices and PSD models, (ii) evolution of PSD from both experimental and mathematical modelling points of view, (iii) effect of PSD on the mechanical and deformational behaviour of granular soils, and (iv) constitutive models of granular soils with consideration of particle breakage.

2.2 PSD quantification subsequent to particle breakage

2.2.1 Description of PSD

The PSD statistically provides information about the distribution of various particle size intervals in terms of their mass, volume, or number in a given soil or material. PSD by mass is commonly adopted in geotechnical engineering and all the PSDs referred to throughout this thesis imply the mass-based PSD. The PSD of granular soils in practical applications is usually determined via the sieving test, in which the soil is allowed to pass through a series of sieves of progressively smaller mesh sizes (i.e., d_n, $d_{n\text{-}1}$ … d_1, where subscript 1 represents the smallest size, and subscript n represents the largest size), and the mass of soil that is stopped by each sieve is weighted as a fraction of the whole mass. Mathematically, it takes the following form

$$p_{(i)} = \begin{cases} \dfrac{m_{(i)}}{\sum_{i=2}^{i=n} m_{(i)}}, for \quad i \geq 2 \\ 0, for \quad i = 1 \end{cases} \tag{2.1}$$

where $m_{(i)}$ is the mass of the d_i-sized particles (with sieve size ranging from d_{i-1} to d_i), and $p_{(i)}$ is the mass fraction of the d_i-sized particles. It should be noted that the smallest sieve size is d_1, which means that none of the particles have a diameter smaller than d_1, and hence, we have $m_{(1)} = p_{(1)} = 0$. The cumulative mass fraction of d_i-sized particles can be expressed as

$$P_{(i)} = \frac{\sum_{1}^{i} m_{(i)}}{\sum_{i=1}^{i=n} m_{(i)}} \tag{2.2}$$

where $P_{(i)}$ is the cumulative mass fraction of d_i-sized particles, and when graphically presented, it is called the PSD curve. It can be easily obtained from Equations (2.1) and (2.2) that $P_{(1)} = 0$, and $P_{(n)} = 100\%$, which means that no particles will pass through the d_1-sized sieve and all the particles will pass through the d_n-sized sieve. The PSD curve obtained through the sieving test is discontinuous because of the limited number of sieve sizes used in the test.

An alternative way to describe a continuous PSD curve is to adopt a suitable mathematical equation that covers the full range of particle sizes with the following general form

$$P_{(x)} = \int_{d_{\min}}^{x} p_{(x)} dx, \quad x \in [d_{\min}, d_{\max}] \tag{2.3}$$

where $p_{(x)}$ is distribution density function; $P_{(x)}$ is the mass percentage of particles passing a particular size x; $d_{\min}$ and $d_{\max}$ are the minimum and maximum particle size, respectively. The continuous PSD curve still satisfies two main properties: i.e., $P_{(x)} = 0$ when $x = d_{\min}$, and $P_{(x)} = 100\%$ when $x = d_{\max}$.

2.2.2 Breakage indices related to the characteristic particle size

The term 'characteristic particle size' in this study means a specific particle size d_x of the PSD curve, at which x% of the sample by mass is smaller. The most commonly used characteristic particle sizes are d_{10}, d_{30}, and d_{60}, which are used to define the coefficient of uniformity C_u (= d_{60}/d_{10}) and the coefficient of curvature C_c (= $d_{30}\times d_{30}/d_{60}\times d_{10}$). To measure the degree of particle breakage, several breakage indices have been proposed based on the change in the characteristic particle size before and after the test and these are summarised below:

(1). **Breakage index B_{15}** (= d_{15i}/d_{15f}, where d_{15} is a characteristic particle size; and subscripts i and f represent the values before and after the test) was proposed by Lee and Farhoomand (Lee & Farhoomand, 1967, see Figure 2.1(a)). As shown in Figure 2.1(a), the minimum value of B_{15} is 1, and the maximum value depends on the ultimate PSD of the granular soil subjected to extreme stresses or strains.

(2). **Breakage index B_{10}** (= 1– d_{10f}/d_{10i}, where d_{10} is a characteristic particle size) was proposed by Lade *et al.* (1996). As shown in Figure 2.1(b), the minimum value of B_{10} is 0, and the maximum value is less than 1, which also depends on the ultimate PSD. One advantage of B_{10} is that it provides an easy approach for computing permeability because of the well-developed relation between d_{10} and the permeability equation (see Hazen's permeability equation (Hazen, 1911)).

(3). **Breakage index B_{r50}** [= (d_{50} – d_{50i})/(d_{50f} – d_{50i}), where d_{50}, d_{50i}, d_{50f} are the characteristic particle sizes of the PSD after the test, PSD before the test, and the ultimate PSD] was proposed by Xiao & Liu (2017). As seen in Figure 2.1(c), the minimum and maximum values of B_{r50} are 0 and 1, respectively.

(4). **Coefficient of uniformity C_u**, which can sometimes be treated as a breakage index (Yan & Dong, 2011; Li *et al.*, 2014). However, the value of C_u does not have a clear range and is highly dependent on the initial PSD. Therefore, Hu *et al.* (2018) proposed a breakage index B_u [= (C_u – C_{ui})/(C_{uf} – C_{ui}), where C_u, C_{ui}, C_{uf} are the current, initial, and ultimate coefficients of uniformity, respectively], named as the 'relative uniformity'. As shown in Figure 2.1(d), the value of B_u ranges from 0 to 1.

(5). **Breakage index B_f** [= R/100, where R is the percentage of particles smaller, after the test, than the smallest particle size in the initial PSD as shown in Figure 2.1(e)] was proposed by Leslie (1963), and Nakata *et al.* (1999). The minimum value of B_f is 0 and the maximum value is less than 1 and is dependent on both the ultimate and the initial PSD.

(6). **Breakage index B_{P10}** [= R_{10}/100, where R_{10} is the increase in the percent of particles passing the characteristic particle size d_{10} of the initial PSD as shown in Figure 2.1(f)] was proposed by Cohen & Leslie (1975). Similar to B_f, the value of B_{P10} ranges from 0 to a number that is less 1 and is dependent on both the ultimate and the initial PSD.

In addition, other forms of indices based on the characteristic particle size have been used to quantify the particle breakage in various studies, for example, the fraction of particles with a size smaller than 0.074 mm (Ghafghazi *et al.*, 2014). In general, these breakage indices defined based on the characteristic particle size are simple in form. However, they cannot capture the whole range of PSD during the particle breakage.

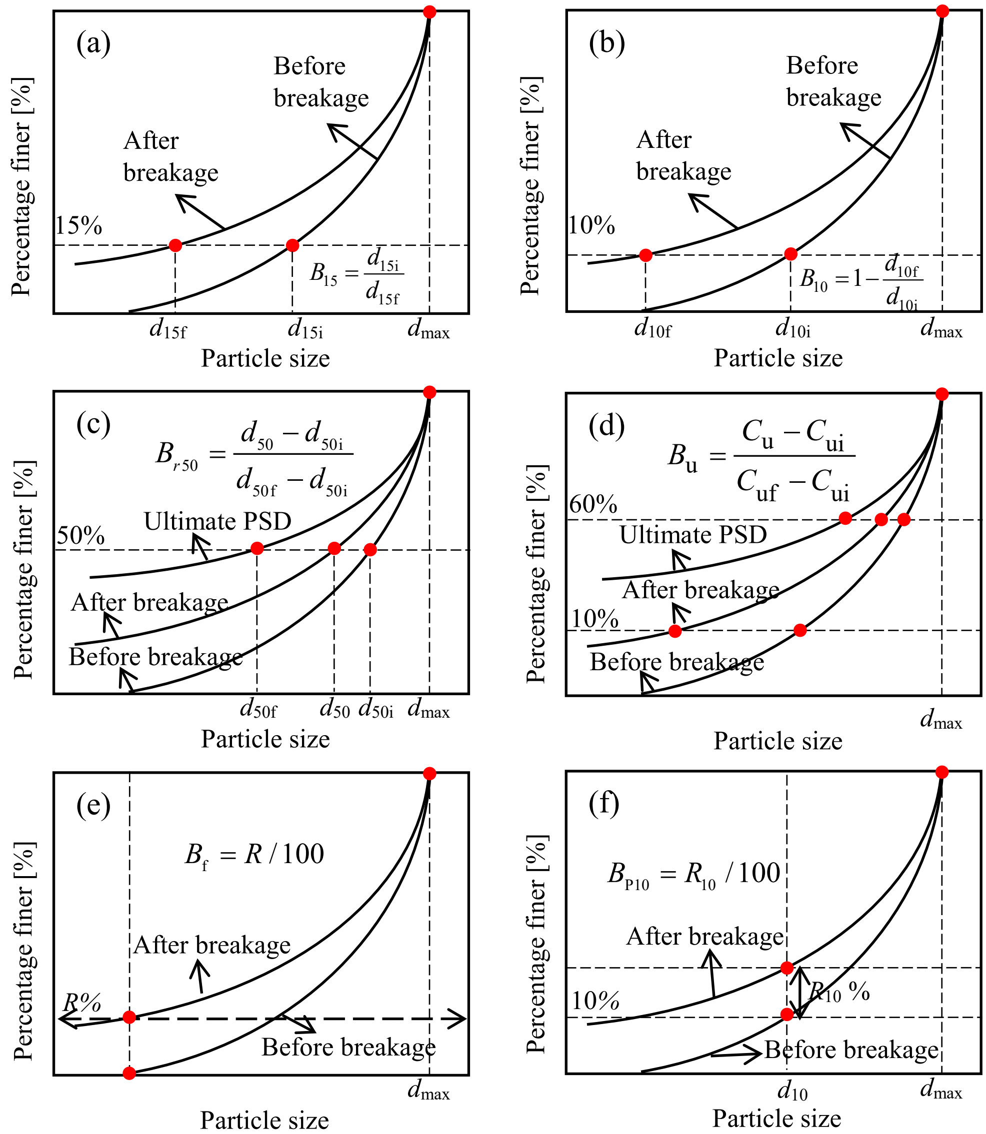

Figure 2.1: Schematic representation of different definitions of particle indices: (a) breakage index B_{15} (Lee & Farhoomand, 1967), (b) breakage index B_{10} (Lade *et al.*, 1996), (c) breakage index B_{r50} (Xiao & Liu, 2017), (d) breakage index B_u (Hu *et al.*, 2018), (e) breakage index B_f (Leslie, 1963; Nakata *et al.*, 1999), and (f) breakage index B_{P10} (Cohen & Leslie, 1975)

2.2.3 Breakage indices related to the whole PSD curve

To overcome the limitation as mentioned above and to measure the particle breakage considering all the particle sizes, some breakage indices based on the whole PSD curve have been proposed as below:

(1). **Breakage index B_g** is defined as the sum of positive or absolute values of the percentage difference of each size-class particles before and after the test (Marsal, 1967). In other words, B_g can be calculated as the maximum percentage difference of the PSD as shown in Figure 2.2(a). The value of B_g ranges from 0 to a number less than 1.

(2). **Relative breakage index B_r** was proposed by Hardin (Hardin, 1985). B_r is defined as the ratio of the 'total breakage' (area ABCA in Figure 2.2(b)) to the 'breakage potential' (area ABDA in Figure 2.2(b)). The minimum and the maximum values of B_r are 0 and 1, respectively, based on the assumption that all the particles will eventually break to a diameter of 0.074 mm. However, this is not well supported by experimental data which shows particle breakage cannot be a never-ending process and an ultimate steady state PSD at high stresses/strains will be observed (McDowell & Bolton, 1998; Coop *et al.*, 2004).

(3). **Modified relative breakage index B_r^*** was developed by Einav (Einav, 2007a; Einav, 2007b) and is shown in Figure 2.2(c). The 'breakage potential' has been modified based on the fractal theory, which presumes that the ultimate PSD is fractal graded, i.e., a straight line in the log (particle size) – log (percentage finer) space. The ultimate PSD is as depicted in Figure 2.2(f). B_r^* is widely used in the study of particle breakage as it considers a limit and well-defined ultimate PSD, perfectly in the range of 0 to 1, with 0 meaning no breakage and 1 full breakage.

(4). **Grading state index I_G** was proposed by Muir Wood (Muir Wood, 2007). As indicated in Figure 2.2(d), I_G is similar to B_r^*, as they both adopt the same limit PSD, although it is not necessary to be fractal-graded, as noted by Muir Wood. However, in the definition of I_G, the samples are assumed to be perfectly uniformly-graded, i.e., all the particles are d_{max}-sized in the initial state. In that case, the minimum value of I_G is highly dependent on the initial PSD, i.e., $I_{Gmin} = 0$, when the initial PSD is perfectly uniformly graded and $I_{Gmin} > 0$ when the initial PSD is non-uniformly graded.

(5). **Ballast breakage index *BBI*** was introduced by Indraratna *et al.* (2005). *BBI* is used for measuring the breakage amount of ballast just as its name implies. The maximum particle size of an arbitrary boundary of PSD is 95% of that of the initial PSD (see Figure 2.2(e)), which is different from other indices. *BBI* is suitable for coarse-grained soils considering the particle size.

(6). **Normalised breakage index B_D** is related to the slope of the straight line in the log (particle size) - log (percentage finer) space and was adopted by some studies (Konrad & Salami, 2018; Yu, 2018b). As mentioned before, the PSD is assumed to evolve towards a fractal distribution as per the fractal theory. The slope of the linear line in the log - log plot might be reasonable enough to quantify the PSD. B_D considers the initial PSD, current PSD, and ultimate PSD as shown in Figure 2.2(f). It should be noted that B_D could be the most ideal breakage index because it can also fully describe the PSD, as long as the initial and current PSDs are well presented by a straight line in the log - log plot. However, the PSDs after particle breakage are not fractal-graded for several granular soils, especially when the initial PSDs are often arbitrarily prepared as indicated by the red dashed lines in Figure 2.2(f).

Apart from the breakage indices analysed above, other breakage indices based on grading entropy theory (Lőrincz *et al.*, 2005), increment of particle surface (Miura & O'Hara, 1979), and probability statistics theory (Zhang *et al.*, 2015) are more or less determined by the distribution of particles within the whole range of sizes. It should be noted that breakage indices based on both characteristic particle size and the whole PSD curve suffer from limitations, such as not being able to describe the whole PSD unless all the PSDs are well fractal-graded as analysed above.

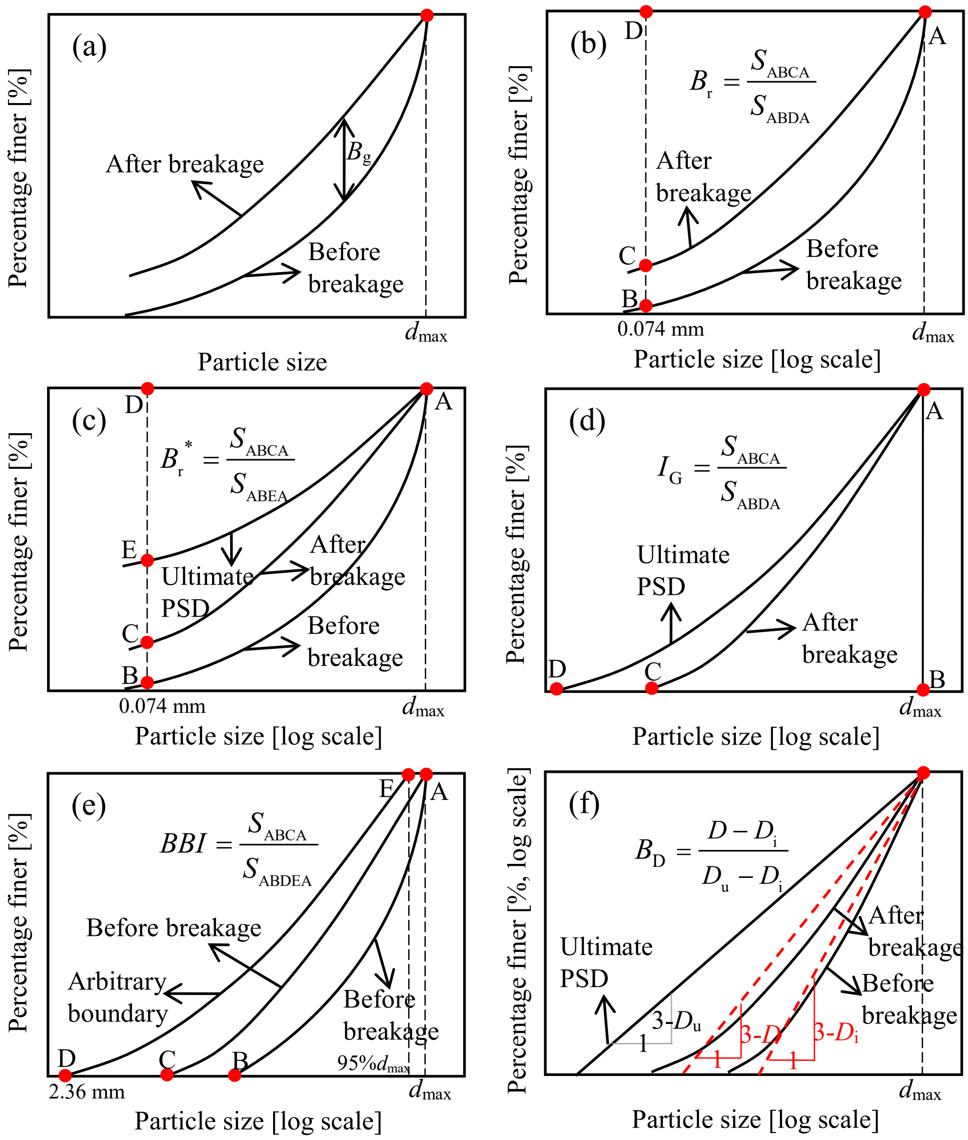

Figure 2.2: Schematic representation of different definitions of particle indices: (a) B_g (Marsal, 1967), (b) B_r (Hardin, 1985), (c) B_r^* (Einav, 2007a; Einav, 2007b), (d) I_G (Muir Wood, 2007), (e) *BBI* (Indraratna *et al.*, 2005), and (f) B_D (Yu, 2018b)

2.2.4 Fractal distribution after breakage

The PSD of a granular soil will eventually evolve toward an ultimate steady state with increasing packing efficiency induced by the particle breakage. An ultimate PSD implies that particles with different sizes will not break further owing to the cushioning effect and the constraining topological effect, which are not necessary for the soils to be fractal-graded. For example, Zhang & Baudet (2013) found that those initial gap-graded samples did not evolve to a fractal PSD even at high stresses. However, the ultimate PSD after breakage is commonly assumed to be fractal-graded based on the fractal theory, or selfsimilarity for most practical cases. According to the fractal model proposed by Turcotte (1986), the relationship between the particle number and the particle size can be expressed as

$$N(d > r) \propto r^{-D} \tag{2.4}$$

where N is the number of particles with size d larger than r and D is the fractal dimension. For a particle size larger than the minimum size $r_{\min}$, Equation (2.4) can be rewritten as

$$N_{\mathrm{M}}(d > r_{\min}) \propto r_{\min}{}^{-D} \tag{2.5}$$

Combining Equations (2.4) and (2.5) gives

$$\frac{N}{N_{\mathrm{M}}} = \left(\frac{r}{r_{\min}}\right)^{-D} \tag{2.6}$$

Similarly, Tyler & Wheatcraft (1989) and Tyler & Wheatcraft (1992) proposed a volume-based approach, whereby

$$V(r > d_i) = C_{\mathrm{V}}\left[1 - \left(\frac{d_i}{\lambda_{\mathrm{V}}}\right)^{3-D}\right] \tag{2.7}$$

where V is the sample volume of particles with size r, d_i is the reference particle size, and C_{V} and λ_{V} are parameters. Assuming all the particles have the same density, Equation (2.7) can be rewritten as

$$M\left(r > d_i\right) = \rho V(r > d_i) = \rho C_{\mathrm{V}}\left[1 - \left(\frac{d_i}{\lambda_{\mathrm{V}}}\right)^{3-D}\right] \tag{2.8}$$

where ρ is the density of soil particles and $M\,(r > d_i)$ is the mass with particle size larger than d_i. Equation (2.8) can be expressed as follows, when $d_i = 0$, and $d_i = d_{\max}$:

$$\begin{cases} M_{\mathrm{T}} = \rho C_{\mathrm{V}} \\ d_{\max} = \lambda_{\mathrm{V}} \end{cases} \tag{2.9}$$

Substituting Equation (2.9) into Equation (2.8) yields

$$P(d_i) = \frac{M\left(r < d_i\right)}{M_{\mathrm{T}}} = 1 - \frac{M\left(r > d_i\right)}{M_{\mathrm{T}}} = \left(\frac{d_i}{d_{\max}}\right)^{3-D} \tag{2.10}$$

$P(d_i)$ is the well-known fractal PSD model. It is a straight line in the log (P) - log (d_i / d_{max}) plot with a slope of 3–D. As indicated by Equation (2.10), the value of the fractal dimension D is physically limited to the range between 0 and 3. The value of the ultimate fractal dimension D_u defines the limit for the PSD of a given granular soil and is an important parameter, when calculating the breakage indices that contain the ultimate PSD (e.g., B_u, B_r^*, I_G, and B_D). However, whether the value of D_u is a soil constant or it varies with different conditions, such as the initial PSD, confining pressure, and test type is still an open question. For the sake of simplicity, D_u is taken as 2.5-2.6 in several studies in the literature (Sammis *et al.*, 1987; McDowell & Bolton, 1998; Coop *et al.*, 2004; Einav, 2007a; Hu *et al.*, 2018).

2.2.5 Existing PSD models

As discussed earlier, the major limitation of the breakage indices is their inability to describe the whole PSD. An alternative method is to adopt a suitable mathematical model that covers the full range of particle sizes. Such a mathematical model has several advantages: (1) the characteristics of the whole PSD curve, such as d_{10}, d_{60}, C_c, and C_u can be obtained when the parameters of the PSD model are determined; (2) it is easier to correlate the entire PSD curve with other properties of the soil. A key challenge here lies in developing a model that has a limited number of parameters while still capturing the widely varying nature of the PSDs.

The subject of PSD models is of great interest to several research disciplines, including soil science, agriculture, powder technology, and geotechnical engineering. PSD models in the literature can be classified into three main types, based on the form of the equation. These are power function (P), exponential function (E), and logarithmic function (L). Some typical PSD models in the literature are summarised in Table 2.1. Although several mathematic models have been proposed for describing the PSDs of soils, their overall performance varies widely for different soils. For example, the lognormal models perform better in silty soils and show poor fit for sandy soils (Buchan, 1989; Hwang *et al.*, 2002; Bayat *et al.*, 2015).

Table 2.1. Typical PSD models in the literature

Reference	No.	Equation	Parameters	Type
Schuhmann (1940) Fuller & Thompson (1907) Talbot & Richart (1923)	1	$P(d)=\left[\dfrac{d}{d_{\max}}\right]^{m}$	m	T
Lassabatere *et al.* (2006)	2	$P(d)=\left[1+\left(\dfrac{d_{g}}{d}\right)^{N}\right]^{-M}, M=1-\dfrac{2}{N}$	M, N, d_g	T
Harris (1968)	3	$P(d)$=1-(1-$\dfrac{d}{d_{\max}})^{k}$	k	T
Smettem *et al.* (1994)	4	$P(d)=cd^{-\beta}$	c, β	T
Pasikatan *et al.* (1999)	5	$P(d)=\left(\dfrac{k_{1}}{1-k_{2}}\right)d^{-(1-k_{2})}$	k_1, k_2	T
Rosin & Rammler (1933)	6	$P(d)=1-e^{\left[-ad^{b}\right]}$	a, b	E
Weibull (1951)	7	$P(d)=a-e^{\left[-\left(\frac{d}{b}\right)^{c}\right]}$	a, b, c	E
Mishra *et al.* (1989)	8	$P(d)=\dfrac{1}{\sqrt{2\pi\sigma}}\int e^{\left[-\frac{1}{2}\left(\frac{d-\mu}{\sigma}\right)^{2}\right]}d(d)$	σ, μ	E
Vipulanandan & Ozgurel (2009)	9	$P(d)=e^{-n\left[k\ln\left(\frac{d}{d_{\max}}\right)\right]^{\frac{d}{d_{\alpha}}}}$	n, k, d_{α}	E
Jaky (1944)	10	$P(d)=e^{\left\{-\frac{1}{p^{2}}\left[\ln\left(\frac{d}{d_{\max}}\right)\right]^{2}\right\}}$	p, $d_{\max}$	E
Zhuang *et al.* (2001)	11	$P(d)=a\left(\ln d\right)+b$	a, b	L
Fredlund *et al.* (2000)	12	$P(d)=\dfrac{1}{\left\{\ln[\exp(1)+\left(\dfrac{a_{gr}}{d}\right)^{n_{gr}}]\right\}^{m_{gr}}}\times\left\{1-\left[\dfrac{\ln\left(1+\dfrac{d_{rgr}}{d}\right)}{\ln\left(1+\dfrac{d_{rgr}}{d_{m}}\right)}\right]^{7}\right\}$	a_{gr}, n_{gr}, m_{gr}, d_{rgr}	L

Fredlund *et al.* (2000)	13	$P(d)=\omega\dfrac{1}{\left\{\ln[\exp(1)+\left(\dfrac{a_{\mathrm{bi}}}{d}\right)^{n_{\mathrm{bi}}}]\right\}^{m_{\mathrm{bi}}}}$ $(1-\omega)\dfrac{1}{\left\{\ln[\exp(1)+\left(\dfrac{j_{\mathrm{bi}}}{d}\right)^{k_{\mathrm{bi}}}]\right\}^{l_{\mathrm{bi}}}}$ $\times\left\{1-\left[\dfrac{\ln\left(1+\dfrac{d_{\mathrm{rbi}}}{d}\right)}{\ln\left(1+\dfrac{d_{\mathrm{rbi}}}{d_{\mathrm{m}}}\right)}\right]^{7}\right\}$	ω, a_{bi}, n_{bi}, m_{bi}, j_{bi}, k_{bi}, l_{bi}, d_{rbi}

A few studies have compared these different models against experimental data. Hwang *et al.* (2002) compared seven PSD models and found that Fredlund's four-parameter model (i.e., Equation No. 12 above) had the best performance for most soils in their database. Hwang (2004) compared nine PSD models using 1385 Korean soils and indicated that the performance of most PSD models could be improved by increasing the content of clay in the soil samples. Again, Fredlund's four-parameter model showed the best overall performance. Zhou *et al.* (2016) compared five PSD models used for granular soils and found that Fredlund's seven-parameter model (i.e., Equation No. 13 above) had the best performance. It is not surprising that a model with more parameters has better performance. However, in some cases, the simpler models yielded more satisfactory results. Buchan *et al.* (1993) came to the conclusion that the one-parameter Jaky's model was superior to the two-parameter standard lognormal model by comparing 23 soils. Vipulanandan & Ozgurel (2009) found that the hyperbolic and S-curve models were comparable to Fredlund's four-parameter model, even though they had fewer parameters.

It should be noted that Equation No. 1 as listed in Table 2.1 has the same form as the fractal model introduced in the previous section, with m = 3–D. However, in Equation No. 1 as listed in Table 2.1, m is a fitting parameter and has no physical meaning. Despite different PSD models being proposed for different soils, the PSD models for granular soils, however, are still limited studied in the literature, especially those that have considered the occurrence of particle breakage, which leads to varying PSDs. The capacity of the existing models in simulating an evolving PSD curve is unknown and needs further study.

2.2.6 Summary

The PSD quantification as a result of the particle breakage can be achieved by adopting breakage indices or continuous PSD models. The former method uses a single parameter to measure the change in PSD. However, it cannot describe the whole PSD; instead, it describes only part of the features of the PSD. The latter method uses a continuous equation to model the whole PSD. In most cases, more than one parameter is required for a good fit performance.

2.3 Evolution of particle breakage

2.3.1 Breakage of a single particle

The breakage of a single particle plays a fundamental role in understanding the breakage of a particle assembly. To date, studies on single-particle breakage have mainly focused on: (1) typical breakage behaviour of a single particle, i.e., force and displacement relations, and breakage (or survival) probability of a single particle; and (2) factors affecting the breakage of a single particle.

The displacement-controlled single-particle uniaxial compression test, referred to as the 'single-particle breakage test' here, is commonly used for measuring the strength and size-scale effect of soil particles. An individual particle is vertically compressed between two rigid horizontal platens, similar to the well-known Brazilian test for rocks. The force-displacement (F-D) curve of a single-particle breakage test is highly dependent on the mineral composition, particle size, particle shape, and failure modes of the single particle. Cavarretta *et al.* (2010) classified the F-D curve, at the initial stage, into three types for three different materials, as shown in Table 2.2.

Table 2.2. Typical F-D curves with three different materials (after Cavarretta *et al.*, 2010)

Material properties	Description	F-D curve

Smaller ballotini, d_{mean}=1.24 mm, and RMS_f =0.08 µm	Initially soft with gradually stiffer response. After reaching the threshold load, the F-D curve is almost linear.	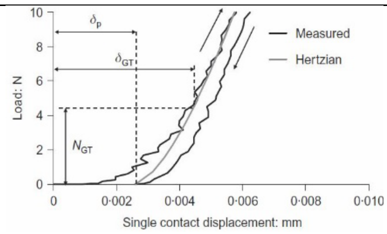
Etched larger ballotini, d_{mean}=2.49 mm, and RMS_f =0.655 µm	Initially soft and quickly becomes linear. After reaching the threshold load, the F-D curve is almost linear with a steep slope.	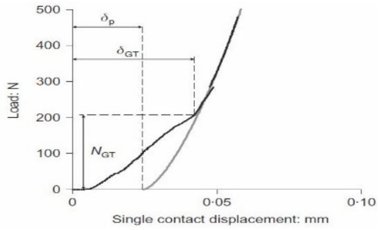
Leighton Buzzard sand, d_{mean}=1.67 mm, and RMS_f =0.3 µm	Initially soft and after reaching the threshold load, the F-D curve is almost linear.	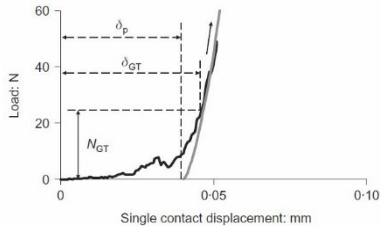

Note: d_{mean} is the mean particle size and RMS_f is the average of the root mean square for measuring the roughness of the particles tested.

Based on the distribution of new particles broken from a single 'mother' particle, Wang & Coop (2016) classified the breakage process into four failure modes and the details of which are summarised in Table 2.3.

Table 2.3. Different failure modes and corresponding typical F-D curves (after Wang & Coop, 2016)

Failure mode	Description	F-D curve
Splitting	Particle splits into two or three large pieces without the creation of numerous small fragments	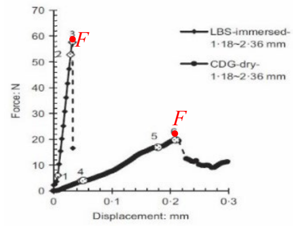
Explosive	Particle undergoes a dramatic and instantaneous blasting into tiny fragments	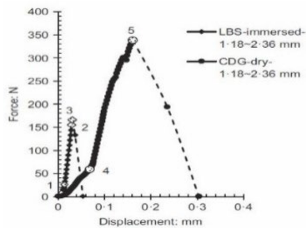

Chipping	A minor part splits away from the particle during compression while the major part may remain between the two loading platens, thus continuing to support substantial loads.	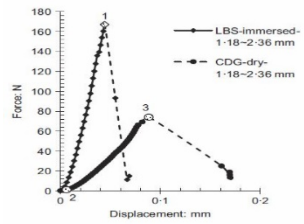
Mixed mode	One smaller part of a particle explodes into several fragments with a high velocity, but leaving the larger part between the platens	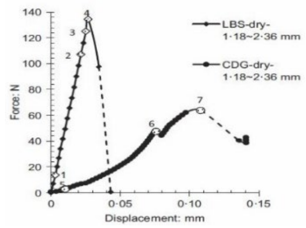

As shown in Table 2.2 and Table 2.3, the F-D responses of single particles differ from those of one another owing to the differences in the material properties. However, it is impossible to find two particles (which are not manufactured through mechanical processes or 3D printing, for example) with the same F-D response because of the variability of the particles in nature. To describe the diversity of particle strength obtained from single-particle breakage tests, a Weibull distribution is commonly employed, which defines the relationship between the survival probability (P_s) of a particle with volume (V) and the tensile strength (σ), which can be expressed as

$$P_s(V) = e^{-\left[\frac{V}{V_0}\left(\frac{\sigma}{\sigma_0}\right)^m\right]} \tag{2.11}$$

Assuming that all the particles tested are spherical in shape, Equation (2.11) can be rewritten as

$$P_s(d) = e^{-\left[\left(\frac{d}{d_0}\right)^3\left(\frac{\sigma}{\sigma_0}\right)^m\right]} \tag{2.12}$$

where d_0 is the reference size, σ_0 is the characteristic strength at which 37% of tested particles with size d_0 will survive, and m is the Weibull modulus. The tensile strength of particle can be calculated as defined by Jaeger (1967)

$$\sigma = \frac{F}{d^2} \tag{2.13}$$

where F is the maximum force measured during the test as indicated in Table 2.3, and d is the particle diameter, i.e., the initial distance between the platens (Nakata *et al.*, 1999). Based on Equation (2.12), the survival probability of particles with size d_0 can be expressed as

$$P_s(d_0) = e^{-\left(\frac{\sigma}{\sigma_0}\right)^m} \tag{2.14}$$

As plotted in Figure 2.3(a), an increasing value of m indicates a decreasing variability in the particle strength. By rewriting Equation (2.14), a linear relationship can be obtained as

$$\ln[\ln(1/P_s(d_0))] = m\ln\sigma - m\ln\sigma_0 \tag{2.15}$$

The values of σ_0 and m can be obtained from the slope and intercept of the linear line as in the example shown in Figure 2.3(b). The survival probability P_s (d_0) with limited tested particles can be calculated using the mean rank position (Cheng *et al.*, 2003)

$$P_s(d_0) = 1 - \frac{i}{N+1} \tag{2.16}$$

where N is the number of the tested particles and i is the rank of the particles sorted in an ascending order.

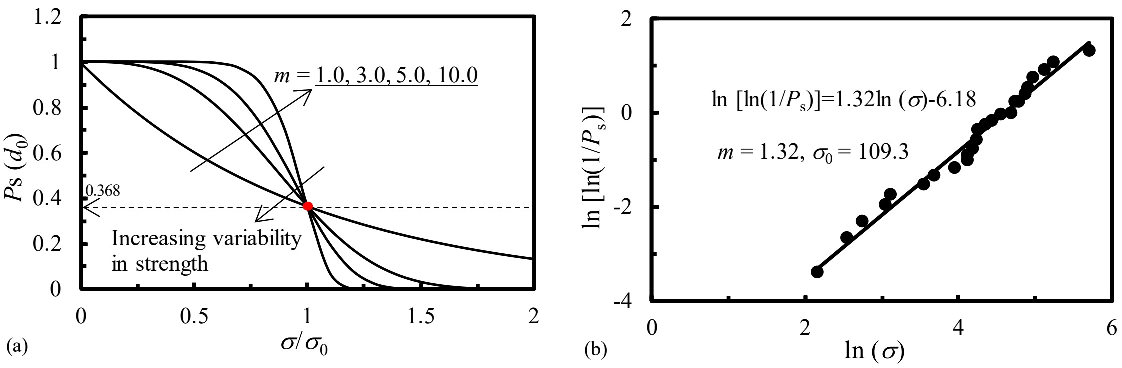

Figure 2.3: Weibull distribution of the survival probability: (a) effect of m on strength, (b) example of linear line (data after McDowell & Amon, 2000)

In general, the strength of a single particle depends on both internal and external factors. The internal factors encompass the properties of the particle itself, including particle shape, particle size, and particle mineralogy. It is clear from Equation (2.12) that a bigger particle has a lower survival probability, mainly owing to the fact that a bigger particle has more inherent flaws than a smaller one (Lobo-Guerrero & Vallejo, 2006). Nakata *et al.* (1999) analysed the strength of quartz and feldspar particles during single-particle breakage tests and reported a significantly larger survival probability for quartz particles at a given tensile strength. This can be explained by the difference in the initial microstructures between the two particles as revealed by Zhao *et al.* (2015), who used X-ray CT to track the whole single-particle breakage process. The effect of particle shape on single-particle breakage is, to a great extent, controversial, largely owing to the difficulty in the description and unification of the particle shapes. For example, Wang & Coop (2016) reported that the 2D sphericity and regularity had little influence on the strength of single particles, while the roundedness played an important role in the breakage mode of single particles. Afshar *et al.* (2017), however, found that particles with a higher degree of sphericity would have lower breakage probability.

The external factors, such as the contact number (or the coordination number), humidity (or water content), affect the single-particle breakage with various degrees. Several studies have shown that an increase in the number of contacts leads to an increase in the failure strength and a decrease in the breakage probability of a soil particle (Gundepudi *et al.*, 1997; Ben-Nun & Einav, 2010; Todisco *et al.*, 2017; Salami *et al.*, 2017). It is worth noting that the effect of humidity on single-particle breakage also depends on the particle mineralogy. For example, particles with intra-particle pores are stronger in dry state than in a saturated state (e.g., decomposed granites or carbonate sands), while the water content has little influence on the strength of those particles with no intra-particle porosity (e.g. quartz sands) (Ovalle *et al.*, 2015; Wang & Coop, 2016).

To summarize the above discussion, more attention has been paid to the breakage probability and the corresponding influencing factors in the studies conducted on single-particle breakage. The distribution of newly generated particles, however, has still not been studied extensively.

2.3.2 Evolution of breakage indices from experiments

For a particle assembly, it is not possible to track each individual particle inside a sample, at least not in a simple way. As discussed previously, the breakage indices calculated based on the PSDs, before and after the test are often used to describe the evolution of the PSD resulting out of particle breakage. To some extent, experimental studies on particle breakage of granular soils mostly comprise post-mortem observations, which means that the PSDs can be obtained only at the end of the test on a particular stress path. Therefore, a series of tests on samples with the same initial conditions subjected to elevated external loads (e.g., stress, strain, input work, grinding time, and number of cycles) need to be performed. A selected breakage index can then calculated based on the measured PSD after each test.

Lu *et al.* (2003) performed a series of comminution tests on quartz sand for simulating the formation of loess by using a high-energy tungsten carbide disc mill. The fractal dimension D was adopted to represent the evolution of PSDs after a progressive grading time. An empirical relation between the fractal dimension D and the grading time was then proposed as follows:

$$D = \frac{t}{a \times t + b} \tag{2.17}$$

where a determines the ultimate fractal dimension D_u (= $1/a$ when $t \to \infty$), and b is a parameter controlling the evolution rate of the PSD.

Lee & Farhoomand (1967) conducted tests on crushed granite gravel with a different constant K_0 stress path and reported that there was no unique relationship between the breakage index B_{15} and the major principal stress, and that the development of B_{15} was highly dependent on the shear stress. Hardin (1985) then proposed a hyperbolic equation for representing the relationship between the breakage effective stress and the breakage index B_r by trial and error as

$$B_r = \frac{\left(\frac{\sigma_b'}{\sigma_r'}\right)^{n_b}}{1+\left(\frac{\sigma_b'}{\sigma_r'}\right)^{n_b}} \tag{2.18}$$

with

$$\begin{cases} \sigma_b' = \sigma_0'\left[1+9\left(\frac{\tau_0}{\sigma_0'}\right)^3\right] = p'\left[1+\frac{2\sqrt{2}}{3}\left(\frac{q}{p'}\right)^3\right] \\ \sigma_r' = 800 p_a \left(n_b - 0.3\right) \end{cases} \tag{2.19}$$

where σ_b' is defined as the breakage effective stress; τ_0 and σ_0 are the effective octahedral normal and shear stresses, respectively; p' and q are the mean effective and deviatoric stresses, respectively; p_a is the atmospheric pressure, and n_b is the breakage number. The use of octahedral normal and shear stresses can show the stress-path dependence of the particle breakage.

Coop & Lee (1993) found that the shear-induced breakage was larger than the compression-induced breakage by conducting a series of one-dimensional (1D) compression tests and triaxial shearing tests on carbonate sand. Furthermore, they reported that B_r was independent of initial density. It is now widely accepted that the relation between B_r and the mean effective stress is not unique, i.e., a denser sample suffers more breakage during shearing (Shahnazari & Rezvani, 2013; Yu, 2017a), while a looser sample suffers more breakage, when subjected to compression (Bopp & Lade, 2005; Altuhafi & Coop, 2011a; Xiao *et al.*, 2017). This phenomenon is mainly attributed to the different energy inputs within the sample. Taking the undrained triaxial test as an example, a dense sample displays strain hardening with substantial particle breakage, while a loose sample may show liquefaction behaviour with negligible particle breakage. Therefore, correlating the breakage index to the energy-based parameter has been adopted more widely.

One of the early studies on this topic was performed by Miura & O'Hara (1979). They found a unique curve between the plastic work and the increase in the surface area during different stress paths in a triaxial test on a decomposed granite soil. Lade *et al.* (1996) proposed a hyperbolic function for describing the evolution of B_{10} with increasing total energy input per unit volume W as

$$B_{10} = \frac{W}{a + bW} \tag{2.20}$$

with

$$W = \int \sigma_{ij} d\varepsilon_{ij} \tag{2.21}$$

where σ_{ij} and ε_{ij} are the stress and the corresponding strain component, respectively. Equation (2.20) is similar to Equation (2.17), with one parameter controlling the evolution rate of PSD and the other being related to the ultimate value of B_{10}. The reason for using the total work input is that the magnitude of plastic work is much larger than that of the elastic work, as a result of the particle breakage. Casini *et al.* (2013) gave a more complex form for linking the modified relative breakage index B_r^* to the input work per unit volume W, based on different kinds of tests on crushed expanded clay pellets

$$\frac{1-B_{\mathrm{r}}^{*}}{1-B_{\mathrm{ri}}}=\left[1+m\left(\frac{W}{W^{*}}\right)^{1/(1-m)}\right]^{-m} \tag{2.22}$$

where m and W^* are the model parameters and B_{ri} is a finite non-zero value. Xiao *et al.* (2017) reported a linear relationship between B_{r}^* and W, based on 1D-compression tests on carbonate sand with various initial densities. It was also emphasized by Xiao et al. that such a relationship was valid only at a small value of B_{r}^* (< 9%). Einav (2007a, 2007b) correlated the modified relative breakage index B_{r}^* with the breakage energy, based on the framework of continuum breakage mechanics (CBM) for the compression tests. However, using the total work input as a mechanical parameter cannot describe the accumulation of particle breakage during cyclic loading. It is therefore, highly beneficial to use the accumulated plastic work (as defined in the following Equation) for correlating with the breakage index.

$$W^{p}=\int\sigma_{ij}d\varepsilon_{ij}^{p} \tag{2.23}$$

where superscript p stands for plastic. A similar equation as Equation (2.20) is widely used to describe the evolution of particle breakage. For example, Hu *et al.* (2018) proposed a unified relation between the breakage index and the plastic work as follows:

$$B_{\mathrm{r}}^{*}/B_{\mathrm{u}}=\frac{W}{a/b+W} \tag{2.24}$$

As indicated by Equation (2.24) the values of B_{r}^* and B_{u} approach unity, when the sample is subjected to an infinite amount of plastic work, and these are the maximum values as analyzed in the previous section.

Other models describing the evolution of breakage indices in terms of energy-based parameters include, but are not limited to, the logarithmic model (Huang *et al.*, 2013) and exponential model (Xiao *et al.*, 2016c). In general, as indicated by all the models proposed in the literature, the breakage rate will eventually decrease to 0 at a high mechanical level, which means that the PSD will ultimately reach a steady state.

2.3.3 Evolution of PSD from mathematical modelling

Mathematical models offer great benefits in describing the evolution of PSD because of their advantages, such as low computational cost and low requirements for test facilities.

In this section, several mathematical models for the evolution of PSD are briefly introduced and discussed.

2.3.3.1 Markov (Chain) Model

Markov model is a stochastic process used to predict a future state using the information of the current state. The future state only depends on the current state and is independent of the past state. This particular property is the so-called 'memorylessness property'. Those models having either a discrete state space or a discrete index set (often representing time) are called Markov chain models. Define a Markov chain model $\{X_n, n \in \mathbb{N}\}$, where $\mathbb{N} = \{1, 2, \cdots n\}$ is a discrete time set. The values of X_i form a countable set $\mathbb{R} = \{R_1, R_2, \cdots, R_n\}$, called the state space. The memorylessness property of the Markov chain model can be expressed as:

$$P\{X_{n+1} = R_{n+1} / X_0 = R_0, X_1 = R_1, \cdots, X_n = R_n\} = P\{X_{n+1} = R_{n+1} / X_n = R_n\} \tag{2.25}$$

where $P\{X_{n+1} = R_{n+1} / X_n = R_n\}$ is the conditional probability, which means that the probability of the system moving to R_{n+1} at time t+1 from state R_n at time t, is defined as: $P_{R_n R_{n+1}}(t)$. When $P_{R_n R_{n+1}}(t)$ is not dependent on time t, it can be simplified as $P_{R_n R_{n+1}}$ and the Markov chain model is called a time-homogeneous Markov chain model. The one-step transition probability matrix $\boldsymbol{P}$ can be expressed as:

$$\boldsymbol{P} = \begin{bmatrix} P_{R_1R_1} & P_{R_1R_2} & \cdots & P_{R_1R_n} & \cdots \\ P_{R_2R_1} & P_{R_2R_2} & \cdots & P_{R_2R_n} & \cdots \\ \vdots & \vdots & \vdots & \vdots & \vdots \end{bmatrix} \tag{2.26}$$

with

$$\begin{cases} P_{R_iR_j} \geq 0, R_i \,\&\, R_j \in \mathbb{R} \\ \sum\limits_{R_j \in \mathbb{R}} P_{R_iR_j} = 1, R_i \in \mathbb{R} \end{cases} \tag{2.27}$$

In addition, we define $P_{R_iR_j}^{(m)} = P\{X_{m+n} = R_j / X_n = R_i\}, (R_i \,\&\, R_j \in \mathbb{R}, m \geq 2)$ as the m-step conditional probability while $\boldsymbol{P}^{(m)}$ is the m-step transition probability matrix. The relationship between $\boldsymbol{P}^{(\mathrm{m})}$ and $\boldsymbol{P}$ can be expressed as:

$$\boldsymbol{P}^{(m)} = \boldsymbol{P}^m \tag{2.28}$$

Defining an initial probability vector $\boldsymbol{R}^T(0) = (X_1, X_2, X_3, \cdots)$, and an absolute probability vector $\boldsymbol{R}^T(m) = (X_1(m), X_2(m), X_3(m), \cdots)$ at time m, the relationship between $\boldsymbol{R}^T(m)$ and $\boldsymbol{R}^T(0)$ is given by:

$$\boldsymbol{R}^T(m) = \boldsymbol{R}^T(0)\boldsymbol{P}^{(m)} = \boldsymbol{R}^T(0)\boldsymbol{P}^m \tag{2.29}$$

Equation (2.29) is then used for predicting the probability vector after an m-step transition.

To understand in a better way, how the Markov chain model works, a simple example introduced by Berthiaux (2000) is adopted here. As shown in Figure 2.4, a goat is able to move in the 11 grids with the same probability of moving to each neighbour grid. Assume that the goat cannot remember its previous step in the grid pattern, the movement of goat, then is a Markov chain model. Assume that the time set $\mathbb{N} = \{1, 2, \cdots n\}$ represents the steps of the goat's movement and the state space set $\mathbb{R} = \{1, 2, \cdots, 11\}$ represents the number or identity of the grid. Let the goat stays in grid #1 at the initial state. The initial probability vector is then expressed as $\boldsymbol{R}^T(0) = (1, 0, 0, \cdots)$. Now, place the lion in grids #8-#11. Once the goat moves to these four grids, it disappears and is out of the system. Otherwise, the goat will survive in the system. The one-step transition probability matrix $\boldsymbol{P}$ can be expressed as:

$$\boldsymbol{P} = \begin{bmatrix} 0 & 1/4 & 1/4 & 0 & 0 & 0 & 0 & 0 & 1/4 & 0 & 1/4 \\ 1/4 & 0 & 0 & 1/4 & 0 & 0 & 1/4 & 1/4 & 0 & 0 & 0 \\ 1/4 & 0 & 0 & 0 & 1/4 & 1/4 & 0 & 0 & 0 & 1/4 & 0 \\ 0 & 1/2 & 0 & 0 & 0 & 0 & 0 & 0 & 1/2 & 0 & 0 \\ 0 & 0 & 1/2 & 0 & 0 & 0 & 0 & 0 & 0 & 0 & 1/2 \\ 0 & 0 & 1/2 & 0 & 0 & 0 & 0 & 0 & 1/2 & 0 & 0 \\ 0 & 1/2 & 0 & 0 & 0 & 0 & 0 & 0 & 0 & 0 & 1/2 \\ 0 & 0 & 0 & 0 & 0 & 0 & 0 & 1 & 0 & 0 & 0 \\ 0 & 0 & 0 & 0 & 0 & 0 & 0 & 0 & 1 & 0 & 0 \\ 0 & 0 & 0 & 0 & 0 & 0 & 0 & 0 & 0 & 1 & 0 \\ 0 & 0 & 0 & 0 & 0 & 0 & 0 & 0 & 0 & 0 & 1 \end{bmatrix} \tag{2.30}$$

The positions of the goat when it moves either 1 step or 6 steps can be calculated based on Equation (2.29) as follows:

$$\begin{cases} \boldsymbol{R}^T(1) = \boldsymbol{R}^T(0)\boldsymbol{P} = \left(0, 1/4,\ 1/4, 0, 0, 0, 0, 0,\ 1/4, 0,\ 1/4\right) \\ \boldsymbol{R}^T(6) = \boldsymbol{R}^T(0)\boldsymbol{P}^6 \\ = \left(0, 9/256,\ 9/256, 0, 0, 0, 0, 11/128,\ 97/256,\ 11/128,\ 97/256\right) \end{cases} \tag{2.31}$$

The survival probabilities of the goat (i.e., it stays in grids #1-#7) after 1 step or 6 steps, obtained from Equation (2.31) are 1/2 and 9/128, respectively.

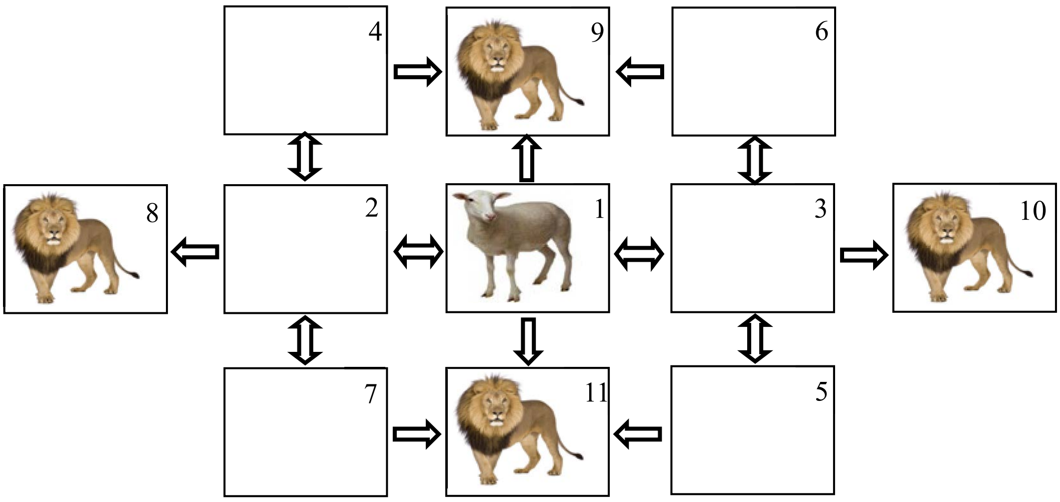

Figure 2.4: Illustration of Markov chain model (modified after Berthiaux, 2000)

The Markov model is widely used for modelling the intentional degradation of PSD in particulate process engineering, such as chemical engineering, pharmaceutical processing, and numerous other fields. More details about the application of Markov model in these fields can be found in the literature (Berthiaux & Mizonov, 2004). In most geotechnical cases, however, the degradation of PSD is inadvertent and the application of the Markov model is still not explored completely.

Ozkan & Ortoleva (2000) proposed a Markov model to describe the evolution of gouge materials in geological faults with two strong hypotheses: (1) the breakage probability depends only on the particle size and the average properties of particles; and (2) a particle will break into smaller particles with the same probability. Inspired by their work, we (Zhang, **Tong**, Li & Sheng, 2015) proposed a new method for studying the evolution of particle breakage. Firstly, the breakage probability p for a uniformly graded sample (d_{n-1}~d_n) is defined as

$$p = \frac{\text{mass of crushed particles (passing } d_{n-1}\text{-sized sieve)}}{\text{total mass of sample}} \tag{2.32}$$

Once the breakage probability is known, the next key question is: how are the new smaller particles generated by the breakage distributed? Instead of a uniform distribution as assumed by Ozkan & Ortoleva (2000), a new two-parameter Weibull distribution function was proposed

$$\begin{cases} F = 1 - e^{-\left[\frac{x_{ij}}{a(1-x_{ij})}\right]^{b}} \\ x_{ij} = \dfrac{d_j}{d_{i-1}} \qquad j = 1, 2, \cdots, i-1 \end{cases} \tag{2.33}$$

where a is a scaling parameter and b is a shape parameter.

For a non-uniformly graded sample, the concept of 'effective breakage probability' was proposed, wherein the breakage of all the particles from different size groups (excluding the minimum-sized particles) was assumed to be the same, and this probability can be expressed as

$$\begin{cases} P_{d_1 d_1} = 0, \quad k = 1 \\ P_{d_k d_k} \equiv p^{m-n}, \quad 2 \le k \le n \end{cases} \tag{2.34}$$

where $p^{m\text{-}n}$ is the effective breakage probability of d_k-sized particles and the superscript $m\text{-}n$ means that the particle breakage is from state m to state n. Because there is no further breakage for the minimum-sized particles, the breakage probability of d_1-sized particles is 0. The one-step transition probability matrix from state m to state n, i.e., $\boldsymbol{P}^{m\text{-}n}$ is then expressed as

$$\boldsymbol{P}^{m-n} = \begin{bmatrix} 1 & 0 & 0 & 0 & \cdots & 0 & 0 \\ \beta_{21} p^{m-n} & q^{m-n} & 0 & 0 & \cdots & 0 & 0 \\ \beta_{31} p^{m-n} & \beta_{32} p^{m-n} & q^{m-n} & 0 & \cdots & 0 & 0 \\ \vdots & \vdots & \vdots & \vdots & \vdots & \vdots & \vdots \\ \beta_{j1} p^{m-n} & \cdots & \beta_{jk} p^{m-n} & \cdots & q^{m-n} & \cdots & 0 \\ \vdots & \vdots & \vdots & \cdots & \vdots & \vdots & \vdots \\ \beta_{i1} p^{m-n} & \beta_{i2} p^{m-n} & \beta_{i3} p^{m-n} & \cdots & \beta_{ii-2} p^{m-n} & \beta_{ii-1} p^{m-n} & q^{m-n} \end{bmatrix} \tag{2.35}$$

where $q^{m\text{-}n}$ (=1-$p^{m\text{-}n}$) is the 'effective survival probability', and β_{jk} is defined as the coefficient of breakage probability which represents the mass ratio between the d_k-sized particles breaking from the d_j-sized particles to the total mass breaking from the d_j-sized particles. Noting that it is physically not possible for particles to break into a larger size, the values in the probability matrix, above the diagonal are 0. In other words, the one-step transition probability matrix is a lower triangular matrix. According to Equation (2.33), the overall mass conservation, β_{jk} is calculated as

$$\begin{cases} \beta_{kl} = F(x_{kl}) - F(x_{kl-1}), \qquad x_{k0} = 0 \\ \sum_{k=1}^{j-1} \beta_{jk} = 1, \qquad j = 2,3,\ldots,i \end{cases} \tag{2.36}$$

The effective breakage probability $p^{m\text{-}n}$ can be calculated based on the PSDs before and after the test. We proposed a framework to study the evolution of both uniformly graded and non-uniformly graded samples as briefly introduced above. However, this model still cannot predict PSDs with different stress paths.

2.3.3.2 Breakage Matrix Model

The breakage matrix model, first proposed by Broadbent & Callcott (1956) is widely used for the mathematical description of the relationship between the initial PSD and the evolving PSD in a grinding process.

$$\boldsymbol{B}_{mn}\boldsymbol{f}_n = \boldsymbol{o}_m \tag{2.37}$$

where $\boldsymbol{f}_n$ and $\boldsymbol{o}_m$ are row vectors of the feed (initial) PSD and the output (final) PSD, respectively, and $\boldsymbol{B}_{mn}$ is the breakage matrix. The subscript mn refers to the dimension of the matrix with m rows and n columns. Equation (2.37) can be expanded as

$$\begin{bmatrix} t_{11} & t_{12} & \cdots & t_{1n} \\ t_{21} & t_{22} & \cdots & \vdots \\ \vdots & \vdots & \ddots & \vdots \\ t_{m1} & t_{m2} & \cdots & t_{mn} \end{bmatrix} \begin{bmatrix} f_1 \\ f_2 \\ \vdots \\ f_n \end{bmatrix} = \begin{bmatrix} o_1 \\ o_2 \\ \vdots \\ o_m \end{bmatrix} \tag{2.38}$$

where coefficient t_{ij} represents the mass fraction of particle size interval j of the output material obtained from the particle size interval i of the input material. It should be noted that the sieve sizes/numbers of the input material are not necessarily the same as those of the output material, i.e., $m \neq n$, especially, for most milling processes. For example, the sizes of feed material are commonly much larger than those of the output material in the field of flour milling. It is, therefore, highly beneficial to use different sieve sizes/numbers for measuring the input and output PSDs with more accuracy (Campbell & Webb, 2001; Campbell *et al.*, 2001). The overall mass conservation requires

$$\sum_{1}^{m} o_i = 1, \sum_{1}^{n} f_i = 1, \sum_{i=1}^{m} t_{ij} = 1, \text{for each } j \in [1, \cdots, n] \tag{2.39}$$

When the sieve sizes/numbers are the same for the input and output PSDs (i.e., $m = n$), for example, as in the case of coal breakage, as suggested by Broadbent & Callcott (1956), the breakage matrix is a square matrix. The square matrix has a similar mathematical form as the one-step transition probability matrix and contains two parts: (1) the breakage function that describes the distribution of newly generated particles broken from the 'mother particles', and (2) the selection function that describes the breakage probability of 'mother particles'. The breakage matrix is more or less an inherent property of the machine that is used for the milling process. In the field of geotechnical engineering, the application of the breakage matrix model is still not studied extensively.

2.3.3.3 Population Balance Model

The population balance model can be a helpful tool for modelling the grinding processes. The population balance equations define how populations of separate entities (such as different size groups) vary in a system over time, through their birth-and-death process (Hulburt & Katz, 1964; Ramkrishna, 2000). The population here can be interpreted as the number/mass of particles. The general form can be expressed as

$$\frac{\partial m(d,t)}{\partial t} = -S(d,t)m(d,t) + \int_{y=d}^{d_{\max}} \beta(d,y)S(y,t)m(y,t)dy \tag{2.40}$$

where $m(d, t)$ means the mass of d-sized particles at time t; $S(d, t)$ is the breakage probability of d-sized particles at time t; and $\beta(d, y)$ is the percentage of the d-sized particles breaking from y-sized particles to the total mass breaking from y-sized particles. $\beta(d, y)$ shares the same meaning as the coefficient of breakage probability.

Ovalle *et al.* (2016) adopted the population balance model to simulate the evolution of PSD in granular assemblies during confined comminution. To describe the mass change of each size fraction, a discrete population balance model in terms of force instead of time was proposed as

$$\frac{\partial m(d_i,\xi)}{\partial \xi_i} = \boldsymbol{B}_{ij} m(d_i,\xi) \tag{2.41}$$

where $\partial \xi_i$ is the increment of the normalized normal contact force of d_i-sized particles. The matrix $\boldsymbol{B}_{ij}$ is defined as follows

$$\boldsymbol{B}_{ij} = \begin{cases} \beta_{ij} S_j & \text{for } i < j \\ -S_i & \text{for } i = j \\ 0 & \text{for } i > j \end{cases} \tag{2.42}$$

This matrix is of the same form as the one-step transition probability matrix discussed earlier. The values of β_{ij} can be obtained by the fractal distribution function

$$\beta_{ij} = \left(\frac{d_{i+1}}{d_j}\right)^{3-D} - \left(\frac{d_i}{d_j}\right)^{3-D} \tag{2.43}$$

The breakage probability of d_i-sized particles S_i is calculated by using a combined breakage probability by taking into consideration (1) the coupling effect of the breakage probability of a single particle (see Equation (2.12)) and (2) the distribution of contact force within the sample, which was first proposed by Marketos & Bolton (2007), and further developed by other scholars (Zhou *et al.*, 2014; Caicedo *et al.*, 2016; Cheng & Wang, 2018).

In general, the three commonly used mathematical models introduced above possess a similarity in terms of correlating the initial PSD and the final PSD with a matrix. The core issue that needs to be tackled here is determining the value of each element in the matrix for the three models, i.e., the breakage probability of d_i-sized particles and the distribution of the newly generated particles from the d_i-sized particles.

2.3.4 Summary

The breakage probability of a single particle is well described by the well-known Weibull distribution. As for the breakage of a particle assembly, the evolution of particle breakage can be tracked with special attention to either the breakage index or the whole PSD. The particle breakage index is commonly correlated with various mechanical parameters, such as plastic shear strain, total input work, and plastic work via different empirical equations, e.g., hyperbolic, linear, logarithmic, and exponential. Three mathematical models, namely Markov, breakage matrix, and population balance models are widely used for correlating the initial and final PSDs with a matrix where the breakage probability of particles and the distribution of newly generated particles are considered.

2.4 Effect of PSD on the constitutive behaviour of granular soils

The mechanical behaviour of granular soils is distinctly different from that of clays with the main features summarised as follows:

(1). The compression curves of granular soils cannot be represented by straight lines in the e (or, v) - ($\ln p$) space, where e is the void ratio, v is the volume (= $1+e$), and p is the mean effective stress. In particular, granular soils are relatively incompressible at low stresses and are subjected to large compression deformation at high stresses.

(2). The isotropic compression line (ICL) is not unique for a granular soil and depends on its initial void ratio, which is significantly different from that of a normal consolidated clay. The ICLs will eventually converge into an asymptotic line at high stresses.

(3). The volumetric and stress-strain responses of granular soils subjected to triaxial shearing are highly dependent on the initial density and the mean effective stress. For a given mean effective stress, contractive and strain hardening behaviour will be observed in a loose sample, whereas a dense sample will show dilative and strain softening behaviour during drained shearing. Moreover, for a given initial density, granular soils may exhibit dilative or contractive behaviours at low or high mean effective stresses, respectively.

(4). For a given mean effective stress, increasing pore water pressure and flow liquefaction behaviour will be observed for a very loose sample, whereas decreasing pore water pressure and non-flow behaviour will be observed for a dense sample during undrained shearing. For a given initial void ratio, samples subjected to higher stress may be more prone to liquefaction.

(5). Granular soils under triaxial shearing will reach a critical state at which plastic shearing could continue indefinitely with no change in the effective stress or specific volume. The critical state lines (CSLs) cannot be represented by straight lines in the classical $e - \ln(p)$ space either. The ICLs and CSL may become parallel at high stresses in the $e - \ln(p)$ space.

(6). Particle breakage is inevitable in various engineering applications with evolving PSD, which will have a great influence on the constitutive behaviour of granular soils.

In the following subsections, a brief review of studies on the effect of PSD on the constitutive behaviour of granular soils will be presented, with particular attention paid to the effect of PSD on the compression and shearing behaviours, and the critical state.

2.4.1 Effect of PSD on compression behaviour

2.4.1.1 Typical compression curves of granular soils

The relationship between the void ratio (or, volume) and the natural logarithm of the applied mean effective stress (for isotropic compression), or vertical effective stress (for 1D-compression) is approximately linear for normal consolidated clay based on the critical state soil mechanics (CSSM) (Roscoe *et al.*, 1958; Muir Wood, 1990). The line called normal consolidation line (NCL), or virgin consolidation line takes the form

$$\begin{cases} e = e_0 - \lambda \ln p' & \text{for isotropic compression} \\ e = e_0 - \lambda \ln \sigma'_\mathrm{v} & \text{for 1D-compression} \end{cases} \tag{2.44}$$

where λ is the slope of the isotropic (1D) compression line and e_0 is the intercept on the line at $p'(\sigma'_\mathrm{v}) = 1$. The results of 1D-compression tests are often plotted in the space defined by the void ratio versus the logarithm of vertical effective stress by using the **compression index C_c** instead of λ

$$e = e_0 - C_\mathrm{c} \log_{10} \sigma'_\mathrm{v} \tag{2.45}$$

where $C_\mathrm{c} = \lambda \ln 10$ (obtained by comparing Equations (2.44) and (2.45)) and is a material constant for the normal consolidated clay. Owing to the nonlinearity and non-uniqueness of the compression curves in the e-log (p/σ'_v) space, the term 'NCL' for granular soils is somewhat controversial. Figure 2.5 shows typical compression curves of granular soils with stiff elastic behaviour followed by linear plastic compression with increasing stress. In most cases, all the compression curves seem to converge into an asymptotic line in the e-log (σ'_v) space at high stresses. This straight line is somewhat treated as the NCL for granular soil with the slope being the compression index C_c, as shown in Figure 2.5 (Altuhafi & Coop, 2011a; Pino & Baudet, 2015). To avoid a negative void ratio at high stresses, which is a major limitation of the NCL, Pestana & Whittle (1995) proposed a double logarithmic approach to describe the asymptotic line named the 'limit compression line' (LCL), as shown in Figure 2.5.

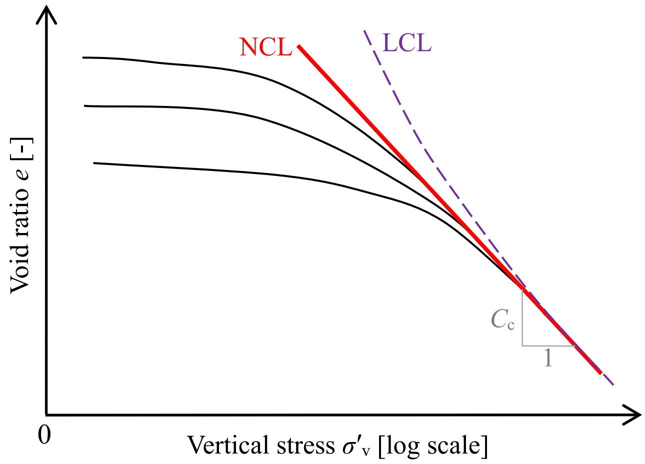

Figure 2.5: Typical compression curves of granular soils and the asymptotic line

To model the nonlinear compression curves of granular soils, several empirical formulas were proposed in different mathematical forms, such as the single logarithmic approach with additional stress shifting parameter (Yao *et al.*, 2019), double logarithmic approach (Butterfield, 1979; Pestana & Whittle, 1995; McDowell, 2005; Sheng *et al.*, 2008; Yao *et al.*, 2018), and exponential function (Gudehus, 1996; Bauer, 1996; Wan & Guo, 2004). More comprehensive comparisons of these approaches can be found in the literature (Pestana & Whittle, 1995).

As summarized by Mesri & Vardhanabhuti (2009), there are three main shapes of compression curves of granular soils (see Figure 2.6)

(1). Type A shape: The **tangent-constrained modulus *M*** (=$\Delta\sigma_v/\Delta\varepsilon_v$, where ε_v is the vertical strain) first increases (denoted as stage 1), then decreases (denoted as stage 2), and finally increases with increasing vertical stress (denoted as stage 3). In stage 1, particle movements will enhance inter-particle locking effect and then dominate the volume change, while a small amount of particle breakage, which, if there is any, mainly includes particle abrasion and breakage of particle corners and edges, will be detected owing to the low stress level. In stage 2, particle fracture occurs when the applied stress exceeds the strength of particles, leading to an unlocked aggregate framework. The unlocking effect due to particle fracture dominates over the locking effect due to the particle movements, which will lead to a decreasing value of *M*. The voids will be filled up by small particles generated by the particle breakage; the rate of particle breakage will slow down and eventually stop during stage 3. At this stage, the particle locking effect regains the dominant role of determining the stiffness of the sample because of a more intimate packing.

(2). Type C shape: The tangent-constrained modulus M increases with an increase in the vertical stress throughout the compression.

(3). Type B shape: This is a transition between types A and C, with an almost constant value of M in stage 2, which indicates a balance between the particle locking and particle breakage effects.

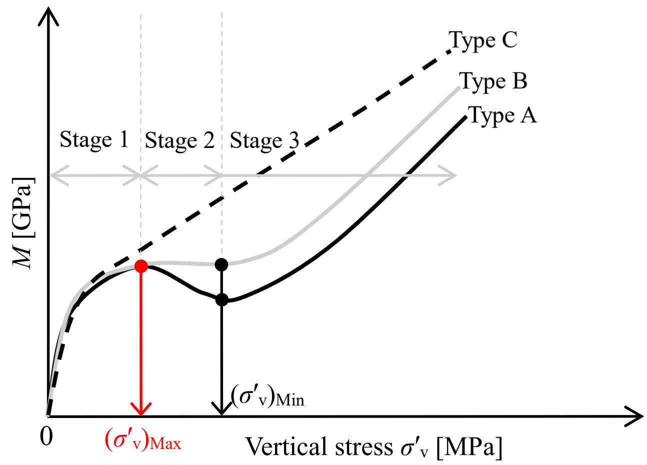

Figure 2.6: Illustration of the three shapes of e-log (σ'_v) curve in terms of σ'_v - M plot

It is generally accepted that the yielding of granular soil is believed to represent the onset of particle breakage (Coop, 1990; Hagerty *et al.*, 1993; Nakata *et al.*, 2001a, Nakata *et al.*, 2001b). The **yield stress $(\sigma_v)_{MC}$** of granular soils is generally determined as the maximum curvature point of the compression curve in the e-log (p/σ'_v) space by the schematic method (Hagerty *et al.*, 1993; Nakata *et al.*, 2001a; Nakata *et al.*, 2001b; Chuhan *et al.*, 2002; Chuhan *et al.*, 2003; Xiao *et al.*, 2018b). As analysed before, there are three distinct stages of the compression curve with abrupt onset of constrained modulus change for type A and type B compression behaviours. As suggested by Mesri & Vardhanabhuti (2009), the first inflection point $(\sigma_v)_{Max}$, and the second inflection point $(\sigma_v)_{Min}$ represent the start and the end of the particle breakage as shown in Figure 2.6.

2.4.1.2 Effect of PSD on compression index

The previous literature on compression tests on granular soils has shown that the compression index of granular soils is independent of the initial PSD for uniformly graded samples, while the initial PSD has a significant influence on the compression index of the non-uniformly graded samples.

Nakata *et al.* (2001b) conducted a series of 1D-compression tests on uniformly graded granular soils with different initial PSDs, mineral compositions, initial void ratios, and particle shapes. Instead of adopting the slope of the NCL as the compression index C_c, they defined a compression index [C_c= (-Δe)/Δlog (σ'_v)] based on Equation (2.45) applicable during the whole compression process. Interestingly, they found that the compression index at high stresses (i.e., C_c as defined from the slope of the NCL) tended to approach a value of 0.4, and seemed to be independent of the initial PSD, mineral composition, initial void ratio, and even particle shape. However, the peak value of the compression index occurred at a lower vertical stress for samples with larger particle sizes. McDowell (2002) reported similar results by testing Leighton Buzzard sands with different initial uniformity gradings. Xiao *et al.* (2018b) demonstrated the PSD-independence of the compression index by conducting 1D-compression tests on uniformly graded rockfill materials with three different sizes. They further gave the value of the compression index of rockfill materials as 0.49. Furthermore, McDowell (2005) and Russell (2011) correlated the compression curve with the fractal breakage theory and explained that the compression index was determined by the ultimate fractal dimension of granular soils, which was thought to be a value between 2.5 and 2.6 as described earlier.

As for the non-uniformly graded granular soils, the compression index appears to be more sensitive to the initial PSD. Altuhafi & Coop (2011a) performed a series of high-stress 1D-compression tests on uniform and non-uniform sands (including carbonate sands, silica sands, and glacial basalt sands). They found that a well-graded sample would have a lower compression index. More specifically, C_c decreased with increasing relative distribution factor R_D (= d_{90}/d_{10}). Pino & Baudet (2015) came to a similar conclusion that the compression index decreased with a better PSD for both reinforced and non-reinforced granular soils. Minh & Cheng (2013) presented 1D-compression tests using the discrete element method (DEM). They created truncated fractal-graded PSDs with a fractal dimension of D between 1.4 and 2.7 and a minimum particle size of 0.092 mm. In addition, the particle breakage was not considered in their simulations. It was found that C_c decreased with increasing D, when $D \leq 2.3$ and increased with increasing D when $D \geq 2.3$. However, a unified trend was observed that the compression index C_c decreased with the increasing coefficient of uniformity C_u (= d_{60}/d_{10}), indicating that the uniformity played a more important role on the compression index than the small particle content.

2.4.1.3 Effect of PSD on tangent-constrained modulus

As discussed above, there are three types of compression curves in terms of the evolution of the tangent-constrained modulus M. The previous studies have shown that the mineral composition had a great influence on the type of compression curve. For example, type A compression behaviour was commonly observed for strong and coarse particles, while type C compression behaviour was always observed for weak and fine particles (Mesri & Vardhanabhuti, 2009). Moreover, the initial density significantly affected the values of M before the linear part of the compression curves was reached, i.e., a dense sample had a larger value of M than that of a loose sample owing to a larger stiffness (Chuhan *et al.*, 2002; Chuhan *et al.*, 2003; Mesri & Vardhanabhuti, 2009). As is already known that in most cases the compression curves with different initial void ratio will approach an asymptotic line at high stresses, where the initial void ratio is no longer a factor affecting the compression deformation, the tangent-constrained modulus is then expected to increase with increasing coefficient of uniformity C_u because that the larger the coefficient of uniformity C_u, the smaller the compression index. However, how the PSD affects the evolution of the tangent-constrained modulus is still rarely studied, especially when the initial relative density is the same.

2.4.1.4 Effect of PSD on yield stress

Nakata *et al.* (2001a) investigated the compression behaviour of silica sands with four different PSDs (both uniformly graded and non-uniformly graded) with the same initial void ratio. They reported that the yield stress $(\sigma_v)_{MC}$ increased with decreasing coefficient of uniformity C_u even for samples with the same mean particle size d_{50}. Nakata *et al.* (2001b), then performed further compression tests on the three different uniformly graded silica sands with identical initial void ratios and found that sands with smaller particles exhibited larger yield stress as expected, which could be explained by the size effect on the strength of a single particle. Several studies, therefore, proposed empirical estimations of the yield stress of a uniformly graded sample when the individual particle strength within the sample is known (Nakata *et al.*, 2001b; McDowell & Harireche, 2002; McDowell & Humphreys, 2002). Based on the survival probability of a single-particle as defined in Equation (2.12), the characteristic stress σ_n at which 37% of the d-sized particles survive, can be expressed as

$$\sigma_{\mathrm{n}} = \left(\frac{d}{d_0}\right)^{(-3/m)} \sigma_0 \propto d^{(-3/m)} \tag{2.46}$$

For a uniformly graded sample with d-sized particles, the yield stress $(\sigma_v)_{MC}$ is considered to be proportional to 37% of the particle strength

$$(\sigma_{\mathrm{v}})_{\mathrm{MC}} = A\sigma_{\mathrm{n}} \tag{2.47}$$

where A is a factor related to the particle shape, and is approximately 0.25 for the real soil particles (McDowell & Humphreys, 2002; McDowell, 2002; Xiao *et al.*, 2018b) and 0.14-0.17 for the DEM spherical particles (McDowell & Harireche, 2002).

As suggested by Mesri & Vardhanabhuti (2009), for type A and type B compression curves, the first inflection point $(\sigma_v)_{Max}$ in the M - σ_v plot indicating the onset of particle fracturing and splitting was a more reasonable definition of yield stress because $(\sigma_v)_{MC}$ was only an artifice of a semilogarithmic plot. The value of $(\sigma_v)_{Max}$ is approximately 0.4-1.4 times $(\sigma_v)_{MC}$, based on a large database of compression curves of granular soils. The values of $(\sigma_v)_{Max}$ are generally smaller for granular soils with a larger value of d_{60} as reported by Chuhan *et al.* (2003).

2.4.2 Effect of PSD on the shearing behaviour

2.4.2.1 Typical response of granular soils during shearing

The void ratio and confining pressure are probably the most two significant factors affecting the stress-strain behaviour of granular soils during shearing. As shown in Figure 2.7, when a sample subjected to drained shearing is initially in a dense state, the strain softening and volume dilation behaviour will be observed, while the sample will exhibit strain hardening and volume contraction if it is in a loosely packed state. However, for the undrained shearing condition, a limited flow (or flow) behaviour, as well as an increase in the pore water pressure (p_u) will be observed in a loose sample, whereas a dense sample will exhibit non-flow behaviour with a continuous increase in the shear stress. Furthermore, it will exhibit a ‘dilation’ behaviour, wherein the pore water pressure initially increases and then decreases. Moreover, three special states are also defined for both drained and undrained conditions in Figure 2.6, namely the phase transformation state, peak state, and critical state.

(1). The phase transformation state is defined as a state wherein (1) the behaviour of granular soils transforms from that of contraction to dilation for the drained conditions (see Figure 2.7(a)), or (2) the maximum pore water pressure of granular soils is generated (see Figure 2.7(b)), which is also associated with the minimum mean effective stress (Ishihara *et al.*, 1975).

(2). The peak state refers to a state wherein the maximum shear stress of the granular soils is reached, which also corresponds to the maximum rate of dilation defined as $(-d\varepsilon_v/d\varepsilon_1)_{max}$, where $d\varepsilon_v$ and $d\varepsilon_1$ are the increments in the volumetric strain and the major principal strain, respectively (Bolton, 1986).

(3). The critical state is defined as a state in which plastic shearing could continue indefinitely with no change in the effective stress or specific volume (i.e., $\partial q/\partial\varepsilon_s = \partial p/\partial\varepsilon_s = /\partial\varepsilon_v/\partial\varepsilon_s = 0$, where p and q are the mean effective stress and shear stress, respectively; ε_s and ε_v are the deviatoric strain and the volumetric strain, respectively) (Roscoe *et al.*, 1958; Muir Wood, 1990). These critical states are reached with a unique line or curve in both *p*-*q* space and *e*-log (*p*) space, which will be discussed later in detail.

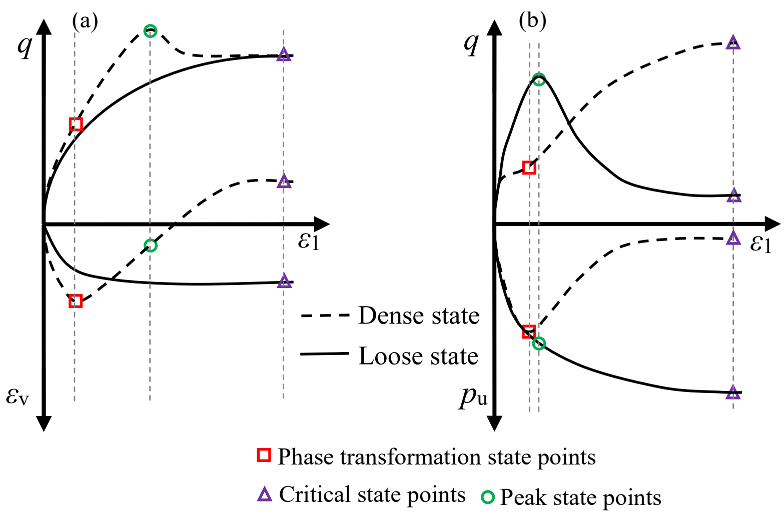

Figure 2.7: Typical response of granular soils during triaxial shearing: (a) drained condition, (b) undrained condition

2.4.2.2 State-dependent dilatancy

As discussed above, the stress-strain relations of granular soils are highly dependent on their initial state. This however, was not considered in the pioneering work by Rowe (1962), who proposed stress-dilatancy relations for granular soils, based on the minimum energy principle with the following general form:

$$\sin\psi_{\mathrm{m}} = \frac{\sin\varphi_{\mathrm{m}} - \sin\varphi_{\mathrm{cs}}}{1 - \sin\varphi_{\mathrm{m}}\sin\varphi_{\mathrm{cs}}} \tag{2.48}$$

where ψ_{m} is the mobilized dilatation angle; φ_{m} is the mobilized friction angle; and φ_{cs} is the critical state friction angle. Equation (2.48) shows the state-independence of the mobilized dilatation angle, which is not appropriate for the granular soils. To describe the state-dependent behaviour of granular soils, the primary issue is to determine whether the sample is in the dense or loose state considering both the void ratio and confining pressure. To date, several parameters have been proposed, based on the distance between the current state and the critical state using CSL as a reference line, as shown in Figure 2.8.

Been & Jefferies (1985) defined a state parameter $\psi = e - e_{\mathrm{cs}}$, where e is the void ratio after the isotropic compression with a mean effective stress of p, and e_{cs} is the critical state void ratio at the mean effective stress of p. Ishihara (1993) proposed a state index I_{s}, based on the loosest state of sands: $I_{\mathrm{s}} = (e_0 - e)/(e_0 - e_{\mathrm{cs}})$, where e_0 is the threshold void ratio. Similarly, Wan & Guo (1998) introduced a state index I_{e}, based on the current and critical state void ratios ($I_{\mathrm{e}} = e/e_{\mathrm{cs}}$). In addition to the comparisons of the void ratio mentioned above, another form of state index that links with the mean effective stress has also been proposed. For example, Wang *et al.* (2002) introduced a state pressure index I_{p} that measures the ratio of current and critical mean effective stresses at the same void ratio (i.e., $I_{\mathrm{p}} = p/p_{\mathrm{cs}}$). Other state indices considering the effect of void ratio and confining pressure can be found in the literature, such as the relative dilatancy index I_{R} [$= I_{\mathrm{D}}(Q - \ln p) - R$, where $I_{\mathrm{D}} = (e_{\max} - e)/(e_{\max} - e_{\min})$ and is the relative density; Q and R are material constants] (Bolton, 1986), the state index incorporating relative density, and current and critical mean effective stresses [$I_{\mathrm{dp}} = I_{\mathrm{D}} \ln(p_{\mathrm{cs}}/p)$] Lashkari (2009), the state index coupling the state indices I_{e} and I_{p} ($I_{\mathrm{ep}} = I_{\mathrm{e}} I_{\mathrm{p}}$) (Xiao & Liu, 2017).

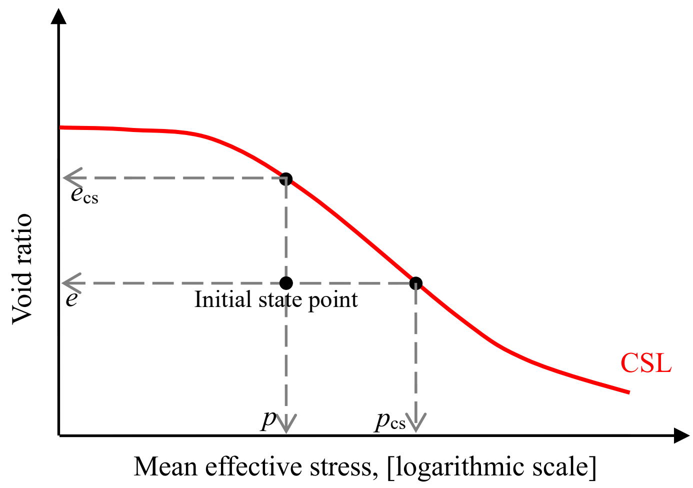

Figure 2.8: Illustration of current and critical states

At present, numerous studies have been carried out on the stress-dilatancy of granular soils. Furthermore, the state-dependent dilatancy equations have been proposed based on the state indices as introduced above. Some selected dilatancy equations are listed in Table 2.4. As shown in Table 2.4, the stress-dilatancy relation with consideration of the particle breakage (or the effect of PSD) is still not completely explored.

Table 2.4. Summary of state-dependent dilatancy equations for granular soils

Reference	State index	Proposed dilatancy equation	Description
Bolton (1986)	I_R	$\varphi_m - \varphi_{cs} = 0.8\psi_m = cI_R$	c = 3 for triaxial compression; c = 5 for plane strain; Q = 10; and R = 1.
Chakraborty & Salgado (2010)		$\varphi_m - \varphi_{cs} = 0.62\psi_m = 3.8I_R$	R = 1; Q = 7.4 + 0.60lnσ_c for triaxial compression; Q = 7.1 + 0.75lnσ_c for plane strain; σ_c is the initial confining pressure.
Amirpour Harehdasht *et al.* (2019)		$\varphi_m - \varphi_{cs} = cI_R$ $c = c_3\left(D_{50}\right)^{-c_4}$	c_3 = 18.89 and c_4 = 0.30 for rounded particles; c_3 = 13.56 and c_4 = 0.21 for subrounded and subangular particles; c_3 = 10.08 and c_4 = 0.13 for subangular and angular particles
Amirpour Harehdasht *et al.* (2017)		$\varphi_m - \varphi_{cs} = b\psi_m$ $b = c_1\left(D_{50}\right)^{-c_2}$	c_1 and c_2 are shape-related parameters and decrease with increasing particle angularity

Wan & Guo (1998)	I_e	$\sin\psi_m = \dfrac{\sin\varphi_m - I_e^{\alpha}\sin\varphi_{cs}}{1 - I_e^{\alpha}\sin\varphi_m\sin\varphi_{cs}}$	α is a material constant modified from Rowe's equation considering state dependency.
Wan & Guo (2001)		$\sin\varphi_f = \dfrac{X\left(\dfrac{F_{33}}{F_{11}}\right)+\gamma^{p*}}{a+\gamma^{p*}} I_e^{\alpha}\sin\varphi_{cs}$	X, a and α are material constants; φ_f is the characteristic friction angle; F_{11} and F_{33} are fabric tensor components in the axial and radial directions; and γ^{p*} is the true shear strain.
Collins *et al.* (1992)	ψ	$\varphi_m - \varphi_{cs} = A[\exp(-\psi)-1]$ $\psi_m = 1.25A[\exp(-\psi)-1]$	A is a parameter ranging from 0.6-0.95.
Li *et al.* (1999)		$d = d_0\left(1-e^{(\mathrm{sgn}\psi)m\lvert\psi\rvert^{n}}\right)$	$d = d\varepsilon_v^p / d\varepsilon_s^p$; d_0, m (> 0); and n (> 0) are parameters.
Li & Dafalias (2000)		$d = d_0\left(e^{m\psi} - \dfrac{\eta}{M}\right)$	$\eta = q/p$; M is the critical state stress ratio; and d_0 and m are material constants.
Lashkari (2009)	I_{dp}	$\varphi_m - \varphi_{cs} = C_1 I_{dp}$ $\psi_m = C_2 I_{dp}$	C_1 and C_1 are soil parameters.

2.4.2.3 Effect of PSD on shear stress

Different initial PSDs lead to different packing efficiencies of the granular soils, which will affects the stress-strain behaviour. To investigate the effect of particle breakage on the drained behaviour of sands, Yu (2017b) conducted a series of drained triaxial shear tests on reconstituted samples with different initial PSDs (i.e., different amounts of particle breakage for a given initial PSD as a basis). The tests showed that particle breakage (i.e., increasing of the fine particles content) would result in the reduction of the peak-state strength and an increase in the volumetric strain (i.e., more contractive behaviour was observed). Similarly, Liu *et al.* (2014b) carried out undrained triaxial shear tests on two different granular materials (i.e., glass balls and Hostun sand) with different initial PSDs and the same mean particle diameter (d_{50} = 0.9 mm). They found that undrained shear strength decreased when the coefficient of uniformity C_u increased from 1.1 to 20 for a similar initial relative density. In other words, increasing the coefficient of uniformity heightened the potential of static liquefaction and the samples became more unstable, which could be largely attributed to the fact that samples with more fine particle content would have larger positive pore water pressures generated (Belkhatir *et al.*, 2014; Yu, 2018a).

Such findings were also observed via the DEM. For example, Yan & Dong (2011) performed a series of 3D numerical drained triaxial tests on samples with different initial PSDs, but with the same mean particle diameter (d_{50} = 0.24 mm), and found that a sample with a wider PSD and larger C_u (i.e., more particle breakage occurred for a given original PSD) exhibited more contractive response, and tended towards strain hardening upon shearing. In other words, the larger the coefficient of uniformity C_u, the lower the peak strength of the sample. Furthermore, a closer examination of the initial PSD effect was conducted by Sitharam & Nimbkar (2000), who adopted DEM analysis and tested the particle assembly with both parallel PSDs (i.e., with different values of d_{50}, but the same value of C_u), and PSDs with fixed minimum particle size and increasing maximum particle size. Figure 2.9 shows the evolution of the internal friction angle in terms of the maximum particle size. It was found that a marginal increase in the internal friction angle was observed for those samples with parallel PSDs as the maximum particle size increased, which indicated that the mean particle diameter d_{50} had limited effect on the internal friction angle. However, the internal friction angle decreased dramatically when the PSD became wider (or the maximum particle size became larger) for the samples with the fixed minimum particle size. Therefore, a conclusion could be drawn that the coefficient of uniformity C_u had a larger effect on the internal friction angle than the mean particle diameter d_{50}, and the larger the coefficient of uniformity C_u, the lower the internal friction angle of the sample.

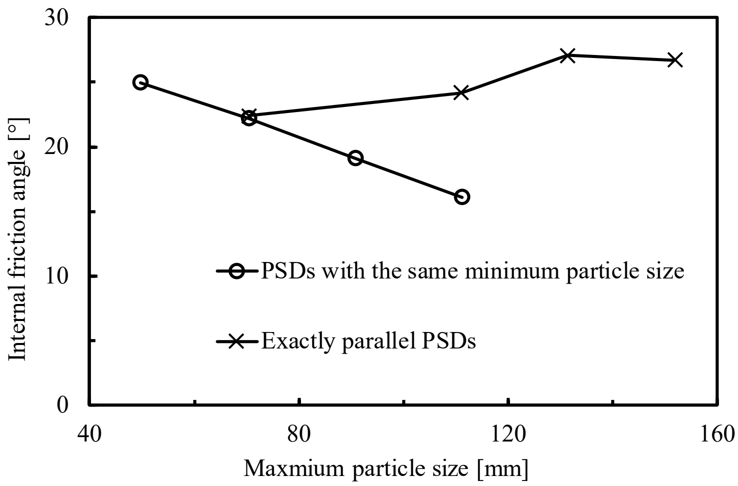

Figure 2.9: Evolution of internal friction angle with maximum particle size (Modified after Sitharam & Nimbkar, 2000)

On the other hand, the initial PSD also affects the stress-dilatancy equation as indicated by Amirpour Harehdasht *et al.* (2019), Amirpour Harehdasht *et al.* (2017) (see Table 2.4), who conducted a series of triaxial shear and direct shear tests on different granular materials with different initial PSDs. It is interesting to note that the contribution of dilatancy to shear strength was found to be independent of the coefficient of uniformity C_u, while it was significantly influenced by the mean particle diameter d_{50}. More specifically, the mobilized friction angle decreased with increasing d_{50} as shown in Table 2.4.

2.4.2.4 Effect of PSD on the critical state line

The concept of critical state is defined as a state, in which plastic shearing could continue indefinitely with no change in effective stress or specific volume (Roscoe *et al.*, 1958; Muir Wood, 1990). These critical states were reached with a unique line or curve in both the *p*-*q* space and the *e*-log (*p*) space. This was a fundamental contribution of the pioneering work on critical state soil mechanics (CSSM) (Roscoe *et al.*, 1958; Schofield & Wroth, 1968). Such a unique line in either *p*-*q* space or *e*-log (*p*) space is called the critical state line (CSL). Several commonly used empirical formulae of granular soils in the *e*-log (*p*) space are list in Table 2.5. The linear CSL used in the CSSM is still used to represent the CSL for granular soils for the sake of simplicity (Been & Jefferies, 1985; Gajo & Muir Wood, 1999; Yin *et al.*, 2016; Hu *et al.*, 2018) although several experimental results have shown that the CSL in the *e*-log (*p*) space is not a straight line (Verdugo & Ishihara, 1996; Yamamuro & Lade, 1996; Lade & Yamamuro, 1996; Yu, 2017c). Other models as listed in the following Table can capture the nonlinearity of the CSL in the *e*-log (*p*) space. The models proposed by Gudehus (1997), Russell & Khalili (2004) and Sheng *et al.* (2008) are also able to describe the CSL at extremely high stresses.

Table 2.5.Summary of typical CSLs of granular soils

Reference	Proposed model	Shape in *e*-log (*p*) space	Description
Roscoe *et al.* (1958)	$e=\Gamma-\lambda\ln\left(p\right)$	Linear	Γ is the void ratio at p =1; λ is the slope of CSL in *e*-log (*p*) space.

Gudehus (1997)	$e = e_{\mathrm{lim}} + \left(e_{\mathrm{ref}} - e_{\mathrm{lim}}\right)\exp\left[-\left(\frac{p}{h_{\mathrm{cs}}}\right)^{n}\right]$	Nonlinear	e_{ref} is the void ratio at p = 0; e_{lim} is the void ratio at extremely stresses; h_{cs} and n are material constants.
Li & Wang (1998)	$e = e_{\mathrm{ref}} - \lambda\left(\frac{p}{p_{\mathrm{a}}}\right)^{\xi}$	Nonlinear	e_{ref} is the void ratio at p = 0; p_{a} is the atmospheric pressure; λ and ξ are material constants.
Wan & Guo (2004)	$e = e_{\mathrm{ref}}\exp\left[-\left(\frac{p}{h_{\mathrm{cs}}}\right)^{n}\right]$	Nonlinear	e_{ref} is the void ratio at p = 0; h_{cs} and n are material constants.
Russell & Khalili (2004)	$v = a + b\tan^{-1}\left[c - d\left(\ln p + F_1\right)\right] + F_2$ $+J\left(\ln p + F_1 - m\right)^3 + K\left(\ln p + F_1 - m\right)^2$ where $a = \left(\hat{v}_{\mathrm{cr}} + \hat{v}_{f}\right)/2; b = \left(\hat{v}_{\mathrm{cr}} - \hat{v}_{\mathrm{f}}\right)/\pi;$ $c = \frac{\pi\lambda_{\mathrm{cr}}}{2\left(\hat{v}_{\mathrm{cr}} - \hat{v}_{\mathrm{f}}\right)}\left[2\left(\frac{\Gamma_0 - \hat{v}_{\mathrm{cr}}}{\lambda_0}\right) + \frac{\hat{v}_{\mathrm{cr}} - \hat{v}_{\mathrm{f}}}{\lambda_{\mathrm{cr}}}\right];$ $d = \frac{\lambda_{\mathrm{cr}}}{b}; m = \frac{c}{d}; J = \frac{\lambda_0 - \lambda_{\mathrm{f}}}{4m^2} - \frac{\Gamma_0 - \hat{v}_{\mathrm{cr}}}{m^3};$ $K = \frac{\lambda_0 - \lambda_{\mathrm{f}}}{4m}; \hat{v}_{\mathrm{cr}} = v_{\mathrm{cr}} + F_3; \hat{v}_{\mathrm{f}} = v_{\mathrm{f}} + F_4$	Three linear segments	λ_0, λ_{cr} and λ_{f} are the slope of the CSL in e-log (p) space before, during and after particle breakage; Γ_0 is the volume at p = 1; v_{cr} and v_{f} are the volume at the onset of particle breakage and at extremely high stresses. F_1, F_2, F_3, F_4 are fitting parameters.
Sheng *et al.* (2008)	$\ln(e) = \ln(\Gamma) - \lambda\ln\left(p + p_{\mathrm{cr}}\right)$ $\ln(e - e_{\mathrm{lim}}) = \ln(\Gamma) - \lambda\ln\left(p + p_{\mathrm{cr}}\right)$	Nonlinear	Γ is void ratio at p + p_{cr} =1; λ and p_{cr} are material constants; e_{lim} is the limit void ratio if an extremely high stress is considered.

The CSL in the p-q space can be represented by a straight line, given by

$$M = \eta_{\mathrm{CS}} = \left(\frac{q}{p}\right)_{\mathrm{CS}} = \frac{6\sin\varphi_{\mathrm{CS}}}{3 - \sin\varphi_{\mathrm{CS}}} \tag{2.49}$$

where M is the critical state stress ratio, and φ_{CS} is the critical state friction angle.

The influence of PSD (or, particle breakage with evolving PSD) on the location of the CSL has been extensively studied. In general, breakage-induced evolving of PSD has a limited effect on the CSL in the p-q space, and the critical state friction angle is assumed to be independent of particle breakage in most studies in the literature (Coop, 1990;

Yamamuro & Lade, 1996; Russell & Khalili, 2004; Coop *et al.*, 2004; Bandini & Coop, 2011; Carrera *et al.*, 2011; Yu, 2017c; Jiang *et al.*, 2018). However, a few studies found that the critical state friction angle increased with increasing fine particle content (Murthy *et al.*, 2007; Kwa & Airey, 2016).

The effect of breakage-induced evolving of PSD on the location of the CSL in the e-log (p) space, however, is more complicated and controversial. It is difficult to obtain the evolving CSLs during the particle breakage. On the other hand, we can test the samples reconstituted from different initial PSDs, representing different degrees of particle breakage for a given initial PSD as a basis, at low stress levels, so that particle breakage is negligible (Murthy *et al.*, 2007; Ghafghazi *et al.*, 2014; Yu, 2017c). However, a question might arise as to whether the CSL in the e-log (p) space has changed because of the particle breakage or the CSL is just only a function of the initial PSD. Bandini & Coop (2011) conducted triaxial tests with two different shearing stages. Here, the first stage was meant to produce different degrees of particle breakage of the original sample and the second stage was to explore whether such a change in the PSD during the first stage would change the CSL under relatively small stresses with undetectable breakage. By comparison, they tested the reconstituted samples with the same PSDs as those of the samples after shearing. The results showed that these two samples had different CSLs, indicating that the samples might be 'aware' of the breakage that they had suffered. In such a case, it appears that the approach of testing the reconstituted samples with different initial PSDs is not fully justified. Nevertheless, a conclusion can still be made that changing of the PSD (or particle breakage) would lead to a change in the intercept of the CSL in the e-log (p) space, as revealed by all the studies in the literature (Daouadji *et al.*, 2001; Murthy *et al.*, 2007; Muir Wood & Maeda, 2008; Bandini & Coop, 2011; Ghafghazi *et al.*, 2014; Xiao *et al.*, 2016b; Yu, 2017c).

2.4.3 Summary

The effect of PSD plays an important role in the mechanical and deformational behaviour of granular soils. More concretely, a soil sample with uniformly graded PSD will yield at larger stress for larger particle size. On the other hand, the compression index appears to be independent of the initial PSD. However, for a uniformly graded sample, the compression index decreases with increasing coefficient of uniformity C_u. An increase in the fine particle content will result in a reduction of the peak-state strength and an increase in the volumetric strain for a soil sample subjected to triaxial shearing. Moreover, changing of the PSD will change the intercept of the CSL in the *e*-log (*p*) space, while the particle breakage-induced evolving of the PSD has no significant influence on the CSL in the *p*-*q* space.

2.5 Constitutive models considering the evolution of PSD due to particle breakage

It has been previously shown that particle breakage will significantly change the PSD and thus, affect the stress-strain behaviour of granular soils. To capture the effect of particle breakage on the stress-strain behaviour of granular soils, numerous constitutive models have been proposed in the literature. Nevertheless, some constitutive models do not take into account the effect of the evolution of the PSD. For example, Sun *et al.* (2007) and Yao *et al.* (2008) proposed new modified hardening parameters and developed constitutive models in the framework of the modified Cam-clay model. In the past two decades, a constitutive model with the specific focus on the evolving PSD has become a hot topic because of the potential benefits in engineering practice (Einav, 2007a). These models can be divided into three main categories: (1) methods based on Rowe's dilatancy equation (see Equation (2.48)), which consider the particle breakage (Ueng & Chen, 2000; Salim & Indraratna, 2004; Liu *et al.*, 2014a), (2) continuum breakage mechanics methods (Einav, 2007a; Einav, 2007b; Buscarnera & Einav, 2012), (3) methods incorporating the state index and particle breakage-induced shifting of the CSL (Muir Wood & Maeda, 2008; Liu & Zou, 2013; Xiao *et al.*, 2014d; Liu & Gao, 2016; Yin *et al.*, 2016; Xiao & Liu, 2017). One selected model under each category will be introduced and analyzed briefly hereafter.

2.5.1 Model proposed by Salim & Indraratna (2004)

A modified Rowe's dilatancy equation, considering the particle breakage-induced energy dissipation was adopted (Ueng & Chen, 2000), which takes the following form:

$$d_{\mathrm{g}} = \frac{d\varepsilon_{\mathrm{v}}^{p}}{d\varepsilon_{\mathrm{s}}^{p}} = \frac{9(M-\eta)}{9+3M-2\eta M} + \frac{dE_{\mathrm{B}}}{p\,d\varepsilon_{\mathrm{s}}^{p}}\left(\frac{9-3M}{9+3M-2\eta M}\right)\left(\frac{6+4M}{6+M}\right) \tag{2.50}$$

where $d\varepsilon_{\mathrm{v}}^{p}$ is the increment of plastic volumetric strain; $d\varepsilon_{\mathrm{s}}^{p}$ increment of plastic shear strain; η is the stress ratio (=q/p); M is the stress ratio at the critical state; and dE_{B} is the energy consumed by particle breakage per unit volume and is assumed to be proportional to the increment of breakage index dB_{g} as

$$dE_{\mathrm{B}} = \beta dB_{\mathrm{g}} \tag{2.51}$$

The breakage index B_{g} was found to be a function of the plastic shear strain via a triaxial shearing test

$$B_{\mathrm{g}} = \frac{\theta\left[1-\exp\left(-\upsilon\varepsilon_{\mathrm{s}}^{p}\right)\right]}{\ln\left(p_{\mathrm{cs(i)}} / p_{\mathrm{(i)}}\right)} \tag{2.52}$$

where θ and υ are two material constants; $p_{\mathrm{(i)}}$ is the mean effective stress at the start of shearing; and $p_{\mathrm{cs(i)}}$ is the value of $p_{\mathrm{(i)}}$ on the CSL at the current void ratio. The relation between $dE_{\mathrm{B}}/d\varepsilon_{\mathrm{s}}^{p}$ and M-$\eta(p/p_{\mathrm{cs}})$ could be represented by a linear form

$$\frac{dE_{\mathrm{B}}}{d\varepsilon_{\mathrm{s}}^{p}} = \frac{\chi+\mu\left[M-\eta\left(p/p_{\mathrm{cs}}\right)\right]}{\ln\left(p_{\mathrm{cs(i)}} / p_{\mathrm{(i)}}\right)} \tag{2.53}$$

where χ and μ are two material constants. Substituting Equations (2.51)-(2.53) in Equation (2.50) yields

$$d_{\mathrm{g}} = \frac{d\varepsilon_{\mathrm{v}}^{p}}{d\varepsilon_{\mathrm{s}}^{p}} = \frac{9\left(M-\eta\right)}{9+3M-2\eta M} + \left(\frac{B}{p}\right)\left(\frac{\chi+\mu\left(M-\eta\left(p/p_{\mathrm{cs}}\right)\right)}{9+3M-2\eta M}\right) \tag{2.54}$$

with

$$B = \frac{\beta}{\ln\left(p_{\mathrm{cs(i)}} / p_{\mathrm{(i)}}\right)}\left[\frac{\left(9-3M\right)\left(6+4M\right)}{6+M}\right] \tag{2.55}$$

The proposed Equation (2.54) is a new dilatancy equation incorporating the evolution of breakage index B_{g}, which defines the plastic potential function for the constitutive model and is not presented here. However, one major limitation of such a dilatancy equation is that it cannot guarantee $d = 0$, when the granular soils is not at the critical state, which is the requirement stated by Li & Dafalias (2000).

2.5.2 Model proposed by Einav (2007a)

Einav (2007a) proposed a thermodynamic framework for crushable materials named 'continuum breakage mechanics' here. A modified relative breakage index B_r^* was defined as:

$$B_{\mathrm{r}}^* = \frac{\int_{d_{\mathrm{m}}}^{d_{\mathrm{M}}} \left(P(d) - P_0(d)\right) d^{-1} \mathrm{d}d}{\int_{d_{\mathrm{m}}}^{d_{\mathrm{M}}} \left(P_{\mathrm{u}}(d) - P_0(d)\right) d^{-1} \mathrm{d}d} \tag{2.56}$$

where $P(d)$, $P_0(d)$, and $P_u(d)$ are the current, initial, and ultimate PSDs as shown in Figure 2.2(c). The PSD with a given B_r^* after the particle breakage can be obtained based on Equation (2.56)

$$P(d) = P_0(d)\left(1 - B_{\mathrm{r}}^*\right) + P_{\mathrm{u}}(d) B_{\mathrm{r}}^* \tag{2.57}$$

The first law of thermodynamics for continuous media can be expressed as

$$\sigma : \delta e = \widetilde{W} = \delta\Psi + \widetilde{\Phi}, \qquad \widetilde{\Phi} \geq 0 \tag{2.58}$$

where σ and e are the stress and strain tensors; Ψ is the Helmholtz free energy; Φ is the non-negative energy dissipation; the use of the tilde symbol represents an increment. The increment of Helmholtz free energy can be associated with the breakage index B_r^* as:

$$\delta\Psi \equiv \frac{\partial \psi_{\mathrm{r}}(\varepsilon)}{\partial \varepsilon}\left[\left(1 - B_{\mathrm{r}}^*\right) m_0 + B_{\mathrm{r}}^* m_{\mathrm{u}}\right] \delta\varepsilon + \psi_{\mathrm{r}}(\varepsilon)\left(m_{\mathrm{u}} - m_0\right) \delta B_{\mathrm{r}}^* \tag{2.59}$$

where m_0 and m_u are the two physical model parameters, which relate to the initial and ultimate particle size distributions, respectively; and $\psi_{\mathrm{r}}(\varepsilon)$ is the free energy density that depends only on the strain. It is assumed that the stored energy in the system is proportional to the energy function at the reference grain-size, and may be expressed as

$$\psi_{\mathrm{r}}(\varepsilon) = \frac{\Psi\left(B_{\mathrm{r}}^* \equiv 0\right)}{m_0} = \Psi\left(B_{\mathrm{r}}^* \equiv 0\right) \tag{2.60}$$

The energy dissipation increment by breakage is given by

$$\widetilde{\Phi}_{\mathrm{B}} = \delta E_{\mathrm{B}}\left(1 - B_{\mathrm{r}}^*\right) - E_{\mathrm{B}} \delta B_{\mathrm{r}}^* \tag{2.61}$$

with

$$E_{\mathrm{B}} = \psi_{\mathrm{r}}(\varepsilon)(m_0 - m_{\mathrm{u}}) \tag{2.62}$$

where E_{B} is defined as the breakage energy which describes the total stored energy that can be released from the system during fracture. A more detailed description can be found in Einav (2007a). The general framework described above provides an alternative approach to model the stress-strain behaviour of crushable materials subjected to 1D-compression stress path with consideration of the evolution of the PSD. However, it still needs more investigations in the triaxial shear stress path for further application.

2.5.3 Model proposed by Muir Wood & Maeda (2008)

Muir Wood & Maeda (2008) proposed a framework to consider the effect of changing PSD on the critical state of granular soils. The critical state parameters as defined in the Cam-clay model changed with different PSDs as demonstrated via DEM tests. The CSL in the traditional e-log$p$ space may be extended with the following form

$$e = \Gamma(I_{\mathrm{G}}) - \lambda(I_{\mathrm{G}})\ln(p) \tag{2.63}$$

Figure 2.10 shows the critical state surface with an additional axis for grading state index I_{G}.

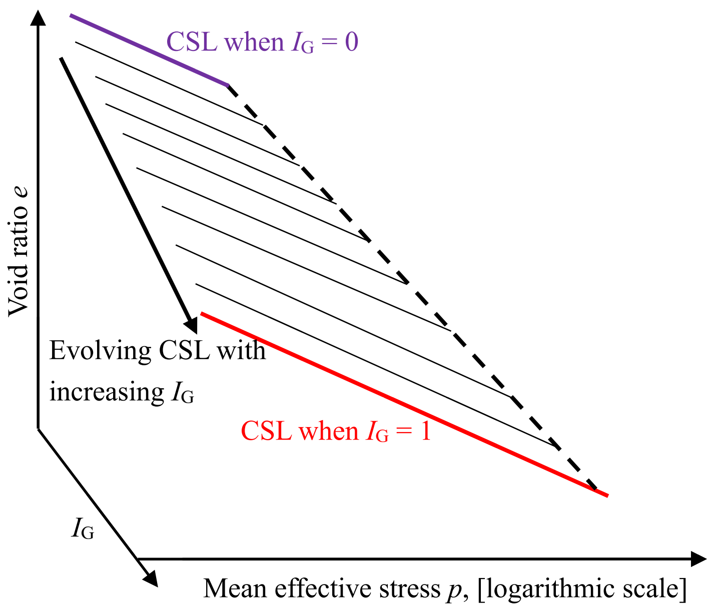

Figure 2.10: Evolution of critical state surface with increasing I_{G} (Modified after Muir Wood & Maeda, 2008)

The state-dependent behaviour of granular soils can be considered using the state parameter with the evolution of PSD is incorporated. Thus, a more complete constitutive model can be developed based on the theory of generalized plasticity (Liu & Ling, 2008; Liu & Zou, 2013), bounding surface plasticity (Sun *et al.*, 2014b; Xiao *et al.*, 2014a; Xiao *et al.*, 2019a), state-dependent dilatancy (Xiao *et al.*, 2014d; Xiao & Liu, 2017), and elasto-plasticity (Daouadji & Hicher, 2010; Hu *et al.*, 2011; Yin *et al.*, 2016). However, the common assumption in most studies that the CSL of a granular sample experiences parallel shifts as particle breakage progresses is not supported by experimental data, especially at a high stress level.

2.5.4 Summary

The constitutive models, which take into account the effect of the grain size distribution can be divided into three main categories: (1) method based on dilatancy equation with consideration of the particle breakage, (2) continuum breakage mechanics approach, and (3) method incorporating the state index and particle breakage-induced shifting of CSL.

Chapter 3 . A simple particle-size distribution model for granular soils

ABSTRACT: Particle size distribution (PSD) is a fundamental soil property that plays an important role in soil classification and soil hydro-mechanical behaviour. A continuous mathematical model representing the PSD curve facilitates the quantification of particle breakage, which often takes place when granular soils are compressed or sheared and the assessment of internal stability of soil sample. This paper proposes a simple and continuous PSD model for granular soils. The model has two parameters (λ_p and κ_p) and is able to represent different types of continuous PSD curves. It is found that parameter κ_p is closely related to the coefficient of non-uniformity (C_u) and the coefficient of curvature (C_c), while parameter λ_p represents a characteristic particle diameter. A database of 53 granular soils with 154 varying PSD curves are analyzed to evaluate the performance of the proposed PSD model, as well as three other PSD models in the literature. The results show that the proposed model has improved overall performance and captures the typical trends in PSD evolution during particle breakage. In addition, the proposed model is also used for assessing the internal stability of 27 widely graded soils.

Keywords: granular soil; PSD; mathematical model; particle breakage; internal stability

This chapter aims to solve the first key issue (i.e., PSD quantification) and is based on a paper published in the journal ***Canadian Geotechnical Journal***:

Tong, C. X*., Burton, G. J., Zhang, S., & Sheng, D. (2018). A simple particle-size distribution model for granular materials. Canadian Geotechnical Journal, 55(2), 246-257.*

Authorship Declaration

By signing below I conform that for the journal paper titled ‘A simple particle-size distribution model for granular materials’ and published by Canadian Geotechnical Journal, that:

Chenxi Tong proposed the model, prepared figures and wrote the manuscript.

Glen J. Burton assisted in the revision of the manuscript.

Sheng Zhang contributed to the discussion of the proposed model

Daichao Sheng is the leader of the research team, and assisted in the revision of the manuscript.

Production Note:

Signature removed
prior to publication.

Chenxi Tong

Dr Glen J. Burton

Prof Sheng Zhang

Prof Daichao Sheng

3.1 Introduction

Particle size distribution (PSD) is a basic soil property and the main basis for soil classification. It is used in analysis of stability of granular filters (Kenney & Lau, 1985; Åberg, 1993; Indraratna *et al.*, 2007), internal instability and suffusion of granular soils (Wan & Fell, 2008; Indraratna *et al.*, 2015; Moraci *et al.*, 2014; Moraci *et al.*, 2015; Ouyang & Takahashi, 2016), groutability of soils (Karol, 1990; Vipulanandan & Ozgurel, 2009; El Mohtar *et al.*, 2015), soil-water characteristic curves (Fredlund *et al.*, 2002; Gallage & Uchimura, 2010), and debris flow (Sanvitale & Bowman, 2017). Particle size distribution curves are widely used to represent soil composition in real engineering practice and academic research. Particle size distribution curves can be obtained by sieving test, where several constrained grain sizes are predetermined. At present, indices such as the coefficient of uniformity C_u and the coefficient of curvature C_c are usually used to evaluate the whole gradation of a soil. For example, the standard for engineering classification of soils in China (GB/T50145-2007) suggest that the soil is well graded when $C_u > 5$ and $1 \leq C_c \leq 3$; otherwise, the soil is poorly graded. However, neither C_u nor C_c can describe a PSD curve completely, as no unique relation exists between these coefficients and a PSD curve.

Another important application of studying the PSD lies in studying particle breakage of granular soils. A large number of studies have shown that soil particles, especially coarse-grained soil particles, can break under loading (Lee & Farhoomand, 1967; Marsal, 1967; Hardin, 1985; Zheng & Tannant, 2016; Hyodo *et al.*, 2017). Some trends have been highlighted when particles break (Mayoraz *et al.*, 2006; Altuhafi & Coop, 2011a; Miao & Airey, 2013), for example, there seems to be an ultimate fractal PSD according to a large number of studies in the literature (Sammis *et al.*, 1987; McDowell *et al.*, 1996; Einav, 2007a). The three key elements in studying the behaviour of a soil that involves particle breakage are: (1) a simple and adequate representation of an evolving PSD, (2) the evolution of the PSD under various stresses and strains, and (3) the correlation between the PSD and soil hydro-mechanical properties (Muir Wood & Maeda, 2008; Zhang *et al.*, 2015). The first element is the foundation for studying the second and third elements, and is the purpose of this study. The second element is studied in Einav (2007a), Zhang *et al.* (2015) and others, while the third element is an area of future interest. In the literature, studies on PSD representation (first element) and PSD evolution (second element) are usually carried out separately, often by different researchers from different backgrounds. However, it will be shown in this paper that these two are somewhat related for soils subjected to particle breakage.

While there are simple quantitative representations of soil PSDs in the literature (for example, C_c and C_u), an alternative way to describe a PSD curve is perhaps to adopt a suitable mathematical model which covers the full range of particle sizes. Such a mathematical model has several advantages: (1) characteristics of the whole PSD curve (such as d_{10}, d_{60}, C_c, C_u, etc.) can be obtained when the parameters of the model are determined; (2) it is easier to correlate the entire PSD curve with other properties of the soil. A key challenge is in developing a model that has a limited number of parameters while still capturing the widely varying nature of soil PSDs. In the case of particle breakage, the PSD model should ideally be able to simulate the evolution of the grading.

A number of studies have attempted to characterize PSD curves using mathematical models, with up to seven input parameters. The most commonly used PSD model is perhaps the Gates-Gaudin-Schuhmann model (GGSM) (Schuhmann, 1940), which was previously proposed by Fuller (Fuller & Thompson, 1907) and Talbot (Talbot & Richart, 1923):

$$P(d)=(\frac{d}{d_{\max}})^{m}, \qquad 0<d<d_{\max} \tag{3.1}$$

where parameter m is a fitting parameter, $d_{\max}$ is the diameter of the largest particle; $P(d)$ is the mass percentage of particles passing a particular size d. Equation (3.1) has the same form with Fractal Models (FM) in the literature (Turcotte, 1986; Einav, 2007a). In a Fractal Model, parameter m equals 3-D, with D being the fractal dimension of the soil specimen. For a uniformly graded soil, the PSD is not fractal, but we can still use an appropriate D value to describe the PSD. In this case, D is not the fractal dimension, but a fitting parameter. However, with particle breakage, the PSD tends to become more and more fractal, and therefore D is usually called the fractal dimension.

Another widely-used one-parameter model is the Gaudin-Melog model (GMM) proposed by Harris (1968):

$$P(d)=1-(1-\frac{d}{d_{\max}})^{k}, \qquad 0<d<d_{\max} \tag{3.2}$$

where k is a fitting parameter.

Equations (3.1) and (3.2) are perhaps the simplest mathematical representations of a PSD. They have one fitting parameter and one specific particle size (d_{max}). Other models in the literature can have as many as two to seven fitting parameters (Vipulanandan & Ozgurel, 2009; Fredlund *et al.*, 2000). A widely used model for well-graded soils is the Fredlund unimodal model (FUM) (Fredlund *et al.*, 2000):

$$P(d)=\frac{1}{\left\{\ln[\exp(1)+\left(\frac{a_{\mathrm{gr}}}{d}\right)^{n_{\mathrm{gr}}}]\right\}^{m_{\mathrm{gr}}}}\left\{1-\left[\frac{\ln\left(1+\frac{d_{\mathrm{rgr}}}{d}\right)}{\ln\left(1+\frac{d_{\mathrm{rgr}}}{d_{\mathrm{m}}}\right)}\right]^{7}\right\} \tag{3.3}$$

where d_{m} is the minimum size particle and a_{gr}, n_{gr}, m_{gr} and d_{rgr} are the four fitting parameters: a_{gr} defines the inflection point, n_{gr} the uniformity of the PSD (i.e. steepness of the PSD), m_{gr} the shape of the curve at small particle sizes and d_{rgr} is related to the amount of fines.

The performance of the different models have been previously compared against experimental data (Hwang *et al.*, 2002; Merkus, 2009; Vipulanandan & Ozgurel, 2009; Luo *et al.*, 2014; Bayat *et al.*, 2015; Zhou *et al.*, 2016). In general, a model with more parameters leads to better fitting of the experimental results. Models currently in the literature are used to fit specific PSD curves, not necessarily an evolving PSD curve due to particle breakage. The evolution of PSD during particle breakage follows certain trends, which are more identifiable for an initially uniformly graded soil specimen (Zhang *et al.*, 2015), and the capacity of existing models in predicting an evolving PSD curve remains unclear.

In this paper, a simple two-parameter PSD model for granular soils is proposed based on the studies of particle breakage. The performance of the proposed model and two other simple one-parameter models (GGSM and GMM listed above) and the four-parameter model (FUM) are compared against experimental data obtained for soil specimens involving particle breakage. The evolution of model parameters during particle breakage is studied. The proposed PSD model is also applied to assess the internal stability of widely graded granular soils.

3.2 A simple PSD model and determination of its parameters

In our previous studies (Zhang *et al.*, 2015; Tong *et al.*, 2015), we considered particle breakage as a probabilistic event, and defined a breakage probability to measure the degree of particle breakage of a uniformly graded soil sample. A two-parameter Weibull distribution was proposed to describe the distribution of new particles generated from the breakage (Figure 3.1). As shown in Figure 3.1, the initially uniformly graded soil sample (with particle sizes between $d_{\max\text{-}1}$ and $d_{\max}$) will break by a percentage (p) of the original mass, leading to a Weibull distribution of new particles (with particle size of d_1, d_2,...,$d_{\max\text{-}1}$) as Equation (3.4):

$$P^* = 1 - e^{-\left[\frac{x_i}{\lambda_p(1-x_i)}\right]^{\kappa_p}} \tag{3.4}$$

where P^* is the distribution of new particles generated from the particle breakage of an initially uniformly graded sample, $x_i = d_i/d_{\max\text{-}1}$ is the particle size ratio, $d_{\max}$ is the diameter of the maximum size particle, and $d_{\max\text{-}1}$ is the second largest particle diameter (second largest sieve size); λ_p is a scale parameter and κ_p is a shape parameter. As shown in Zhang *et al.* (2015), the main advantage of the proposed Weibull distribution is twofold: (1) it captures particle breakage of different patterns such as asperity breakage, surface grinding and particle splitting; and (2) it can be integrated into a Markov chain model to describe the breakage process of a non-uniformly graded soil sample.

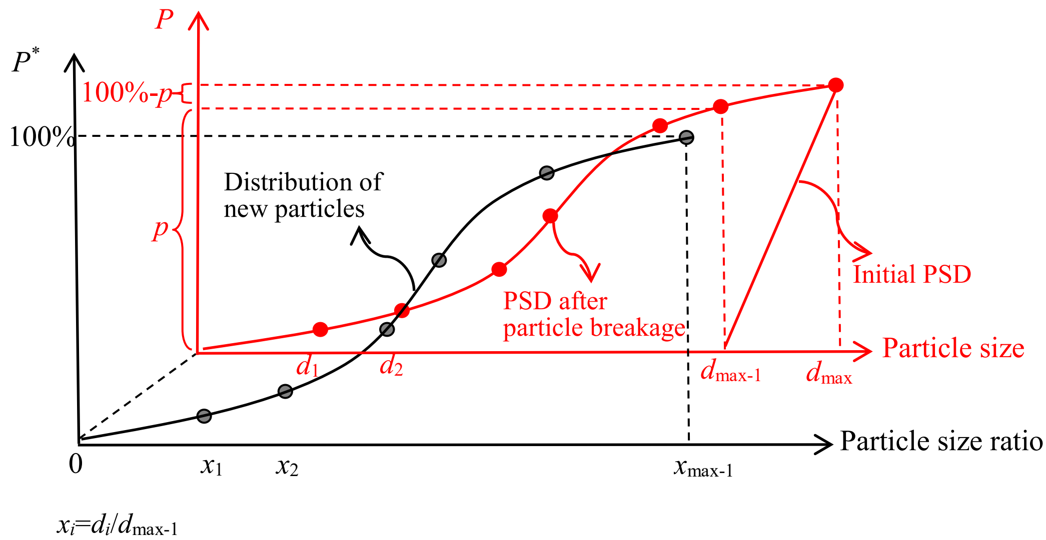

Figure 3.1: Schematic diagram of PSD of uniformly graded sample after particle breakage

Equation (3.4) defines the distribution of new particles, with sizes less than d_{max-1}, generated as a result of breakage, for example. The PSD of the whole specimen after breakage, is then based on the breakage probability or the percentage of broken mass (p). The percentages of particles in different size groups can then be calculated as follows:

$$\begin{cases} P(d) = \left\{ 1 - e^{-\left(\frac{\frac{d}{d_{\max-1}}}{\lambda_{\mathrm{p}} (1 - \frac{d}{d_{\max-1}})} \right)^{\kappa_{\mathrm{p}}}} \right\} \times p, & 0 < d \le d_{\max-1} \\ P(d) = p + \dfrac{1-p}{d_{\max} - d_{\max-1}} \times (d - d_{\max-1}), & d_{\max-1} < d \le d_{\max} \end{cases} \tag{3.5}$$

Equation (3.5) is a two-part function that is not continuously differentiable. It can be treated as a PSD model to some extent. When the size of particles is between 0 and d_{max-1}, $P(d)$ can be calculated from the first part of Equation (3.5). When the particle size is between d_{max-1} and d_{max}, the $P(d)$ can be obtained by linear interpolation as used in the second part of Equation (3.5). Equation (3.5) is supposed to describe the PSD of a granular soil of an arbitrary breakage probability (p). For a uniformly graded sample and a zero breakage probability, the PSD of the soil is $P(d) = (d-d_{max-1})/(d_{max}-d_{max-1})$. It represents a line in the $P(d)$-d space, as shown in Figure 3.1. It is important to note that for real samples, the second largest particle may not be determined, as the PSD is defined at distinct points. Here, for a uniformly graded sample, the second largest particle size d_{max-1} is the same as d_{min}.

The PSD of an initially uniformly graded granular soil after breakage tends to be continuous, or well graded, after breakage (Nakata *et al.*, 2001a; Zhang & Baudet, 2013). Here, we consider the PSD curve of a granular soil after breakage as a continuous curve, with the second largest particle size d_{max-1} infinitely approaching the maximum particle size d_{max}. In this case, the particle breakage probability p approaches 100% as shown in Figure 3.1. Equation (3.5) is then reduced to

$$P(d) = \lim_{d_{\max-1} \to d_{\max}} \{ 1 - e^{-\left(\frac{\frac{d}{d_{\max-1}}}{\lambda_{\mathrm{p}} (1 - \frac{d}{d_{\max-1}})} \right)^{\kappa_{\mathrm{p}}}} \} = 1 - e^{-\left(\frac{d}{\lambda_{\mathrm{p}} (d_{\max} - d)} \right)^{\kappa_{\mathrm{p}}}} \tag{3.6}$$

Equation (3.6) is a new PSD model for non-uniformly graded granular soils broken from uniformly graded sample. It is also a modified Weibull distribution model, with two parameters: a scale parameter λ_p and shape parameter κ_p. This model reflects the fact that the mass percentage of particles $P(d)$ has a limit value of 1 when passing a particular size d_{max}. The values of the two parameters can be calculated if two PSD points, such as: (d_{10}, $P(d_{10})$) and (d_{60}, $P(d_{60})$) are known. Once the values of the two parameters are determined, the PSD of a granular soil can be determined uniquely.

As shown in Equation (3.6), when $d = \lambda_p * d_{max}/(1+\lambda_p)$, the value of $P(d) \equiv 1\text{-}1/e \approx 0.632$, irrespective of κ_p value. Parameter λ_p is then determined as

$$\lambda_p = \frac{d_{63.2}}{d_{max} - d_{63.2}} \tag{3.7}$$

where $d_{63.2}$ is the characteristic particle diameter at which 63.2% of the sample by mass is smaller. Equation (3.7) is the theoretical solution of parameter λ_p. It is a non-dimensional parameter and is only related to characteristic particle diameters $d_{63.2}$ and d_{max}. Substituting Equation (3.7) into Equation (3.6) leads to the final form of the PSD model:

$$P(d) = 1 - e^{-\left(\frac{d(d_{max} - d_{63.2})}{d_{63.2}(d_{max} - d)}\right)^{\kappa_p}} \tag{3.8}$$

Equation (3.8) is an exponential function. If the values of d_{max} and parameter λ_p are known, the parameter κ_p can easily be obtained by using MATLAB fitting toolbox (cftool) (Matlab R2016b, The MathWorks. 2016b, MATLAB. Inc, Natick, Massachusetts, United States). The performance of the proposed PSD model can be evaluated according to the coefficient of determination R^2, defined as following:

$$R^2 = 1 - \frac{\sum_1^N (Y_i - Y_j)^2}{\sum_1^N (Y_i - \overline{Y}_i)^2} \tag{3.9}$$

where Y_i and Y_j are actual and calculated cumulative mass of particles finer than d, respectively. $\overline{Y}_i$ is mean of actual value.

The flow chart for obtaining and assessing parameter λ_p and κ_p is shown in Figure 3.2. The fitting process can be summarised as follows:

(1) Experimental characteristic diameter $d^*_{63.2}$ is determined by linear interpolation of the sieving test data.

(2) Parameter λ_p is calculated using Equation (3.7).

(3) Parameter κ_p is found by a nonlinear least square fitting of the experimental PSD data, based on the trust-region algorithm method in Matlab.

(4) The calculated characteristic diameter $d^\#_{63.2}$ is determined from Equation (3.6), and is compared with the experimental characteristic diameter $d^*_{63.2}$.

(5) Optimal values of λ_p and κ_p are obtained only when the coefficient of determination R^2 obtained in step 3 is sufficiently large ($R^2 \geq 0.95$) and the difference between the calculated and experimental values of $d_{63.2}$ is sufficiently small ($\Delta d_{63.2} = \left| d^*_{63.2} - d^\#_{63.2} \right| / d^*_{63.2} \leq 0.01$). Otherwise, the experimental characteristic diameter $d_{63.2}$ is reset to the calculated value and the above steps are repeated.

(6) The maximum iteration is set to 5. If either $R^2 < 0.95$ or $\Delta d_{63.2} > 0.01$ is satisfied, exit the iteration with the latest values of λ_p and κ_p.

The iterative process in Figure 3.2 converges to a unique solution, typically within 1-2 iterations. The number of sieves used in the experimental data affects the convergence rate, and the more sieves lead to a faster convergence.

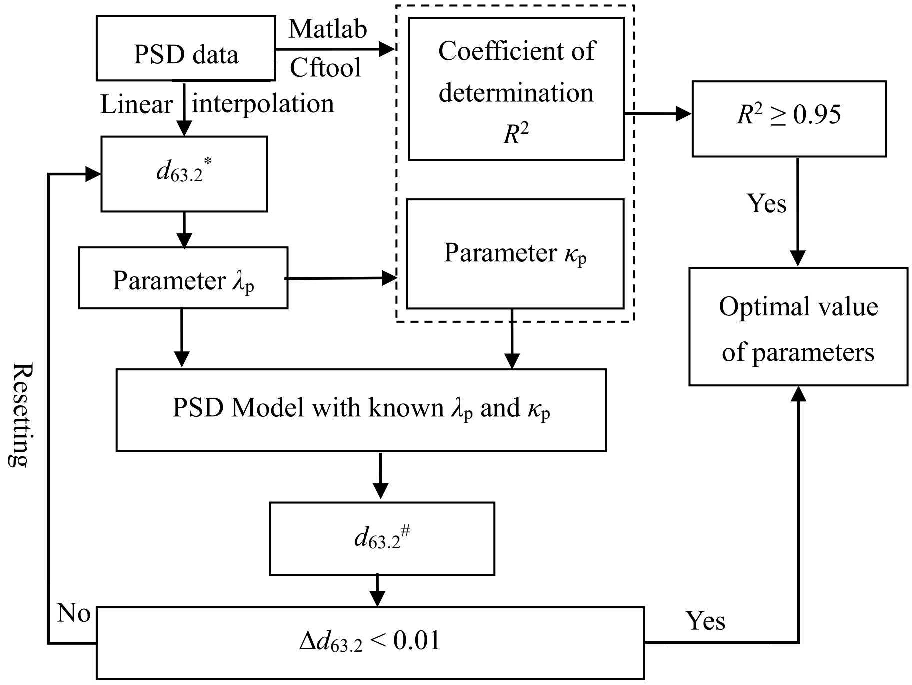

Figure 3.2: Flow chart for obtaining and assessing parameter λ_p and κ_p

3.3 Parametric study and validation of model

In this section, we focus on the influences of model parameters on the shape of PSD and the relationship between the model parameters and classification systems commonly used in geotechnical engineering, such as the coefficient of uniformity C_u and the coefficient of curvature C_c. Besides, the proposed PSD model is verified and compared with other three PSD models (GGSM, GMM, FUM) based on a database of 154 continuous PSD curves (with 127 PSD curves broken from initial uniformly graded or non-uniformly graded samples and 27 PSD curves mixed by different group sizes, see the details in section 3.4 and section 3.5, respectively).

The most frequent particle size can directly be obtained by a particle size probability density function (PDF) plotted in a log(d) scale (Fredlund *et al.*, 2000). The differentiation of the proposed PSD model in a logarithm form is given by:

$$p(d) = \frac{dP(d)}{d\log(d)} = \frac{\ln(10)\kappa_p d_{max}}{\lambda_p^{\kappa_p}} \times \frac{d^{\kappa_p}}{(d_{max}-d)^{\kappa_p+1}} \times e^{-[\frac{d}{\lambda_p(d_{max}-d)}]^{\kappa_p}} \tag{3.10}$$

There are three main types of continuous PSD curves in $P(d)$-log(d) space: hyperbolic (Type 1), S shaped (Type 2), and nearly linear (Type 3) (Zhu *et al.*, 2015). In order to verify the performance of the proposed model, we fix d_{max} at 50mm, and change the values of parameter λ_p and κ_p. The results are shown in Figure 3.3 and Figure 3.4.

As shown in Figure 3.3(b), the PSD of Type 1 is a hyperbolic shaped curve in the $P(d)$-log(d) space, and the PDF first increases and then decreases with increasing particle size. Type 2 in Figure 3.3(c) is an S shaped curve in the $P(d)$-log(d) space. The value of $p(d)$ shares the similar tendency with that of Type 1: first increases and then decreases with increasing particle size. Both of Type 1 and Type 2 PSD are unimodal distribution. However, a soil with Type 1 PSD has much more larger particles than Type 2 PSD. PSD of Type 3 as shown in Figure 3.3(a) is a nearly linear shaped curve in the P(d)-log(d) space, and the logarithmic density function increases with increasing particle size, which means a larger particle size has a larger mass percentage. General speaking, a soil with Type 3 PSD has the largest amount of large particles.

Figure 3.3 shows the influence of λ_p on PSD. For a constant κ_p (0.8) in Figure 3.4(b), the shape of the PSD curves are hyperbolic and of Type 1. As λ_p increases, the PSD becomes steeper. Figure 3.4(c) shows a plot of PSD with a constant κ_p (1.5) and varying λ_p. Particle sizes become smaller with a decreasing λ_p, but the shape of the PSD curves remains almost unchanged (Type 2). For a constant κ_p at 0.2, the PSD curves tend to be more linear (Type3, Figure 3.3(a)). In general, λ_p does not affect the shape of the PSD curves much if the value of κ_p is fixed, but it affects the characteristic particle sizes, for example d_{10} or d_{50}.

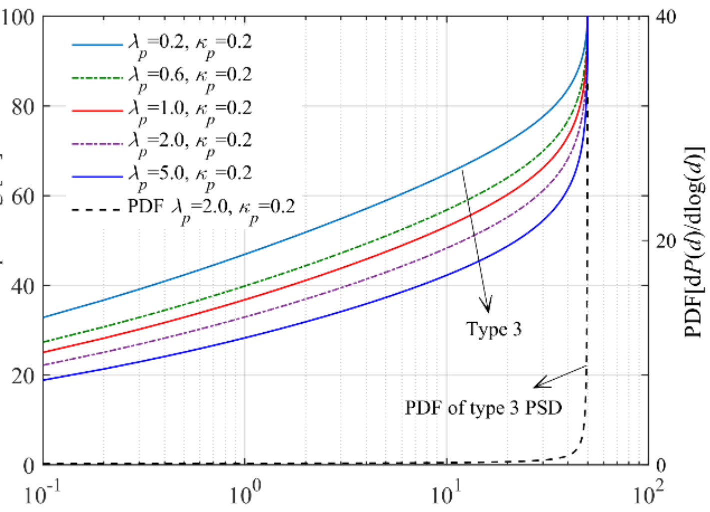

(a)

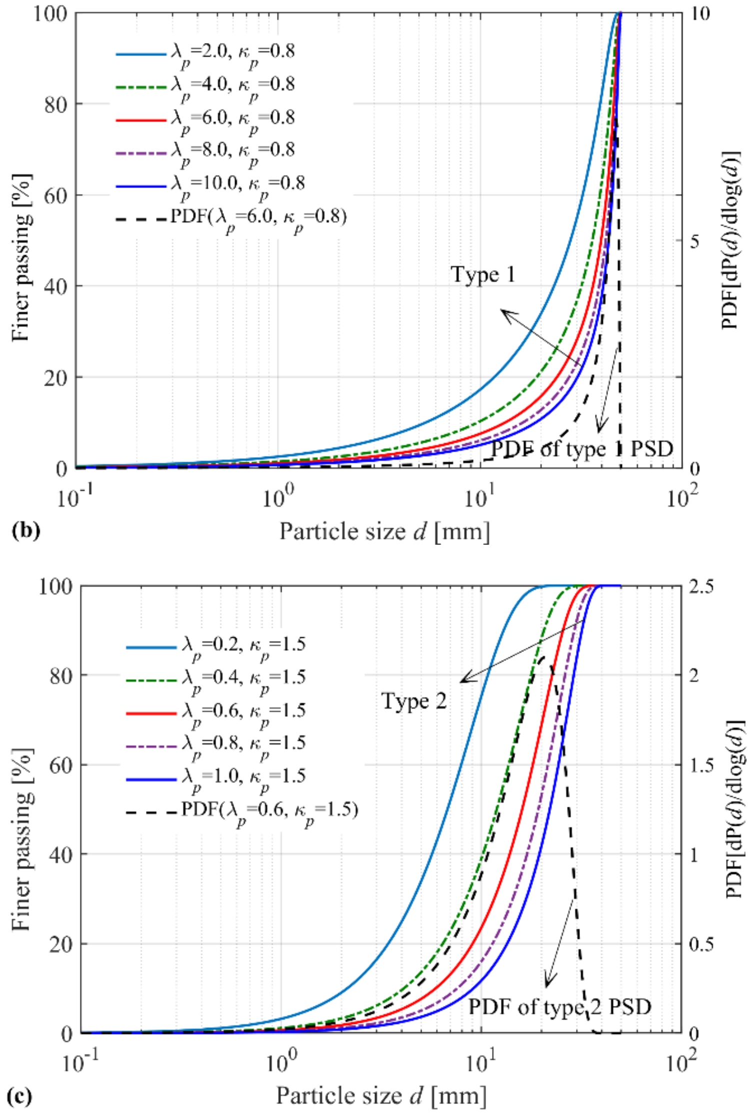

Figure 3.3: Influence of parameter λ_p on particle size distribution: (a) varying of λ_p with a fixed $\kappa_p = 0.2$; (b) varying of λ_p with a fixed $\kappa_p = 0.8$; (c) varying of λ_p with a fixed $\kappa_p = 1.5$

Figure 3.4 shows the influence of κ_p on PSD. In this figure, for a constant λ_p, the shape of PSD changes with parameter κ_p and all the PSD curves intersect at one point ($d_{63.2}$, 0.632). For example, for $\kappa_p = 0.2$, the PSD curves are more or less in a linear shape (Type 3, also see Figure 3.3(c)), irrespective of λ_p. As κ_p increases and λ_p is kept small (Figure 3.4(a) and Figure 3.4 (b)), the shape of the PSD curves changes from a linear shape (Type 3) to a hyperbolic one (Type 1) and then to an S shaped (Type 2).

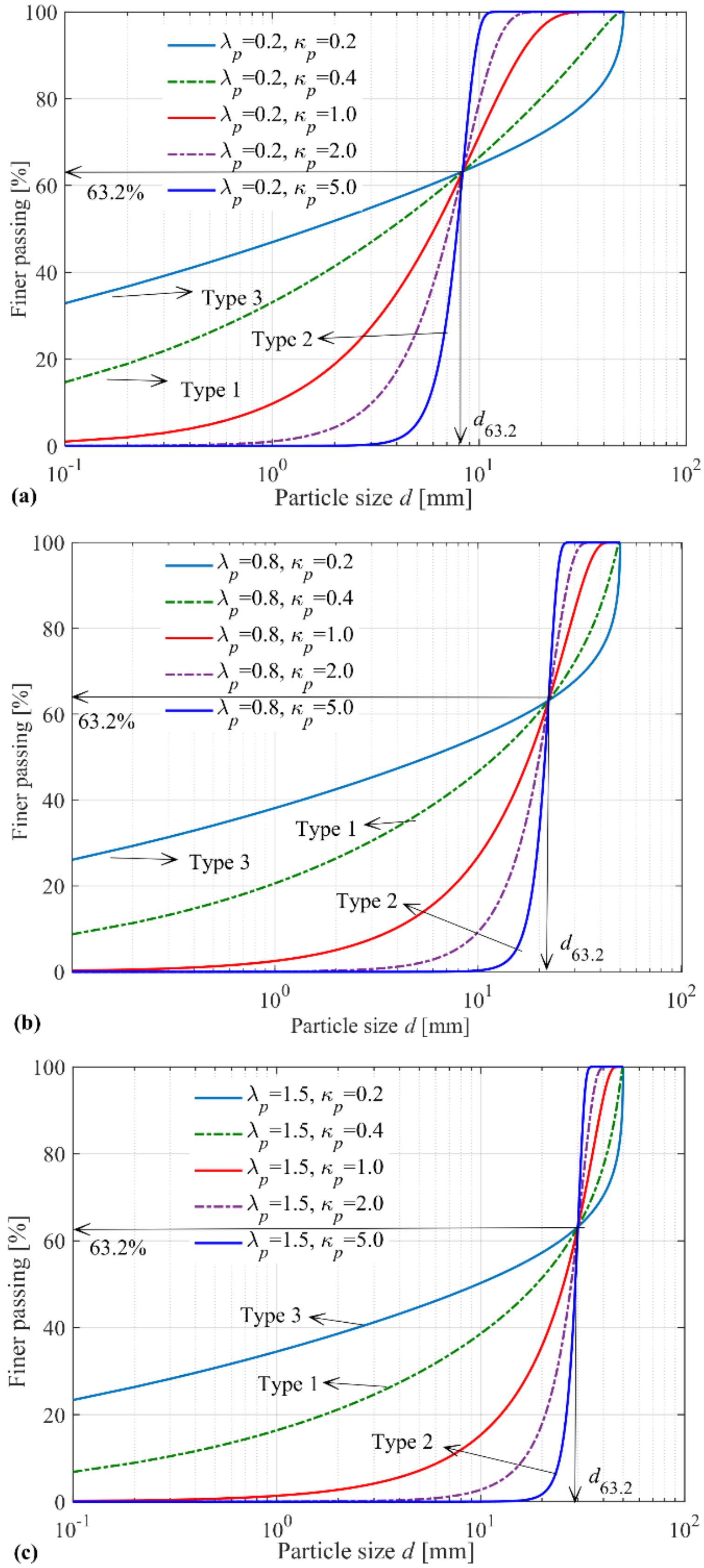

Figure 3.4: Influence of parameter κ_p on particle size distribution: (a) varying of κ_p with a fixed $\lambda_p = 0.2$; (b) varying of κ_p with a fixed $\lambda_p = 0.8$; (c) varying of κ_p with a fixed $\lambda_p = 1.5$

Figure 3.5 shows the influence of κ_p on logarithmic PDF. Again, the PSD curve type will change from Type 3 to Type 1 and then Type 2 with the increasing κ_p for a fixed λ_p. According to Figure 3.5, the most frequent particle size (the size corresponding to the peck value of PDF) will decreases with increasing κ_p.

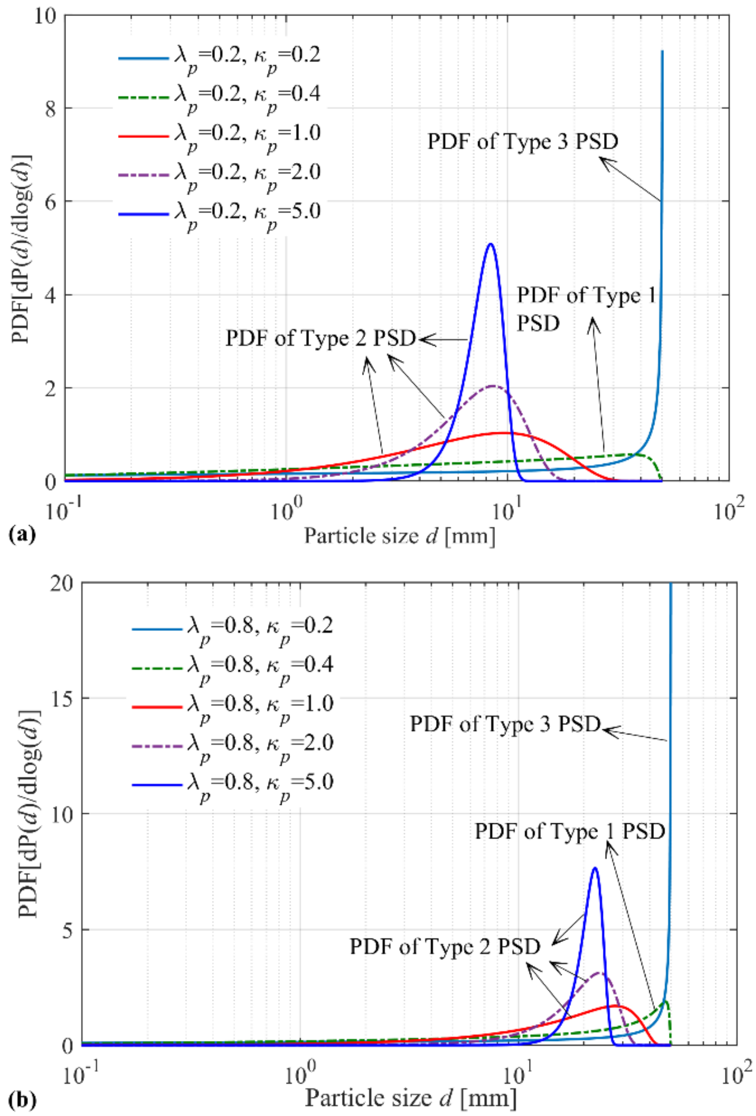

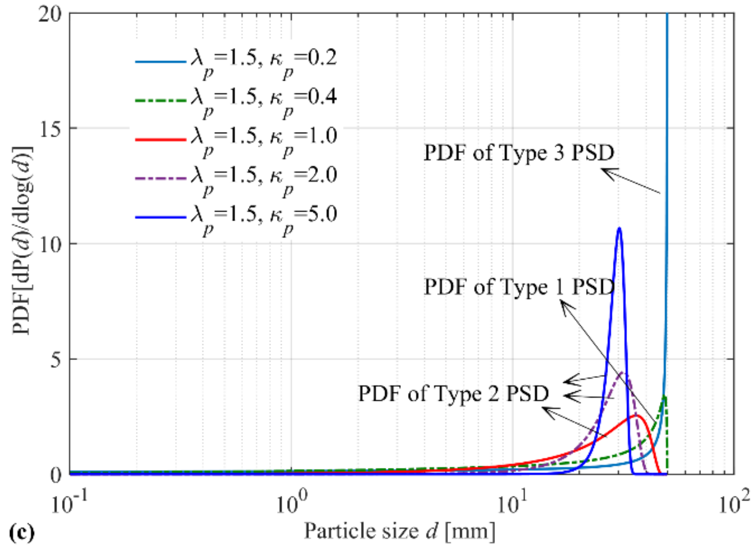

Figure 3.5: Influence of parameter κ_p on logarithmic PDF: (a) varying of κ_p with a fixed λ_p = 0.2; (b) varying of κ_p with a fixed λ_p = 0.8; (c) varying of κ_p with a fixed λ_p = 1.5

In summary, the proposed PSD model is able to describe continuous PSD curves of the three main types. Moreover, the shape of a PSD curve is mainly affected by parameter κ_p, with parameter λ_p affecting characteristic particle diameters.

Parameters such as the coefficient of uniformity C_u and the coefficient of curvature C_c are commonly used as basic properties of soil in engineering field. Parameter λ_p has a theoretical solution as shown by Equation (3.7), and it is an index similar with C_u. The relationship between parameter κ_p and the coefficient of uniformity C_u, the coefficient of curvature C_c were investigated based on 154 PSD curves (see details in section 3.4 and section 3.5).

Figure 3.6 and Figure 3.7 show the correlation between parameter κ_p and C_c or C_u. Both C_c and C_u decrease with increasing κ_p and show an asymptote around κ_p = 0.35. The relationship between κ_p and C_c or C_u can be expressed as power functions as shown in Figure 3.6 and Figure 3.7. These relationships seem to be independent of the tested material or the testing method, as the experimental data listed in Table 3.1 include different soils in different tests. The correlations shown in Figure 3.6 and Figure 3.7 indicate that parameter κ_p can be estimated with confidence from commonly used soil grading parameters. For example. as the red square points shown in Figure 3.6 and Figure 3.7, parameter κ_p = 0.927, 0.372, 3.00 when C_u = 5, C_c = 1 and C_c = 3, respectively, which means the parameter κ_p should be within the range of 0.372 to 0.927 if the soil sample is expected to be well graded based on the standard for engineering classification of soils in China (GB/T50145-2007).

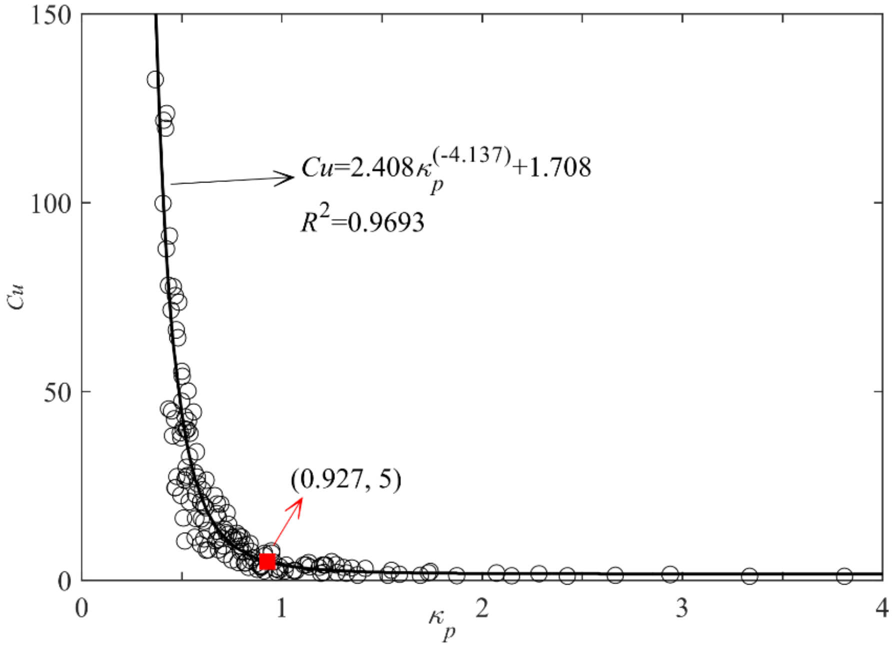

Figure 3.6: Correlation between parameter κ_p and coefficient of non-uniformity C_u

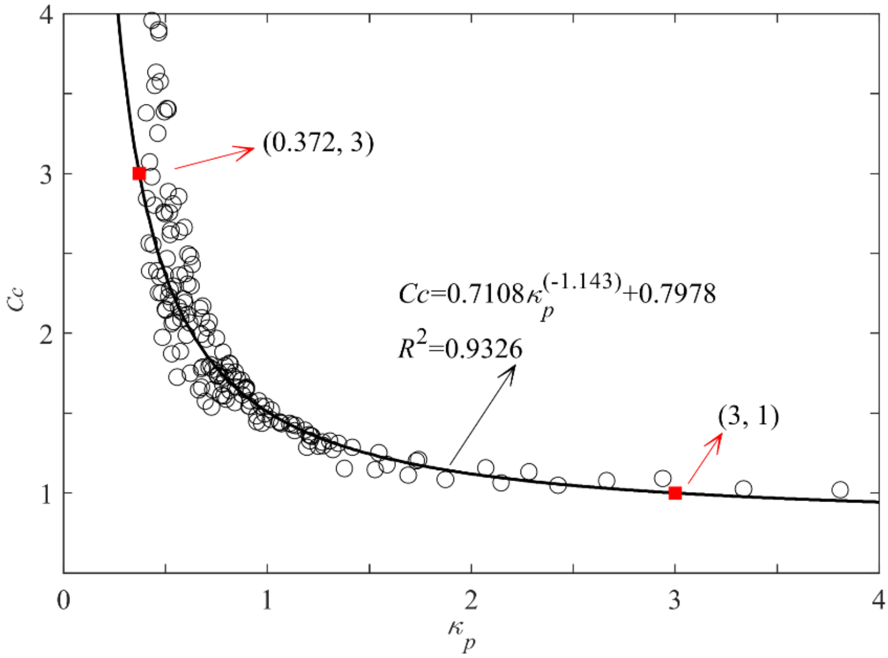

Figure 3.7: Correlation between parameter κ_p and coefficient of curvature C_c

To verify the proposed PSD model, fifty-three (53) sets of granular materials with 154 PSD curves are used to evaluate the applicability of proposed model. Those PSD curves are all non-uniformly and continuous graded, some of them break from uniformly graded samples (see the details in section 3.4) and others are an arbitrary mixture of particles from different group sizes (see the details in section 3.5). Moreover, other three PSD models (GGSM, GMM, and FUM) are also used for comparison. The results are shown in Figure 3.8.

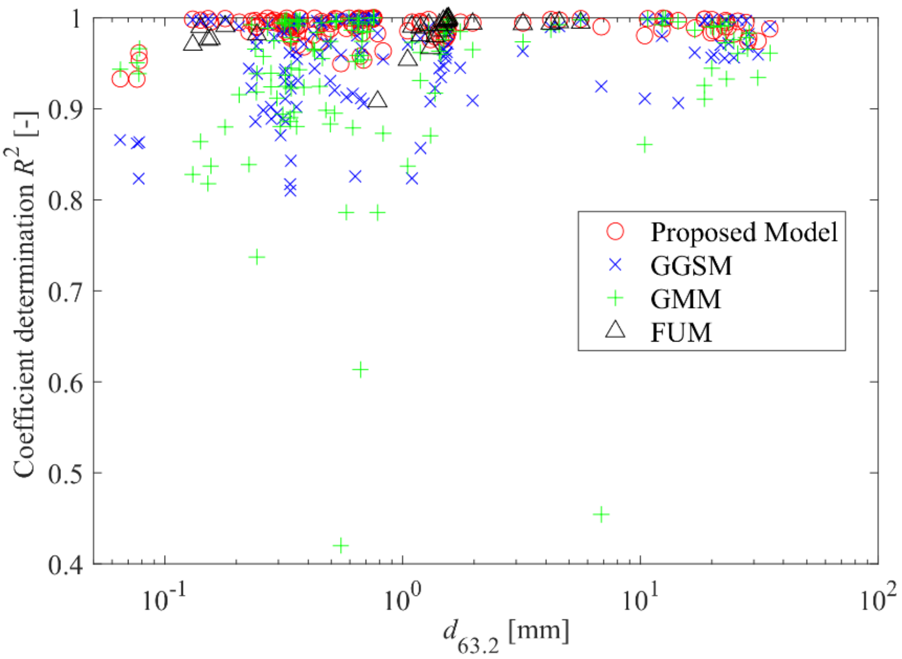

Figure 3.8: Performance of the four PSD models at different particle diameters $d_{63.2}$

Figure 3.8 shows the variation of the correlation coefficient R^2 versus the particle diameter $d_{63.2}$. The reason that we choose $d_{63.2}$ is that $d_{63.2}$ is an important particle size and determines the value of λ_p in this study. The values of $d_{63.2}$ are obtained by setting $P(d_{63.2}) = 0.632$ to Equation (3.6). An R^2 value closer to 1 indicates a better fitting. As shown in Figure 3.8, the performance of the proposed model is relatively good across different values of $d_{63.2}$. The overall performance of the GGSM model is better than the GMM model, although some values of R^2 of the GMM are larger than those of GGSM's in certain cases. The model proposed in this paper and FUM are superior to the previous two models. In general, the model proposed in this paper is able to capture a wide variety of PSDs from the literature and it performs better than the FUM model while having less fitting parameters and simple mathematical form.

3.4 Evolving particle size distributions due to breakage

In this section, twenty-six (26) sets of granular materials with 127 PSD curves are used to evaluate the applicability of the proposed model involving particle breakage. The selected experimental data covers different material properties and loading types and most of the curves are obtained from tests designed to induce particle crushing tests (Bard, 1993; Hagerty *et al.*, 1993; Luzzani & Coop, 2002; Coop *et al.*, 2004; Russell & Khalili, 2004; Okada *et al.*, 2004; Mayoraz *et al.*, 2006; Guimaraes *et al.*, 2007; Kikumoto *et al.*, 2010; Xiao *et al.*, 2014b; Xiao *et al.*, 2016c; Zhang *et al.*, 2017). Some typical detailed fitting results are shown in Table 3.1. The fitting of experimental data in Table 3.1 was done individually for each PSD curve, which allows us to examine the general capacity of the proposed model in predicting evolving PSD curves.

Table 3.1 shows the fitting results of the experimental data of the four PSD models. The performances of different PSD models can be evaluated by the correlation coefficient R^2, with the highest value for each PSD highlighted in red. In Table 3.1, there is a consistent and monotonic evolution of the 2 fitting parameters (λ_p and κ_p) of the proposed model in most cases, except for the data from Coop *et al.* (2004) at very large strains. The reason for this inconsistent and non-monotonic evolution of 2 parameters is either an experimental error or particle aggregation. The test results in Coop *et al.* (2004) showed that the number of fine particles first increased with increasing strain and then dropped at very high strains, which is not possible unless particle aggregation occurs at large strains. The proposed model does not consider particle aggregation. It is noted that the performance of FUM model is only verified by those PSD data with more than eight sieving points in Figure 3.8 and Table 3.1, because the fitting results may be unreliable when the sieving points are too few to fit for the four fitting parameters.

According to the data in Table 3.1, the GGSM model and GMM model have a relatively good performance for describing PSD curves for specimens at relatively low stresses or strains (with less particle breakage). However, at large stress or strain, the performance of the proposed model and FUM model become significantly better than the GGSM model and GMM model, implying that the proposed model captures the particle breakage better than the GGSM and the GMM models.

Table 3.1. Performance of four PSD models for different materials

Reference	Property/Loading	Proposed Model			GGMM	GMM	FUM
		λ_p	κ_p	R^2	R^2	R^2	R^2
Coop *et al.* (2004)	CS/UG/RS/VS1/no shearing	6.498	1.528	0.9997	0.9981	0.9959	
	CS/UG/RS/VS1/ γ=52%	5.572	0.911	0.9833	0.9545	0.9963	
	CS/UG/RS/VS1/ γ=104%	3.664	0.632	0.9935	0.9616	0.9912	

	CS/UG/RS/VS1/ γ=171%	2.716	0.611	0.9959	0.9848	0.9947	
	CS/UG/RS/VS1/ γ=251%	2.101	0.537	0.9976	0.9785	0.9746	
	CS/UG/RS/VS1/ γ=730%	1.129	0.422	0.9845	0.9444	0.8389	
	CS/UG/RS/VS1/ γ=1430%	0.729	0.500	0.9992	0.9981	0.8800	0.9908
	CS/UG/RS/VS1/ γ=2780%	0.579	0.472	0.9955	0.9955	0.8373	0.9768
	CS/UG/RS/VS1/ γ=2860%	0.556	0.458	0.9989	0.9988	0.8179	0.9757
	CS/UG/RS/VS1/ γ=11030%	0.444	0.467	0.9984	0.9979	0.8280	0.9702
	CS/UG/RS/VS1/ γ=11100%	0.496	0.480	0.9976	0.9965	0.8641	0.9896
	CS/UG/RS/VS2/ γ=285%	3.235	0.750	0.9994	0.9855	0.9982	
	CS/UG/RS/VS2/ γ=1180%	1.742	0.626	0.9996	0.9924	0.9888	
	CS/UG/RS/VS2/ γ=3350%	1.325	0.496	0.9894	0.9691	0.9181	
	CS/UG/RS/VS2/ γ=10920%	1.343	0.406	0.9905	0.9388	0.7373	0.9815
	CS/UG/RS/VS2/ γ=13280%	0.931	0.507	0.9952	0.9906	0.9154	
	CS/UG/RS/VS2/ γ=26650%	1.343	0.522	0.9943	0.9779	0.9388	
	CS/UG/RS/VS3/ γ=9040%	5.126	0.877	0.9892	0.9626	0.9979	
	CS/UG/RS/VS3/ γ=23900%	3.908	0.593	0.9900	0.9224	0.9736	
	CS/UG/RS/VS3/ γ=31700%	3.960	0.623	0.9894	0.9283	0.9782	
	CS/UG/RS/VS3/ γ=37500%	3.062	0.475	0.9964	0.9111	0.9371	
	CS/UG/RS/VS3/ γ=147000%	3.137	0.495	0.9852	0.8863	0.9248	
Bard (1993)	PC/UG/1DC/ VS=5MPa	1.278	0.793	0.9989	0.9982	0.9980	0.9946
	PC/UG/1DC/ VS=7.5MPa	0.836	0.793	0.9976	0.9906	0.9923	0.9950
	PC /UG/1DC/ VS=10MPa	0.723	0.722	0.9982	0.9896	0.9871	0.9935
	PC /UG/1DC/ VS=20MPa	0.471	0.676	0.9945	0.9635	0.9737	0.9932
	PC /UG/1DC/ VS=40MPa	0.245	0.677	0.9945	0.9091	0.9649	0.9935
	PC /UG/1DC/ VS=57MPa	0.135	0.695	0.9958	0.8569	0.9618	0.9894
	PC /UG/1DC/ VS=100MPa	0.123	0.726	0.9953	0.8238	0.9729	0.9906
Russell & Khalili (2004)	QS/NG (initial)	1.478	1.731	0.9912	0.9022	0.8804	
	QS/NG/DT/MES=410kPa	1.044	2.939	0.9944	0.8711	0.8805	
	QS/NG/DT/MES=760kPa	1.090	2.283	0.9930	0.8893	0.8939	
	QS/NG/DT/MES=1417kPa	0.975	2.071	0.9944	0.8946	0.9117	
	QS/NG/DT/MES=2395kPa	0.874	1.741	0.9957	0.8890	0.9242	
	QS/NG/DT/MES=3006kPa	0.873	1.547	0.9953	0.9022	0.9393	
	QS/NG/DT/MES=5705kPa	0.760	1.306	0.9959	0.8983	0.9573	
	QS/NG/DT/MES=7800kPa	0.666	1.204	0.9967	0.8859	0.9657	
Zhang *et al.* (2017)	ST/NG (initial)	1.666	1.185	0.9745	0.9598	0.9342	
	ST/NG/1DC/VS=2MPa	1.304	1.139	0.9742	0.9680	0.9657	
	ST/NG/1DC/VS=5MPa	0.977	1.121	0.9823	0.9561	0.9759	
	ST/NG/1DC/VS=10MPa	0.883	0.845	0.9902	0.9719	0.9949	
	ST/NG/1DC/VS=15MPa	0.771	0.763	0.9839	0.9701	0.9913	
	ST/NG/1DC/VS=20MPa	0.689	0.733	0.9857	0.9594	0.9897	
	SM/NG (initial)	2.351	0.991	0.9879	0.9905	0.9612	
	SM/NG/1DC/VS=2MPa	1.336	0.958	0.9778	0.9822	0.9832	
	SM/NG/1DC/VS=5MPa	0.826	0.914	0.9903	0.9556	0.9913	
	SM/NG/1DC/VS=10MPa	0.657	0.755	0.9835	0.9565	0.9905	
	SM/NG/1DC/VS=15MPa	0.512	0.682	0.9887	0.9617	0.9866	
	SM/NG/1DC/VS=20MPa	0.406	0.787	0.9969	0.9066	0.9959	
Xiao *et al.* (2016c)	CS/UG/IL/SH1, IW=4.71KJ	1.808	0.669	0.9982	0.9895	0.9867	0.9922
	CS/UG/IL/SH1, IW=9.71KJ	1.454	0.527	0.9940	0.9773	0.9309	0.9808
	CS/UG/IL/SH1, IW=19.42KJ	1.105	0.433	0.9856	0.9709	0.8371	0.9538
	CS/UG/IL/SH1, IW=38.85KJ	0.644	0.438	0.9827	0.9830	0.786	0.9079
	CS/UG/IL/SH2, IW=4.71KJ	2.851	0.818	0.9873	0.9650	0.9871	0.9965
	CS/UG/IL/SH2, IW=9.71KJ	2.490	0.683	0.9820	0.9447	0.9632	0.9921
	CS/UG/IL/SH2, IW=19.42KJ	2.157	0.569	0.9795	0.9224	0.917	0.9796
	CS/UG/IL/SH2, IW=38.85KJ	1.890	0.514	0.9760	0.9079	0.8707	0.9666
	CS/UG/IL/SH3, IW=4.71KJ	3.351	1.070	0.9914	0.9819	0.9971	0.9990
	CS/UG/IL/SH3, IW=9.71KJ	3.145	0.897	0.9811	0.9597	0.9859	0.9966
	CS/UG/IL/SH3, IW=19.42KJ	2.924	0.814	0.9763	0.9473	0.9758	0.9918
	CS/UG/IL/SH3, IW=38.85KJ	2.637	0.715	0.9746	0.9347	0.9603	0.9860
	CS/UG/IL/SH3, IW=4.71KJ	3.566	1.208	0.9932	0.9863	0.9981	0.9995

	CS/UG/IL/SH3, IW=9.71KJ	3.449	1.060	0.9839	0.9711	0.9920	0.9980
	CS/UG/IL/SH3, IW=19.42KJ	3.298	0.969	0.9801	0.9624	0.9874	0.9967
	CS/UG/IL/SH3, IW=38.85KJ	3.125	0.895	0.9780	0.9556	0.9828	0.9951
Mayoraz *et al.* (2006)	ST/UG/ML/MMP=0.5MPa	3.348	1.059	0.9872	0.9799	0.9922	
	ST/UG/ML/MMP=1MPa	1.872	0.463	0.9806	0.9114	0.8608	
	ST/UG/ML/MMP=3MPa	0.748	0.300	0.9902	0.9246	0.4546	
	LT/UG/ML/MMP=0.5MPa	3.870	1.587	0.9990	0.9984	0.9996	
	LT/UG/ML/MMP=1MPa	3.522	1.321	0.9998	0.9989	0.9991	
	LT/UG/ML/MMP=3MPa	2.027	0.842	0.9990	0.9987	0.9985	

Note: CS-Carbonate Sand, PC-Petroleum Coke, QS-Quartz Sand, SM-Sandy Mudstone, ST-Sandstone, LT-Limestone
UG-uniformly graded, NG-non-uniformly graded
RS-Ring shear test, 1DC-One dimensional compression, DT-Drained triaxial test, IL-Impact loading test, ML- Monotonic loading test
VS-vertical stress, VS1-vertical stress ranges 650–930 kPa, VS2-vertical stress ranges 248–386 kPa, VS3-vertical stress ranges 60–97 kPa, MES- mean effective stress, MMP-maximum mean pressure
SH1-specimen height = 31.8 mm, SH2-specimen height = 63.7 mm, SH3-specimen height = 95.5 mm, SH4-specimen height = 127.3 mm, IW-input work

As mentioned above, the evolution of PSD curves during particle breakage exhibits certain trends, which are easily identifiable for initially uniformly graded samples. Ideally these trends should be captured in the PSD model. Figure 3.9 shows the evolution of the two model parameters (λ_p and κ_p) with stresses or strains for a range of tests and materials. Both parameters follow clear trends during breakage, decreasing with increasing stresses or strains (or increasing extent of breakage) and approaching stationary values at high degrees of breakage. The following equation provides a relatively good prediction of the evolution of the two parameters (λ_p and κ_p):

$$\lambda_p = a_\lambda + b_\lambda e^{c_\lambda \sigma(\gamma, p)}, \qquad \kappa_p = a_\kappa + b_\kappa e^{c_\kappa \sigma(\gamma, p)} \tag{3.11}$$

where a, b, c are fitting parameters, $\sigma(\gamma, p)$ is stress (strain) in the test. With Equation (3.11), only two sets of parameters (a, b, c) or total six parameters are needed to predict the PSD curve at an arbitrary degree of breakage, which is an important advantage of the proposed model.

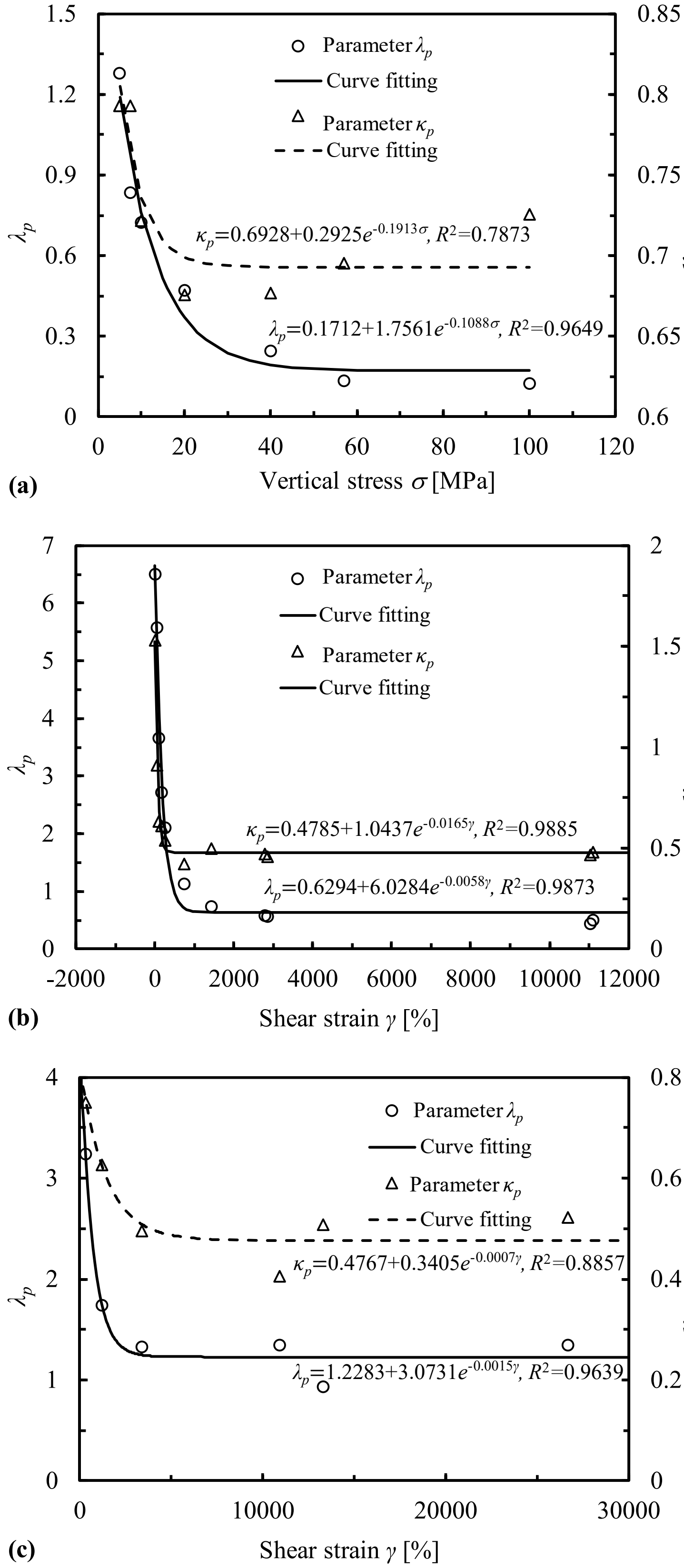

(a)
Parameter λ_p
Curve fitting
Parameter κ_p
Curve fitting
κ_p=0.6928+0.2925$e^{-0.1913\sigma}$, R^2=0.7873
λ_p=0.1712+1.7561$e^{-0.1088\sigma}$, R^2=0.9649
λ_p
κ_p
Vertical stress σ [MPa]
(b)
Parameter λ_p
Curve fitting
Parameter κ_p
Curve fitting
κ_p=0.4785+1.0437$e^{-0.0165\gamma}$, R^2=0.9885
λ_p=0.6294+6.0284$e^{-0.0058\gamma}$, R^2=0.9873
λ_p
κ_p
Shear strain γ [%]
(c)
Parameter λ_p
Curve fitting
Parameter κ_p
Curve fitting
κ_p=0.4767+0.3405$e^{-0.0007\gamma}$, R^2=0.8857
λ_p=1.2283+3.0731$e^{-0.0015\gamma}$, R^2=0.9639
λ_p
κ_p
Shear strain γ [%]

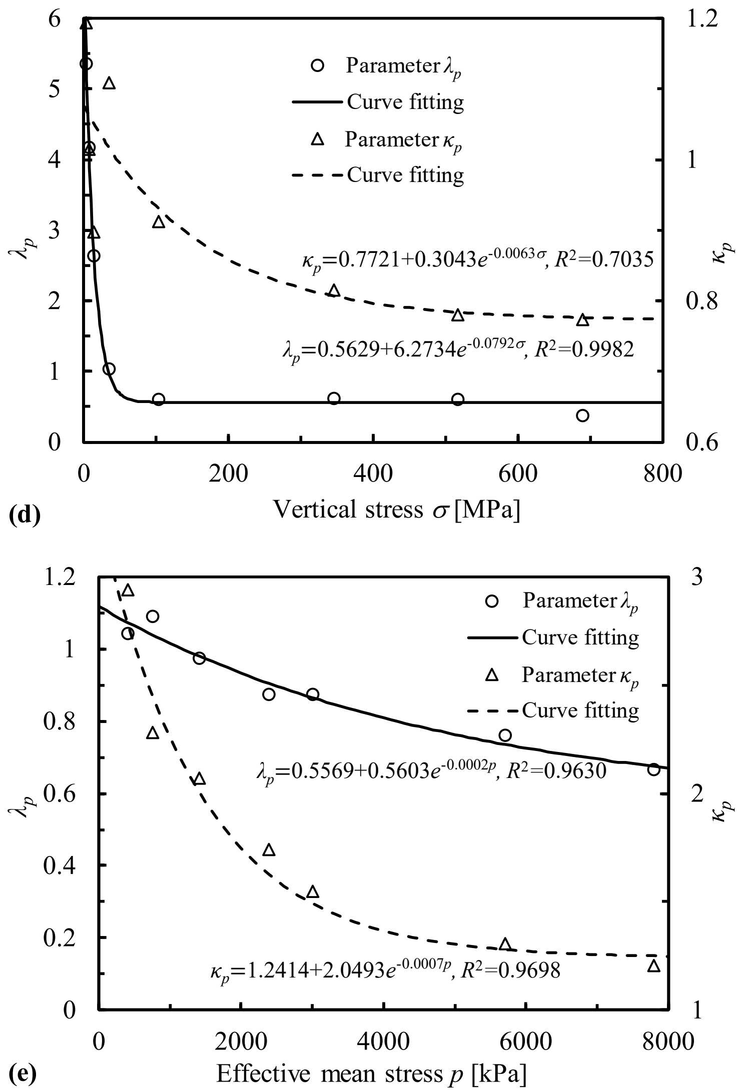

Figure 3.9: Evolution of model parameters with particle breakage: (a) data from Bard (1993); (b)-(c) data from Coop *et al.* (2004); (d) data from Hagerty *et al.* (1993); (d) data from Russell & Khalili (2004)

3.5 Assessing internal stability of widely graded granular soils

In additional to particle breakage, the PSD model proposed in this paper can also be applied to assess internal stability of granular filters. One of the most commonly used geometric criteria is the criterion by Kenney & Lau (1985); Kenney & Lau (1986). A geometric index ratio of H/F was proposed and applied in the analysis of internal stability of granular soils. A granular sample would be considered as unstable if

$$(H/F)_{\min} < 1 \tag{3.12}$$

where H is the mass fraction of particles with size from d to $4d$, F is the mass fraction of particles with size finer than d as shown in Figure 3.10. For a widely graded and uniformly graded sample, the search for the minimum value of H/F will end at $F = 20\%$ and $F = 30\%$ respectively.

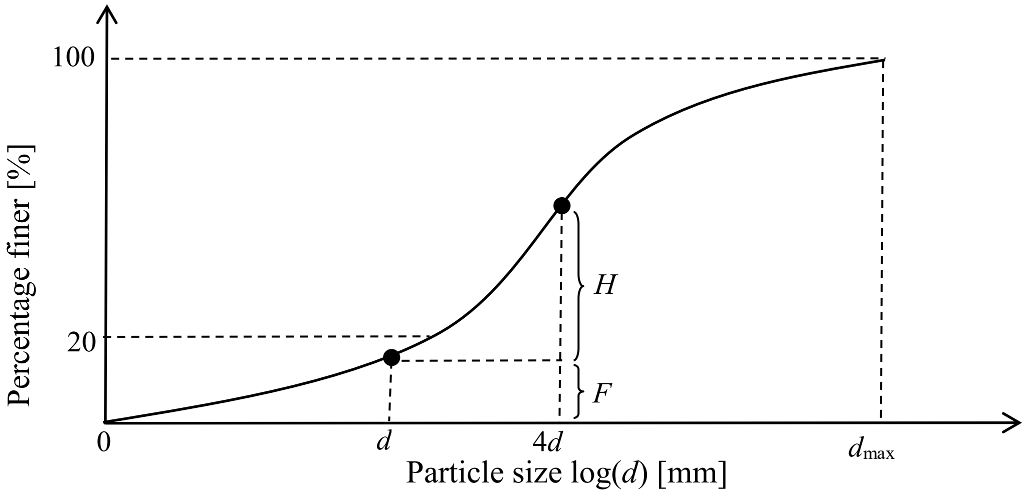

Figure 3.10: Illustration of Kenny and Lau's criterion

For a widely graded granular soil (with minimum particle size 0.063 mm), the whole PSD curve can be represented by the proposed PSD model as shown in Equation (3.6). Substituting Equation (3.6) into Equation (3.12) leads to:

$$\left\{ \frac{e^{-\left(\frac{d}{\lambda_{\mathrm{p}}(d_{\max}-d)}\right)^{\kappa_{\mathrm{p}}}} - e^{-\left(\frac{4d}{\lambda_{\mathrm{p}}(d_{\max}-4d)}\right)^{\kappa_{\mathrm{p}}}}}{1-e^{-\left(\frac{d}{\lambda_{\mathrm{p}}(d_{\max}-d)}\right)^{\kappa_{\mathrm{p}}}}} \right\}_{\min} < 1, \qquad 0.063 < d \le \frac{d_{\max}}{4} \tag{3.13}$$

Equation (3.13) means that for a given particle size d (from 0.063 to $d_{\max}/4$), the value of H/F is always less than 1. It is a linear programming problem to some extent. The maximum value of $d_{\max} \le 100$ mm for most granular soils. Letting $d_{\max}/d=y$, the range of y values should be from 4 to 100/0.063($\approx$ 1600). Equation (3.13) can then be expressed as

$$\begin{cases} (2e^{-\left(\frac{1}{\lambda_{\mathrm{p}}(y-1)}\right)^{\kappa_{\mathrm{p}}}} - e^{-\left(\frac{1}{\lambda_{\mathrm{p}}(\frac{1}{4}y-1)}\right)^{\kappa_{\mathrm{p}}}} - 1)/_{4\le y\le 1600} < 0 \\ \lambda_{\mathrm{p}} > 0 \\ \kappa_{\mathrm{p}} > 0 \end{cases} \tag{3.14}$$

Letting $f(y)=2e^{-\left(\frac{1}{\lambda_p(y-1)}\right)^{\kappa_p}}-e^{-\left(\frac{1}{\lambda_p(\frac{1}{4}y-1)}\right)^{\kappa_p}}-1$, we can plot $f(y) = 0$ in $\lambda_p - \kappa_p$ space for any $4 \leq y \leq 1600$, as shown in Figure 3.11.

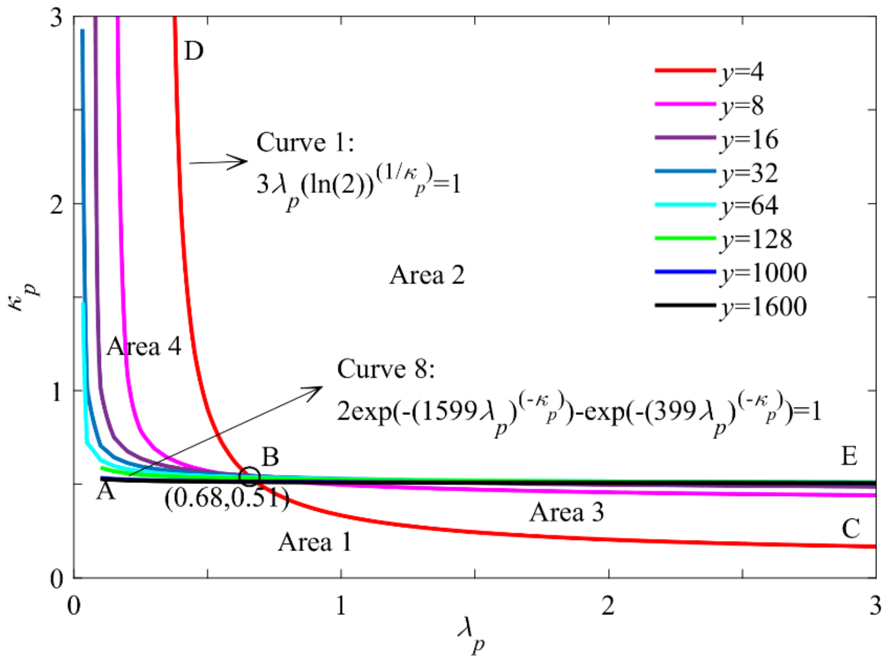

Figure 3.11: Curves of $f(y) = 0$ in $\lambda_p - \kappa_p$ space

Figure 3.11 shows some typical curves of $f(y) = 0$ in $\lambda_p - \kappa_p$ space for given y. In general, the curve of $f(y) = 0$ tends to be flat with increasing y. In the case of $y = 4$, the relationship between λ_p and κ_p is be plotted as curve 1, while, in the case of $y = 1600$, the relationship between λ_p and κ_p is plotted as curve 8. Since for any y ($4 \leq y \leq 1600$), $f(y)$ needs to satisfy $f(y) < 0$, that is to say, the range of λ_p and κ_p needs to below all the curves of $f(y) = 0$ for any y ($4 \leq y \leq 1600$). In other words, if the granular sample would be considered unstable, the range of λ_p and κ_p should fall within the area below curves AB & BC (Area 1, the intersection of all the range of λ_p and κ_p for any y) as shown in Figure 3.11. Point B is the intersection of curve 1 and curve 8.

The same method for determining the range of λ_p and κ_p for the consideration of stable of granular soils since the criterion should be rewritten as:

$$(H/F)_{\min} \geq 1 \tag{3.15}$$

Similar conclusion can be obtained that the granular sample would be considered stable if the range of λ_p and κ_p falls in the area above curves DB & BE (Area 2). It is worth noting that this area is not, but very close to, the real area because the intersections of all the curves of λ_p and κ_p for any given y are close to, but not exactly at point B. Here, for simplicity, we use point B to distinguish the area of λ_p and κ_p when assessing the internal stability for soil samples.

Data of internal stability tests on 27 widely graded granular soils from the literature (Kenney & Lau, 1985; Åberg, 1993; Indraratna *et al.*, 2015; Skempton & Brogan, 1994) are collected and used for verifying the stable and unstable areas proposed in the $\lambda_p - \kappa_p$ space. PSD parameters λ_p and κ_p are first obtained using fitting process as shown in Figure 3.2, and their values are then plotted in the $\lambda_p - \kappa_p$ space. The results are shown in Figure 3.12.

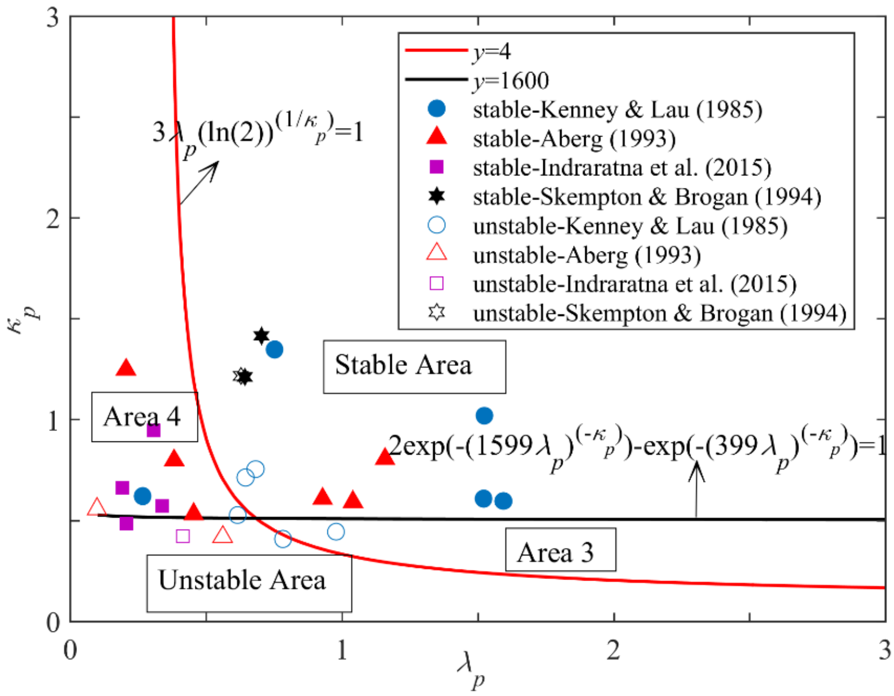

Figure 3.12: Validation of internal stability of well-graded granular soil

Figure 3.12 shows that more than 50% (10/18) of the stable grading fall into the proposed stable area, 7 stable grading fall into area 4, while, and only 1 stable grading falls into the unstable area. Unstable gradings tested in the laboratory fall into stable area, unstable area and other two areas with the same proportion (3/9). For areas 3 & 4, Equation (3.12) & Equation (3.15) are not always satisfied for any y. If both Equation (3.12) (or Equation (3.15)) and $F \leq 20\%$ are met, the granular soil sample can be regarded as unstable (or stable). That is to say, for the PSD parameters λ_p and κ_p falling into area 3 & area 4, the internal stability of the granular soil cannot be determined and needs further assessment.

The stable area and unstable area proposed in this paper are based on Kenney & Lau's criterion. It is a more straightforward and simpler way for assessing internal stability of widely graded granular soils, compared against other methods in the literature. As shown in Figure 3.12, the stable and unstable area defined in the $\lambda_p - \kappa_p$ space are in relatively good agreement with experimental results.

3.6 Conclusions

A simple particle size distribution model for granular materials is proposed in this paper. The model contains two parameters, one parameter (λ_p) representing a characteristics particle diameter, and the other parameter κ_p closely correlated to the coefficient of uniformity (C_u) or the coefficient of curvature (C_c). Parameter κ_p mainly affects the shape of the PSD curve, while parameter λ_p affects characteristic particle sizes of the soil sample.

The proposed PSD model can capture the main types of continuous PSD curves. Its performance is compared against the Gates-Gaudin-Schuhmann model, Gaudin-Melog model and Fredlund unimodal model by analysing 53 soil specimens with 154 PSD curves. It is shown that the proposed PSD model performs better than the Gates-Gaudin-Schuhmann model and the Gaudin-Melog model, particularly for PSD curves obtained at high degrees of particle breakage. The proposed two-parameter PSD model displays a similar performance to the four-parameter Fredlund unimodal model. It is shown that the two parameters in the proposed model follow clear trends identifiable during particle breakage of initially uniformly graded soil samples. Equations are proposed for these trends, with which the evolution of PSD curves during particle breakage of one soil sample can be simulated with two sets of model parameters.

A continuous particle size distribution model provides a quantitative method for estimating other soil properties and is an important element in studying problems such as particle breakage and assessment of internal stability. An initially non-uniformly graded sample can be treated either as the product of a uniformly graded sample due to particle breakage, or an arbitrary mixture of particles from different group sizes (Zhang *et al.*, 2015). For initially non-uniformly graded samples, the situation can be more complex. The proposed model can be extended to capture more complex PSDs (e.g. bimodal distributions representative of gap-graded soils) through superposition of two or more unimodal PSDs.

List of symbols

PSD	particle size distribution
PDF	probability density function
C_u	coefficient of uniformity
C_c	coefficient of curvature
m	fitting parameter in Equation (3.1)
d_{max} and d_{max-1}	diameter of the largest and second largest particle
D	fractal dimension
k	fitting parameter in Equation (3.2)
a_{gr}, n_{gr}, m_{gr} and d_{rgr}	fitting parameters in Equation (3.3)
λ_p and κ_p	scale parameter and shape parameter in Equation (3.4)
x_i	particle size ratio
P^*	distribution of new particles generated from the particle breakage of an initially uniformly graded sample
$d_{63.2}$	characteristic particle diameter at which 63.2% of the sample by mass is smaller
R^2	coefficient of determination
a, b, c	fitting parameters in Equation (3.11)
H	mass fraction of particles with size from d to $4d$
F	mass fraction of particles with size finer than d

Chapter 4 . A breakage matrix model for carbonate sands subjected to one-dimensional compression

ABSTRACT: The breakage matrix model has great potential in describing particle size degradation of granular materials. A series of one-dimensional compression tests were performed on uniformly graded calcareous sand to obtain the breakage matrix. This straightforward method has successfully simulated the particle size evolution of non-uniformly graded samples with different initial particle size distribution.
Keywords: Breakage matrix; calcareous sand; one-dimensional compression test;

This chapter aims to solve the second key issue (i.e., breakage evolution law) and is based on a conference paper of GeoShanghai 2018:

Tong, C. X, *Zhang, S., & Sheng, D. (2018). A Breakage Matrix Model for Calcareous Sands Subjected to One-Dimensional Compression. In GeoShanghai International Conference (pp. 17-24), Shanghai, China.*

Authorship Declaration

By signing below I conform that for the conference paper titled 'A breakage matrix model for calcareous sands subjected to one-dimensional compression' and published at the GeoShanghai 2018 conference, that:

Chenxi Tong proposed the model, conducted the tests and wrote the manuscript.

Sheng Zhang contributed to the discussion of the proposed model.

Daichao Sheng is the leader of the research team, and assisted in the revision of the manuscript.

Production Note:

Signature removed
prior to publication.

Chenxi Tong

Prof Sheng Zhang

Prof Daichao Sheng

4.1 Introduction

Grinding related problems accompanied with degradation of particle size have always been a hot topic in many particulate fields: chemical engineering, minerals, foods, pharmaceuticals, geotechnical engineering, etc. Particle size degradation is mainly manifested on the change of particle size distribution (PSD) due to particle breakage caused by mechanical forces like shear, compression and impact. In some cases, the change of PSD is intentional, for example, to obtain a target PSD of wheat by using a roller milling and controlling the feed characteristics like initial PSD, feed rate, etc. (Campbell & Webb, 2001; Campbell *et al.*, 2001). However, in most geotechnical cases, such a degradation in PSD is inadvertent and unfavorable. For example, the degradation of ballast increases the settlement of ballast bed and maintenance costs (Indraratna *et al.*, 1997; Sun *et al.*, 2014a). The degradation of PSD deteriorates the mechanical properties of carbonate sands (Bandini & Coop, 2011) and rockfill materials (Tapias *et al.*, 2015; Xiao *et al.*, 2015).

The breakage matrix model proposed by Broadbent & Callcott (1956) is widely used for mathematical description of the relationship between the initial PSD and the evolving PSDs in a process of particle breakage:

$$\boldsymbol{p} = \boldsymbol{f}.\boldsymbol{T}_m \tag{4.1}$$

where $\boldsymbol{p}$ and $\boldsymbol{f}$ are row vectors of the output PSD and initial PSD, and $\boldsymbol{T}_m$ is the breakage matrix.

The breakage matrix has two statistical functions: a breakage function for describing the distribution of new particles generated from 'mother' particles and a selection function for describing the breakage probability of 'mother' particles. It is interesting to note that Equation (4.1) has the same form as the one-step transition matrix based on the Markov Chain model for non-uniform samples (Zhang *et al.*, 2015). The one-step transition matrix was used for the same purpose, i.e. calculating the new mass percentages within particle size groups from the original mass percentages, but was difficult to determine either theoretically or experimentally.

For both statistical approach and stochastic approach, the core issue needs to be tackled is to determine the value of each element in the breakage matrix. The mathematical models for describing both breakage function and selection function have been established in many grinding process (Broadbent & Callcott, 1956; Austin *et al.*, 1976; Campbell & Webb, 2001; Campbell *et al.*, 2001; Jekel & Tam, 2007), and most of them are suitable for intentional particulate degradation without considerations of particle-particle interactions, because the breakage patterns depend only on properties of particles (Campbell *et al.*, 2001).

For an involuntary degradation process in geotechnical field, breakage patterns are more complex, only very limited research has been conducted on breakage function and selection function in the literature. Zhang *et al.* (2015) proposed a two-parameter Weibull distribution to describe breakage function of uniformly graded samples and assumed that particles within different size groups of a non-uniformly graded sample had the same distribution. The breakage probability of different particle sizes was simplified as the concept of effective breakage probability. Ovalle *et al.* (2016) adopted a self-similar distribution (or fractal distribution) to describe the breakage function and a Weibull strength statistics equation (Weibull, 1951) combined with contact forces between particles to describe the selection function. Caicedo *et al.* (2016) used a very similar method: a Beta function to describe breakage function and a Weibull strength statistics equation combined with filling coefficient of particle to describe selection function. However, it is difficult to determine the breakage function and selection function of a non-uniformly graded sample for a given particle size and the precision of related models for describing both breakage function and selection function is not yet very clear, especially when the effect of particle size cannot be ignored. For example, particles within different size groups of a non-uniformly graded sample may suffer different breakage patterns, which is difficult to consider in the models mentioned before.

The aim of this work is to explore an alternative breakage model for non-uniformly graded samples, using the concept of breakage matrix. More specifically, we will attempt a straightforward experimental method for determining the breakage matrix through a series of one-dimensional compression tests of calcareous sands. Some insightful observations on the breakage matrix are revealed by studying the effects of initial particle size distributions and stress paths on particle breakage.

4.2 Breakage matrix model

A particle sample contains particles falling between sieve size d_1 and d_n (subscript 1 represents the finest particles, subscript n represents the coarsest particles). For simplicity, we use subscript 1, 2,…, n to represent particle size. The coefficient t_{ij} represents the mass fraction of particle size interval i that falls into particle size interval j ($n \geq i \geq j \geq 1$). Thus, expanded form of Equation (4.1) can be rewritten as:

$$\begin{bmatrix} p_1 & p_2 & \cdots & p_n \end{bmatrix} = \begin{bmatrix} f_1 & f_2 & \cdots & f_n \end{bmatrix} \begin{bmatrix} t_{11} & 0 & \cdots & \cdots & 0 \\ t_{21} & t_{22} & & & \vdots \\ \vdots & & \ddots & & \vdots \\ \vdots & & & \ddots & 0 \\ t_{n1} & t_{n2} & \cdots & \cdots & t_{nn} \end{bmatrix} \tag{4.2}$$

Where p_i represents mass fraction of particle size i after breakage, and f_i represents mass fraction of particle size i before breakage. The overall mass conservation requires,

$$\begin{cases} \sum_{1}^{n} p_i = 1 \\ \sum_{1}^{n} f_i = 1 \\ \sum_{j=1}^{i} t_{ij} = 1 \end{cases} \tag{4.3}$$

The matrix is a lower triangular matrix; the elements of diagonal of matrix t_{ii} are related to selection function, and the elements below diagonal of matrix t_{ij} (i>j) are related to breakage function.

4.3 Materials and test procedures

Calcareous sand used in our previous work (Zhang *et al.*, 2015) was still used in a series of one-dimensional compression tests in this study. Five sieve size classes are selected, that is 1 mm, 2 mm, 2.5 mm, 3 mm and 5 mm. The finest particle size is less than 1 mm, and the coarsest particle size ranges from 3 mm to 5 mm. Firstly, one-dimensional compression tests with different particle size of uniformly graded calcareous sand (D = 5 mm, D = 3 mm, D = 2.5 mm and D = 2 mm) were carried out to determine the breakage matrix. The assumption that the finest particles cannot break any more is still adopted in this study. Because the breakage matrix is highly dependent on vertical stress, we fix the vertical stress σ_v = 3.2 MPa in all the compression tests. To ensure the repeatability of the tests, each test had been conducted for three times. After that, non-uniformly graded samples with different initial PSDs were prepared and compressed at some stress conditions. The details of the tests conducted in this study are summarized in Table 4.1.

Table 4.1. Details of tests in this study

Test No.	Vertical Stress/MPa	Mass fraction of each particle size/ %				
		1 mm	2 mm	2.5 mm	3 mm	5 mm
UCS5	3.2	0	0	0	0	100
UCS3	3.2	0	0	0	100	0
UCS2.5	3.2	0	0	100	0	0
UCS2	3.2	0	100	0	0	0
NCS1	3.2	0	25	25	25	25
NCS2	3.2	0	14.3	14.3	14.3	57.1
NCS3	3.2	0	57.1	14.3	14.3	14.3
NCS4	3.2	0	0	42.9	0	57.1
NCS5	3.2	0	28.6	0	28.6	42.8
NCS6	3.2	0	0	0	50	50
NCS7	3.2	20	20	20	20	20

The specimens were compressed in high-pressure consolidation apparatus as shown in Figure 4.1. The inside diameter and height of wreath knife is 6.18 cm and 2 cm respectively. Each specimen has the same mass to ensure the same initial void ratio e_0. To make calcareous sand break completely, the maximum vertical stress of the apparatus (3.2 MPa) was applied. Since the main concern of this study is about the breakage matrix and the e-logσ_v relationship is not the focus of this study, we applied the stress by a single loading instead of multilevel loading. When the change of the dial indicator less than 0.01 mm/hour, the breakage is considered stable and the test can be stopped. A series of sieving tests were carried out for the specimens after breakage. The results and analyses are shown in the following section.

Figure 4.1: Schematic view of consolidation apparatus

4.4 Test and validation and analyses

Five sieve size classes mean the breakage matrix is a 5×5 matrix. Each row in the matrix represents the breakage distribution of the each size class. For a uniformly graded particles (D = 5 mm), the value of t_{51}-t_{55} can be obtained by the compression test no. UCS5 as shown in Figure 4.2. As for the particles with the finest size, since there is no further breakage as assumed before, the value of t_{11} should be 1.

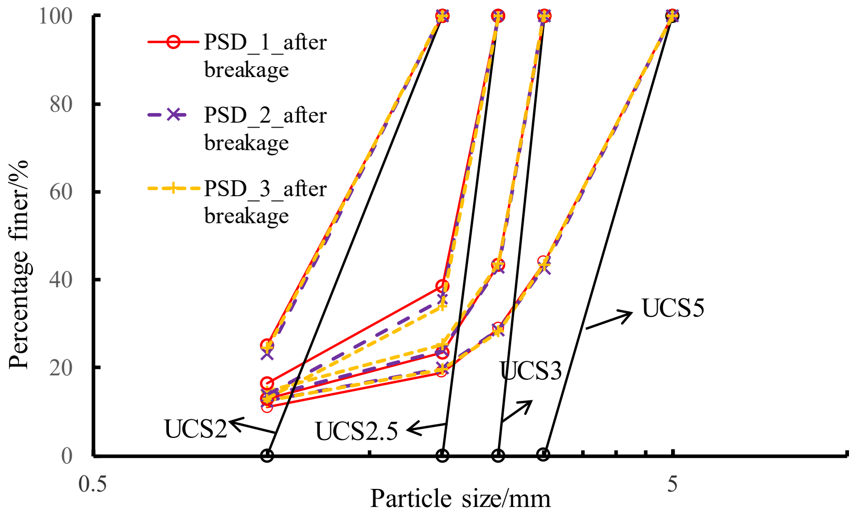

Figure 4.2: PSDs of uniformly graded samples before and after breakage

Figure 4.2 shows that there is no significant difference between three PSDs after breakage for uniformly graded sample with different particle size class, which means the repeatability of the tests is good and the test results are reliable. The breakage matrix $\boldsymbol{T}_{m1}$, $\boldsymbol{T}_{m2}$, $\boldsymbol{T}_{m3}$, obtained from the first to third experiment (as shown in Figure 4.2) can be written as:

$$\boldsymbol{T}_{m1} = \begin{bmatrix} 1 & 0 & 0 & 0 & 0 \\ 0.251 & 0.749 & 0 & 0 & 0 \\ 0.166 & 0.219 & 0.615 & 0 & 0 \\ 0.130 & 0.104 & 0.199 & 0.568 & 0 \\ 0.110 & 0.079 & 0.101 & 0.150 & 0.560 \end{bmatrix} \tag{4.4}$$

$$\boldsymbol{T}_{m2} = \begin{bmatrix} 1 & 0 & 0 & 0 & 0 \\ 0.231 & 0.769 & 0 & 0 & 0 \\ 0.139 & 0.217 & 0.644 & 0 & 0 \\ 0.137 & 0.103 & 0.189 & 0.571 & 0 \\ 0.125 & 0.074 & 0.088 & 0.140 & 0.573 \end{bmatrix} \tag{4.5}$$

$$\boldsymbol{T}_{m3} = \begin{bmatrix} 1 & 0 & 0 & 0 & 0 \\ 0.245 & 0.755 & 0 & 0 & 0 \\ 0.13 & 0.209 & 0.661 & 0 & 0 \\ 0.146 & 0.107 & 0.184 & 0.563 & 0 \\ 0.125 & 0.072 & 0.086 & 0.152 & 0.565 \end{bmatrix} \tag{4.6}$$

Seven specimens with different mass fraction of each particle size are compressed at the same conditions with the previous tests for determining breakage matrix.

Case 1: the specimen with test no. NCS1, the row vector $\boldsymbol{f}$ can be written as $\boldsymbol{f}_1$= [0 25% 25% 25% 25%], the three output row vectors of PSD $\boldsymbol{p}_{1\_1}$, $\boldsymbol{p}_{1\_2}$, $\boldsymbol{p}_{1\_3}$ can be obtained by Equation (4.2) and three breakage matrix $\boldsymbol{T}_{m1}$, $\boldsymbol{T}_{m2}$, $\boldsymbol{T}_{m3}$:

$$\boldsymbol{p}_{1\_1} = \boldsymbol{f}_1.\boldsymbol{T}_{m1} = [16.4\% \quad 28.8\% \quad 22.9\% \quad 18.0\% \quad 14.0\%] \tag{4.7}$$

$$\boldsymbol{p}_{1\_2} = \boldsymbol{f}_1.\boldsymbol{T}_{m2} = [15.8\% \quad 29.1\% \quad 23.0\% \quad 17.8\% \quad 14.3\%] \tag{4.8}$$

$$\boldsymbol{p}_{1\_3} = \boldsymbol{f}_1.\boldsymbol{T}_{m3} = [16.2\% \quad 28.6\% \quad 23.3\% \quad 17.9\% \quad 14.1\%] \tag{4.9}$$

The three calculated output of PSDs with three breakage matrices after breakage are compared with measured values as shown in Figure 4.3.

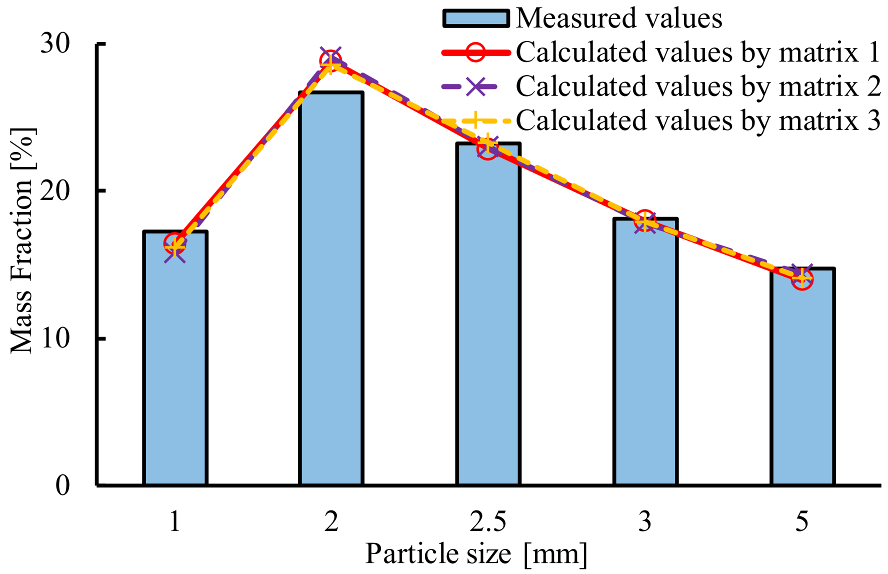

Figure 4.3: The comparison of three calculated PSDs and measured values

Figure 4.3 illustrates that the calculated PSDs have a general good agreement with the measured ones, which indicates that breakage matrix model is promising to predict PSD, although the breakage matrix needs to be known for a specific loading condition in this study. It can also be seen from Figure 4.3 that there is little difference between the three calculated PSDs because of the little difference in breakage matrix. Thus, the average breakage matrix $\boldsymbol{T}_m$ of calcareous sand with a given sieve class (1 mm, 2 mm, 2.5 mm, 3 mm, 5 mm) at a specific vertical stress (3.2 MPa) can be obtained:

$$\boldsymbol{T}_m = \frac{1}{3}(\boldsymbol{T}_{m1} + \boldsymbol{T}_{m2} + \boldsymbol{T}_{m2}) = \begin{bmatrix} 1 & 0 & 0 & 0 & 0 \\ 0.242 & 0.758 & 0 & 0 & 0 \\ 0.145 & 0.215 & 0.64 & 0 & 0 \\ 0.138 & 0.105 & 0.191 & 0.567 & 0 \\ 0.120 & 0.075 & 0.092 & 0.147 & 0.566 \end{bmatrix} \tag{4.10}$$

Case 2-Case 7: the specimen with test no. NCS2-test no. NCS7, the row vector $\boldsymbol{f}$ can be written as: $\boldsymbol{f}_2$= [0 14.3% 14.3% 14.3% 57.1%], $\boldsymbol{f}_3$= [0 57.1% 14.3% 14.3% 14.3%], $\boldsymbol{f}_4$= [0 0 42.9% 0 57.1%], $\boldsymbol{f}_5$= [0 28.6% 0 28.6% 42.8%], $\boldsymbol{f}_6$= [0 0 0 50% 50%], $\boldsymbol{f}_7$= [20% 20% 20% 20% 20%]; the calculated output of PSDs can be obtained by Equation (4.2) and average breakage matrix $\boldsymbol{T}_m$:

$$\boldsymbol{p}_2 = \boldsymbol{f}_2.\boldsymbol{T}_m = \begin{bmatrix} 14.2\% & 19.7\% & 17.1\% & 16.6\% & 32.4\% \end{bmatrix} \tag{4.11}$$

$$p_3 = f_3.T_m = [19.6\% \quad 48.9\% \quad 13.2\% \quad 10.2\% \quad 8.1\%] \tag{4.12}$$

$$p_4 = f_4.T_m = [12.9\% \quad 13.4\% \quad 32.8\% \quad 8.4\% \quad 32.4\%] \tag{4.13}$$

$$p_5 = f_5.T_m = [15.9\% \quad 27.8\% \quad 9.4\% \quad 22.5\% \quad 24.3\%] \tag{4.14}$$

$$p_6 = f_6.T_m = [12.8\% \quad 8.9\% \quad 14.2\% \quad 35.8\% \quad 28.4\%] \tag{4.15}$$

$$p_7 = f_7.T_m = [32.9\% \quad 23.0\% \quad 18.5\% \quad 14.3\% \quad 11.3\%] \tag{4.16}$$

The calculated and measured PSDs are plotted in Figure 4.4 - Figure 4.9. As shown in Figure 4.4 - Figure 4.9, the agreement between the calculated and measured PSDs is quite good.

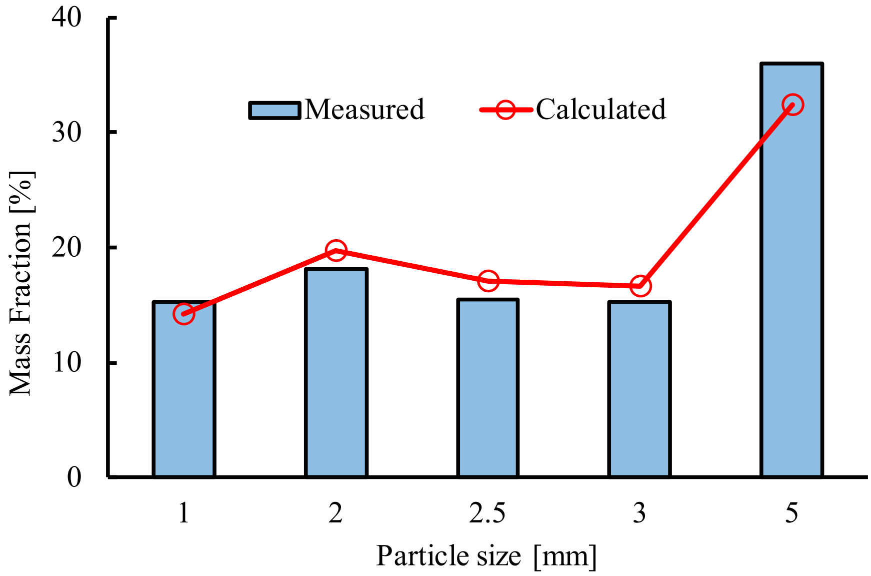

Figure 4.4: Comparison of calculated and measured PSD of test no. NCS2 specimen

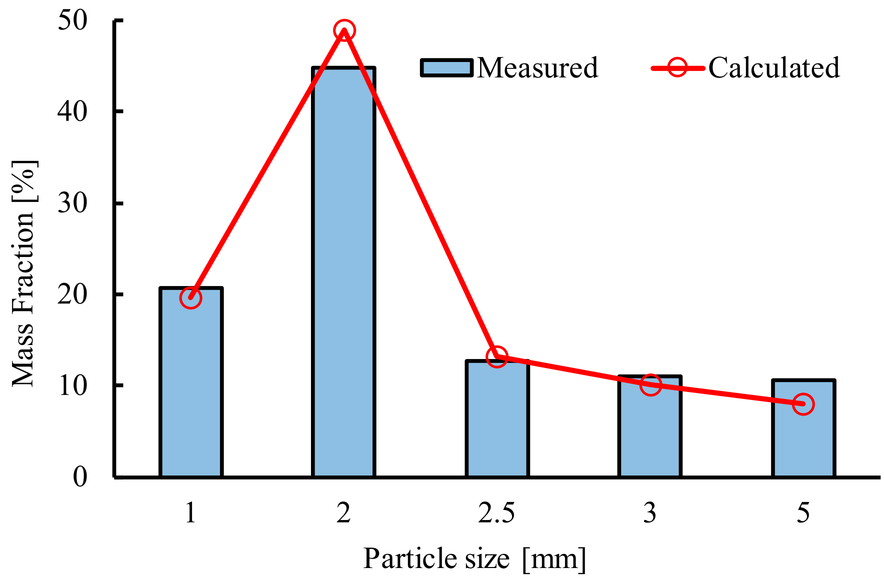

Figure 4.5: Comparison of calculated and measured PSD of test no. NCS3 specimen

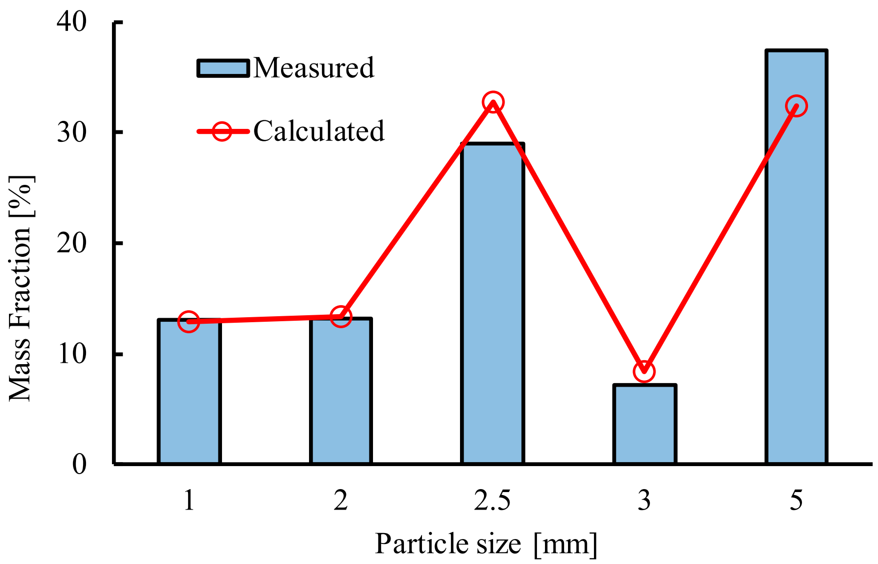

Figure 4.6: Comparison of calculated and measured PSD of test no. NCS4 specimen

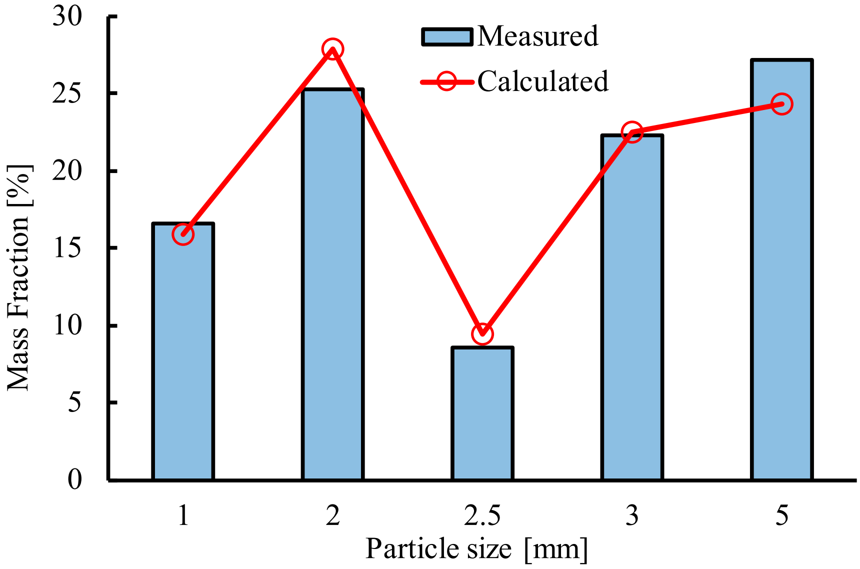

Figure 4.7: Comparison of calculated and measured PSD of test no. NCS5 specimen

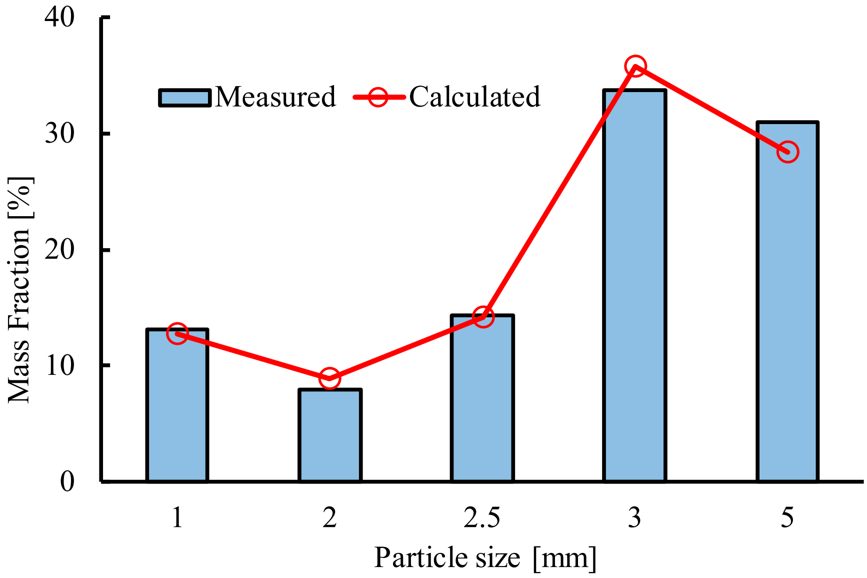

Figure 4.8: Comparison of calculated and measured PSD of test no. NCS6 specimen

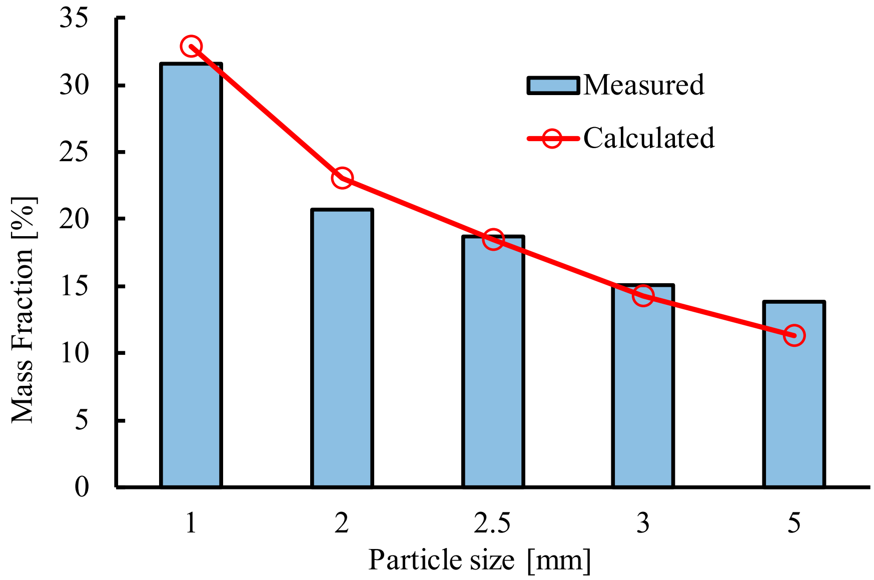

Figure 4.9: Comparison of calculated and measured PSD of test no. NCS7 specimen

Figure 4.3 - Figure 4.9 indicate that the method for determining breakage matrix by pre-separating the specimen into different size classes and testing the breakage behaviour individually for consisting each row of breakage matrix has approved to be appropriate to some extent, although there are still remaining problems, for example, the calculated mass fraction of coarsest particles are always lower than the measured values for all the cases in this study. This can be explained by the theory of coordination number that larger particles have higher coordination number and lower probability of failure of those particles (Muir Wood & Maeda, 2008).

4.5 Conclusions

A series of one-dimensional compression tests of calcareous sand were conducted to determine the breakage matrix straightforwardly. Firstly, non-uniformly graded specimen was separated into different uniformly graded samples. Then, those uniformly graded samples were tested and the breakage distribution of each size can be obtained. Finally, breakage distributions of all the size classes constitute the breakage matrix. Each row of the breakage matrix tells the details of breakage function and selection function of the each size class directly. The breakage matrix model is a promising method for simulating the evolution of particle breakage effectively.

The breakage matrix model also provides an alternative way for describing the evolution of particle loss which has the opposite evolution of PSD compared with that of particle breakage (Muir Wood, 2007, Muir Wood & Maeda, 2008, Muir Wood *et al.*, 2010) because of the 'magic form' of breakage matrix. That still needs further research.

List of symbols

PSD	particle size distribution
$\boldsymbol{p}$	row vector of the output PSD
$\boldsymbol{f}$	row vector of the input PSD
$\boldsymbol{T}_{\mathrm{m}}$	breakage matrix
t_{ij}	mass fraction of particle size interval i that falls into particle size interval j
p_i	mass fraction of particle size i after breakage
f_i	mass fraction of particle size i before breakage

Chapter 5 . A stochastic particle breakage model for granular soils subjected to one-dimensional compression with emphasis on the evolution of coordination

ABSTRACT: Prediction of the evolution of particle size distribution (PSD) is of great importance for studying particle breakage. This paper presents a stochastic approach, namely a Markov chain model, for predicting the evolution of PSD of granular materials during one-dimensional compression tests. The model requires the survival probability of each size group particles in an assembly, named as the survival probability matrix. The Weibull distribution is used to capture the particle size and particle strength effects of single particles. The evolution of the coordination number is investigated via 3D discrete element simulations. The proposed analytical form of survival probability matrix with consideration of the coupling effect of particle-scale factors (i.e., particle size, particle strength) and evolution of the coordination number during one-dimensional compression shows that the largest particles in an assembly do not always have the maximum breakage probability (or the minimum survival probability). This also confirms the dominant role of the coordination number on the balance of evolution of PSD within granular soils. The proposed model is validated against experimental data from one-dimensional compression tests on different granular materials. The limitations as well as possible future developments of the model are discussed.
Keywords: granular soil; particle size distribution; one-dimensional compression; coordination number; discrete element simulation; particle breakage

This chapter aims to solve the second key issue (i.e., breakage evolution law) with consideration of coordination number effect and is based on a paper published in the journal ***Computers and Geotechnics***:

Tong, C. X., *Zhang, K. F., Zhang, S., & Sheng, D. (2019a). A stochastic particle breakage model for granular soils subjected to one-dimensional compression with emphasis on the evolution of coordination number. Computers and Geotechnics, 112, 72-80.*

Authorship Declaration

By signing below I conform that for the journal paper titled 'A stochastic particle breakage model for granular soils subjected to one-dimensional compression with emphasis on the evolution of coordination number' and published by Computers and Geotechnics, that:

Chenxi Tong proposed the model, conducted the numerical analyses and wrote the manuscript.

Kenfen Zhang contributed to the numerical analyses

Sheng Zhang contributed to the discussion of the proposed model

Daichao Sheng is the leader of the research team, and assisted in the revision of the manuscript.

Production Note:

Signature removed
prior to publication.

Chenxi Tong

Kenfen Zhang

Prof Sheng Zhang

Prof Daichao Sheng

5.1 Introduction

Degradation of particle size is important in many fields, such as in chemical engineering, minerals processing, foods, pharmaceuticals, and geotechnical engineering. Particle breakage is manifested by the change in particle size distribution (PSD), due to mechanical forces, like shearing, compression or impact. In some cases, the change of PSD is intentional. For example, the PSD of processed wheat can be controlled by varying the characteristics (e.g. feed rate) of a roller mill (Campbell & Webb, 2001; Campbell *et al.*, 2001). In most geotechnical cases, however, the degradation of PSD is inadvertent and may be detrimental to performance. For example, degradation of railway ballast increases with train speeds and axle loads, which leads to settlement of the ballast, reduction of its permeability and increases maintenance costs (Indraratna *et al.*, 1997; Sun *et al.*, 2014a). Similarly, particle breakage deteriorates the mechanical and deformational response of other geomaterials, such as: carbonate sand (Bandini & Coop, 2011; Xiao *et al.*, 2016c; Xiao *et al.*, 2017; Tong *et al.*, 2019a), rockfill material (Ovalle *et al.*, 2014; Xiao *et al.*, 2014c; Tapias *et al.*, 2015; Xiao *et al.*, 2016b; Yin *et al.*, 2016), silica sand (Nakata *et al.*, 1999; Nakata *et al.*, 2001a; Hyodo *et al.*, 2017; Yu, 2017c), and to name a few.

Different methods for capturing the degradation process of PSD of geomaterials have been proposed during last decades, from laboratory investigation (Hardin, 1985; Hagerty *et al.*, 1993; Coop *et al.*, 2004; Zheng & Tannant, 2016; Tong *et al.*, 2018b; Tong *et al.*, 2019a) to discrete element simulations (Cheng *et al.*, 2003; Cheng *et al.*, 2004; Xu *et al.*, 2017; Zheng & Tannant, 2018; de Bono & McDowell, 2018). To some extent, experimental studies on particle breakage are usually based on post-mortem inspection, because the PSD can be obtained only at the end of the test, usually via sieving test. With the developments in high-tech measurement, X-ray CT-based (Zhao *et al.*, 2015; Guida *et al.*, 2018) and high-speed camera-based (Wang & Coop, 2016; Wang & Coop, 2018) methods are more frequently used to observe the whole breakage process. However, tracking individual particles inside a sample is time-consuming and costly, and is not easily available in most geotechnical laboratories.

Mathematical models can be of great benefit for describing the evolution of PSD because of the low computational cost and low requirements for test facilities (Caicedo *et al.*, 2016;

Tong *et al.*, 2018a). Nakata *et al.* (1999) proposed a statistical approach for estimating the survival probability of a single particle within the soil sample. They simplified the stress distribution within the sample and ignored the evolution of coordination number during compression and shearing, leading to an underestimated survival probability of particles. Marketos & Bolton (2007) proposed a probabilistic model for quantifying particle breakage of granular materials. They firstly obtained the distribution of normal contact force within a particle assembly and then simulated particle breakage with assumed breakage criterion. Based on their work, Zhou *et al.* (2014) and Cheng & Wang (2018) developed a probabilistic model with different breakage criteria and applied it to one-dimensional compression and biaxial shearing, respectively. Other mathematical models such as Markov chain model (Zhang *et al.*, 2015), population balance model (Ovalle *et al.*, 2016) and combined linear packing and Markov chain model (Caicedo *et al.*, 2016) were also proposed to estimate the evolution of PSD of granular soils subjected to different loading conditions successfully. The core idea of these models is trying to combine the inter-particle force distribution with particle-scale effects when calculating the survival probability (or breakage probability) of an individual particle or particles with the same size-class within the granular packing. The models mentioned above enrich the studies of the evolution of particle breakage. However, most of them only consider the particle-scale effects, but failed to consider the effects of an evolving of coordination number.

The coordination number and the particle size are considered as two of the most important factors affecting particle breakage. The particle-scale effects (including particle size and particle strength) are usually considered by employing the well-known Weibull distribution and will be introduced in the next section. The coordination number of a single particle is defined as the number of contact points with neighbouring particles, reflecting the geometrical structure characteristic in a granular system. The influence of coordination number on breakage characteristic of particles has been investigated by both experimental and numerical studies. Gundepudi *et al.* (1997) studied glass and alumina spheres under uniaxial compression (two-point), three, four and six-point compression, and found the maximum internal tensile strength decreased with increasing coordination number. According to the numerical study by Sukumaran *et al.* (2006), the crushing strength of particle increases as the coordination number increases. Similarly, Todisco *et al.* (2017) confirmed that an increase in the coordination number would lead to an increase in the critical stress threshold, i.e. failure stress of a single particle. Salami *et al.* (2015), Salami *et al.* (2017) found that both the coordinate number and contact positions influenced breakage properties of single particles by conducting a series of tests on cylindrical specimens. Those specimens with higher coordination number were harder to break.

In general, the survival probability of a single particle increases with increasing coordination number, but with decreasing particle size. These two factors (i.e., particle size and coordination number) play opposite roles in the evolution of PSD. They are competing through the whole breakage process, and finally, reach a dynamic balance when an ultimate PSD of a granular packing is observed (McDowell & Bolton, 1998). However, in a particle assembly, the coordination number of a single particle is dependent on its size and evolves with external loading, which makes it more difficult for modelling particle breakage. To date, however, these coupling effects are rarely considered and incorporated into a mathematical model for predicting PSD during breakage.

This paper follows on from our previous work (Zhang *et al.*, 2015) and aims to establish a new stochastic approach for predicting the evolution of particle breakage of granular soils subjected to one-dimensional compression, with emphasis on the evolution of coordination number. For simplicity, the effect of contact position on particle breakage is ignored and the average coordination number is used for representing the overall coordination number of particles with the same particle size. The basic concept of the Markov chain model is firstly introduced. The relationship between the particle size, the average coordination number of particles with the same size and the vertical stress is then investigated by using 3D discrete element simulations on uncrushable particles. After that, an analytical form of survival probability of particles within a particle assembly is deducted, with consideration of the coupled effects of particle size and coordination number. Finally, the proposed model is validated against experimental data of different granular soils subjected to one-dimensional compression tests.

5.2 Markov chain model

5.2.1 Basic concept

The process of particle breakage can be treated as a Markov chain if the breakage event is discretized into discrete state space and discrete time. The state space is formed by a set of discrete values of particle size since the evolution of particle size is the objective of this study. A granular soil sample contains particles between sieve size d_1 and d_n (subscript 1 represents the finest particles, subscript n represents the coarsest particles). Define a Markov chain model $\{X_n, n \in \mathbb{N}\}$, where $\mathbb{N} = \{1, 2, \cdots n\}$ is the discrete time set. The values of X_i form a countable set $\mathbb{R} = \{d_1, d_2, \cdots, d_n\}$ is called the state space. The memorylessness property of a Markov chain model can be expressed as:

$$P\{X_n = d_n / X_1 = d_1, \cdots, X_{n-1} = d_{n-1}\} = P\{X_n = d_n / X_{n-1} = d_{n-1}\} \tag{5.1}$$

where $P\{X_n = d_n / X_{n-1} = d_{n-1}\}$ is the conditional probability, which means the probability of particle size d_{n-1} at time n-1 breaking into particle size d_n at time n. This conditional probability is denoted as $P_{d_{n-1}d_n}(n)$ and simplified as $P_{n-1n}(n)$. In this paper, the degradation process of PSD is treated as one breakage event irrespective of the external loading. That is to say, only one load increment is considered, indicating the discrete time n is adopted as 1. In that case, time '0' means the initial state before particle breakage, and time '1' means the final state after particle breakage. The advantage of doing this is to avoid a more complex and non-homogeneous model, because the conditional probability P_{n-1n} (n) highly depends on current PSD and is variable with time n (or the number of load increment), and which will be discussed in details in **Section 5.4**. Noting that it is impossible for particles to break into a larger size, we have $P_{ij}(1)$ (simplified as P_{ij}) = 0 when $i < j$. The diagram of particle size transition is shown in Figure 5.1.

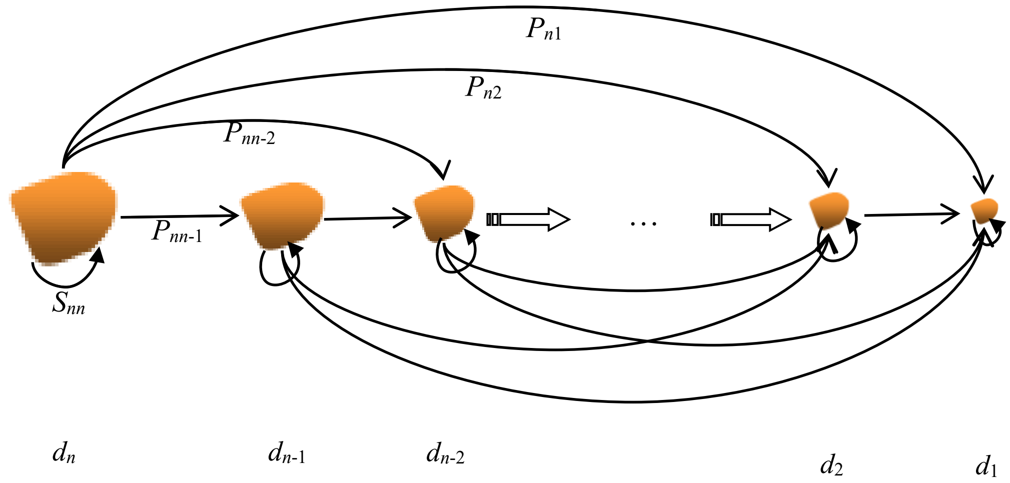

Figure 5.1: Diagram of particle size transition

As shown in Figure 5.1, the one-step transition probability matrix $\boldsymbol{P}$ composed of the conditional probability of particles with all the size-classes is a lower triangular matrix, which can be expressed as:

$$\boldsymbol{P} = \begin{bmatrix} S_{11} & 0 & \cdots & 0 \\ P_{21} & S_{22} & \cdots & 0 \\ \vdots & \vdots & \ddots & \vdots \\ P_{n1} & P_{n2} & \cdots & S_{nn} \end{bmatrix} \tag{5.2}$$

with

$$\begin{cases} P_{ij} \geq 0, \overset{n-1}{\underset{i=2}{S_{ii}}} \geq 0, S_{nn} > 0 \\ S_{11} = 1, \quad when\, i = 1 \\ \sum_{j=1}^{i-1} P_{ij} + S_{ii} = 1, \quad when\, i > 1 \end{cases} \tag{5.3}$$

where S_{ii} is the survival probability of d_i-sized particles as shown in Figure 5.1, and can be defined as:

$$S_{ii} = \frac{\text{Total mass of } d_i\text{-sized particles after loading}}{\text{Total mass of } d_i\text{-sized particles before loading}} \tag{5.4}$$

It is assumed that the finest particles will not break under external loading, indicating that S_{11} equals to 1. It is also commonly assumed that not all the largest particles will break completely, implying that $S_{nn} > 0$.

Define an initial probability vector $\boldsymbol{I}^T(0) = (X_1(0), X_2(0), X_3(0), \cdots)$ that represents the PSD before particle breakage (i.e., at time '0'), and an absolute probability vector $\boldsymbol{F}^T(1) = (X_1(1), X_2(1), X_3(1), \cdots)$ that represents the PSD after particle breakage (i.e., at time '1'), where $X_i(0)$ and $X_i(1)$ represent the mass percentage of d_i-sized particles before and after particle breakage, respectively. The relationship between $\boldsymbol{F}^T(1)$ and $\boldsymbol{I}^T(0)$ is given by:

$$\boldsymbol{F}^T(1) = \boldsymbol{I}^T(0)\boldsymbol{P} = \boldsymbol{I}^T(0)(\boldsymbol{S} + \boldsymbol{\beta} - \boldsymbol{S}.\boldsymbol{\beta}) \tag{5.5}$$

where $\boldsymbol{S}$ is the survival probability matrix and $\boldsymbol{\beta}$ is the crushing state matrix, which can be expressed as:

$$\boldsymbol{S} = \begin{bmatrix} S_{11} & & & \\ & S_{22} & & \\ & & \ddots & \\ & & & S_{nn} \end{bmatrix}, \boldsymbol{\beta} = \begin{bmatrix} 0 & 0 & \cdots & 0 \\ \beta_{21} & 0 & & \vdots \\ \vdots & \vdots & \ddots & 0 \\ \beta_{n1} & \beta_{n2} & \cdots & 0 \end{bmatrix} \tag{5.6}$$

where β_{kl} is defined as the coefficient of breakage probability, which represents the mass ratio between the d_l-sized particles breaking from the d_k-sized particles to the total mass breaking from d_k-sized particles. It can be calculated as suggested by Zhang *et al.* (2015):

$$\begin{cases} x_{ij} = \dfrac{d_j}{d_{i-1}} \\ F(x_{ij}) = 1 - e^{-\left[\frac{x_{ij}}{a(1-x_{ij})}\right]^b} \\ \beta_{kl} = F(x_{kl}) - F(x_{kl-1}), x_{k0} = 0 \\ \sum_{l=1}^{k-1} \beta_{kl} = 1, k = 2, 3, ..., i \end{cases} \tag{5.7}$$

where, x_{ij} is defined as the particle size ratio; $F(x_{ij})$ is the cumulative percentage of the total crushed mass, and it is a function of the particle size ratio, which should be distinguished from that of PSD; a is a scaling parameter and b is a shape parameter, and both of them can be obtained from the breakage tests on a uniformly graded sample. As can be seen from Equations (5.3) - (5.7), once the survival probability matrix of a sample is determined, the PSD after test can be obtained by using Equation (5.5). The survival probability of a single particle of a given size in a particle assembly will be discussed herein.

5.2.2 Survival probability of particles of a given size-class in a soil matrix

5.2.2.1 Breakage characteristics of a single particle

The survival probability of a brittle material of a given size d_i when subjected to a tensile stress of σ is widely considered to follow the Weibull distribution (Weibull, 1951):

$$S_{ii}(d_i,\sigma)=\exp\left[-\left(\frac{d_i}{d_0}\right)^3\left(\frac{\sigma}{\sigma_0}\right)^m\right] \tag{5.8}$$

where d_0 is the characteristic size, σ_0 is the characteristic stress at which 37% (=1/e, e is the natural logarithm) of particles of size d_0 will survive, m is the Weibull modulus.

Equation (5.8) is verified by extensive experimental data of a wide range of materials in the literature (Nakata *et al.*, 1999; McDowell & Amon, 2000; Lobo-Guerrero & Vallejo, 2006). It is worth noting that Equation (5.8) is applicable only when a single particle is crushed with two contact points in a uniaxial compression test as shown in Figure 5.2(a), which is analogous to the well-known Brazilian test. The tensile strength σ was found to be corresponding to the failure force F and the particle size d (defined as the distance between top and bottom plates as shown in Figure 5.2(a)), which was defined by Jaeger (1967):

$$\sigma=\frac{F}{d^2} \tag{5.9}$$

However, for the breakage of a single particle with multiple contacts as shown in Figure 5.2(b), the survival probability depends not only on the stress level but also on the coordination number. As mentioned before, a particle surrounded with more particles (i.e., a higher coordination number) will have a higher survival probability because of the larger critical stress threshold. In that case, Equation (5.8) can be modified as suggested by Ben-Nun & Einav (2010):

$$S_{ii}(d_i,\sigma)=\exp\left[-\left(\frac{d_i}{d_0}\right)^3\left(\frac{\sigma}{\sigma_0(C-1)\exp\left(\xi(C-2)(C-3)/4C\right)}\right)^m\right], C>1 \tag{5.10}$$

where C is the coordination number of the crushed particle, ξ is a particle shape factor. Setting $C=2$ in Equation (5.10) recovers the survival probability of a single particle with two-point compression as shown in Equation (5.8).

Equation (5.10) is the survival probability of a single particle when considering the effect of coordination number. In order to calculate the survival probability of each single particle in a particle assembly as shown in Figure 5.2(c), three key issues are needed to be considered: (1) the relationship between force acting on a single particle and the external loading acting on the sample, (2) the distribution of coordination number for particles with different size-classes, and (3) how the coordination number evolves with increasing vertical stress.

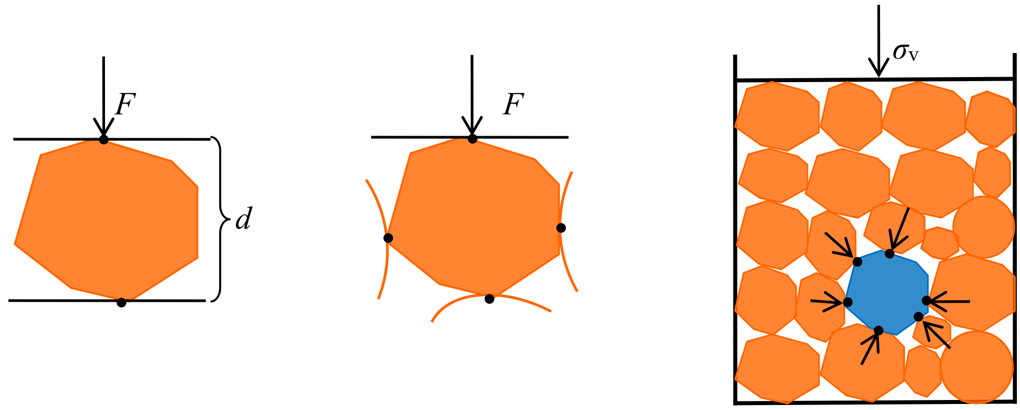

Figure 5.2: Illustration of different contacts of single particle: (a) two contacts of a single particle; (b) multiple contacts of a single particle; (c) multiple contacts of a single particle from a particle assembly

5.2.2.2 Particle breakage characteristics within a particle assembly

Nakata *et al.* (1999) proposed a simplified method to correlate the stress acting on a single particle in a soil matrix and the external loading acting on the soil sample, which takes the following form:

$$\sigma = \sigma_{\text{sample}} \left[\frac{(1+e_0)\pi}{6} \right]^{\frac{2}{3}} = 0.65\sigma_{\text{sample}} (1+e_0)^{\frac{2}{3}} \tag{5.11}$$

where σ_{sample} is the maximum principal stress σ_1 in the triaxial compression as stated by Nakata *et al.* (1999). For the one-dimensional compression test, σ_{sample} is simplified as the vertical stress σ_v in this paper, and e_0 is the initial void ratio of sample. Substituting Equation (5.11) in Equation (5.10) gives the average survival probability of d_i-sized particles in a soil matrix:

$$\widetilde{S_{ii}}(d_i,\sigma_\mathrm{v})=\exp\left[-\left(\frac{d_i}{d_0}\right)^3\left(\frac{0.65\sigma_\mathrm{v}(1+e_0)^{2/3}}{\sigma_0(\widetilde{C_i}-1)\exp\left(\xi(\widetilde{C_i}-2)(\widetilde{C_i}-3)/4\widetilde{C_i}\right)}\right)^m\right] \quad (5.12)$$

where, $\widetilde{S_{ii}}(d_i,\sigma_\mathrm{v})$ is the average survival probability of d_i-sized particles when subjected to vertical stress of σ_v; and $\widetilde{C_i}$ is the average coordination number of d_i-sized particles, which is defined as:

$$\widetilde{C_i}=\frac{\sum_{j=1}^{N}C_{ij}}{N} \quad (5.13)$$

where C_{ij} is the coordination number of the j-th particle with d_i size, N is the total number of d_i-sized particles.

As assumed before, no further breakage occurs for the minimum-sized particles. Equation (5.12) can then be modified as:

$$\widetilde{S_{ii}}(d_i,\sigma_\mathrm{v})=\exp\left[-\left(\frac{d_i}{d_0}\right)^3\left(\frac{0.65\sigma_\mathrm{v}(1+e_0)^{2/3}(\widetilde{C_i}-\widetilde{C_{\min}})}{\sigma_0(\widetilde{C_i}-1)(\widetilde{C_i}-\widetilde{C_{\min}}+1)\exp\left(\xi(\widetilde{C_i}-2)(\widetilde{C_i}-3)/4\widetilde{C_i}\right)}\right)^m\right]$$

(5.14)

where $\widetilde{C_{\min}}$ is the average coordination number of the minimum-sized particles. The average survival probability of the minimum-sized particles: $\widetilde{S_{11}}(d_1,\sigma_\mathrm{v})=\widetilde{S_{ii}}(d_i,\sigma_\mathrm{v})/_{\widetilde{C_i}=\widetilde{C_{\min}}}=1$.

5.2.2.3 Relationship between $\widetilde{C_i}$ and d_i & σ_v via discrete element simulations

It should be noted that the value of $\widetilde{C_i}$ is highly dependent on both particle size d_i and external stress σ_v in one-dimensional compression. For example, $\widetilde{C_i}$ increases with increasing d_i as reported by discrete element simulation by others (Muir Wood & Maeda, 2008; Nguyen *et al.*, 2015; de Bono & McDowell, 2016). To understand the particle-scale statistical distribution of the coordination number and to incorporate the coupling effects of $\widetilde{C_i}$, d_i and σ_v into the survival probability matrix of a soil sample subjected to one-dimensional compression, several one-dimensional compression tests on uncrushable granular sphere particles were performed using 3D discrete element simulations (PFC^{3D}, Itasca, 2018). The reason that we choose a 3D approach is because it is more realistic than a 2D approach for a real soil sample. A 3D approach can provide the spatial distribution information, while 2D can only provide the planar distribution information of a soil sample. Although the relation between the average coordination number and particle size has been proved linear for both 3D and 2D approach (see below for details), the average coordination number for a 3D approach should be much larger than that of a 2D approach.

All the samples tested are 90 mm in diameter and 30 mm in height and with different uniform gradings. The initial void ratio for all samples is about 0.67. The particle size span $R_D=d_{max}/d_{min}$ (where, d_{max} is the maximum particle size, and d_{min} is the minimum particle size) varies from 1.2 to 7.5 as shown in Figure 5.3(a)-(b). For computational efficiency, the minimum particle size d_{min} for all the 3D discrete element simulations is set to be no less than 1.5 mm, resulting in the number of spherical particles ranging from 1500 to 9390. During the test, the sample was confined by the cylindrical wall and was subjected to a the vertical compression by moving the top and bottom plates towards each other at a constant rate of 5 mm/s until the vertical strain reaches approximately 23% to 32%. The vertical stresses, ranging from 100 kPa to up to 500 MPa, as well as the corresponding distributions of the coordination number were recorded and input at each certain vertical strain for each test. The parameters used in the simulations are given in Table 5.1.

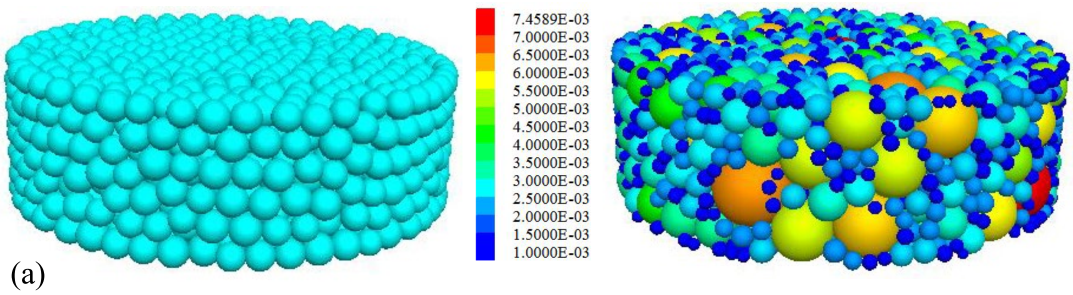

(a)

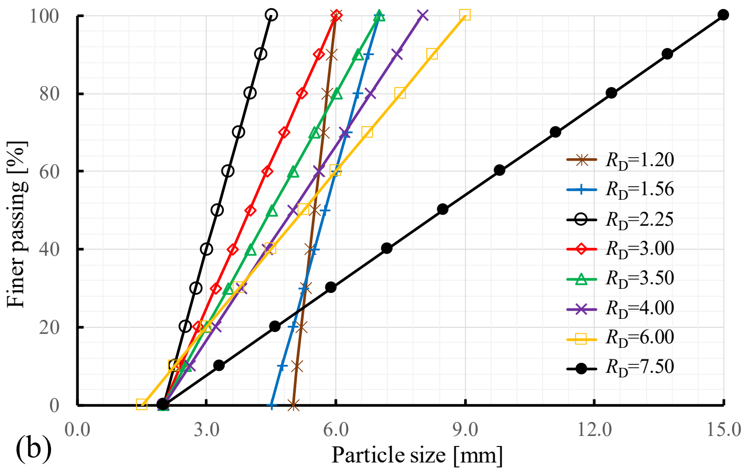

(b)

Figure 5.3 (a): 3D discrete element simulation samples: R_{D}=1.2 (left sample), and R_{D}=7.5 (right sample); (b): Initial gradings with different size span used in discrete element simulations

Table 5.1. Parameters for all the discrete element simulations

Parameters	Value
Contact model	Hertz contact model
Particle density (kg/m^3)	2650
Interparticle friction coefficient	0.577
Particle shear stiffness (N/m)	3.0×10^9
Particle passion ratio	0.3
Particle-wall friction coefficient	0
Damping coefficient	0.7
Wall normal stiffness (N/m)	1.5×10^{14}

Figure 5.4 shows a nearly linear relationship between the normalized average coordination number $\widetilde{C_i}/\widetilde{C_{\max}}$ and the particle size index I_{d} [= $(d-d_{\min})$ / $(d_{\max}-d_{\min})$] during varying vertical stress for different values of particle size span R_{D}. The slope of the line depends on the initial value of R_{D}. However, for the same initial value of R_{D}, such a linear relationship seems to be independent of the vertical stress, as shown in Figure 5.4. This is similar to the founding by Nguyen *et al.* (2015), who used a 2D discrete element approach and found the average coordination number $\widetilde{C_i}$ was as a nearly linear function of the particle size index I_{d}:

$$\frac{\widetilde{C_i}}{\widetilde{C_{\max}}} = A \times I_{\mathrm{d}} + B \tag{5.15}$$

where B is the normalized average coordination number of the minimum-sized particles ($I_d = 0$), and (A+B) is the normalized average coordination number of the maximum-sized particles ($I_d = 1$), i.e., A+B=1. $\widetilde{C_{max}}$ is the average coordination number of the maximum-sized particles.

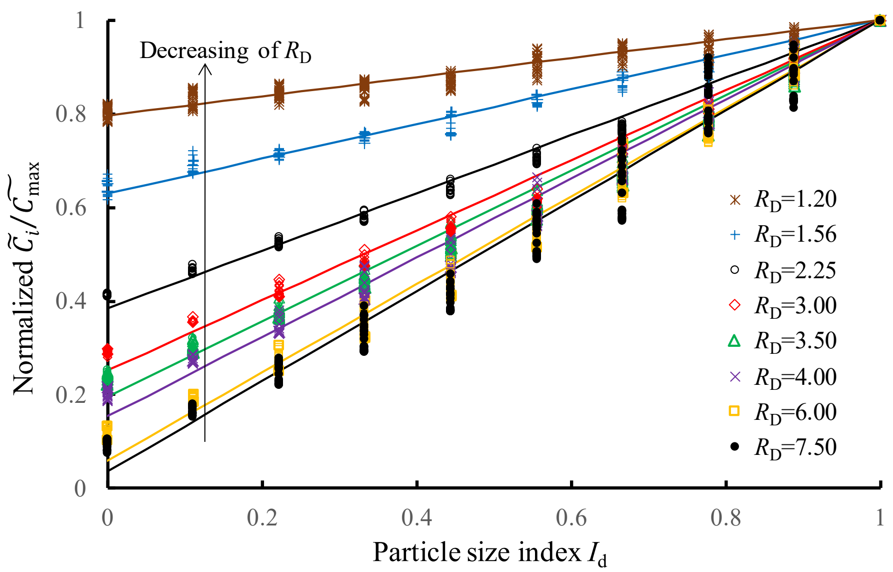

Figure 5.4: Relationship between particle size index I_d and normalized average coordination number $\widetilde{C}_i/\widetilde{C_{max}}$.

As obtained from Figure 5.4, the values of parameter A are 0.20, 0.37, 0.62, 0.75, 0.80, 0.85, 0.94 and 0.96 for R_D = 1.20, 1.56, 2.25, 3.00, 3.50, 4.00, 6.00 and 7.50, respectively. As expected, the value of parameter B decreases with increasing R_D, which means the average coordination number tends to be more homogenous with decreasing R_D. Figure 5.5 shows the relationship between parameter A and particle size span R_D, which can be described by the following best fitting curve:

$$A = -0.024R_D^{\ 2} + 0.304R_D \tag{5.16}$$

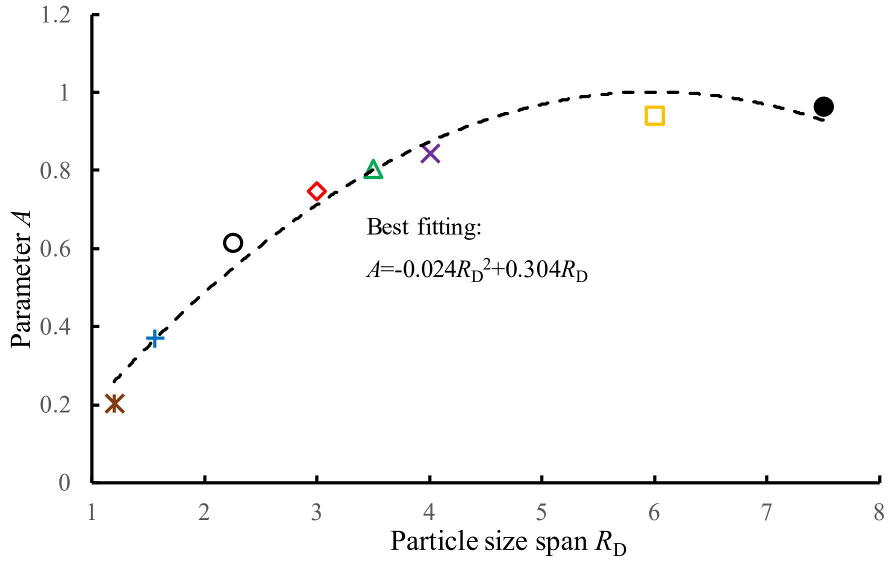

Figure 5.5: Relationship between particle size span R_D and parameter A

Figure 5.6 shows the evolution of $\widetilde{C_{\max}}$ with increasing vertical stress. The value of $\widetilde{C_{\max}}$ experiences a significant initial increases, and the increasing rate slows down as the vertical stress increases. The reason might be that the sample will densify in a short time as it changes from an initially isotropic state towards a K_0 state. However, when the sample is sufficiently dense, the change in the coordination number will slow down. This is similar to the observation reported by Shen *et al.* (2017). Furthermore, it is not surprising that the value of $\widetilde{C_{\max}}$ of a wider-graded sample (with larger R_D) is also larger than that of a more narrowly-graded sample under the same vertical stress. One possible form for correlating with the average coordination number of the maximum-sized particles and the applied vertical stress can be written as suggested by Shen *et al.* (2017):

$$\widetilde{C_{\max}} = \kappa_1 \left(\frac{\sigma_v}{p_a} \right)^{\kappa_2} \tag{5.17}$$

where κ_1 and κ_2 are R_D-dependent parameters as shown in Figure 5.7, p_a is the atmospheric pressure (≈ 100 kPa). The relationships between R_D and κ_1, and R_D and κ_2 can be fitted by a quadratic polynomial equation and a linear equation, respectively, as expressed by Equation (5.18).

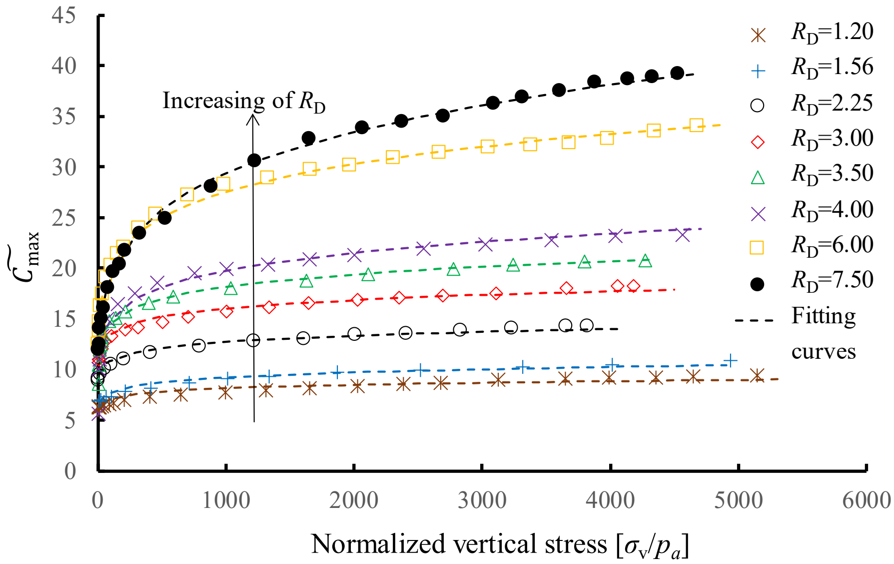

Figure 5.6: Evolution of $\widetilde{C_{max}}$ with normalized vertical stress

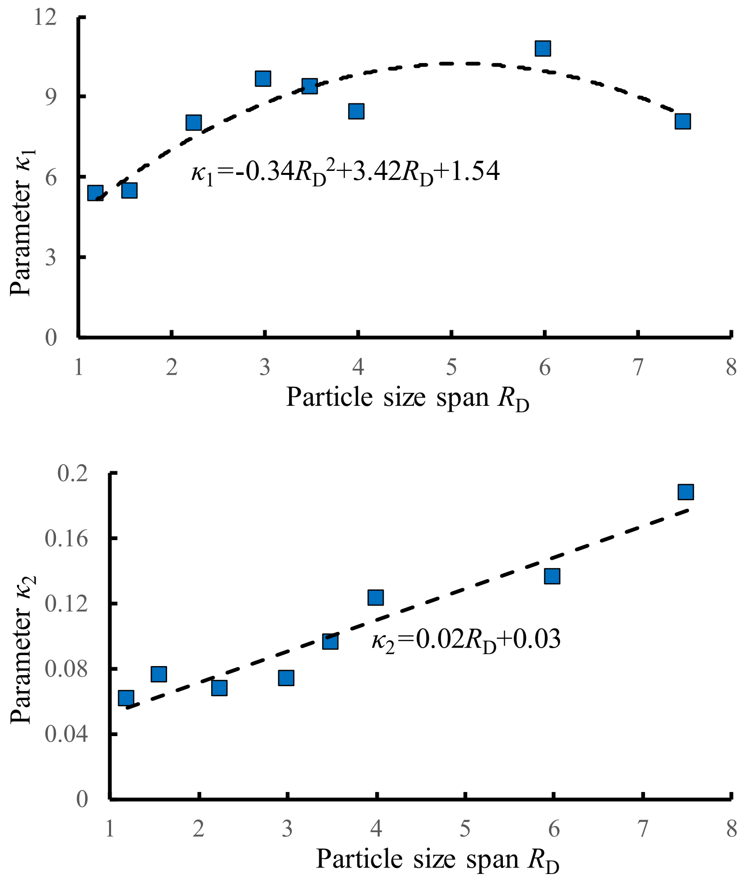

Figure 5.7: Relationship between particle size span R_D and parameters κ_1 & κ_2

$$\begin{cases} \kappa_1 = -0.34 R_D{}^2 + 3.42 R_D + 1.54 \\ \kappa_2 = 0.02 R_D + 0.03 \end{cases} \tag{5.18}$$

Substitution of Equations (5.15) - (5.18) into Equation (5.14) gives the relationship between the average survival probability, the particle size index and the vertical stress:

$$\begin{cases} \widetilde{S_{ii}}(I_{\mathrm{d}}, \sigma_{\mathrm{v}}) = \exp\left[-\left(\dfrac{\left(d_{\max} - d_{\min}\right) I_{\mathrm{d}} + d_{\min}}{d_0} \right)^3 \times \left(\dfrac{0.65\sigma_{\mathrm{v}}(1+e_0)^{2/3}(\widetilde{C_i} - \widetilde{C_{\min}})}{\sigma_0(\widetilde{C_i} - 1)(\widetilde{C_i} - \widetilde{C_{\min}} + 1)\exp\left(\xi(\widetilde{C_i} - 2)(\widetilde{C_i} - 3)/4\widetilde{C_i}\right)} \right)^m \right] \\ \widetilde{C_i} = \left[\left(-0.024R_{\mathrm{D}}^2 + 0.304R_{\mathrm{D}}\right) I_{\mathrm{d}} + 0.024R_{\mathrm{D}}^2 - 0.304R_{\mathrm{D}} + 1\right] \times \\ \left(-0.34R_{\mathrm{D}}^2 + 3.42R_{\mathrm{D}} + 1.54\right)\left(\dfrac{\sigma_{\mathrm{v}}}{p_{\mathrm{a}}}\right)^{(0.02R_{\mathrm{D}} + 0.03)} \end{cases} \tag{5.19}$$

It should be noted that the proposed model only consider the first breakage process or one breakage event as mentioned before. Equation (5.19) may not be appropriate when considering the second or subsequent breakage because of the changing particle arrangements and the consequent change of PSD. In that case, the failure force as defined in Equation (5.9) is adopted as the first breakage force of parent particles tested in the single-particle breakage test.

Figure 5.8 shows the theoretical simulations of the survival probability of particles with different sizes in a particle assembly during one-dimensional compression test using Equation (5.19). It is interesting noted that for a given vertical stress, the maximum-sized particles do not always have the minimum survival probability or the maximum breakage probability as indicated by the black solid circles in Figure 5.8(b). This is not in agreement with the breakage law for single particle, i.e. Equation (5.8), where the largest particles exhibit the lowest survival probability. It is commonly accepted that the PSD will tend to a non-uniform state (for example, fractal distributed state), which means not all the largest particles will break completely because of the balance between the effect of particle size and the effect of coordination number. The larger particles have more flaws and internal cracks, but have a larger coordination number and thus might survival with the protection of neighbouring particles, via the so-called cushion effect. While, the small particles are stronger because of fewer flaws and internal cracks, but have fewer particles surrounded. As also observed in the case of Figure 5.8(b), the maximum-sized particles have the minimum survival probability when the vertical stress is 5 MPa, indicating that particle size dominates over the coordinate number in the evolution of PSD. However, the particle size corresponding to the minimum survival probability decreases with increasing vertical stress as observed in Figure 5.8(b), which indicates that coordination number plays a more dominant role on the evolution of PSD with increasing vertical stress.

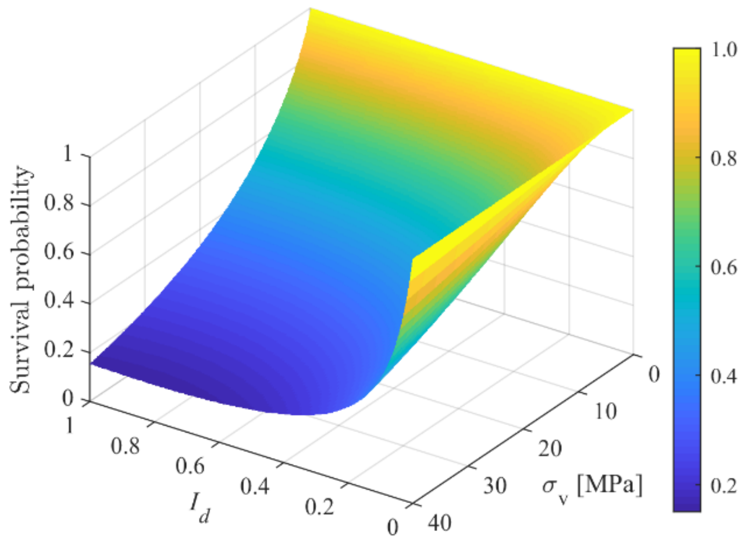

(a)

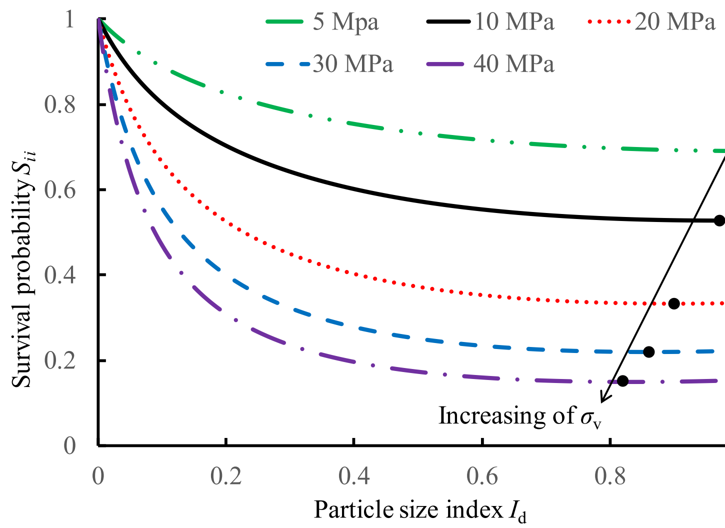

(b)

Figure 5.8: Relationship between survival probability, particle size I_d and the vertical stress σ_v, with $e_0 = 1.0$, $\xi = 1.0$, $m = 3.0$, $D_{max} = 4.0$ mm, $D_{min} = 2.0$ mm, $D_0 =3.0$ mm, $\sigma_0 =3.0$ MPa; (a) 3D view, (b) 2D view. Black solid circles represent the minimum survival probability point for each σ_v

Figure 5.9 shows the effects of particle size span R_D, the characteristic stress σ_0, the Weibull modulus m and the particle shape ξ on the survival probability of the maximum-sized particles (i.e., $I_d = 1$). For a well-graded sample, the maximum-sized particles have a higher coordination number as shown in Figure 5.4 and thus have a higher survival probability for given vertical stress as shown in Figure 5.9(a). Moreover, the survival probability increases with increasing σ_0 and ξ, but with decreasing m as shown in Figure 5.9(b)-5.9(d).

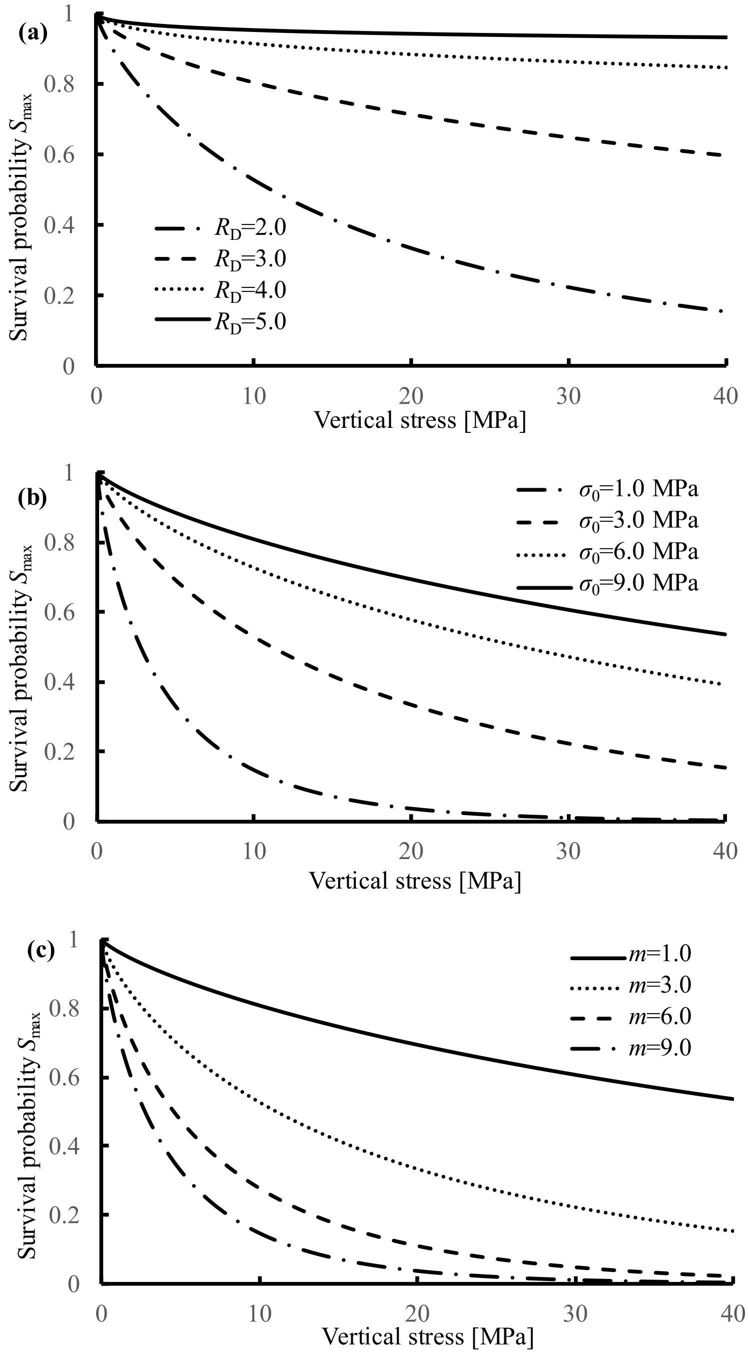

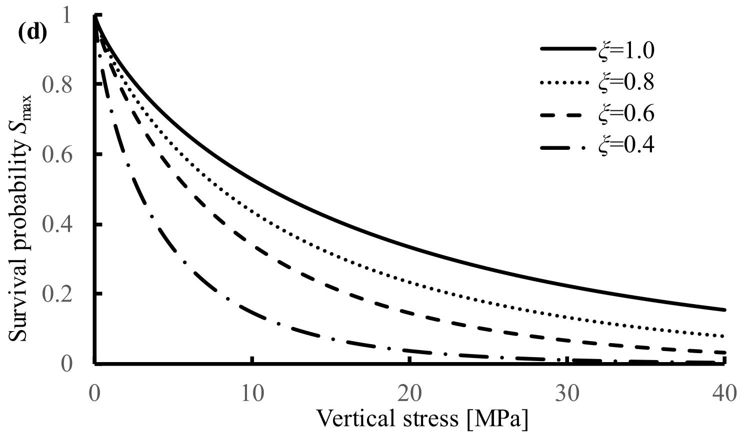

Figure 5.9: The evolution of survival probability of the maximum-sized particles in a particle assembly; (a) effect of R_D with fixed d_{max} = 4.0 mm, e_0=1.0, ξ=1.0, m=3.0, σ_0=3.0 MPa, d_0=3.0 mm; (b) effect of σ_0, e_0=1.0, ξ=1.0, D_{max}=4.0 mm, d_{min}=2.0 mm, m=3.0, d_0=3.0 mm; (c) effect of m, e_0=1.0, ξ=1.0, d_{max}=4.0 mm, d_{min}=2.0 mm, σ_0=3.0 MPa, d_0=3.0 mm; and (d) effect of ξ, e_0=1.0, d_{max}=4.0 mm, d_{min}=2.0 mm, m=3.0, σ_0=3.0 MPa, d_0=3.0 mm

5.3 Experimental Validation

In order to verify the model, experimental data of different granular materials in the literature were adopted, i.e., silica sand (Nakata *et al.*, 2001a), carbonate sand (Tong *et al.*, 2018b; Tong *et al.*, 2019a), and glass beads (Hagerty *et al.*, 1993).

5.3.1 Silica sand

A series of single-particle breakage tests and one-dimensional compression tests on silica sand were conducted by Nakata *et al.* (1999), Nakata *et al.* (2001a). The single-particle breakage tests indicated that the Weibull modules (m) of silica sand was 4.2 (Nakata *et al.*, 1999) and the characteristic stress (σ_0) was adopted as 18.5 MPa (Nakata *et al.*, 2001a). For the one-dimensional compression tests, samples were initial uniformly graded with d_{max} of 1.7 mm and d_{min} of 1.4 mm, which gives the value of R_D of 1.21. The particle shape parameter ξ was set to be 0.75 as a medium round particle. The sample with an initial void ratio of 0.67 was compressed at the vertical stresses ranging from 1.7 MPa to up to 92 MPa. The calculated PSDs during one-dimensional compression by the proposed model are shown as dotted lines in Figure 5.10. The comparison between the experimental data and calculations is reasonably good, especially the patterns.

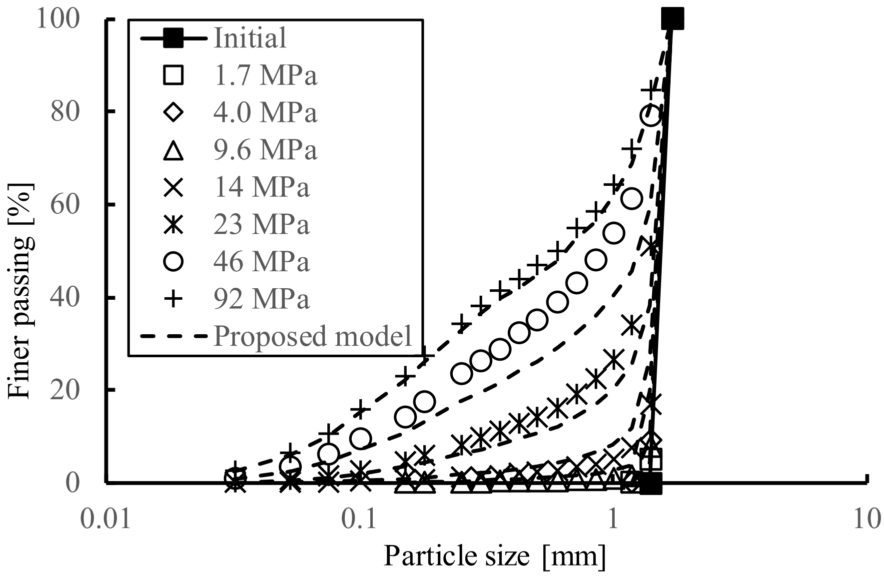

Figure 5.10: Measured (points) and calculated (dotted lines) PSDs in semi-logarithmic scale for silica sand under one-dimensional compression tests with ξ = 0.75, d_0 =1.5 mm, σ_0 =18.5 MPa

5.3.2 Carbonate sand

Tong *et al.* (2019a) conducted a series of one-dimensional compression tests on uniformly graded carbonate sand to investigate the evolving PSD with increasing vertical stress. The sample was initially uniformly graded with d_{max} of 1.18 mm and d_{min} of 0.6 mm, which gives the value of R_D of 1.97. Because no experimental breakage tests on individual carbonate sand were conducted, the Weibull modules (m) of carbonate sand cannot be determined directly. According to the extensive study on the values of m in the literature, materials such as feldspar, limestone, and carbonate have a m value of 1 to 3 (Ovalle *et al.*, 2014). In this paper, m of carbonate sand was adopted as 3.0, which is less than that of silica sand because of the smaller single-particle strength. The particle shape parameter ξ was set to 0.65 as a less round particle. The sample with an initial void ratio of 1.1 was compressed at the vertical stresses ranging from 2.0 MPa to 32 MPa. As shown in Figure 5.11(a), the proposed approach can capture the evolution of the PSD during one-dimensional compression very well.

Tong *et al.* (2018b) conducted one-dimensional compression tests at a fixed vertical stress (= 3.2 MPa) on different initial non-uniformly graded carbonate sand with the initial void ratio of 1.3. The initial particle size ranges from 1 mm to 5 mm for PSD1 and 2.5 mm to

5 mm for PSD2, indicating the value of R_D is 5 for PSD1 and 2.5 for PSD2, respectively as shown in Figure 5.11(b). The Weibull modules and the particle shape parameter are adopted as 3.0 and 0.65, respectively, as in the previous study. The characteristic size (d_0) and the characteristic stress (σ_0) for PSD1 are 2.5 mm and 2 MPa, respectively. While, d_0 of PSD2 is larger than that of PSD1 (= 4 mm), leading to a smaller value of σ_0 (= 1.2 MPa). As shown in Figure 5.11(b), the calculations of PSD for different initially non-uniformly graded samples are in good agreement with the measured PSDs.

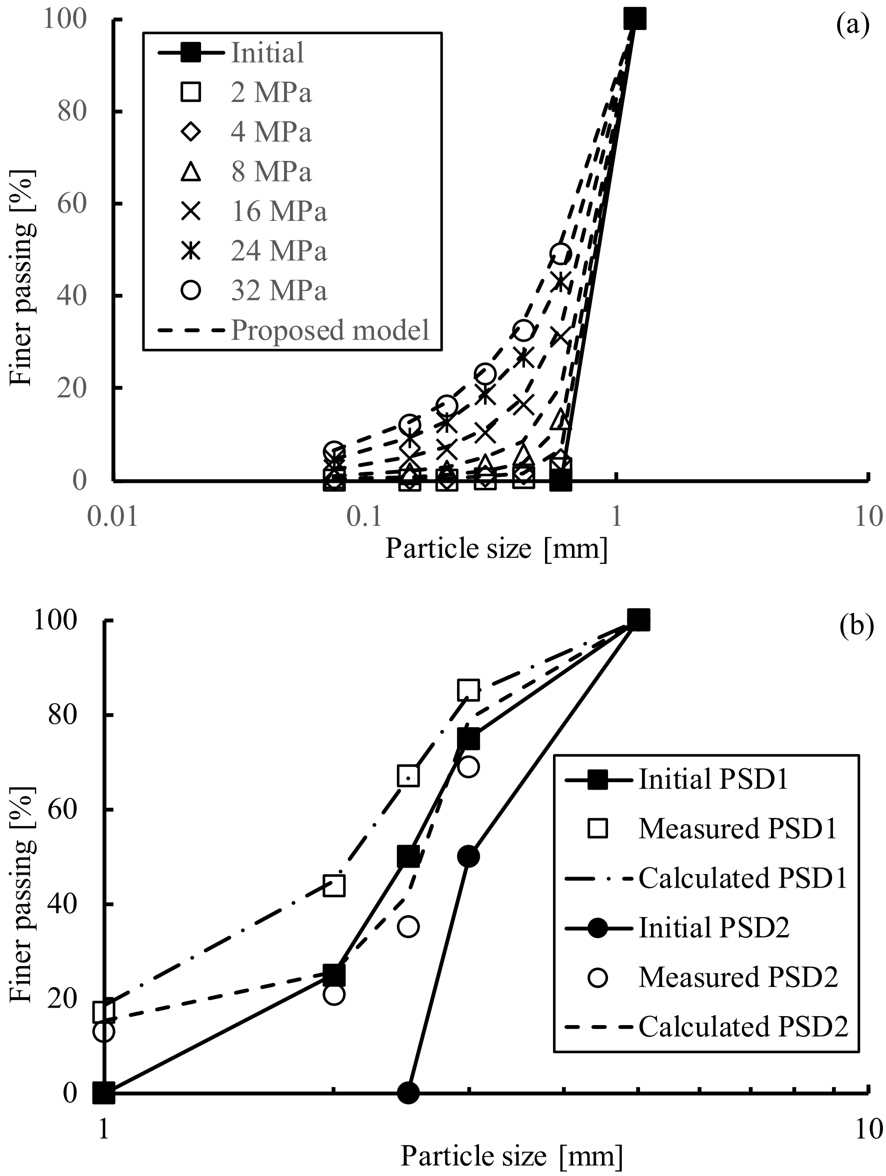

Figure 5.11: Measured (points) and calculated (dotted lines) PSDs in semi-logarithmic scale for carbonate sand under one-dimensional compression test with $\xi = 0.65$; (a) D_0 =1.0 mm, σ_0 =8.0 MPa; (b) D_0 =2.5 mm, σ_0 =2.0 MPa for PSD1 and D_0 =4.0 mm, σ_0 =1.2 MPa for PSD2

5.3.3 Glass beads

Hagerty *et al.* (1993) investigated the breakage property of glass beads at extremely high vertical stress (up to 689 MPa). The components of glass beads are of 72.5% silicon dioxide, 13.7% sodium oxide, 9.8% calcium oxide, 3.3% magnesium oxide, 0.4% aluminium oxide and 0.2% iron oxide. The maximum and minimum particle size is 0.84 mm and 0.6 mm, which means the value of $R_D = 1.4$. The Weibull modules (m) of glass beads was set to 8.0 according to the study by Takei *et al.* (2001), which is larger than silica sand because of the higher characteristic stress (σ_0) of 150 MPa. The glass beads are spherical in shape, leading to the particle shape parameter $\xi = 1.0$. Figure 5.12 shows the comparisons between the experimental data and the results calculated by the proposed model. The proposed model can simulate the evolving PSD well especially at the low and high vertical stresses. There are some discrepancies noted for the results at stress level of 345 MPa.

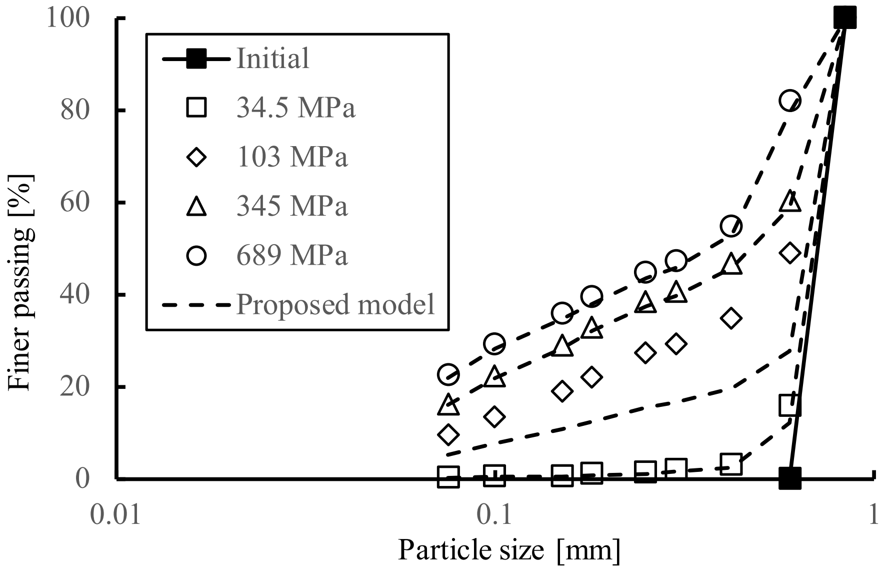

Figure 5.12: Measured (points) and calculated (dotted lines) PSDs in semi-logarithmic scale for glass beads under one-dimensional compression test with $\xi = 1.0$, d_0 =0.7 mm, σ_0 =150 MPa

5.4 Discussion and Limitations of the Model

The development and validation of the proposed theoretical model have been shown in the previous sections. The core of the model is to calculate the survival probabilities of particles with different sizes within a sample, which are expected to be dependent on many factors, i.e., particle-scale factors (mineralogy, strength, size, shape of a single particle), sample-scale factors (initial PSD, initial void ratio, spatial distribution of the coordination number, etc.), and external factors (load type, stress path, sample preparation method, water content, etc.). It should be noted that some factors are independent of others; while some are coupled. It is difficult or even impossible to tackle all these factors in the calculation of survival probability. In this paper, most particle-scale factors, sample-scale factors, and their coupling effects are considered as shown in Equation (5.19) when the sample is subjected to one-dimensional compression, which is the reason why the proposed model performs well in simulating the evolution of PSD. In theory, the proposed model also has potential application in other stress paths as long as the coupling effects of the average coordination number, particle size, and stress (strain) can be obtained via discrete element approach.

The major limitation of the proposed model is the limited range of initial PSD and the sphere particles adopted in the discrete element simulations. This limitation will result in the uncertainty in the applicability of the model when the sample is well graded and the particles are irregular. Although the particle shape factor is considered in a simplified form as shown in Equation (5.10), the influence of particle shape on the relations between $\widetilde{C}_i$, d_i and σ_v are not considered. The next phase of model development can focus on the coupling effect of particle shape on the survival probability of particles in a particle assembly.

Another limitation of the model comes from the assumption that the model considers only one breakage event, which in turn greatly simplifies the model. Actually, the proposed model has great potential to describe the multiple load increments. In that case, Equation (5.5) can be expressed as:

$$\boldsymbol{F}^T(t) = \boldsymbol{I}^T(0)\boldsymbol{P}^{(0)-(1)}\boldsymbol{P}^{(1)-(2)}\cdots\boldsymbol{P}^{(t-1)-(t)} \tag{5.20}$$

where $\boldsymbol{F}^T(t)$ is the PSD vector after t-th load increment, $\boldsymbol{P}^{(t-1)-(t)}$ is the one-step transition probability matrix for the t-th load increment. The survival probability for each load increment should be dependent on the 'initial' PSD, which, however, is determined by the 'final' PSD of previous load increment. Equation (5.20) may provide a framework for further study of the evolution of particle breakage when considering multiple breakage events.

5.5 Conclusions

In this paper, a stochastic-based approach, namely a Markov chain model is proposed with the aim of modelling the evolution of PSD of granular materials during one-dimensional compression tests. The survival probability of particles with different sizes in a particle assembly is captured by employing the Weibull distribution with emphasis on the evolution of coordination number obtained by using discrete element simulations on uncrushable sphere particles.

The discrete element simulations show that the normalised average coordination number displays a linear distribution in terms of the particle size index I_d, which is independent of vertical stress but dependent on initial particle size span R_D. The proposed approach confirms that the role of the coordination number is becoming more dominant with increasing vertical stress on the survival probability of particles. The proposed model was validated against experimental results of one-dimensional compression tests on different granular materials. It has been shown that the Markov chain model with consideration of both particle-scale effect and evolution of the coordination number is able to capture the evolution of PSD of geomaterials during particle breakage process.

List of symbols

D_i	particle size
$\mathbb{N}=\{1,2,\cdots n\}$	discrete time set
$\mathbb{R}=\{D_1,D_2,\cdots,D_n\}$	state space
P_{ij}	probability of particle size moving to D_i from D_j
$\boldsymbol{P}$	one-step transition probability matrix for one load increment
$\boldsymbol{P}^{(t\text{-}1)\text{-}(t)}$	one-step transition probability matrix for the t-th load increment
S_{ii} and $\widetilde{S}_{ii}$	survival probability and average survival probability of D_i-sized particles
$\boldsymbol{I}^T(0)$	PSD vector before breakage
$\boldsymbol{F}^T(1)$ and $\boldsymbol{F}^T(t)$	PSD vector after 1st breakage and t-th breakage
$X_i(0)$ and $X_i(1)$	mass percentage of D_i-sized particles before and after particle breakage
$\boldsymbol{S}$ and $\boldsymbol{\beta}$	survival probability matrix and crushing state matrix
β_{kl}	coefficient of breakage probability
x_{ij} and $F(x_{ij})$	particle size ratio and cumulative percentage of the total crushed mass
a and b	scaling parameter and shape parameter
D_0 and σ_0	characteristic size and characteristic stress
m	Weibull modulus
ξ	particle shape factor
e_0	initial void ratio of sample
C_{ij} and $\widetilde{C}_i$	coordination number of the j-th particle with D_i size and average coordination number of D_i-sized particles
σ_v	vertical stress applied on the sample
I_d and R_D	particle size index and particle size span
A and B	normalized average coordination number related parameters
κ_1 and κ_2	average coordination number of the maximum-sized particles related parameters

Chapter 6 . Particle breakage of uniformly graded carbonate sands in dry/wet condition subjected to compression/shear tests

ABSTRACT: The behaviour of a granular material is primarily affected by its particle size distribution (PSD), which is not necessarily a soil constant as assumed in traditional soil mechanics. The PSD may change over time due to mechanical as well as environmental actions. In this study, a series of ring shear tests and one-dimensional compression tests were completed on a carbonate sand, in both dry and saturated conditions. Samples were prepared with different initial uniform gradings, to investigate: (1) the influence of the saturation state and initial grading on mechanical and deformational behaviour of carbonate sands and, (2) the evolution of the PSD as a result of breakage. The ring shear tests show that the residual friction angle remains almost constant, but dilatancy reduces with increasing saturation degree. In the one-dimensional compression test, the yield stress decreases with increasing saturation degree, but the compressibility (as defined by C_c) remains almost constant, irrespective of the saturation state. Moreover, saturated samples suffer more breakage than dry samples during ring shear tests, while there is no obvious effect of saturation state on particle breakage in one-dimensional compression. A recently proposed PSD model with only two parameters (λ_p and κ_p) is employed to model the evolution of PSD, as it can more broadly capture the whole PSD throughout the breakage process than existing breakage indices. Test results demonstrate that parameter λ_p is linearly related to Einav's breakage index B_r^* and is dependent on initial grading, but independent of test mode. Parameter κ_p is in power relationship with B_r^*, and is independent of initial grading or test mode. The evolution of parameters λ_p and κ_p are related to the input work for both ring shear and compression tests, with λ_p being hyperbolically related to input work and κ_p in power relationship with input work. Using such an evolution law provides an alternative approach to capture the effects of particle breakage in constitutive models.

Keywords: Carbonate sands; particle breakage; particle size distribution (PSD); input work

*This chapter aims to solve the second key issue (i.e., breakage evolution law) via experimental observations and is based on a paper under review in the journal **Acta Geotechnica**:*

***Tong, C. X.**, Burton, G. J., Zhang, S., & Sheng, D. (2020a). Particle breakage of uniformly graded carbonate sands in dry/wet condition subjected to compression/shear tests. Acta Geotechnica. https://doi.org/10.1007/s11440-020-00931-x.*

Authorship Declaration

By signing below I conform that for the journal paper titled 'Particle breakage of uniformly graded carbonate sands in dry/wet condition subjected to compression/shear tests' and submitted to Acta Geotechnica, that:

Chenxi Tong conducted the tests and wrote the manuscript.

Glen J. Burton assisted in the discussion of the tests and revision of the manuscript.

Sheng Zhang contributed to the discussion of the tests and manuscript.

Daichao Sheng is the leader of the research team, and assisted in the revision of the manuscript.

Production Note:

Signature removed
prior to publication.

Chenxi Tong

Dr Glen J. Burton

Prof Sheng Zhang

Prof Daichao Sheng

6.1 Introduction

Particle breakage of carbonate sands has attracted significant attention, largely due to the increased number of offshore structures and their widespread distribution (Poulos, 1980). In comparison to silica-based sands, carbonate sands, where many offshore structures are constructed on, have a high friction angle but are more prone to break, which may have important consequences for the design and performance of geotechnical infrastructure. For example, the axial capacity reduced by up to 90% when a pile was driven into a calcareous sand deposit in the Bass Strait off Australia (Angemeer *et al.*, 1973). This reduction was thought to be due to particle breakage and a loss of lateral stress as a result of volume change. Particle breakage will greatly change the particle size distribution (PSD). Thus, knowing how PSD changes under various loading conditions and how such a change in PSD affects the mechanical and deformational behaviour is important to better understand and assess the potential hazards caused by particle breakage.

The mechanical and deformational behaviour of granular soils undergoing particle breakage have been investigated through a number of laboratory methods. These studies highlight the importance of mineralogy (Lee & Seed, 1967; Nakata *et al.*, 1999; Luzzani & Coop, 2002; Shahnazari & Rezvani, 2013), initial PSD (Nakata *et al.*, 2001a; Indraratna *et al.*, 2016), particle size (McDowell, 2002; Li *et al.*, 2017; Xiao *et al.*, 2018b), particle shape (Cho *et al.*, 2006; Xiao *et al.*, 2018a; Xiao *et al.*, 2019c; Zhao *et al.*, 2019), relative density (Altuhafi & Coop, 2011a; Hyodo *et al.*, 2017; Xiao *et al.*, 2017; Zhao *et al.*, 2019), stress path (Hardin, 1985; Ezaoui *et al.*, 2011), test mode (Altuhafi & Coop, 2011b; Miao & Airey, 2013; Nanda *et al.*, 2018; Xiao *et al.*, 2019b), sample preparation method (Sadrekarimi & Olson, 2010), microstructure (Cheng *et al.*, 2003; Bolton *et al.*, 2008; Ciantia *et al.*, 2019; Tong *et al.*, 2019b) and saturation state (Lee & Farhoomand, 1967; Miura & Yamanouchi, 1975; Ovalle *et al.*, 2015) on particle breakage. It is commonly accepted that liquid water induces corrosion at the tip of water-sensitive micro-cracks, triggering crack propagation (known as stress corrosion cracking phenomenon), and thus promote particle breakage of many granular soils, such as Antioch sand (Lee & Farhoomand, 1967), quartz-rich sand (Miura & Yamanouchi, 1975), quartzitic slate gravel (Oldecop & Alonso, 2007), decomposed granite soil (Ham *et al.*, 2010), shale quartzite sand (Ovalle *et al.*, 2015). These materials display micro flaws that exacerbate the extent of particle breakage. However, carbonate sands often have large inter-particle voids (e.g. visible to the naked eye), and the role of water on the compression/shear characteristics and the corresponding breakage is still not fully understood.

In this paper, three different uniform gradings of a carbonate sand have been tested in a series of ring shear and one-dimensional compression tests, in both dry and saturated conditions. The objective of this study is to investigate: (1) the influence of the saturation state and initial grading on the mechanical and deformational behaviour of carbonate sands, and (2) the evolution of PSD with breakage. These results are used to develop a unified and optimal evolution law of particle breakage of uniformly graded carbonate sand for different initial gradings and different type of tests. Two PSD parameters (i.e., λ_p and κ_p) of the newly proposed PSD model (Tong *et al.*, 2018a) are adopted as PSD indices for correlating to input work per unit volume. This evolution law is verified through the results of other carbonate sands in the literature.

6.2 Materials and tested procedures

6.2.1 Material tested

A commercially available carbonate sand was tested as part of this study. The mineral composition, as shown in Table 6.1, is almost pure calcium carbonate. The original material was sieved to produce samples with three different initial uniform gradings (0.3-0.425 mm, 0.425-0.6 mm and 0.6-1.18 mm) as shown in Figure 6.1 and Figure 6.2. Prior to testing, the sieved material was oven-dried (24h at 105°C). The specific gravity of carbonate sand was measured to be 2.80 by using an automated gas pycnometer (Micromeritics Autopyc II 1340 with an accuracy of 0.05%).

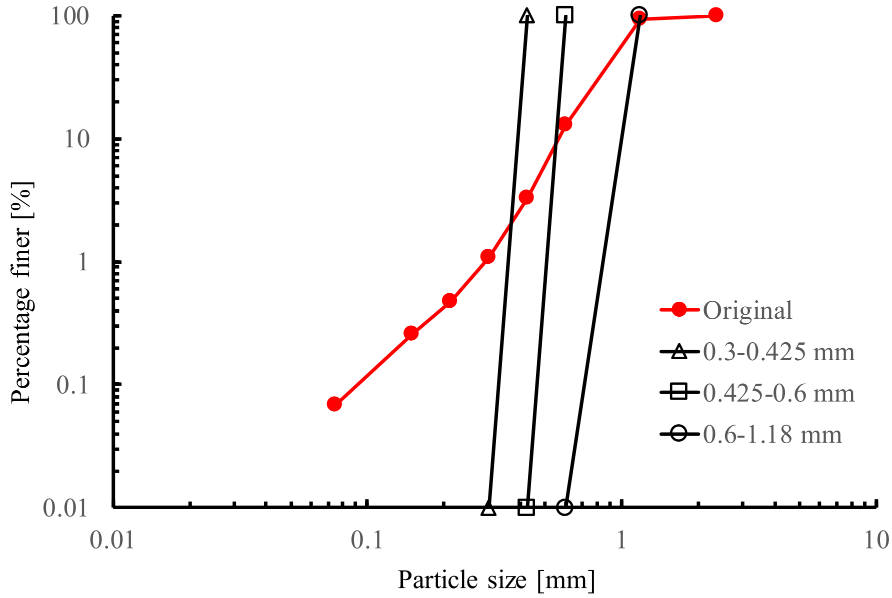

Figure 6.1: PSDs of original and three tested carbonate sands

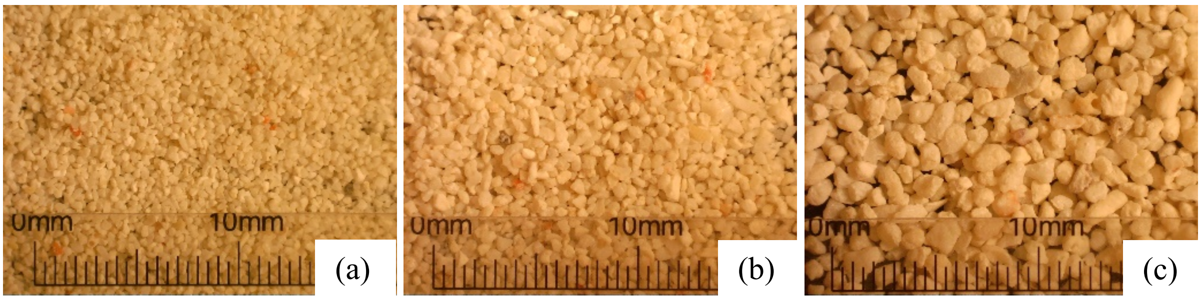

Figure 6.2: Micrographs of the three different gradings before test: (a) 0.3-0.425 mm; (b) 0.425-0.6 mm; (c) 0.6-1.18 mm

Table 6.1. Mineral composition of carbonate sand

Mineral composition	$CaCO_3$	SiO_2	MgO	Al_2O_3	SO_4	Fe_2O_3
Percentage	99.8%	0.07%	0.05%	0.05%	0.03%	40ppm

6.2.2 One-dimensional compression test with controlled strain rate

Samples were prepared for the strain rate controlled one-dimensional compression (60 mm in diameter and average 19.80 mm in height) by dry pluviation. The compression apparatus used in this paper is shown in Figure 6.3. The tests were carried out using a constant displacement rate of 1 mm/min to six target vertical stresses (2, 4, 8, 16, 24 and 32 MPa). The measured displacement was corrected for apparatus compliance. Saturated samples were prepared from an initially dry sample by percolating distilled water from the base of the sample at a small water pressure of 15-25 kPa until no air bubble was observed from the top. The sample is considered to be saturated when the volume of percolated water is about three times of the pore volume of the dry sample. Finally, the water pressure of 50 kPa was applied under an effective vertical stress equals to 1-5 kPa. Details of the one-dimensional compression tests are summarized in Table 6.2. After the test, the PSD of the saturated sample was analysed after oven drying (24h at 105°C).

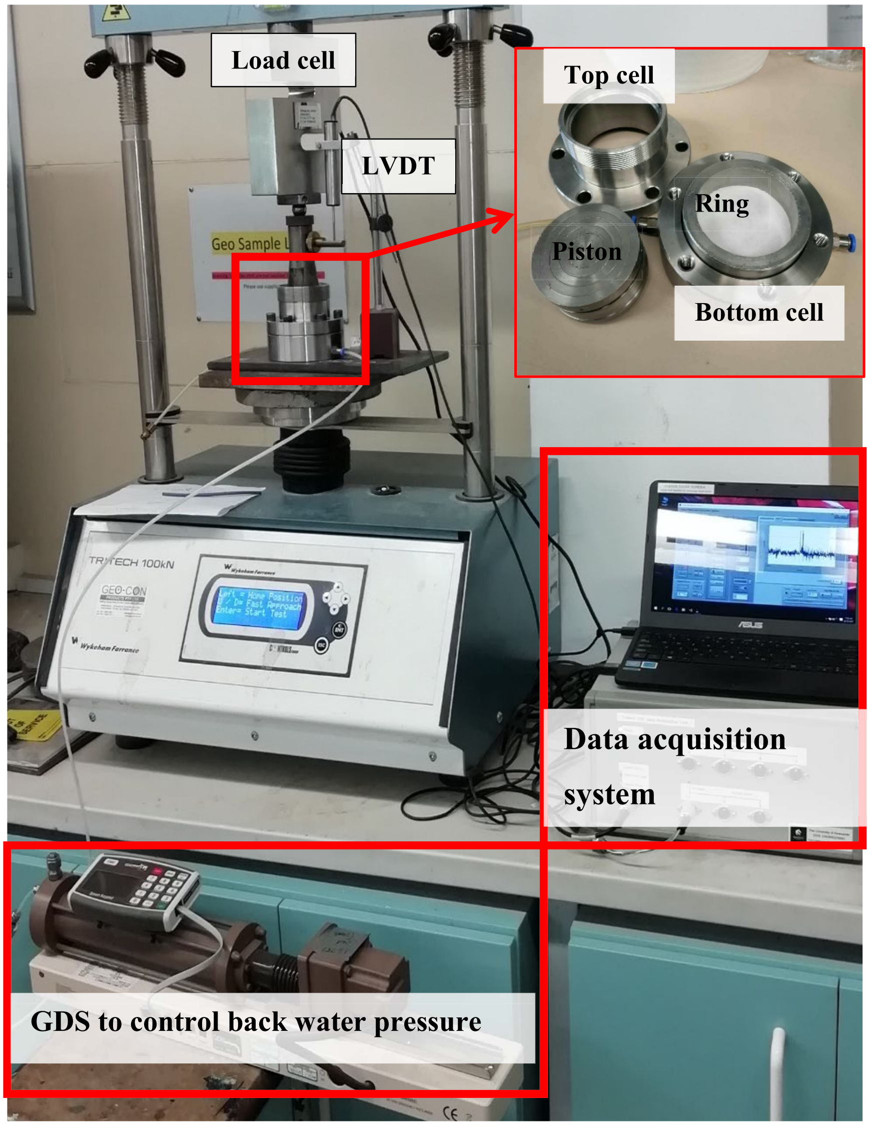

Figure 6.3: The one-dimensional compression apparatus. The LVDT (Solartron Metrology) has capacity of 15 mm, and the load cell (Kelba) has capacity of 10 t

Table 6.2. Details of strain rate controlled one-dimensional compression tests on initial uniformly graded samples

Test No.	Initial grading [mm]	Saturation state	Sample mass [g]	Initial void ratio e_0 [-]	Effective vertical stress [MPa]
OD1_1	0.6-1.18	Dry	74.48	1.099	2

OD1_2		Dry		1.096	4
OD1_3		Dry		1.097	8
OD1_4		Dry		1.094	16
OD1_4#		Saturation		1.106$^{\$}$	16
OD1_5		Dry		1.103	24
OD1_5#		Saturation		1.097$^{\$}$	24
OD1_6		Dry		1.105	32
OD1_6#		Saturation		1.106$^{\$}$	32
OD2_1		Dry		1.077	2
OD2_2		Dry		1.077	4
OD2_3		Dry		1.075	8
OD2_4		Dry		1.075	16
OD2_4#	0.425-0.6	Saturation	75.21	1.079$^{\$}$	16
OD2_5		Dry		1.076	24
OD2_5#		Saturation		1.076$^{\$}$	24
OD2_6		Dry		1.083	32
OD2_6#		Saturation		1.075$^{\$}$	32
OD3_1		Dry		1.135	2
OD3_2		Dry		1.145	4
OD3_3		Dry		1.140	8
OD3_4		Dry		1.142	16
OD3_4#	0.3-0.425	Saturation	73.00	1.142$^{\$}$	16
OD3_5		Dry		1.148	24
OD3_5#		Saturation		1.138$^{\$}$	24
OD3_6		Dry		1.144	32
OD3_6#		Saturation		1.142$^{\$}$	32

$^{\$}$ represents the void ratio reached after full saturation

6.2.3 Ring shear test

Ring shear tests were conducted in a Bromhead type of apparatus (Bromhead, 1979), generally in accordance with British standard (BS1377-7, 1990), as shown in Figure 6.4. Shearing was conducted at a rate of ω = 2.4 degree/min (≈ 1.80 mm/min). Following the work of Coop *et al.* (2004), the notional definition of shear strain (γ) and vertical strain (ε_v) are adopted for presentation of the experimental results:

$$\gamma = \frac{\delta S}{h}, \varepsilon_v = \frac{\delta v}{h} \tag{6.1}$$

where δS is the variation in shear displacement, h is the initial sample height, δv is the variation in vertical displacement. Based on some preliminary tests, the samples were prepared in a dry state with a target initial void ratio of e_0 = 1.00. Samples with the same initial PSDs to the one-dimensional compression test were compressed to 5 different normal stresses and subsequently sheared to between 2 and 7 different shear strains in dry and saturated conditions as summarised in Table 6.3. The saturated samples were prepared in the same way as the dry samples, with the cell flooded with distilled water prior to the application of normal stress and throughout the remainder of the test, which is commonly adopted for carbonate sand saturation in ring shear test (Coop *et al.*, 2004; Wei *et al.*, 2018). In tests with a high normal stress, the maximum shear strain was limited to a relatively small value to limit particle loss. After the test, the whole sample was oven dried (24h at 105°C) and sieved.

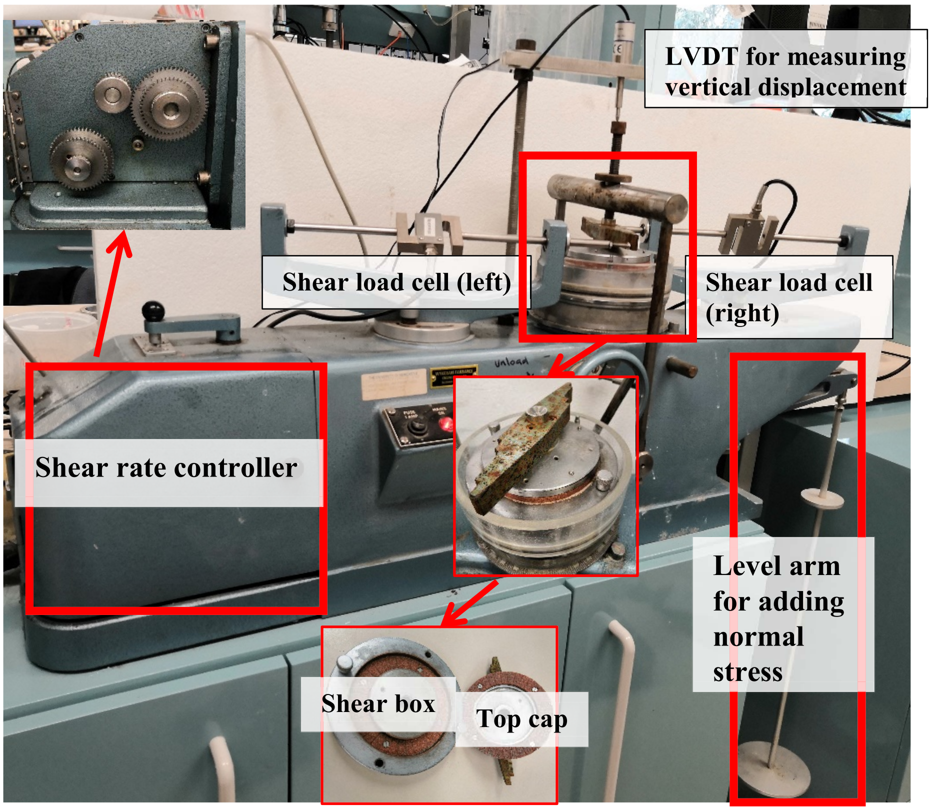

Figure 6.4: The ring shear apparatus. The capacity of LVDT (RDP Electronics) is 2.5 mm; the capacity of shear load cell is 100 kg. The ring shear specimen is annular with an outer diameter of 100 mm, an inner diameter of 70 mm, and a height of 5 mm

Table 6.3. Details of ring shear tests on initial uniformly graded samples

Test No.	Initial grading [mm]	Vertical stress σ_v [kPa]	Shear strain γ [%]	Test No.	Initial grading [mm]	Vertical stress σ_v [kPa]	Shear strain γ [%]
RS1_1		48.93	2158	RS7_3		391.46	4314
RS1_2		48.93	30033	RS7_4		391.46	8094
RS2_1		195.73	1996	RS8_1		611.65	534
RS2_2	0.6-1.18	195.73	3238	RS8_2*	0.425-0.6	611.65	1076
RS2_3		195.73	5417	RS8_3*		611.65	2152
RS2_4		195.73	7702	RS8_4		611.65	4320
RS2_5		195.73	12950	RS9_1		782.92	107

RS3_1		391.46	1073	RS9_2		782.92	288
RS3_2		391.46	2308	RS9_3		782.92	530
RS3_3		391.46	5392	RS9_4*		782.92	1073
RS3_4		391.46	7558	RS9_5		782.92	1613
RS3_5		391.46	12950	RS9_6		782.92	2140
RS4_1		611.65	537	RS9_7		782.92	2698
RS4_2*		611.65	1073	RS10_1		48.93	539
RS4_3*		611.65	2155	RS10_2		48.93	1078
RS4_4		611.65	6469	RS10_3		48.93	2157
RS5_1		48.93	2152	RS11_1		195.73	538
RS5_2		48.93	4314	RS11_2		195.73	1078
RS5_3		48.93	8985	RS11_3		195.73	2157
RS5_4		48.93	17217	RS12_1		391.46	539
RS5_5		48.93	26960	RS12_2	0.3-0.425	391.46	1078
RS6_1	0.425-0.6	195.73	1073	RS12_3		391.46	2158
RS6_2		195.73	2152	RS13_1		611.65	538
RS6_3		195.73	5393	RS13_2*		611.65	1079
RS6_4		195.73	8631	RS13_3		611.65	2159
RS6_5		195.73	12950	RS14_1		782.92	538
RS7_1		391.46	1076	RS14_2*		782.92	1079
RS7_2		391.46	2155	RS14_3		782.92	2149

* means samples were tested in both dry and saturated conditions, the rest tested only in dry condition.

6.3 Test results

6.3.1 One-dimensional compression test with controlled strain rate

Figure 6.5 shows the volumetric response of samples and the corresponding evolution of the compressibility index C_c (C_r) = (-Δe)/Δlog (σ'_v), where e is the void ratio and σ'_v is the effective vertical stress. C_c is defined as the compression index when the effective vertical stress is larger than the yield stress, and C_r is defined as the recompression index when the effective vertical stress is smaller than the yield stress. The initial void ratio of samples in each loading series was made almost the same as shown in Table 6.2. For both dry and saturated samples, similar compression curves (e-log (σ'_v)) as well as C_c (C_r) - σ'_v curves are observed in Figure 6.5(a) - Figure 6.5(c) and Figure 6.5(d) - Figure 6.5(f), respectively, indicating good repeatability of the sample preparation. As shown in Figure 6.5(d) - Figure 6.5(f), C_c first increases and reaches a peak value as the effective vertical stress increases from the yield stress to 15-20 MPa, then gradually decreases to a relative constant value with increasing σ'_v. The saturated samples plot at a lower void ratio than the dry samples as shown in Figure 6.5(a) - Figure 6.5(c). This is because the saturation of sample can trigger collapse, which is in consistent with the recent study by Ovalle (2018), who summarized the results of one-dimensional compression tests on saturated and dry, flat, angular sand derived from quartzite shale rock. However, as shown in Figure 6.5(d) - Figure 6.5(f), the value of C_c in both saturated and dry samples lies within a narrow band, indicating very limited effect of the saturation state on compressibility when defined by C_c. This is in contrast to the results of Ovalle (2018) where saturated samples have a higher C_c and experience more particle breakage. The saturated carbonate sands tested in this paper have similar particle size distributions as the dry samples as shown in Figure 6.7, even after compression to a high vertical stress. Those samples with more particle breakage observed after compression are more compressible and have higher values of C_c.

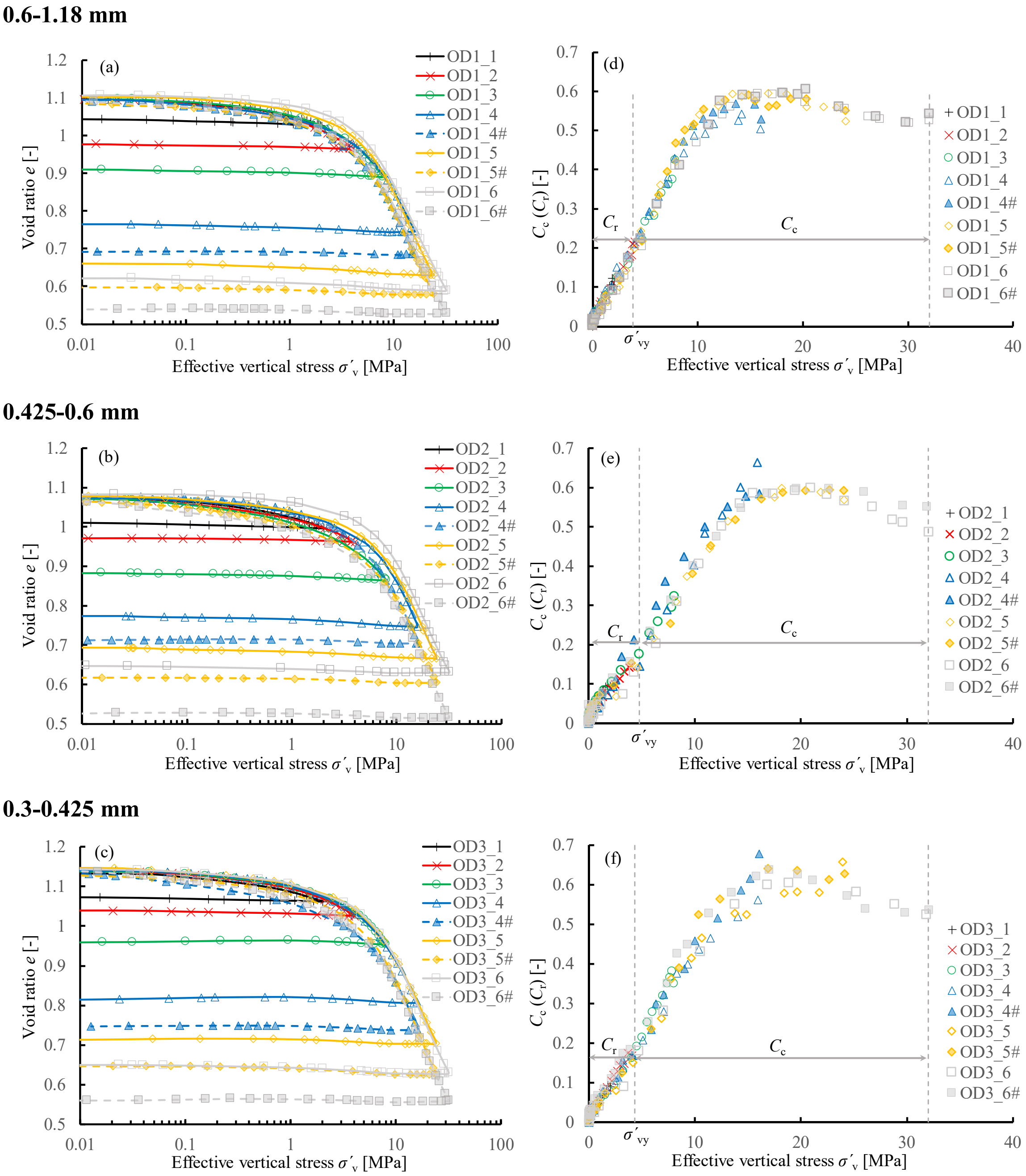

Figure 6.5: One-dimensional compression of uniformly graded carbonate sand: (a)-(c) e-log(σ'_v) curves, (d)-(f) the corresponding evolving of compressibility index C_c (C_r)

The vertical yield stresses (σ'_{vy}) have been calculated based on the work input criterion proposed by Becker *et al.* (1987) and plotted in Figure 6.6 in terms of the average particle size d_{50}. As shown in Figure 6.6, the yield stress of carbonate sand first increases, then decreases with increasing particle size based on the test results in this paper and data from Yan & Shi (2014). This is similar with the observation of silica sand as reported by McDowell (2002), who found the yield stress of uniformly graded silica sand with average particle size larger than 0.45 mm decreased with increasing particle size. Figure 6.6 also shows that saturated specimens have a lower yield stress than that of dry specimens. The reduction of yield stress also explains why the compression curves of saturated samples plot below the dry samples as shown in Figure 6.5(a) - Figure 6.5(c).

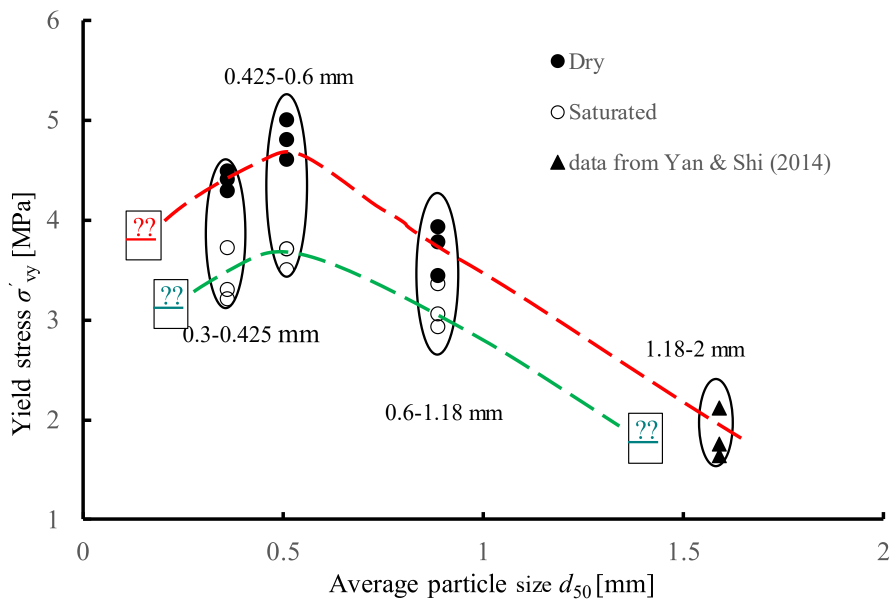

Figure 6.6: Relationship between average particle size and yield stress of dry and saturated samples

Figure 6.7 shows the evolution of PSDs (in a double logarithmic form) of the initially uniformly graded carbonate sands during one-dimensional compression tests with controlled strain rates. The PSDs progressively become finer with increasing effective vertical stress and the PSD of the saturated samples is almost the same, or slightly coarser, than the dry samples (excluding test No. OD2_4#) as shown in Figure 6.7. It can also been seen from Figure 6.7 that in double logarithmic space, the PSDs approach a straight line and evolve towards a fractal grading as the effective vertical stress is increased. For a fractal grading, the relationship between percentage finer P and particle size d is represented by a straight line in log(P)-log(d) space, as indicated by the black dashed line in Figure 6.7 and Figure 6.9.

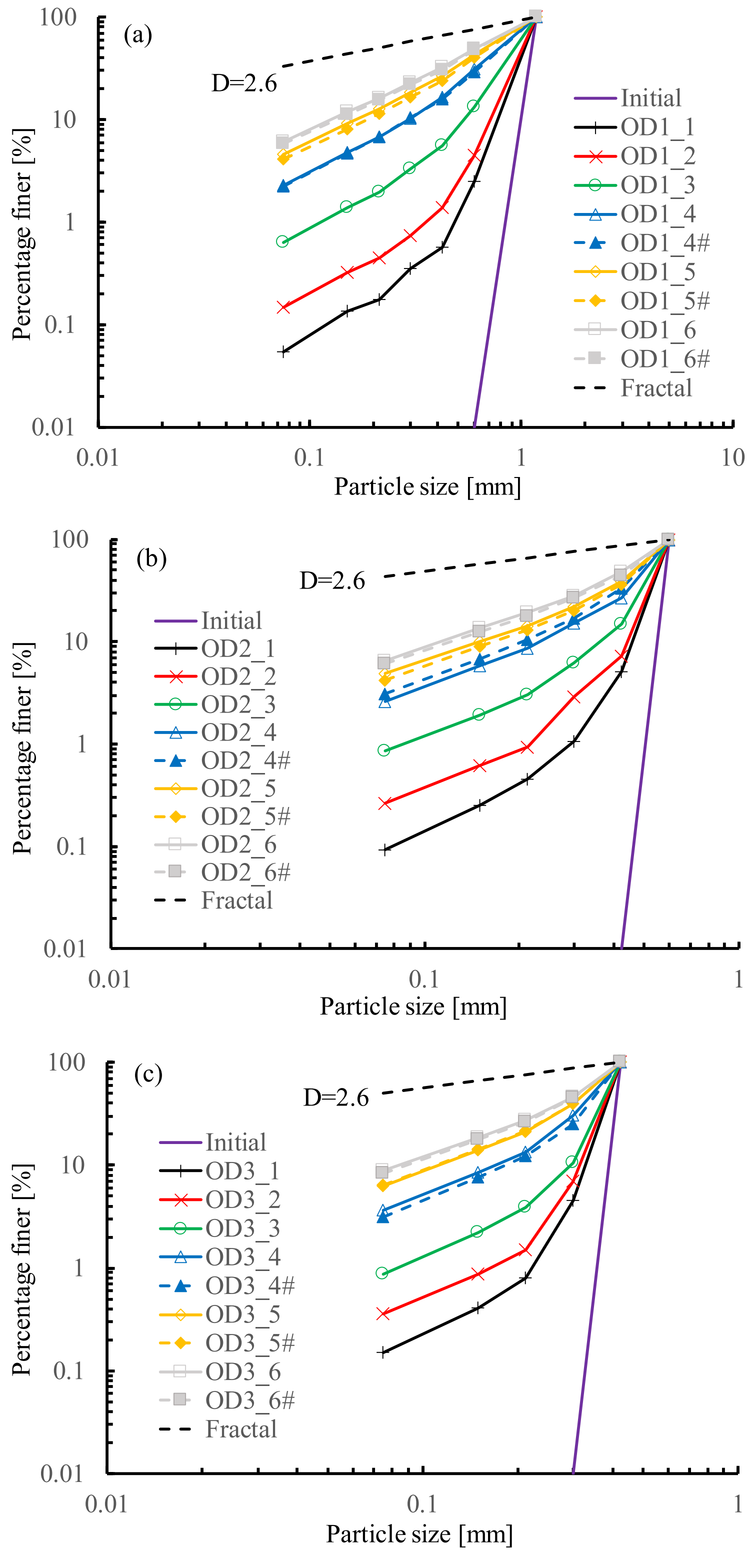

Figure 6.7: Evolution of PSD of uniformly graded carbonate sand during one-dimensional compression test; (a) 0.6-1.18 mm, (b) 0.425-0.6 mm, (c) 0.3-0.425 mm

6.3.2 Ring shear test

Figure 6.8 shows the evolution of the normalised shear stress (τ_n/σ_v) and volumetric strain obtained from the ring shear test for uniformly graded specimens in both dry and saturated conditions. The normal stresses adopted in the ring shear tests remained below the vertical yield stress (σ'_{vy}) obtained from the one-dimensional compression tests (2.5 MPa < σ'_{vy} < 5.0 MPa). This indicates that the samples were in an 'over-consolidated' state, despite not having been previously loaded. In agreement with this observation, the samples show an obvious strain-softening behaviour as indicated in Figure 6.8(a) - Figure 6.8(c). The stress ratio first increases to a peak value at a relative small shear strain of approximately 70% < γ < 100% (see peak zone in Figure 6.8(a) - Figure 6.8(c)), which corresponds with the maximum rate of dilation ($\psi_{max} = [-d\varepsilon_v/d\gamma]_{max}$, Bolton, 1986) as indicated by the points in Figure 6.8(d) - Figure 6.8(f), and then decreases to a constant value at a shear strain γ > 200% (see residual zone in Figure 6.8(a) - Figure 6.8(c)).

The peak mobilised friction angle ($\phi_{peak} = \tan^{-1}[(\tau_n/\sigma_v)|_{peak}]$) of the dry specimens vary with particle size, while the average mobilised residual friction angle ($\phi_{residual} = \tan^{-1}[(\tau_n/\sigma_v)|_{residual}]$) of the dry specimen is relatively constant as summarised in Table 6.4, and seems to be independent of the initial grading over the stress range applied in these tests. As shown in Table 6.4, the values of ϕ_{peak} of the saturated specimens are smaller than that of dry specimens, while the values of $\phi_{residual}$ of the saturated specimens with three initial gradings are almost the same with the dry specimens (within the range of 1 degree), which means that an increase in the saturation degree reduces the ϕ_{peak}, but has almost no effect on $\phi_{residual}$.

Table 6.4. Details of ϕ_{peak} and $\phi_{residual}$ of ring shear tests on initial uniformly graded samples

Initial PSD [mm]	ϕ_{peak} [Deg]		$\phi_{residual}$ [Deg]	
	Dry	Saturated	Dry	Saturated
0.3-0.425	34.1	33.1	32.9	33.7
0.425-0.6	36.4	34.3	32.9	33.2
0.6-1.18	35.9	34.8	32.2	32.9

Figure 6.8(d) - Figure 6.8(f) illustrate the volumetric strains of the samples during shearing in both dry and saturated conditions. As shown in those Figures, the dry samples first contract at low shear strain ($\gamma < 40\%-50\%$) and then begin to dilate until a shear strain of $\gamma \approx 50\%$ - 100%. After that, contraction dominates the deformation behaviour due to the particle breakage that occurs during shearing. However, the dilatancy tendency appears to have been suppressed because of the increasing saturation degree. For example, dilatancy almost disappears for samples with size range from 0.3-0.425 mm under normal stresses of 611.65 kPa and 782.92 kPa as shown in Figure 6.8(f). There are two potential reasons behind: one being that water can promote particle breakage (see results in Figure 6.9) which leads to a denser sample; the other being that water reduces the inter-particle friction.

Another interesting observation from the ring shear test is the 'jump' in τ_n/σ_v-γ curves at shear strains of 15%-30%, as indicated by the hollow ellipses in Figure 6.8(a) - Figure 6.8(c), where the rate of volume change slows down as shown in Figure 6.8(d) - Figure 6.8(f). At this stage, it is the particle re-arrangement, i.e., particle sliding and rolling, instead of particle breakage, that dominates the volume change. Furthermore, both dry and saturated samples under different shear strains show a very similar stress ratio and volumetric strain as shown in Figure 6.8, which also means the good repeatability of tests.

0.6-1.18 mm

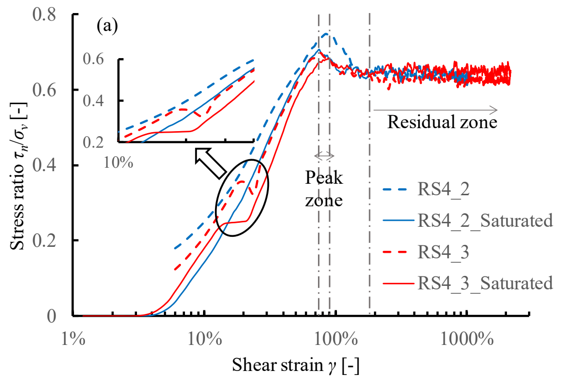

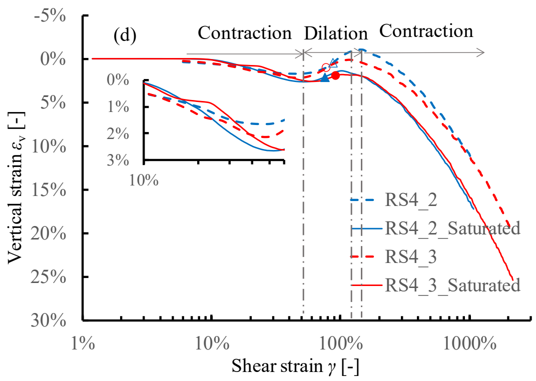

0.425-0.6 mm

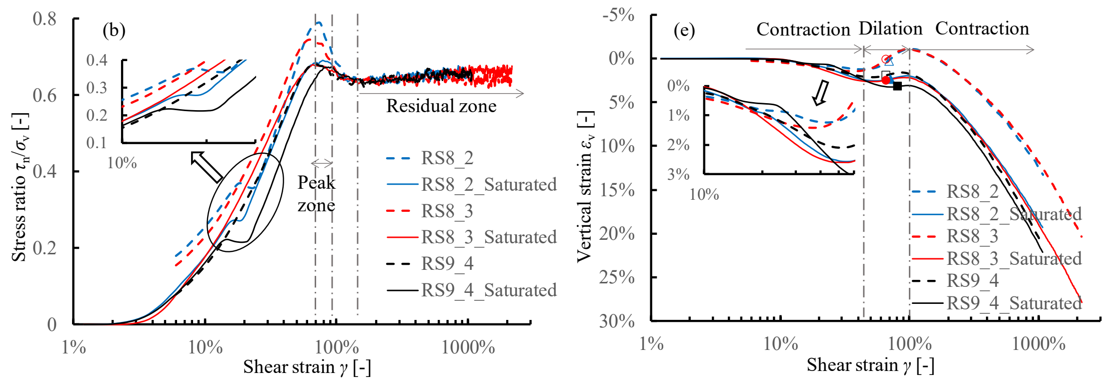

0.3-0.425 mm

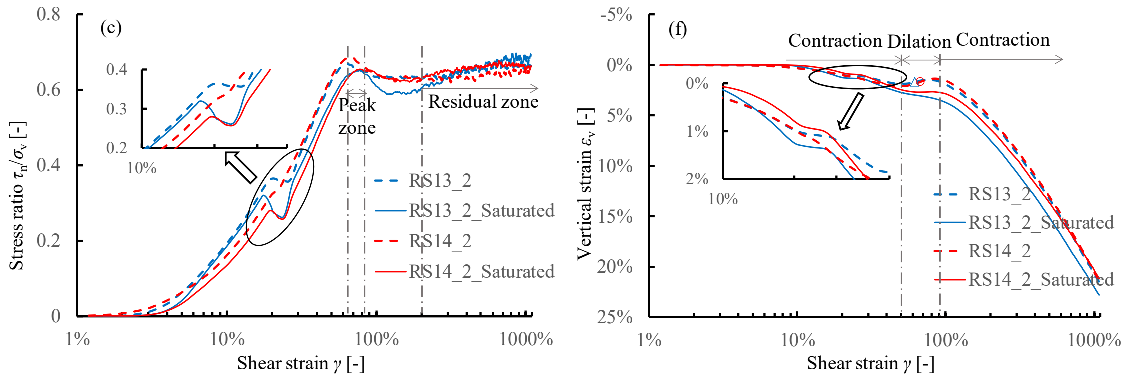

Figure 6.8: Stress & volumetric response of dry and saturated samples with different gradings during ring shear test. The hollow points in (d)-(f) represent the maximum rate of dilation of dry samples, and the solid points mean the maximum rate of dilation of saturated samples

<table>
<tr><th>σ´v [kPa]</th><th>0.6-1.18 mm</th><th>0.425-0.6 mm</th><th>0.3-0.425 mm</th></tr>
<tr><td>48.93</td><td>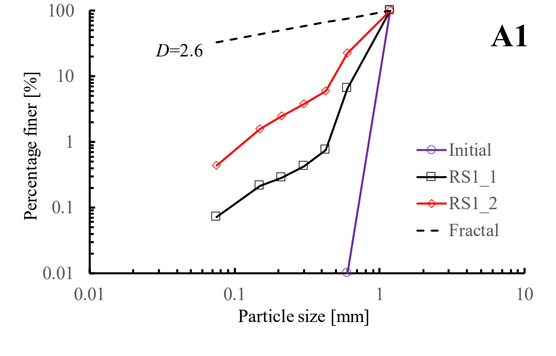
</td><td>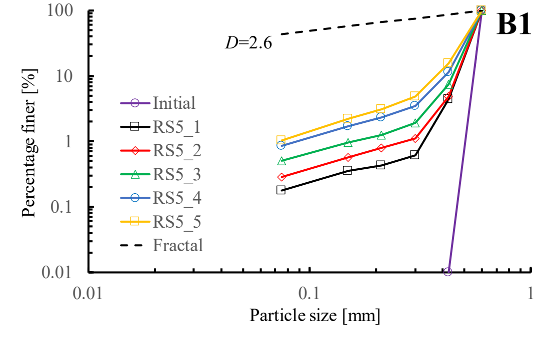
</td><td>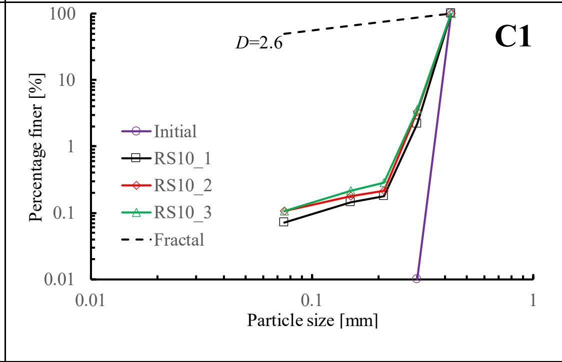
</td></tr>
<tr><td>195.73</td><td>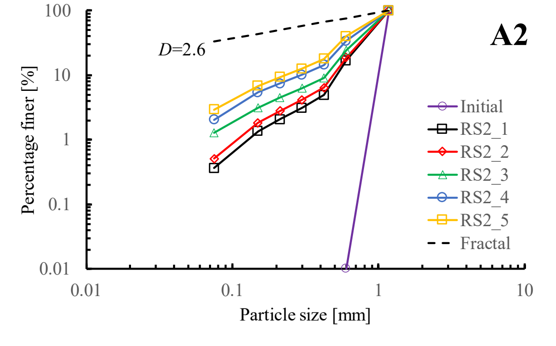
</td><td>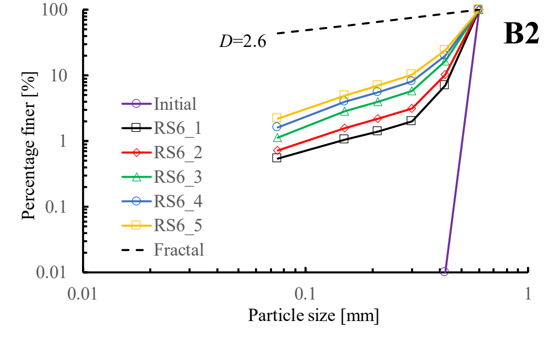
</td><td>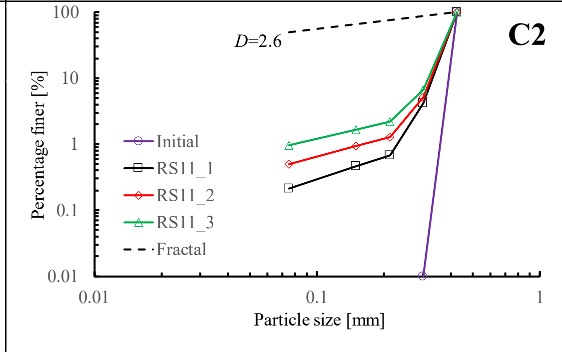
</td></tr>
<tr><td>391.46</td><td>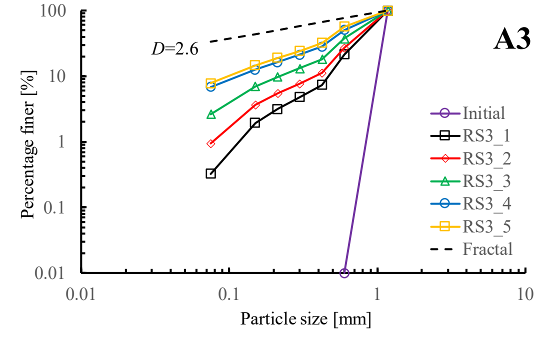
</td><td>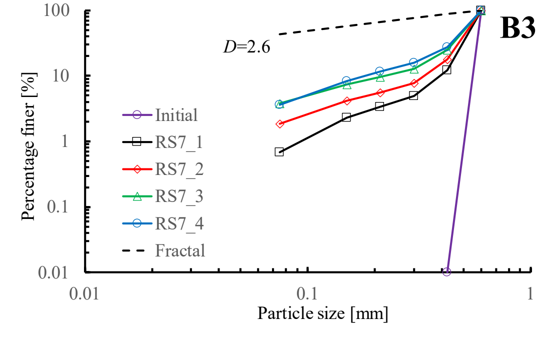
</td><td>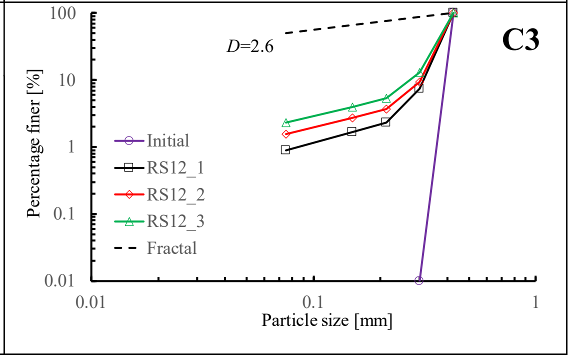
</td></tr>
</table>

<table>
<tr>
<td>611.65</td>
<td>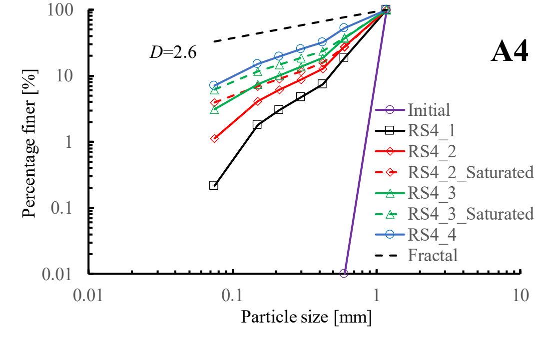
</td>
<td>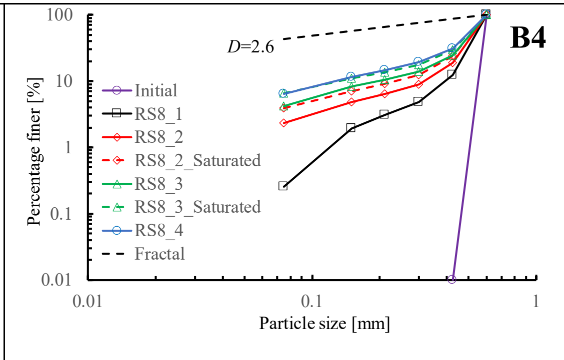
</td>
<td>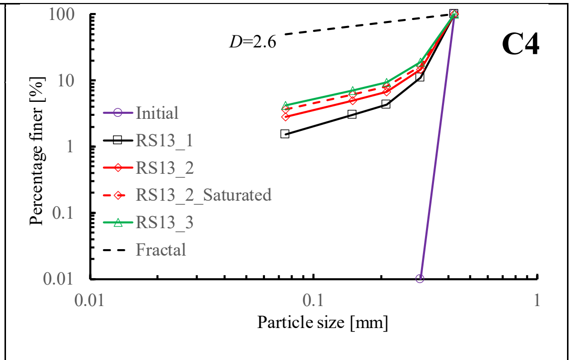
</td>
</tr>
<tr>
<td>782.92</td>
<td></td>
<td>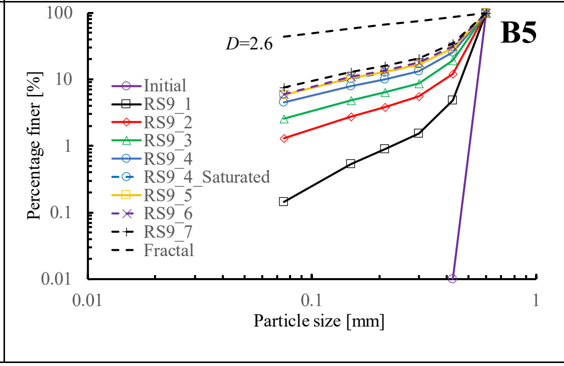
</td>
<td>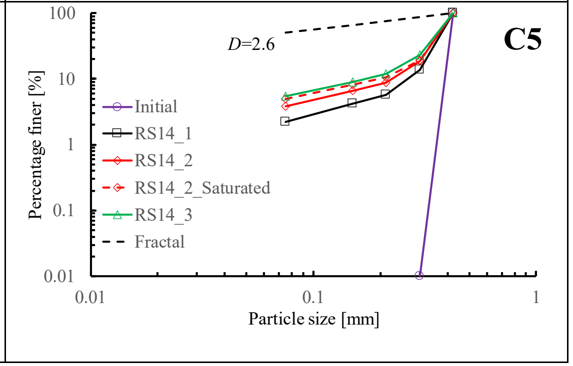
</td>
</tr>
</table>

Figure 6.9: Evolution of PSDs of uniformly graded carbonate sand during ring shear test

Figure 6.9 shows the evolution of PSDs (in a double logarithmic form) of uniformly graded carbonate sands after ring shear tests. The PSDs become finer with increasing shear strain and vertical stress. A fractal grading, as suggested by other studies (e.g. Coop *et al.*, 2004; Miao & Airey, 2013), is not reached at small normal stresses despite the relatively high shear strain as shown in Figures 6.9(A1), 6.9(B1) and 6.9(C1). However, fractal characteristics become more obvious at the higher normal stresses with the progression of particle breakage, even though the shear strain is not large enough as shown in Figures 6.9(B4), 6.9(B5).

In comparison with the results of the one-dimensional compression tests, the PSD of the sample in the ring shear test uplifts significantly in the presence of water, as shown in Figures 6.9(A4), 6.9(B4), 6.9(B5), 6.9(C4) and 6.9(C5), implying that water strongly promotes particle breakage when the sample is subjected to shearing.

6.4 Evolution of PSD due to particle breakage

6.4.1 Quantification of particle breakage

To study the evolution of particle breakage, we first need to find appropriate indices to represent the whole PSD of a sample. After that, we need to establish evolution laws that describe how these indices evolve under various loading paths and hydraulic scenarios (Zhang *et al.*, 2015). To tackle the first issue, several different indices have previously been proposed. Some can reflect changes in the characteristic particle size such as the coefficient of uniformity C_u (Yan & Dong, 2011; Li *et al.*, 2014), Lee's breakage index B_{15} (Lee & Farhoomand, 1967), Lade's breakage index B_{10} (Lade *et al.*, 1996), Xiao's breakage index B_{50} (Xiao & Liu, 2017). Some can provide an indication of the overall shape of the PSD, for example, the slope β of the straight line in $\log(P)$-$\log(d/d_{max})$ space (Konrad & Salami, 2018), while others can describe the overall change of the PSD with consideration of all the size fractions, such as, increase of surface area ΔS (Miura & O'Hara, 1979), Hardin's breakage index B_r (Hardin, 1985) and Modified Hardin's breakage index B_r^* (Einav, 2007a).

The modified Hardin breakage index B_r^* (Einav, 2007a) is widely adopted as it considers the ultimate fractal grading at extreme conditions, as defined in Figure 6.10. The ultimate fractal grading can be described as

$$P(d) = \left(\frac{d}{d_{\max}} \right)^{\beta} \tag{6.2}$$

where β=3-D, D is the fractal dimension. For carbonate sands, the average value of D was found to be around 2.6 as reported by others (Coop *et al.*, 2004; Xiao *et al.*, 2016c).

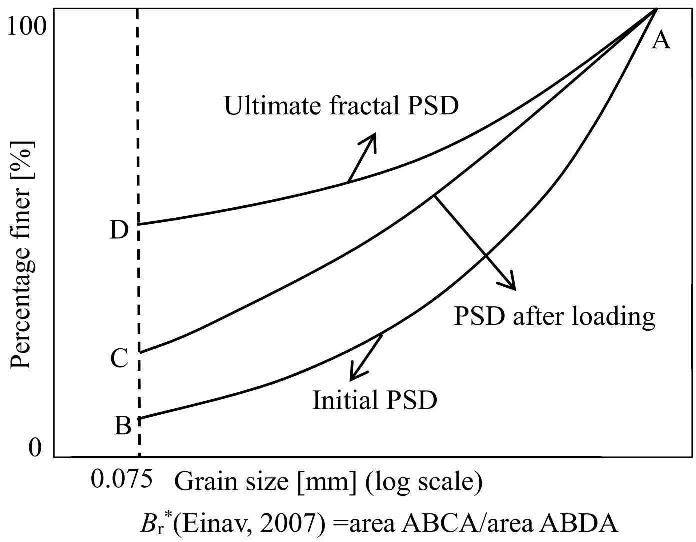

Figure 6.10: Definition of modified Hardin's breakage index B_r^* (Einav, 2007a)

However, representation of PSD based on a single parameter suffers limitations, such as not being able to describe the whole PSD (Tong *et al.*, 2018a, Konrad & Salami, 2018). Thus, using a simple mathematical model for representing the whole PSD is considered to be an effective way to track particle breakage.

Tong *et al.* (2018a) proposed a simple two-parameter PSD model, which is able to capture the typical trends in PSD evolution during particle breakage. The model is written as

$$P(d) = 1 - e^{-\left(\frac{d}{\lambda_p (d_{\max} - d)} \right)^{\kappa_p}} \tag{6.3}$$

where $\lambda_p = \dfrac{d_{63.2}}{d_{\max} - d_{63.2}}$ is a scale parameter, $d_{63.2}$ is the characteristic particle diameter at which 63.2% of the sample by mass is smaller and κ_p is a shape parameter. This two-parameter PSD model shows some advantages over other PSD indices in representing the whole PSD. Nevertheless, the variation of λ_p and κ_p during particle breakage has not been explored in detail.

To address this, the relationship between λ_p and κ_p, with B_r^* is explored to further analyse the evolution of particle breakage of uniformly graded carbonate sand reported above and other tests in the literature (Xiao *et al.*, 2016c; Xiao *et al.*, 2017). The evolution of these particle breakage indices during compression/shearing will then be discussed.

6.4.2 Relationship between λ_p, κ_p, and B_r^*

Figure 6.11 shows the relationship between B_r^* and λ_p for both dry and saturated samples with different initial PSDs. The relationship between B_r^* and λ_p is rather linear and of the general form

$$\lambda_p = \lambda_{\text{initial}} - \alpha_\lambda B_r^* \tag{6.4}$$

where α_λ is a parameter related to the initial PSD, and λ_{initial} is a parameter related to the initial PSD. As can be seen from Equation (6.4), parameter λ_p equals to λ_{initial} at the initial state where no particle breakage happens ($B_r^* = 0$). For a uniformly graded sample, the particle size ranges from d_{min} to d_{max} and the characteristic particle diameter $d_{63.2}$ is calculated based on linear interpolation as $d_{63.2} = 0.632d_{max} + 0.368d_{min}$. Then PSD parameter at the initial state, λ_{initial}, can be calculated as

$$\lambda_{\text{initial}} = \frac{d_{63.2}}{d_{\max} - d_{63.2}} = \frac{0.632R_D + 0.368}{0.368R_D - 0.368} \tag{6.5}$$

where $R_D = d_{max}/d_{min}$ is the ratio of maximum to minimum particle size at the initial state. The values of λ_{initial} and α_λ based on Equations (6.4) - (6.5)with different initial PSD are summarised in Table 6.5. As shown in Table 6.5, λ_{initial} and α_λ decreases with increasing R_D. The relationship between B_r^* and λ_p is dependent on grading index R_D for the uniformly graded samples.

Table 6.5. Relationship between λ_{initial}, α_λ and R_D

Initial PSD	R_D [-]	λ_{initial} [-]	α_λ [-]
0.3-0.425 mm	1.42	8.24	12.79
0.425-0.6 mm	1.41	8.32	13.52
0.6-1.18 mm	1.97	4.53	6.88
1-2 mm, Xiao *et al.* (2016c)	2.00	4.44	4.47
0.8-1 mm, Xiao *et al.* (2017)	1.25	12.59	32.55

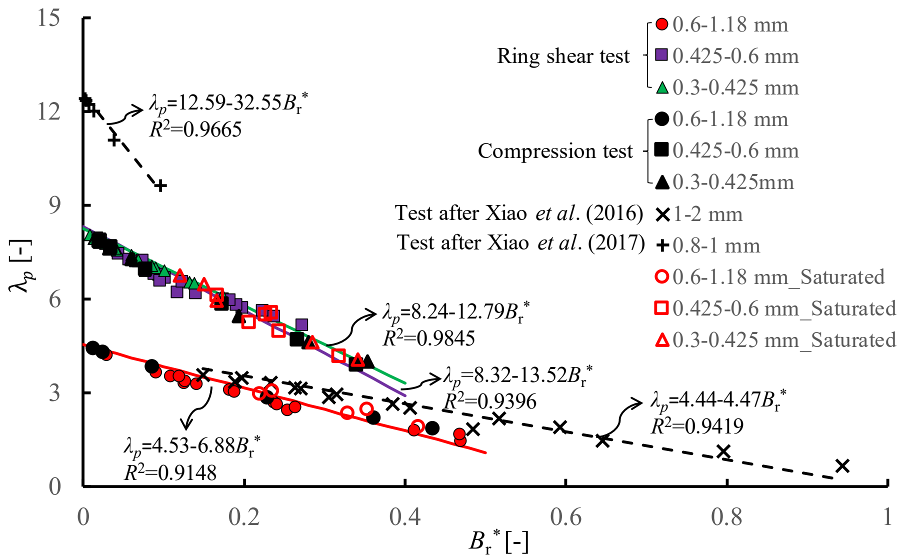

Figure 6.11: Relationship between breakage index B_r^* and PSD parameter λ_p for dry and saturated samples with different initial PSDs during different test modes. Solid point means dry sample, hollow point means saturated sample subjected to both compression and shearing

Figure 6.12 shows the relationship between B_r^* and κ_p for both dry and saturated samples with different initial uniformly PSDs. It is interesting to note that the relationship between κ_p and B_r^* can be described by a unique power function despite the difference in initial PSDs and test modes, which can be expressed as

$$\kappa_p = 3.96 B_r^{*(-0.11)} - 3.61 \tag{6.6}$$

As shown in Equation (6.6), when the ultimate state is reached and all particle breakage has occurred (B_r^* =1.0), the parameter κ_p = 0.35, which matches previous findings (Tong *et al.*, 2018a).

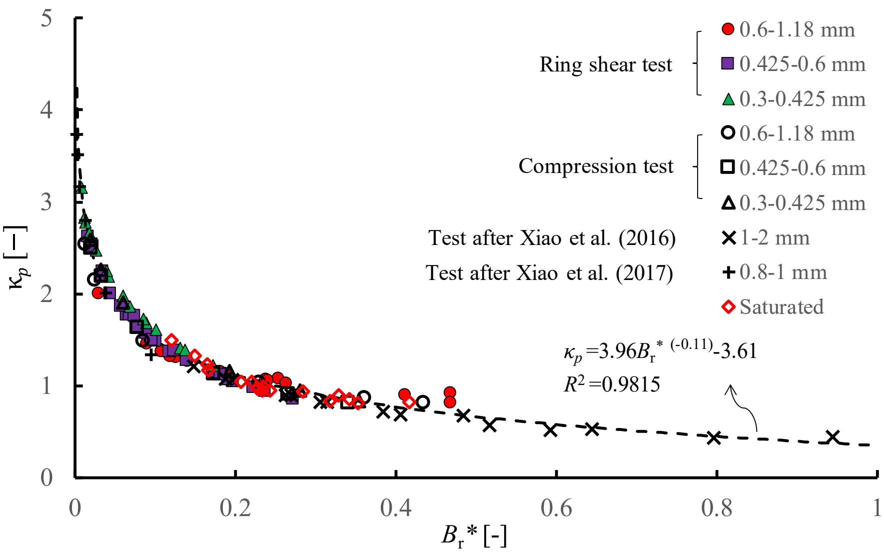

Figure 6.12: Relationship between breakage index B_r^* and PSD parameter κ_p for dry and saturated samples with different initial PSDs during different test modes

From Figure 6.11 and Figure 6.12, it is clear that the two PSD parameters can be well correlated to B_r^*. Parameter λ_p is linearly related with B_r^*, but dependent on the initial PSD and independent of the test mode. Whereas, κ_p is in a power function with B_r^* and is independent of both the initial PSD and the test mode. In general, using the two PSD parameters as breakage indices has two main benefits: (1) a full PSD curve can be drawn, and (2) the extent of particle breakage (i.e. B_r^*) can be derived.

6.4.3 Evolution of λ_p, κ_p during ring shear test

Figure 6.13 and Figure 6.14 shows the relationship between two PSD parameters (i.e., λ_p and κ_p) with shear strain γ and normal stress σ_v during the ring shear tests, respectively. As shown in Figure 6.13, both λ_p and κ_p decrease with increasing shear strain. For samples with the same initial PSD but different applied vertical stresses, λ_p and κ_p evolve as a power function under different strains, i.e., a nearly linear relation is observed in log-log space. It is not surprising that λ_p and κ_p decreases with increasing normal stress because of more particle breakage. According to Figure 6.14, both λ_p and κ_p decrease with increasing normal stress, and display a linear relation in λ_p (κ_p) - σ_v space over the range of vertical stresses applied in this paper.

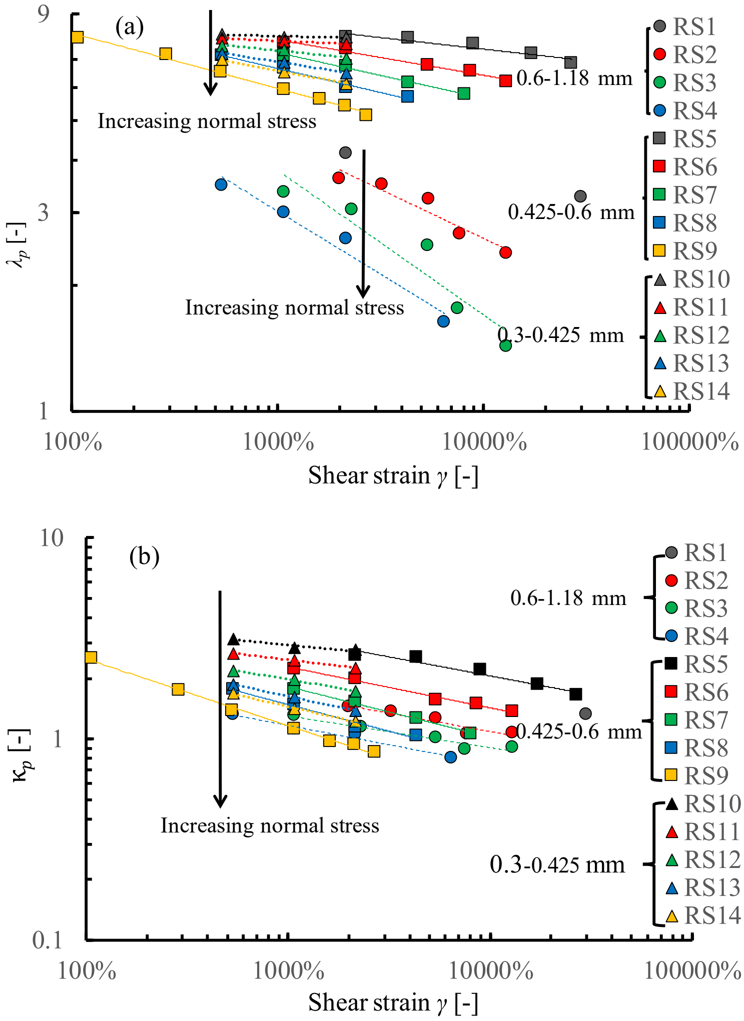

Figure 6.13: Relationship between shear strain and PSD parameters in ring shear test: (a) γ vs. λ_p, (b) γ vs. κ_p

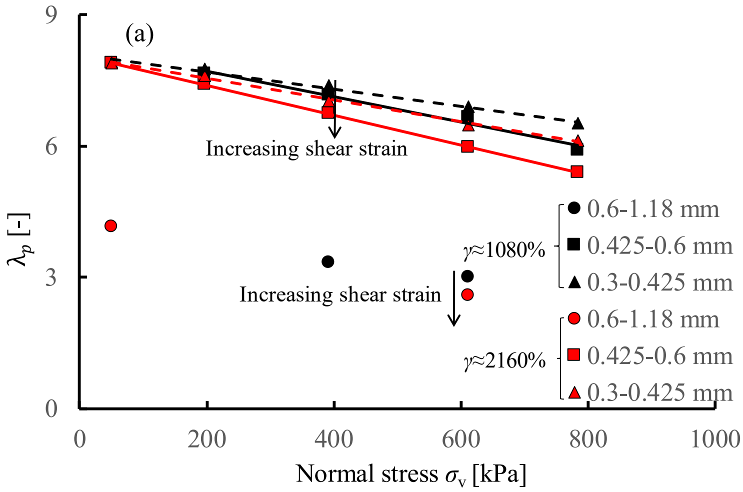

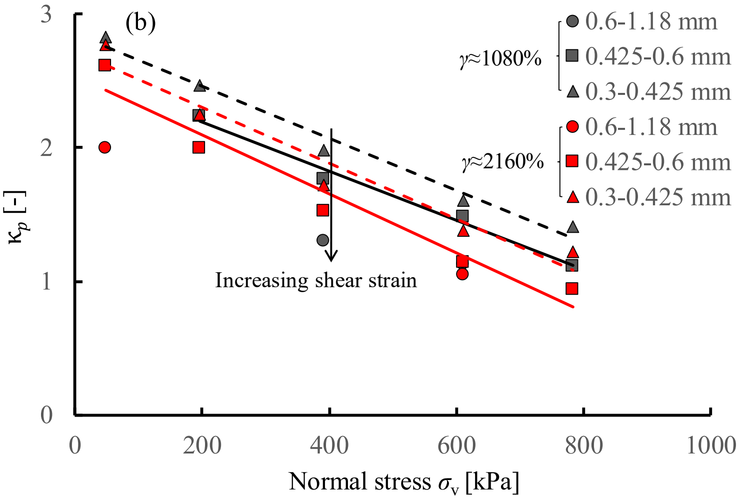

Figure 6.14: Relationship between normal stress and PSD parameters in ring shear test: (a) σ_v vs. λ_p, (b) σ_v vs. κ_p

As shown in Figure 6.13 and Figure 6.14, the evolution of two PSD parameters are highly dependent on both shear strain and normal stress during ring shear test. Recognising that particle breakage is influenced by both shear and normal components of stress and strain, a mechanical parameter that combined with normal stress and shear strain, for example, input work, might be appropriate for correlation with PSD indices. One of the early studies on correlating input work with breakage index was performed by Miura & O'Hara (1979). They found a unique curve between plastic work and increase in surface area during different stress paths in triaxial test on a decomposed granite soil. The flexibility and advantages of using input work as a mechanical parameter have been confirmed by many studies (Lade *et al.*, 1996; Daouadji *et al.*, 2001; Kelly & Airey, 2005; Xiao *et al.*, 2016c; Xiao *et al.*, 2017; Hu *et al.*, 2018; Wang & Arson, 2018). The total input work per unit volume is adopted and its relations with λ_p and κ_p will be explored in the following study.

The total input work per unit volume W_V in a ring shear test can be calculated as (Kelly & Airey, 2005)

$$W_V = \left(\sum_{SOT}^{EOS} \sigma_v \dot{\varepsilon}_v + \sum_{SOS}^{EOS} \tau_n \dot{\varepsilon}_s \right) / V \tag{6.7}$$

where *SOT* means start of test; *SOS* means start of shearing; *EOS* means end of shearing; σ_v is the normal stress; τ_n is the shear stress; $\dot{\varepsilon}_v$ and $\dot{\varepsilon}_s$ are normal strain increment and horizontal strain increment, respectively; V is the volume of sample.

Figure 6.15(a) shows the relationship between W_V and λ_p of both dry and saturated samples during the ring shear tests. In general, λ_p decreases as W_V increases. The relationship between W_V and λ_p can be expressed by the following general hyperbolic curve

$$\lambda_p = \lambda_{initial} - \frac{W_V}{\alpha_W \times W_V + W_{VR}} \tag{6.8}$$

In the equation above, $\lambda_{initial}$ is parameter related to the initial grading as mentioned before, the values of $\lambda_{initial}$ of samples with different initial gradings are summarised in Table 6.5. Parameter α_W is corresponding to the ultimate state, and can be calculated as $\alpha_W = 1/[\lambda_{initial}-\lambda_{ultimate}]$, with $\lambda_{ultimate}$ being the value of λ_p at the ultimate state (i.e., W_V approaches to infinity). The values of α_W for the three initial gradings are 0.28, 0.31, 0.33, respectively. Parameter W_{VR} is a reference input work and the values of W_{VR} for the three initial gradings are 2209 kN.m/m^3, 1282 kN.m/m^{3}and 1806 kN.m/m^3, respectively. As shown in Figure 6.15(a), such a relationship between λ_p and W_V seems to depend on the initial grading and is applicable for both dry and saturated sample.

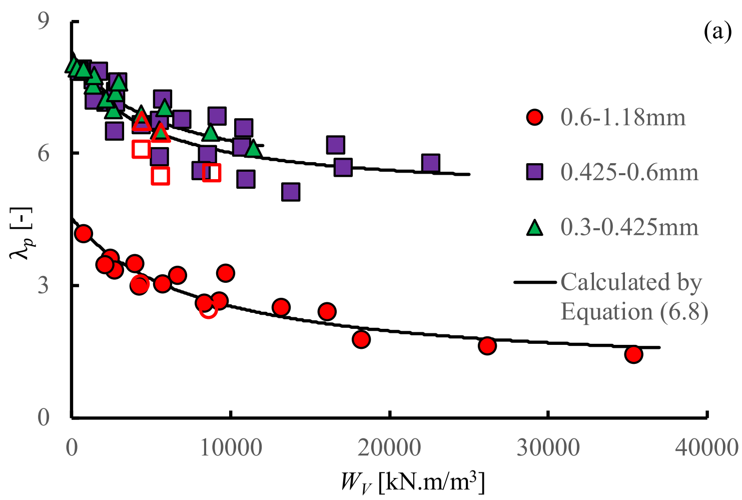

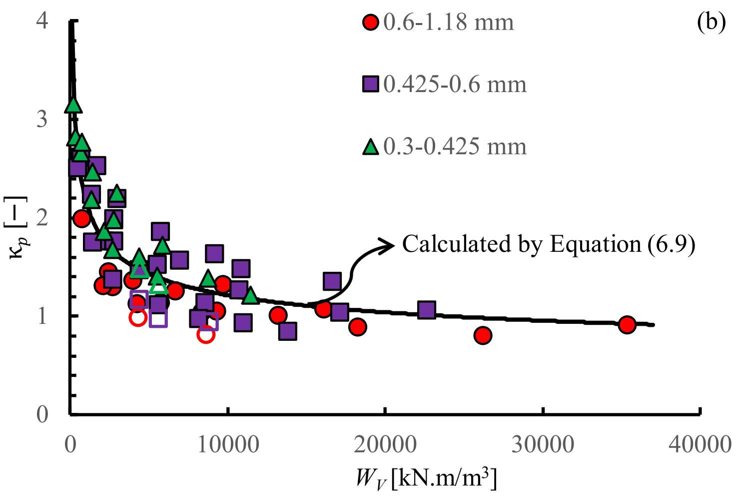

Figure 6.15: Relationship between W_V and PSD parameter in ring shear test: (a) W_V vs. λ_p, (b) W_V vs. κ_p. Solid point means dry sample, hollow point means saturated sample

Figure 6.15(b) shows the relationship between W_V and κ_p, based on the ring shear test results. As seen from Figure 6.15(b), κ_p decreases with increasing W_V. The relationship between W_V and κ_p can be expressed by the following unified power function

$$\kappa_p = a \times \left[\frac{W_V}{\langle W_{VR} \rangle} \right]^{-b} + 0.35 \tag{6.9}$$

where $\langle W_{VR} \rangle$ is the average of the reference input work obtained from Equation (6.8), with fitting parameters a = 1.51 and b = 0.32. As shown in Equation (6.9), the ultimate value of κ_p equals to 0.35 when W_V approaches to infinity. Moreover, the above equation is independent of the initial grading and again applicable for both dry and saturated sample.

The energy based evolutional law for both λ_p and κ_p proposed in Equations (6.8) - (6.9) seems to be independent of shear strain and normal stress, as shown in Figure 6.15, indicating that using the input work for correlation with PSD parameters is appropriate for both dry and saturated sample in the ring shear test.

6.4.4 Application to the other testing conditions

The evolution of PSD parameters proposed in the ring shear test is used for validating in the other test modes mentioned in this study, i.e., one-dimensional compression tests with controlled strain rates, impact tests (Xiao *et al.*, 2016c) and one-dimensional compression tests with controlled stress rates (Xiao *et al.*, 2017).

The input work per unit volume W_V in one-dimensional compression test, and impact test can be defined as

$$W_V = \left(\int \sigma'_v d\varepsilon_v\right) / V, \qquad W_V = \sum_{i=1}^{n} mgh_i / V \tag{6.10}$$

where m is the mass of harmer during impact test, g is the acceleration of gravity, h_i is the dropping height of hammer of i-th impact, and n is the number of impact.

The relationships between W_V and λ_p, κ_p of uniformly graded carbonate sands were plotted in Figure 6.16 and Figure 6.17 by using Equations (6.8) - (6.9). It is clear that the proposed evolutional laws of particle breakage from the ring shear test are also applicable to other test modes.

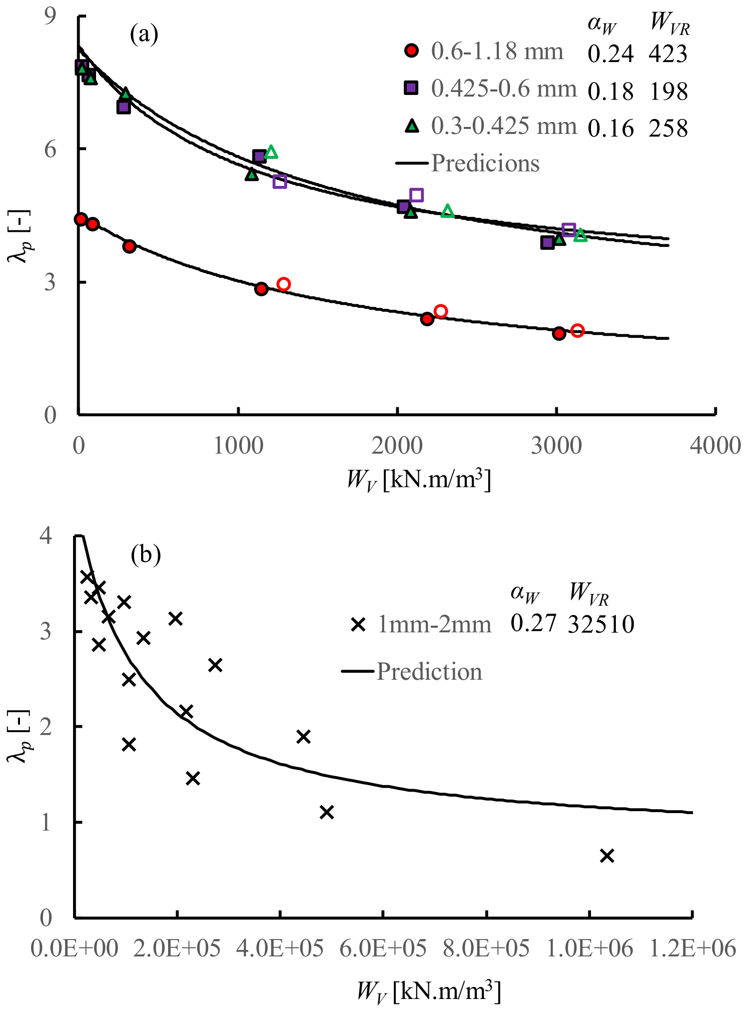

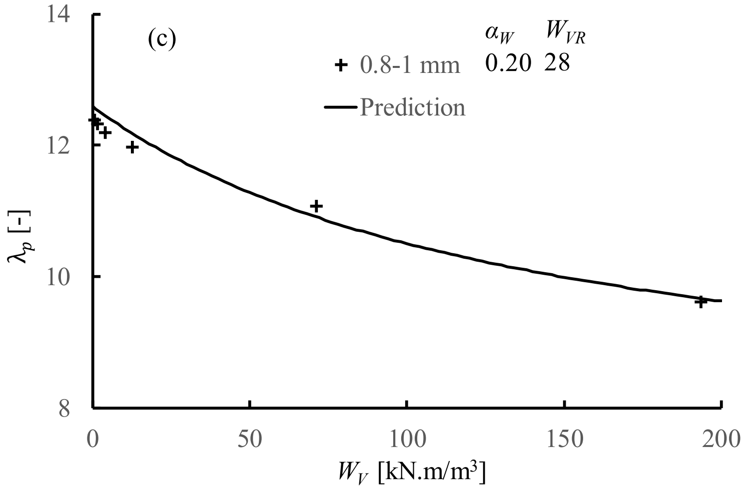

Figure 6.16: Relationship between W_V and PSD parameter λ_p in other test modes: (a) one-dimensional compression tests with controlled strain rates (this study), (b) impact test (after Xiao *et al.*, 2016c), (c) one-dimensional compression tests with controlled stress rates (after Xiao *et al.*, 2017)

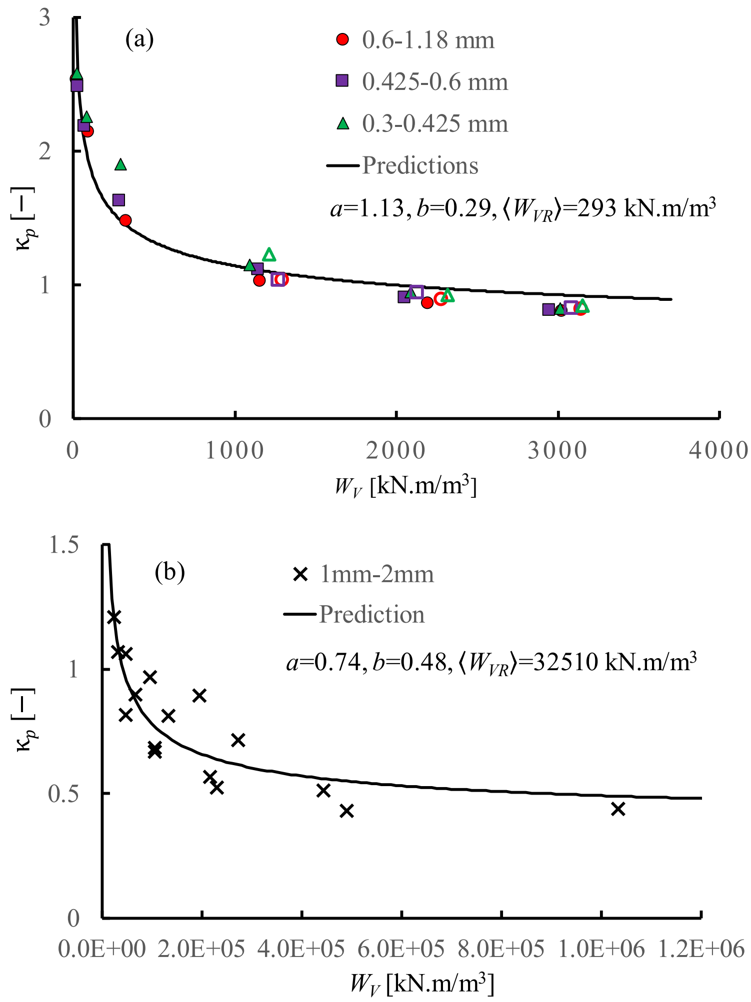

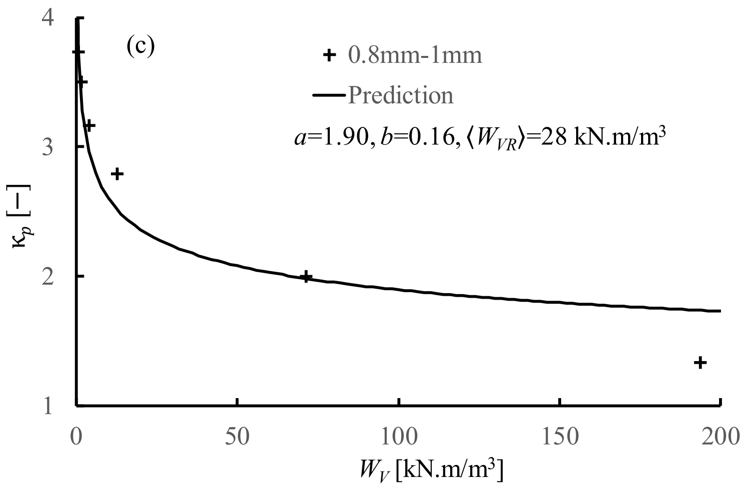

Figure 6.17: Relationship between W_V and PSD parameter κ_p in other test modes: (a) one-dimensional compression tests with controlled strain rates (this study), (b) impact test (after Xiao *et al.*, 2016c), (c) one-dimensional compression tests with controlled stress rates (after Xiao *et al.*, 2017)

The evolutional laws of correlating the two PSD parameters to the input work per unit volume need four parameters as summarised in Table 6.6, which are appropriate for different test modes. We note that a limited number of test modes were considered in this study, and that the stress paths in those tests are relatively simple. For a more complex stress path, for example, in a triaxial test, the evolution of the two PSD parameters under different stress paths still needs further research.

Table 6.6. Summary of parameters related to λ_p and κ_p

Initial PSD [mm]	Test mode	λ_p related parameters		κ_p related parameters		Reference
		α_W [-]	W_{VR} [kN.m/m^3]	a [-]	b [-]	
0.3-0.425 0.425-0.6 0.6-1.18	Ring shear/ 1D compression	0.33/0.16 0.31/0.18 0.28/0.24	1806/258 1282/198 2209/423	1.51/1.13	0.32/0.29	This paper
1-2	Impact	0.27	32510	0.74	0.48	Xiao *et al.* (2016c)
0.8-1	1D compression	0.20	28	1.90	0.16	Xiao *et al.* (2017)

6.5 Conclusions

This paper presents the results of a series of ring shear and one-dimensional compression tests on a carbonate sand prepared with three different initial uniform gradings, in both dry and saturated conditions to investigate the mechanical and deformational behaviour and the corresponding particle breakage properties when subjected to different testing conditions. The main conclusions are summarised as follows:

1. The mechanical and deformational behaviour and breakage of the carbonate sand during both ring shear and one-dimensional compression tests was affected by the saturation state. In one-dimensional compression test, the yield stress decreases, but the compressibility (as defined by C_c) remains almost constant with increasing saturation degree. In ring shear test, the saturation degree reduces the peak mobilised friction angle ϕ_{peak} and the dilatancy tendency, but has almost no effect on the residual mobilised friction angle $\phi_{residual}$. Furthermore, particle breakage of the carbonate sand increased with increasing saturation degree during ring shear test; while in the one-dimensional compression test, saturation state had no obvious effect on particle breakage.
2. The two PSD parameters (i.e. λ_p and κ_p) of a recently proposed PSD model (Tong *et al.*, 2018a) were used as PSD indices for further study on evolution of particle breakage for two main reasons: (1) it can describe the whole PSD curve, which is usually the limitation of traditional single PSD index; and (2) both of the PSD parameters are well correlated with the modified Hardin breakage index B_r^*, which implies that the two parameters can reflect the overall change of PSD with consideration of all the size fractions. More specifically, parameter λ_p is linearly related to B_r^*, and the linear relationship is dependent on the initial PSD, but independent of the testing conditions, while parameter κ_p and B_r^* are in a power relationship. However, such a power relationship seems to be independent of the initial grading and testing conditions.
3. The input work per unit volume W_V was used as a mechanical parameter for correlating with λ_p and κ_p during the ring shear tests to characterize particle breakage. The evolutional law of λ_p is hyperbolically related to W_V and shows a high dependency on the initial grading. Parameter κ_p is in a power relation with W_V, but this relationship is independent of the initial grading. Such evolution laws were also verified by the results from one-dimensional compression test and by experimental data on uniformly graded carbonate sands in the literature.

List of symbols

PSD	Particle size distribution
γ	shear strain
ε_v	vertical strain
h	sample height
δS and δv	variation in shear and vertical displacement
C_c	compression index
σ'_v and σ'_{vy}	effective vertical stress and yield stress
d_{50}	particle size at 50% finer of size distribution curve
$d_{63.2}$	particle size at 63.2% finer of size distribution curve
P	percentage finer
d, d_{max}, and d_{min}	particle size, the maximum particle size and the minimum particle size
D	fractal dimension
τ_n/σ_v	normalised shear stress
ψ_{max}	the maximum rate of dilation
ϕ_{peak} and $\phi_{residual}$	peak mobilised friction angle and mobilised residual friction angle
B_r^*	Einav's breakage index (Einav, 2007)
λ_p and κ_p	PSD indices
$\lambda_{initial}$ and $\lambda_{ultimate}$	PSD index at initial state and PSD index at ultimate state
R_D	ratio of maximum to minimum particle size
α_λ	parameter related to initial PSD
W_V	total input work per unit volume
α_W and W_{VR}	parameters related to λ_p
a and b	parameters related to κ_p

Chapter 7 . Particle breakage observed in both transitional and non-transitional carbonate sands

Abstract: Particle breakage of carbonate sands is widely encountered during the construction of harbor facilities. In this study, a series of one-dimensional (1D) compression tests on carbonate sands with different initial particle size distributions (PSDs) and initial void ratios were completed at high vertical stress (32 MPa) to investigate the influence of PSD and void ratio on the compression behaviour of carbonate sands and the corresponding particle breakage properties. The PSDs used in this study were prepared by fractal distribution with two different fractal dimensions, i.e., 0.5 and 2.0. The results show that samples with a fractal dimension of 0.5 have a unique normal compression line (NCL), implying the occurrence of non-transitional behaviour. However, when the samples tend to be better-graded with a fractal dimension of 2.0, the non-convergent compression paths are likely to occur, which means a transitional behaviour is identified. Particle breakage is observed after the compression tests on samples with two different initial PSDs. It can, therefore, be concluded that particle breakage may happen in both transitional and non-transitional behaviour soils.
Keywords: Particle breakage, Carbonate sands, Compressibility.

This chapter aims to investigate the effect of PSD on the compression behaviour of granular soils (i.e., third key issue) and is based on a conference paper submitted for the 4th International Conference on Transportation Geotechnics:

Tong, C. X*., Zhang, S., & Sheng, D. (2020c). Particle breakage observed in both transitional and non-transitional carbonate sands. The 4th International Conference on Transportation Geotechnics. Chicago, USA. (Abstract accept, full paper under review)*

Authorship Declaration

By signing below I conform that for the conference paper titled ‘Particle breakage observed in both transitional and non-transitional carbonate sands’ submitted to the 4th International Conference on Transportation Geotechnics, that:

Chenxi Tong conducted the tests and wrote the manuscript.

Sheng Zhang contributed to the discussion of the manuscript.

Daichao Sheng is the leader of the research team, and assisted in the revision of the manuscript.

Production Note:

Signature removed
prior to publication.

Chenxi Tong

Prof Sheng Zhang

Prof Daichao Sheng

7.1 Introduction

Particle breakage of carbonate sands has gained significant attention, largely due to the increasing number of offshore structures, harbor facilities, and their widespread distribution. Particle breakage will change the particle size distribution (PSD), which will greatly affect the mechanical and deformational behaviour of carbonate sands. Particle breakage is strongly affected by the initial PSD and initial void ratio. For example, a well-graded sample will suffer less particle breakage and different breakage patterns comparing with the poor-graded one (Nakata *et al.*, 1999; Nakata *et al.*, 2001a). This is mainly attributed to the different packing efficiency that the better distributed of a sample, the higher coordination number for the larger particles, resulting in a smaller breakage probability within the sample (McDowell & Bolton, 1998; Altuhafi & Coop, 2011a; Tong *et al.*, 2019b).

The effect of PSD on the packing characteristics and compressive behaviour of carbonate sand is rare studied. Altuhafi & Coop (2011a) reported that a wider graded carbonate sand had a lower compression index and was more difficult in determining the normal compression line (NCL). When the sample was fractal-graded with a fractal dimension larger than 2.57, which was thought to be the ultimate PSD for a uniformly graded carbonate sand, a transitional behaviour with non-convergent compression paths was observed during the 1D-compression at high vertical stress of 30 MPa. As expected, no detectable particle breakage was found for such samples with transitional behaviour.

In this study, we report the results of 1D-compression tests on carbonate sands with two different initial fractal-graded PSDs and various initial void ratios at high vertical stress (32 MPa). A more compressive investigation on the effect of PSD and void ratio on the compression behaviour of carbonate sand in terms of the compression index, tangent-constrained modulus, and particle breakage is also presented with both qualitative and quantitative approaches.

7.2 Material tested and procedures

7.2.1 Material tested

The carbonate sand tested in this paper is commercially available and with almost pure calcium mineral composition. The specific gravity of carbonate sand was measured to be 2.80 using an automated gas pycnometer (Micromeritics Autopyc II 1340 with an accuracy of 0.05%). The original material was sieved carefully to separate into different particle sizes before preparing different initial PSDs that are fractal-graded with the following expression

$$F(d) = \left(\frac{d}{d_{\max}}\right)^{3-D} \tag{7.1}$$

where $F(d)$ is the mass percentage finer than particle size d, $d_{\max}$ is the maximum particle size, and D is the fractal dimension. In this study, two different values of D (i.e., $D = 0.5$, 2.0) are adopted by mixing particles from each size fraction in the target proportion. The minimum particle size of sample is 0.1 μm, and the distribution of the silt fraction as shown in the red line in Figure 7.1 was determined using the Micromeritics X-Ray particle size system (Sedigraph 5120). Since it is difficult and even impossible to separate the silt fraction into different size intervals, an average grading for the silt fraction was adopted for calculating the overall PSD of sample as shown in the black lines in Figure 7.1.

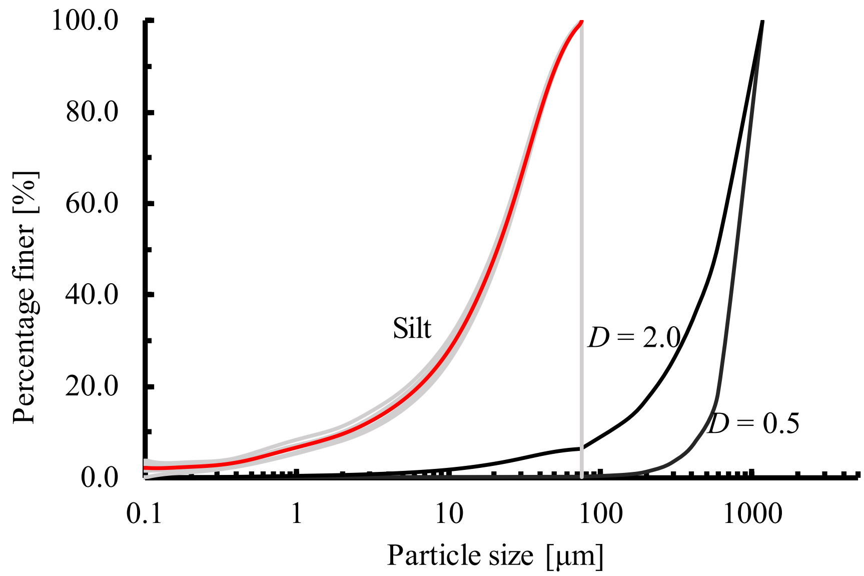

Figure 7.1: Initial PSDs of the tested carbonate sand in the in semi-log plot

7.2.2 1D-compression test

The constant rate of strain (CRS) 1D-compression tests were carried out with sample diameter of 60 mm. Samples with a wide range of initial densities and PSDs were tested dry to a high vertical stress of 32 MPa. The tests were carried out at the displacement rate of 1 mm/min with the sample height of 20 mm for consistency with previous work (Tong *et al.*, 2019a). Samples were prepared by 10 mm/layer and the undercompaction method proposed by Ladd (1978) was adopted to obtain a homogenous of PSD and a uniform density over the entire range of the sample height. The measured displacement was corrected for apparatus compliance for the samples.

The initial void ratio was calculated by measuring the initial dry weight (readability of 0.01 g) and initial sample height (at least three height measurements with a difference less than 0.1 mm). The final void ratio could be calculated from the initial void ratio and vertical displacement recorded during the loading process as shown in the final void ratio 1 in Table 7.1 or could be measured from the final sample height as shown in the final void ratio 2 in Table 7.1. The difference of ±0.02 in the final void ratio was acceptable as suggested by Shipton & Coop (2012). Details of the 1D-compression tests are summarized in Table 7.1.

Table 7.1. Summary of 1D-compression tests reported in this study

Test Number	Initial void ratio [-]	Final void ratio 1† [-]	Final void ratio 2‡ [-]
FG0.5_1§	1.148	0.545	0.546
FG0.5_2	1.099	0.529	0.533
FG0.5_3	1.056	0.528	0.528
FG0.5_4	0.955	0.532	0.531
FG0.5_5	0.907	0.526	0.529
FG2.0_1	0.975	0.504	0.484
FG2.0_2	0.925	0.490	0.481
FG2.0_3	0.862	0.469	0.455
FG2.0_4	0.756	0.462	0.463
FG2.0_5	0.664	0.440	0.435

Note: § FG0.5_1 the first number means the initial fractal dimension is 0.5, the second number means the different initial void ratio; † means the final void ratio is calculated from initial void ratio and vertical displacement measured by LVDT; ‡ means the final void ratio is calculated from final measurement of sample height.

7.3 Test results

The compression curves of the two carbonate sands with various initial void ratios are presented in Figure 7.2. It is clear from Figure 7.2(a) that samples with narrow-graded PSD (i.e., D = 0.5) tend to have a unique one-dimensional normal compression line (1D-NCL) in the e-log(σ_v) space. The slope of the NCL, i.e., the compressibility index C_c (= (-Δe)/Δlog (σ_v), where e is the void ratio and σ_v is the effective vertical stress) is calculated to be approximately equal to 0.51. Figure 7.2(b) shows little convergence of compression paths for wide-graded carbonate sands with D = 2.0. The difference of void ratio at vertical stress of 32 MPa is three times of the estimated accuracy of the void ratio of 0.02, which indicates that a transitional behaviour is observed.

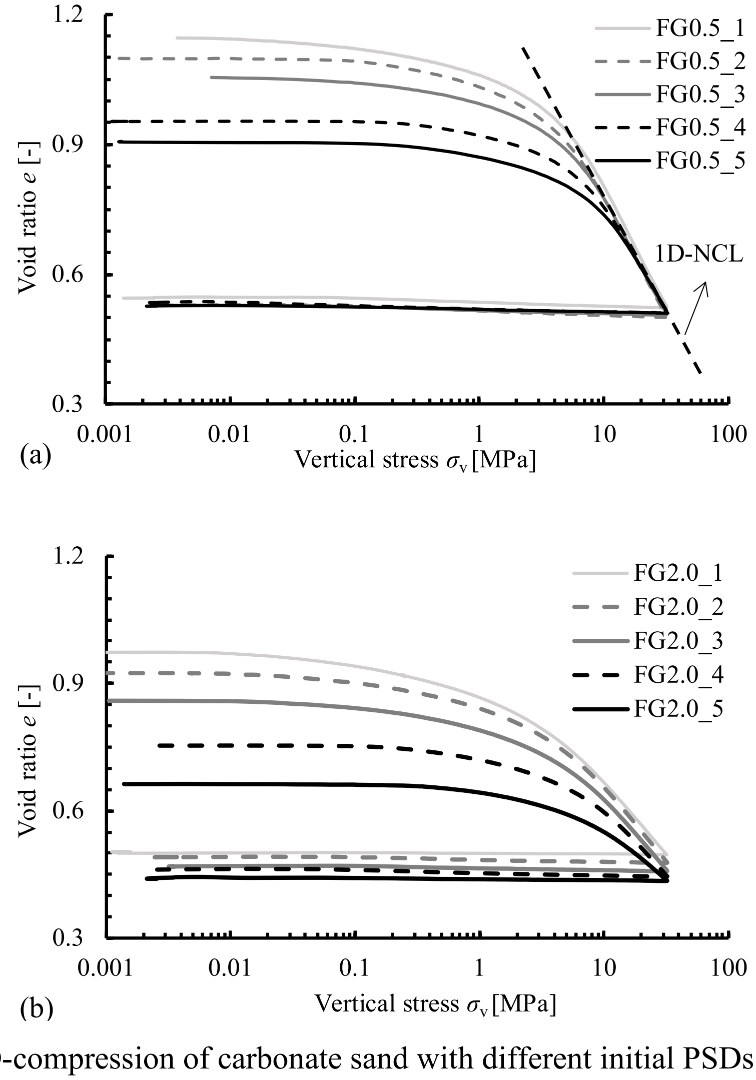

Figure 7.2: 1D-compression of carbonate sand with different initial PSDs: (a) D=0.5, (b) D=2.0

A closer look at the compression behavior of the samples with two different initial PSDs is presented in Figure 7.3 in terms of the relation between the tangent-constrained modulus M (=$\Delta\sigma_v/\Delta\varepsilon_v$, where ε_v is the vertical strain) and vertical stress. As summarized by Mesri & Vardhanabhuti (2009), there are three main shapes of e-log (σ_v) curve of granular soils during compression, i.e., the type A, type B, and type C. In the type A compression curve, M first increases, then decreases, and finally increases with increasing vertical stress. In the type B compression curve, M first increases, then almost keeps constant (see the red lines in Figure 7.3(a)), and finally increases with increasing vertical stress. In the type C compression curve, M increases with an increase in the vertical stress throughout the whole compression stage. As shown in Figure 7.3(a), a type B compression curve for the dense sample and a type C compression curve for the loose sample are observed for the samples with D = 0.5. All the values of M for different initial void ratios at high vertical stresses approach to almost the same value, indicating all the compression curves will eventually be coincident at high vertical stresses as seen in Figure 7.2(b).

As for the wide-graded samples with D = 2.0, only a type C compression curve is observed with various initial void ratios. The values of M for all the compression curves (except for the densest sample) tend to be identical at large stresses. As shown in Figure 7.2(b), the densest sample yields a very large vertical stress, and the linear part of the compression curve in the e-log (σ_v) space is still not obvious. It is reasonably assumed that the compression curve of the densest sample will be eventually parallel with those of samples with other initial void ratios if the vertical stress is large enough. Considering the fact that the other four compression curves have been parallel already at the given stress level, it is still convincing that the behaviour of the sample with D = 2.0 is transitional. As shown in Figure 7.3(a) and Figure 7.3(b), a decrease in the value of M can be observed as the initial PSD becomes more uniform.

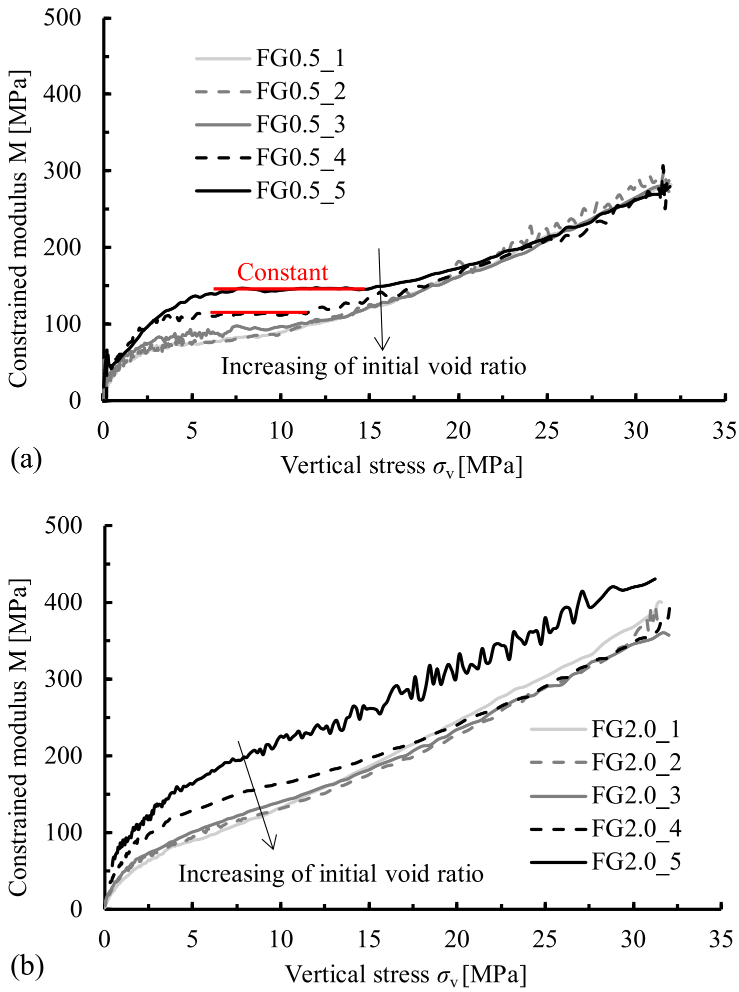

Figure 7.3: The tangent-constrained modulus of carbonate sand with different initial PSDs: (a) D=0.5, (b) D=2.0

Post-test samples were sieved using a standard sieving apparatus to obtain the evolution of PSD due to particle breakage. The PSDs before and after tests are shown in Figure 7.4 in a log-log scale. It is interesting noting that the PSDs are more or less straight lines in the double logarithmic plot, which means the PSD after the test is also fractal-graded. To quantify particle breakage, the modified Hardin's breakage index B_r^* proposed by Einav (2007a) is widely used as it considers the ultimate fractal grading at extreme conditions, as defined in Figure 7.5. Inspiring from the fact that PSDs after the tests are fractal-graded, a new breakage index is defined as

$$B_D = \frac{D - D_{\text{initial}}}{D_{\text{ultimate}} - D_{\text{initial}}} \tag{7.2}$$

where D is the fractal dimension after test, D_{initial} and D_{ultimate} are the fractal dimensional at the initial and ultimate state, respectively. D_{ultimate} is adopted 2.6 for carbonate sand as reported by others (Coop *et al.*, 2004; Xiao *et al.*, 2016c).

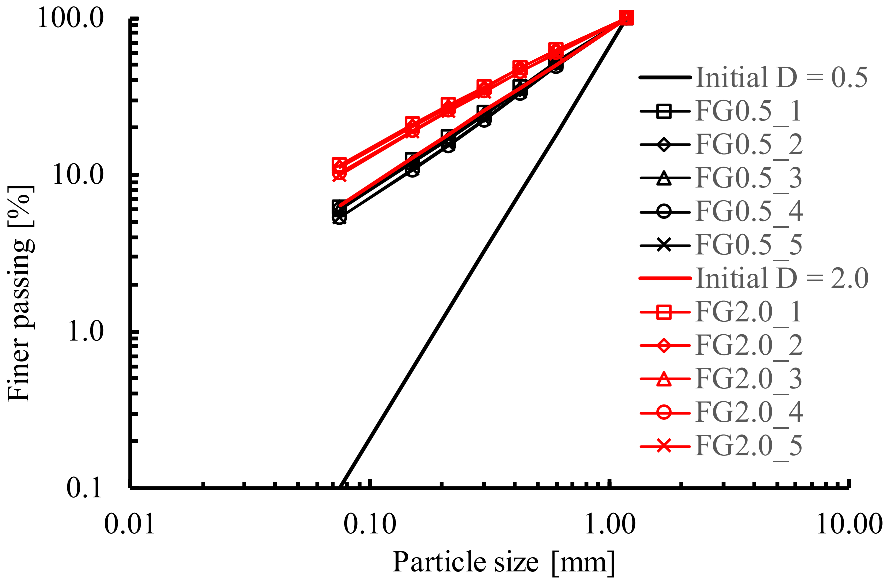

Figure 7.4: PSDs of the two soils before and after test

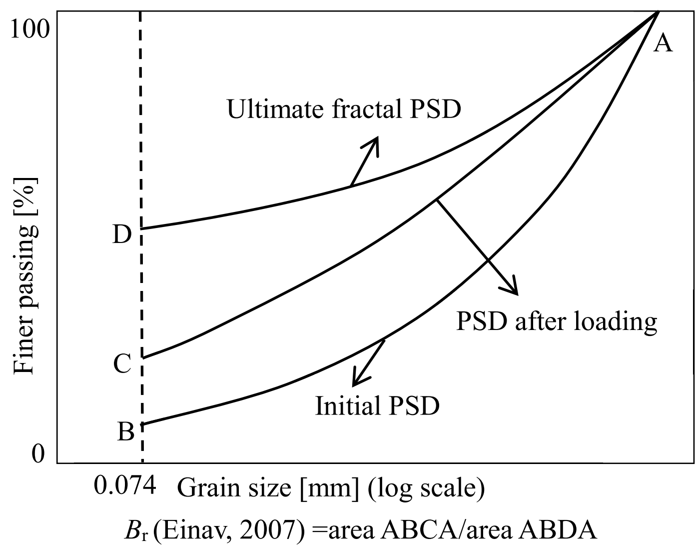

Figure 7.5: Definition of modified Hardin's breakage index B_r^* (Einav, 2007a)

Figure 7.6 shows the values of B_r^* and B_D for the samples with different PSDs and initial void ratios. In general, a denser sample will suffer less particle breakage in terms of both breakage indices B_r^* and B_D, which is in accordance with previous findings (Altuhafi & Coop, 2011a; Xiao *et al.*, 2017). It seems that the effect of initial PSD on particle breakage is not obvious when using B_r^*, which is different with what is commonly accepted that initial PSD plays a significant role in the particle breakage. In that case, using B_D as a breakage index will highlight the importance of initial PSD. Overall, particle breakage is observed for the narrow-graded with non-transitional behavior and wide-graded carbonate sand with transitional behaviour when using both the breakage indices B_r^* and B_D.

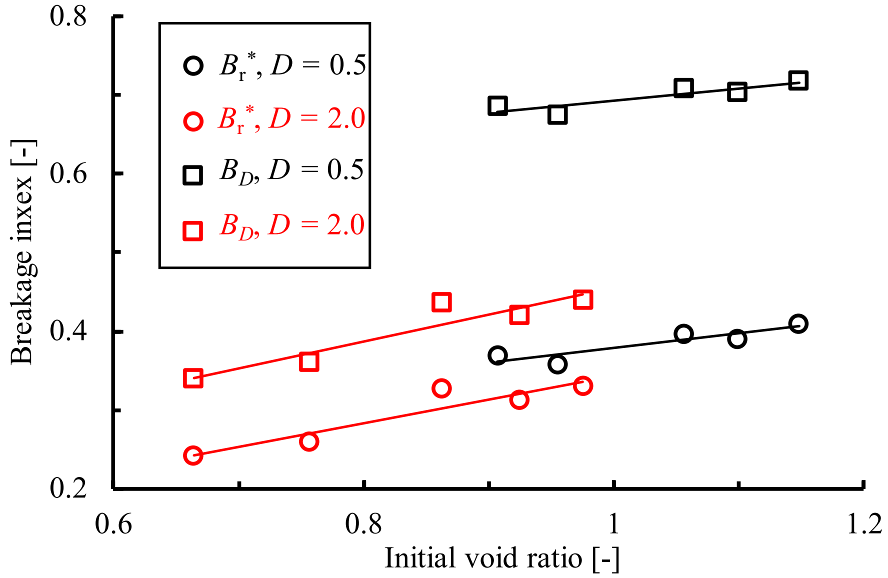

Figure 7.6: Values of B_r^* and B_D for the two soils with different initial PSD after the test

7.4 Conclusions

This study presents 1D-compression tests on carbonate sand with two different initial fractal-graded PSDs. The narrow-graded sample shows non-transitional behaviour with a unique 1D-NCL. The type B compression curve for the dense sample and type C compression curve for the loose sample are observed for the narrow-graded samples. The wide-graded sample, however, shows a typical feature of transitional behaviour with non-convergent compression paths. The type C compression curve is observed for the wide-graded samples with a wide range of initial void ratios. Detectable particle breakage could be observed in both transitional and non-transitional carbonate sands.

List of symbols

PSD	Particle size distribution
$F(d)$	mass percentage finer than particle size d
$d_{\max}$	maximum particle size
D	fractal dimension
M	tangent-constrained modulus
C_c	compression index
B_r^*	Einav's breakage index (Einav, 2007)
B_D	new breakage index
D_{initial} and D_{ultimate}	fractal dimensional at initial state and PSD index at ultimate state

Chapter 8 . A critical state framework for granular soils experiencing particle breakage

ABSTRACT: Typical behavioural features of granular materials include: (1) the critical state line (CSL) and isotropic compression lines (ICLs) cannot be represented by straight lines in the e - log(p) space, (2) the stress-strain behaviour is dependent on void ratio and confining pressure, and (3) particle breakage occurs and affects the location of the CSL and the stress-strain behaviour. A practical approach for considering particle breakage in constitutive modelling is to incorporate the breakage-induced movement of the CSL into the well-known state parameter. However, such an approach suffers from two main limitations, especially at high stresses: (1) the CSL is not suitable as a reference line for defining the state parameter because of the different PSDs between the current state and the reference state, (2) the common assumption that the CSL experiences parallel shifts as particle breakage progresses is not supported by experimental data. This paper aims to develop a state-dependent constitutive model based on a new definition of the state parameter and a new evolution law for the CSL. We adopt a double logarithmic approach for modelling the nonlinearity of the CSL and ICLs. We assume that the CSL shifts downwards with increasing particle breakage under a relatively low stress level. Furthermore, the CSLs with various degrees of particle breakage will eventually converge to a steady state at a high stress level where particle breakage completes and is no longer the main deformation mechanism of granular soils. The proposed model is validated against experimental data with satisfactory performance.
Keywords: Granular soil; critical state; state parameter; particle breakage; constitutive modelling

This chapter aims to solve the third key issue (i.e., constitutive law), and is based on a journal paper submitted to Computers and Geotechnics:

Tong, C. X., *Sheng, D., & Zhang, S. (2020b). A critical state framework for granular soils experiencing particle breakage. Computers and Geotechnics. Under review (Manuscript number: COGE-D-20-00037).*

Authorship Declaration

By signing below I conform that for the journal paper titled ‘A critical state framework for granular soils experiencing particle breakage’ submitted to Computers and Geotechnics, that:

Chenxi Tong proposed the model and wrote the manuscript.

Daichao Sheng is the leader of the research team, and assisted in the revision of the manuscript and discussion of the proposed model.

Sheng Zhang contributed to the discussion of the proposed model.

Production Note:

Signature removed
prior to publication.

Chenxi Tong

Prof Daichao Sheng

Prof Sheng Zhang

8.1 Introduction

The mechanical behaviour of granular soils is significantly different from that of other soils with smaller particle sizes like clay, mainly reflected by the three main properties, i.e., (1) the nonlinear critical state line (CSL) and isotropic compression lines (ICLs) in the space of void ratio e (or, specific volume v = 1+e) versus the logarithm of mean effective ln$p$, (2) the state dependency, and (3) the crushability of granular soils. It is commonly accepted that particle breakage will change the CSL and also affect the stress-strain behaviour of granular soils.

The concept of critical state is defined as a state at which plastic shearing could continue indefinitely with no change in effective stress or specific volume ($\partial q/\partial \varepsilon_s = \partial p/\partial \varepsilon_s = /\partial \varepsilon_v /\partial \varepsilon_s = 0$, where p and q are the mean effective stress and shear stress; ε_v and ε_s are the volumetric strain and deviatoric strain) (Roscoe *et al.*, 1958; Muir Wood, 1990). These critical states were reached with a unique line or curve in both p - q space and e - log(p) space, which is the fundamental of the pioneering work of critical state soil mechanics (CSSM) (Roscoe *et al.*, 1958; Schofield & Wroth, 1968). The application of CSSM to granular soils was less successful than that of clay, mainly due to the fact that the ICL (or, normal compression line as defined for the normal consolidated clay) cannot be determined (Been *et al.*, 1991). Strictly speaking, the ICL of a granular soil is not unique, and depends on its initial void ratio. Those ICLs will eventually converge into a unique line referred to as the limit compression line (LCL, Pestana & Whittle, 1995), which is considered to be parallel to the CSL at high stresses (de Bono & McDowell, 2018). It should be noted that the CSSM is not applicable for those samples with transitional behaviour where the occurrence of non-convergent compression paths is observed (Altuhafi & Coop, 2011a; Shipton & Coop, 2012; Shipton & Coop, 2015; Xiao *et al.*, 2016a). To model the nonlinear CSL and ICLs as observed by many laboratory studies (Verdugo & Ishihara, 1996; Yamamuro & Lade, 1996; Yu, 2017c), several empirical formulas had been proposed, such as single logarithmic approach (Yao *et al.*, 2019), double logarithmic approach (Butterfield, 1979; Pestana & Whittle, 1995; McDowell, 2005; Sheng *et al.*, 2008; Yao *et al.*, 2018), power approach (Li & Wang, 1998), composite function approach (Gudehus, 1996; Bauer, 1996; Wan & Guo, 2004), and three linear segments approach (Russell & Khalili, 2004). More comprehensive comparisons of these approaches can be found in the literature (Sheng *et al.*, 2008, de Bono, 2013).

The stress-strain behaviour of granular soils are highly dependent on both the mean effective stress and initial density. Constitutive models of granular soils developed in the past tend to adopt different sets of parameters for the same material for different initial states, which is of great inconvenience. In order to understand, describe and normalise the behaviour of granular soils, several parameters have been proposed based on the concept of critical state. The core ideal is to measure the distance between the current state and the critical state by using the CSL as a reference line. Been & Jefferies (1985) defined the state parameter ψ as the difference between the current and the critical void ratios at the same mean effective stress (= e - e_{cs}). Ishihara (1993) proposed a state index I_s based on the loosest state of sands (= (e_0 - e) / (e_0 - e_{cs}), where e_0 is the threshold void ratio). Similarly, Wan & Guo (1998) introduced the state index I_e defined as the ratio of the current to the critical state void ratios at the same mean effective stress (= e / e_{cs}). Other forms of state indices have also been proposed. For example, Wang *et al.* (2002) introduced a state index, which measures the ratio of the current to the critical mean effective stresses at the same void ratio. Those state indices have been successfully used in modelling the behaviour of sand (Jefferies, 1993; Manzari & Dafalias, 1997; Gajo & Muir Wood, 1999; Li & Dafalias, 2000; Jin *et al.*, 2017), ballast (Sun *et al.*, 2014b; Chen *et al.*, 2016), and rockfill materials (Liu & Zou, 2013; Liu *et al.*, 2014a; Liu & Gao, 2016; Xiao & Liu, 2017, Yin *et al.*, 2016).

Particle breakage is important for many engineering applications, which will greatly change particle size distributions (PSDs) of granular soils, and thus significantly affect their stress-strain behaviour. In fact, the nonlinearity of ICLs in the e - log(p) space is thought to be mainly attributed to particle breakage, while the maximum curvature points of the ICLs are generally considered as the beginning of particle breakage (e.g. Hagerty *et al.*, 1993; Nakata *et al.*, 2001a; Chuhan *et al.*, 2003; Xiao *et al.*, 2018b). The influence of particle breakage on the location of the CSL has been extensively studied. In general, particle breakage has a very limited effect on the CSL in the p - q space, and the critical state friction angle is assumed to be independent of particle breakage in most studies in the literature (e.g. Coop, 1990; Yamamuro & Lade, 1996; Russell & Khalili, 2004; Coop *et al.*, 2004; Bandini & Coop, 2011; Kan & Taiebat, 2014; Yu, 2017c). The effect of particle breakage on the location of CSL in the e - log(p) space, however, is more complicated and controversial. It is difficult to obtain the evolving CSLs during particle breakage. On the other hand, we can test samples reconstituted from different initial PSDs, representing different degrees of particle breakage for a given initial PSD as a basis, at low stress levels to so that particle breakage is negligible (Murthy *et al.*, 2007; Ghafghazi *et al.*, 2014; Yu, 2017c). However, a question might arise as to whether the CSL in the *e* - log(*p*) space changes because of particle breakage or because CSL is just only a function of the initial PSD. Bandini & Coop (2011) conducted triaxial tests with two different shearing stages, the first stage is to produce different degrees of particle breakage of the original sample, and the second stage is to explore whether such a change in PSD during the first stage will change the CSL under relative small stresses with undetectable breakage. By comparison, they tested the reconstituted samples with the same PSDs as those samples after shearing. The results showed that these two samples had different CSLs, indicating that samples might be able to 'know' about the breakage that they have suffered. In that case, it seems that the approach of testing the reconstituted samples with different initial PSDs is not fully justified. Nevertheless, a conclusion still can be made that particle breakage will lead to a change of intercept of CSL in the *e* - log(*p*) space revealed by all the studies in the literature (e.g. Daouadji *et al.*, 2001; Murthy *et al.*, 2007; Muir Wood & Maeda, 2008; Bandini & Coop, 2011; Ghafghazi *et al.*, 2014; Xiao *et al.*, 2016c; Yu, 2017c).

Intuitively, particle breakage produces more fine particles, which leads to the suppression of dilatancy (or, the promotion of contraction), and the reduction of the strength of granular soils. The effects of particle breakage on dilatancy have been investigated on the basis of energy dissipation (Ueng & Chen, 2000; Salim & Indraratna, 2004; Liu *et al.*, 2014a), or state indices where the effect of particle breakage on the CSL is incorporated (Kikumoto *et al.*, 2010; Liu & Zou, 2013; Xiao *et al.*, 2014c; Liu & Gao, 2016; Xiao & Liu, 2017). Although the commonly-used state parameter proposed by Been & Jefferies (1985) provides a normalised description of samples at various mean effective stresses and densities and is also flexible when considering the effect of particle breakage, it has some limitations, especially when the sample is very loose and subjected to high stresses. For example, assuming that a sample is initially consolidated to point A (as shown in Figure 8.1) with the mean effective stress less than that of the maximum curvature point of the ICL (see point D in Figure 8.1), which means only limited particle breakage occurs at this stage. After that, the sample is sheared under undrained condition to point B where the flow liquefaction is observed because it is in the instable liquefaction zone. In that case, the sample reaches to the CSL with almost no change in PSD. However, according to the definition of state parameter, the corresponding reference point at the CSL (point C as shown in Figure 8.1) corresponds to a certain amount of breakage. Therefore, point C is not suitable for a reference point for point A when calculating the state parameter, because of the different PSDs. Such a limitation had also been stated by Ghafghazi *et al.* (2014) and Javanmardi *et al.* (2018). Javanmardi *et al.* (2018) then proposed a new reference line instead of the CSL with satisfactory performance. However, constitutive models based on this new reference line are not available.

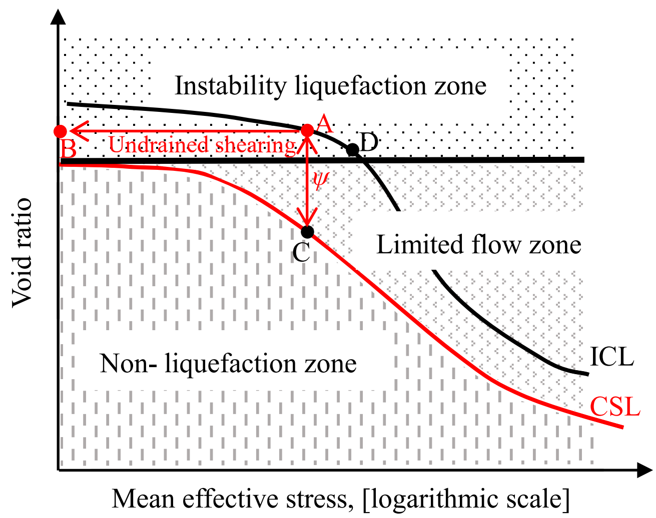

Figure 8.1: Illustration of the limitation of state parameter under undrained shearing

The aim of this paper is to propose a simple constitutive model considering the three main properties of granular soils. Firstly, a double logarithmic approach proposed by Sheng *et al.* (2008) is adopted for modelling the nonlinear CSL and ICLs in the e - log(p) space. The state-dependent behaviour is then developed by using the modified state parameter where a new reference compression line (RCL) suggested by Javanmardi *et al.* (2018) is employed. The particle breakage effects are incorporated with consideration of the change of intercept of the CSL in the e - log(p) space. Finally, the proposed model is validated against experimental triaxial test data in the literature.

8.2 Notation and definitions

The following stress and strain invariants are used for developing the constitutive model in terms of the principal stress space:

$$\begin{cases} \sigma_{\mathrm{m}} = \left(\sigma_{11} + \sigma_{22} + \sigma_{33}\right)/3 \\ s_{ij} = \sigma_{ij} - \sigma_{\mathrm{m}}\delta_{ij} \\ p = \sigma_{kk}/3 \\ q = \sqrt{\dfrac{3}{2}s_{ij}s_{ij}} \end{cases}, \begin{cases} \varepsilon_{\mathrm{m}} = \left(\varepsilon_{11} + \varepsilon_{22} + \varepsilon_{33}\right)/3 \\ e_{ij} = \varepsilon_{ij} - \varepsilon_{\mathrm{m}}\delta_{ij} \\ \varepsilon_{\mathrm{v}} = \varepsilon_{kk} \\ \varepsilon_{\mathrm{s}} = \sqrt{\dfrac{2}{3}e_{ij}e_{ij}} \end{cases} \tag{8.1}$$

where σ_{ij} is the stress tensor (i, j = 1, 2, 3); σ_{m} (p) is the mean stress; s_{ij} is the deviatoric stress tensor; δ_{ij} is the Kronecker delta (i.e., $\delta_{ij} = 1$ for $i = j$, otherwise $\delta_{ij} = 0$); q is the deviatoric stress; ε_{ij} is the strain tensor (i, j = 1, 2, 3); ε_{m} is the mean strain; e_{ij} is the deviatoric strain tensor; ε_{v} is the volumetric strain; ε_{s} is the deviatoric strain. All stresses used in this paper are referred as to effective stresses.

For the conventional triaxial test where the specimen is subjected to an axisymmetric stress (i.e., $\sigma_{22} = \sigma_{33}$ and $\varepsilon_{22} = \varepsilon_{33}$), the stress and strain invariants can be simplified as

$$\begin{cases} p = \left(\sigma_1 + 2\sigma_3\right)/3 \\ q = \sigma_1 - \sigma_3 \\ \varepsilon_{\mathrm{v}} = \varepsilon_1 + 2\varepsilon_3 \\ \varepsilon_{\mathrm{s}} = 2(\varepsilon_1 - \varepsilon_3)/3 \end{cases} \tag{8.2}$$

8.3 Modified state parameter

8.3.1 Nonlinear CSL and ICLs

As shown by Pestana & Whittle (1995), the Limit Compression Line (LCL) can be expressed as a perfect straight line in the space of logarithm of void ratio versus logarithm of mean effective stress

$$\ln(e_{\mathrm{LCL}}) = \ln(N) - \lambda \ln(p/p_{\mathrm{r}}) \tag{8.3}$$

where p_{r} is the unit pressure (= 1 kPa) for ensuring the dimensionally consistency, e_{LCL} is the void ratio on the LCL, N is the void ratio on the LCL when p = 1 kPa, λ is the slope of LCL in the ln(e) - ln(p) space. A family of Isotropic Compression Lines (ICLs) can be given by adding one parameter in the Equation (8.3) (Sheng *et al.*, 2008)

$$\ln(e_{\mathrm{ICL}}) = \ln(N) - \lambda \ln\left[\left(p + p_{\mathrm{ICL}}\right)/p_{\mathrm{r}}\right] \tag{8.4}$$

where e_{ICL} is the void ratio on the ICLs, p_{ICL} is defined as a shifting stress controlling the curvature of the ICL, which depends on the initial void ratio of sample, i.e., a smaller initial void ratio leads to a larger p_{ICL} value (as shown in Figure 8.2). A similar form of CSL with Equation (8.4) is also defined by Sheng *et al.* (2008), which takes the form

$$\ln(e_{\mathrm{CSL}}) = \ln(\Gamma) - \lambda \ln\left[\left(p + p_{\mathrm{CSL}}\right) / p_{\mathrm{r}}\right] \tag{8.5}$$

where e_{CSL} is the void ratio on the CSL, Γ is the void ratio on the CSL when $p + p_{\mathrm{CSL}} =$ 1kPa, p_{CSL} is defined as a shifting stress controlling the curvature of the CSL.

8.3.2 A New RCL

Javanmardi *et al.* (2018) found that the Reference Compression Line (RCL) would approximately be represented by an ICL that coincides with the CSL at a very low mean effective stress. In this paper, we assume that the RCL intersects with the CSL at $p = 0$, $e = e_{\mathrm{CS0}}$. Substituting this point into Equation (8.5) gives

$$p_{\mathrm{ICL}} = \left(\frac{N}{e_{\mathrm{CS0}}}\right)^{1/\lambda} p_{\mathrm{r}} \tag{8.6}$$

The new RCL can be obtained by substituting Equation (8.6) into Equation(8.5), expressed as

$$\ln(e_{\mathrm{RCL}}) = \ln(N) - \lambda \ln\left[p + \left(\tfrac{N}{e_{\mathrm{CS0}}}\right)^{1/\lambda}\right] \tag{8.7}$$

The new RCL is shown in Figure 8.2 for a sample with $N = 5$, $\lambda = 0.25$, $\Gamma = 4$, $e_{\mathrm{CS0}} = e_{\mathrm{CSL}}$ = 0.9 at p = 10 kPa. As shown in Figure 8.2, all the ICLs converge into the LCL that is parallel to the CSL at very high stresses in the e - ln(p) space.

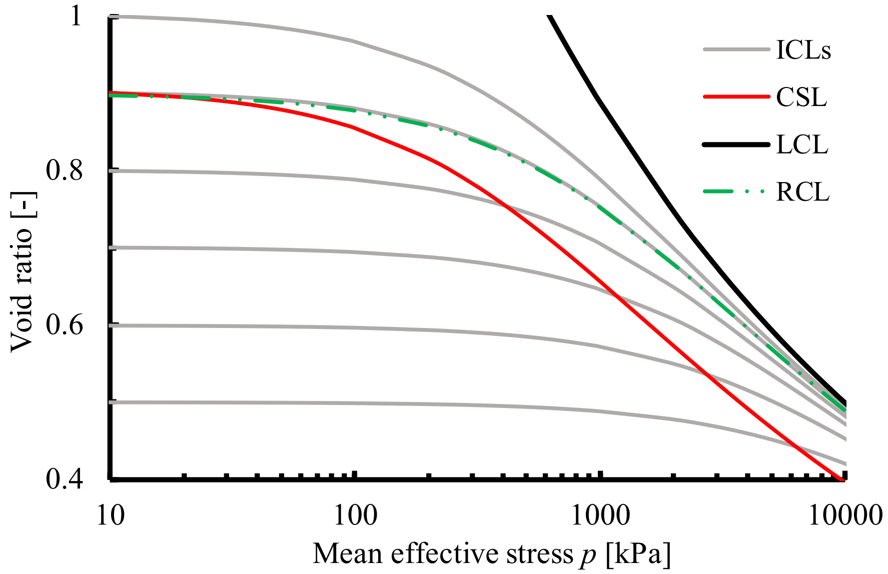

Figure 8.2: Illustration of ICLs, CSL, LCL, and RCL ($N = 5$, $\lambda = 0.25$, $\Gamma = 4$, $e_{CS0} = e_{CSL}$ = 0.9 at p = 10 kPa)

According to Equation (8.7), the new RCL needs three parameters: the void ratio on the LCL at p = 1 kPa, the slope of LCL in the ln(e) - ln(p) space, and the void ratio on the CSL at p = 0. It should be noted that the third parameter can be adopted as the void ratio on the CSL at a low mean effective stress if the critical state void ratio at 0 stress is not available. Figure 8.2 demonstrates that the RCL obtained from Equation (8.7) with $e_{CS0} = e_{CSL}$ at p = 10 kPa almost coincides with the ICL, with some minor differences at low stresses as shown in Figure 8.3.

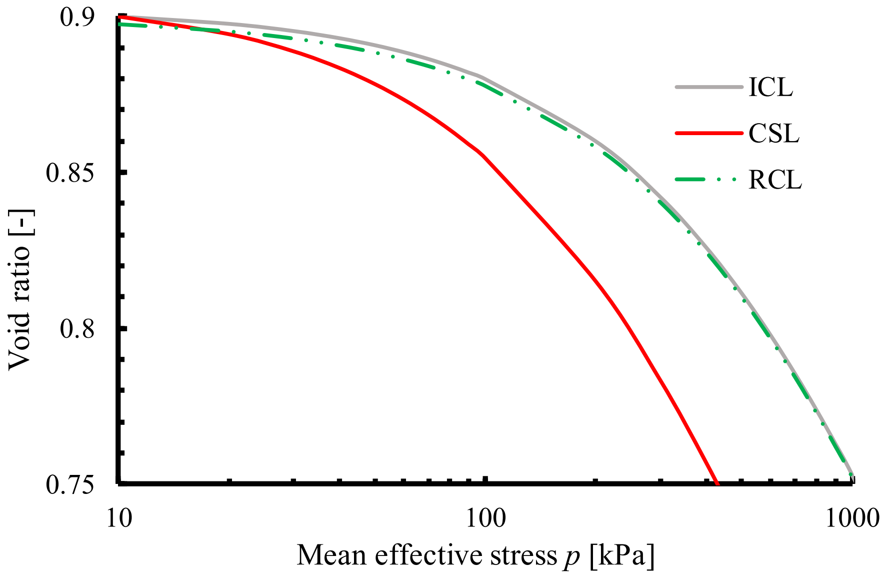

Figure 8.3: Magnified figure 8.2 at low stresses

8.3.3 Modified state parameter

The modified state parameter Ψ is defined as the difference between the current void ratio and the void ratio on the RCL at the same mean effective stress (see Figure 8.4) based on the definition of state parameter ψ proposed by Been & Jefferies (1985) as follows

$$\Psi = e - e_{\mathrm{RCL}} = e - \frac{N}{\left[p + \left(\frac{N}{e_{\mathrm{CS0}}}\right)^{1/\lambda}\right]^{\lambda}} \tag{8.8}$$

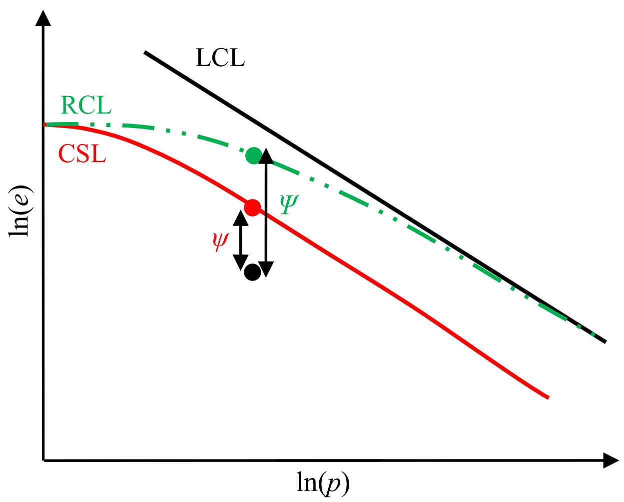

Figure 8.4: Definition of the modified state parameter Ψ

8.4 Particle breakage of granular soils

8.4.1 Particle breakage index

An appropriate constitutive model of granular soils should consider the evolution of PSD during stress path, which means the PSD should be treated as a variable in a constitutive model (Einav, 2007a; Muir Wood & Maeda, 2008; Zhang *et al.*, 2015). In that case, it is necessary to adopt a simple variable that can represent the PSD and measure the degree of particle breakage of a sample, preferably within the range of 0 to 1, with 0 meaning no breakage and 1 full breakage. During the last decades, several indices have been proposed and are based either on the initial PSD, the current PSD or the ultimate PSD. Some indices can reflect changes in the characteristic particle size, such as the change of the coefficient of uniformity C_u (= d_{60}/ d_{10}) (Li *et al.*, 2014; Hu *et al.*, 2018), the change of d_{10} (i.e., B_{10}

as defined by Lade *et al.*, 1996), the change of d_{15} (i.e., B_{15} as defined by Lee & Farhoomand, 1967). Some indices can indicate the overall shape of the PSD, such as the slope of linear fitting line of PSD in the log-log space (Konrad & Salami, 2018; Yu, 2018b). Some other indices can describe the overall change of the PSD with consideration of all the size fractions, such as breakage index B proposed by Marsal (1967), increase of surface area ΔS (Miura & O'Hara, 1979), relative breakage index B_r (Hardin, 1985) and modified relative breakage index B_r^* (Einav, 2007a), grading state index I_g (Muir Wood, 2007). With increased understanding and knowledge of particle breakage, especially the development of fractal breakage theory, the modified relative breakage index B_r^* proposed by Einav (2007a) can be considered as an appropriate variable. This index considers the ultimate fractal PSD, and thus its value is in the range of 0 (no breakage) to 1 (complete breakage), although it cannot fully describe the whole PSD (Konrad & Salami, 2018; Tong *et al.*, 2018a).

An alternative option is to start with the recently proposed PSD model (Tong *et al.*, 2018a), which can capture the evolving PSD of granular soils duo to particle breakage well. The model is expressed as

$$P(d) = 1 - e^{-\left(\frac{d}{\lambda_p (d_{max} - d)}\right)^{\kappa_p}} \tag{8.9}$$

where λ_p is a scale parameter, and κ_p is a shape parameter, d_{max} is the maximum particle size. Parameter λ_p is a function of d_{max} and $d_{63.2}$

$$\lambda_p = \frac{d_{63.2}}{d_{max} - d_{63.2}} \tag{8.10}$$

where $d_{63.2}$ is the characteristic particle diameter at which 63.2% of the sample by mass is smaller. According to the study by Tong *et al.* (2019a), λ_p is linearly related to Einav's B_r^*, indicating that λ_p can not only consider the overall change of PSD, but also sufficiently describe the whole PSD for a given κ_p. Therefore, particle breakage index named as 'relative PSD index' B_λ is defined to quantify the degree of breakage as given by

$$B_\lambda = \frac{\lambda_{pi} - \lambda_{pc}}{\lambda_{pi} - \lambda_{pu}} \tag{8.11}$$

where λ_{pi} is the initial value of λ_p, λ_{pu} is the ultimate value of λ_p, λ_{pc} is the current value of λ_p. All the values can be calculated by using Equation (8.10) when knowing the corresponding value of $d_{63.2}$. The value of B_λ ranges from 0 to 1 as the PSD evolves from the initial state to the ultimate state. The ultimate state, however, is commonly assumed to follow fractal distribution (Steacy & Sammis, 1991; McDowell & Bolton, 1998) with the value of

$$d_{63.2u} = 0.632^{\frac{1}{3-D}} d_{max} \tag{8.12}$$

Substitution of Equation (8.10) and Equation (8.12) into Equation (8.11) yields

$$B_\lambda = \frac{\dfrac{d_{63.2i}}{d_{max} - d_{63.2i}} - \dfrac{d_{63.2u}}{d_{max} - d_{63.2u}}}{\dfrac{d_{63.2i}}{d_{max} - d_{63.2i}} - \dfrac{0.632^{\frac{1}{3-D}}}{1 - 0.632^{\frac{1}{3-D}}}} \tag{8.13}$$

where $d_{63.2i}$, $d_{63.2c}$, and $d_{63.2u}$ are the $d_{63.2}$ at the initial state, current state and ultimate state, respectively (as shown in Figure 8.5), and D is the ultimate fractal dimension.

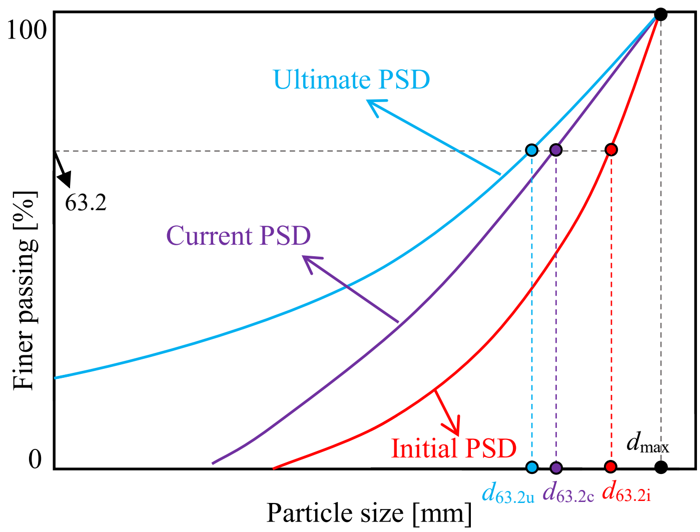

Figure 8.5: Definition of the breakage index B_λ

8.4.2 Evolution of breakage index

The evolution of particle breakage has been extensively studied, such as from mathematical modelling aspect (e.g. Marketos & Bolton, 2007; Zhang *et al.*, 2015; Caicedo *et al.*, 2016; Ovalle *et al.*, 2016; Cheng & Wang, 2018; Tong *et al.*, 2019b), and from constitutive modelling aspect (e.g. Hardin, 1985; Lade *et al.*, 1996; Daouadji *et al.*, 2001; Einav, 2007a; Hu *et al.*, 2018). The former can describe the evolution of the whole PSD more accurately, but is difficult to consider in constitutive models; while the latter provides the relationship between breakage indices and loading condition, and is easy to use in constitutive models.

A large number of tests have indicated that particle breakage is affected by both stress and strain (e.g. Coop *et al.*, 2004; Tong *et al.*, 2019a). Breakage indices are often correlated to energy quantities which are combinations of stress and strain. There is not much difference when using total input work and plastic work because the amount of elastic work is often several orders of magnitude smaller than that of plastic work in many cases, such as in ring shear test (Tong *et al.*, 2019a), impact test (Xiao *et al.*, 2016c), triaxial test with considerable particle breakage (Lade *et al.*, 1996). However, the accumulation of particle breakage during cyclic loading cannot be predicted when using total input work. In general, correlating plastic work with particle breakage indices provides a unified and flexible approach when considering particle breakage in constitutive models subjected to both monotonic and cyclic loading (Daouadji *et al.*, 2001, Hu *et al.*, 2018).

The plastic work W^p in a conventional triaxial test can be expressed as follows

$$W^p = \int \left\langle \sigma_{ij} \mathrm{d}\varepsilon_{ij}^p \right\rangle = \int \left\langle p \mathrm{d}\varepsilon_{\mathrm{v}}^p + q \mathrm{d}\varepsilon_{\mathrm{s}}^p \right\rangle \tag{8.14}$$

where the symbol $\langle\ \rangle$ is the Macaulay's brackets (i.e., $\langle x \rangle = x$, if $x \geq 0$; $\langle x \rangle = 0$, if $x <$ 0). The relationship between the plastic work and breakage index can be described by a unified hyperbolic function, regardless of the initial density or stress path. For example, Hu *et al.* (2018) showed that both B_{r}^* and B_{u} (defined as relative uniformity) could be hyperbolically related to the plastic work by extensive experimental results of different granular soils. Similarly, the relationship between B_λ and W^p can be given as

$$B_\lambda = \frac{W^p}{b \times p_{\mathrm{r}} + W^p} \tag{8.15}$$

where b is a material parameter controlling the evolution rate of PSD.

8.4.3 Incorporating with particle breakage effect

The CSL in the p - q space can be represented by a straight line and is assumed independent of particle breakage in this paper, which is consistent with most studies in the literature

$$M = \frac{q_{CS}}{p_{CS}} = \frac{6\sin\phi_{CS}}{3-\sin\phi_{CS}} \tag{8.16}$$

where M is the critical state stress ratio, and ϕ_{CS} is the critical state friction angle.

The CSL in the e - log(p) space, however, will be significantly affected by particle breakage in a complicated way. In this paper, a simple method for describing the evolution of the CSL, RCL, and LCL considering particle breakage is proposed as follows:

- The CSL shifts downwards with increasing B_λ value as observed by various experimental investigations under a relatively low stress level (Murthy *et al.*, 2007; Bandini & Coop, 2011; Ghafghazi *et al.*, 2014; Yu, 2017c). However, it is not possible to explore the effect of PSD on the CSL at a high stress level because of the evolving PSD at such high stresses. Realising that experimental results tend to show a steady ultimate state of particle breakage, we assume that the CSLs of samples with various degrees of particle breakage will eventually converge to steady state at a high stress level where particle breakage completes and is no longer the main deformation mechanism. As shown in Figure 8.6, the proposed evolution of CSL moves downwards with decreasing slope of CSL at the same mean effective stress (not high stress level), as particle breakage progresses. This assumption is reasonable and in consistent with the experimental results by Bandini & Coop (2011) and Xiao *et al.* (2016b), who found that particle breakage will not only result in a downward shift, but also a rotation of the CSL in the e - log(p) space. In other words, the intercept of CSL (value of e_{CS0} at $p = 0$), can be expressed as a function of B_λ.
- Since the RCL and CSL intersect at a very low mean effective stress (ideally at $p = 0$), the RCL will shift downwards subsequently as the proposed RCL is a function of e_{CS0} (as shown in Equation (8.7)). Again, all the RCLs of samples with various degrees of particle breakage will eventually converge to a steady state at a high stress level.

- The ICL will not change as it is an asymptotic line of the RCL at high stresses, which is similar with the observations by McDowell, who found the compression index ($C_c = (-\Delta e)/\Delta\log(\sigma'_v)$) is independent of the initial PSD (McDowell, 2002) and the slope of LCL in the log (e)-log (p) space depends on the ultimate fractal dimension, but is independent of the initial PSD (McDowell, 2005). The parameter N and λ of the LCL as shown in the Equation (8.3) are then independent of B_λ.

To quantify the evolution law of the CSL, RCL, and ICL, the relation between e_{CS0} and B_λ could be expressed in the following simple form

$$e_{\mathrm{CS0}} = e_{\mathrm{CS,ref}} \exp\left(-aB_\lambda\right) \tag{8.17}$$

where $e_{\mathrm{CS,ref}}$ is the intercept of the CSL without particle breakage ($B_\lambda = 0$), a is a material parameter that controls the rate of the CSL movement caused by particle breakage.

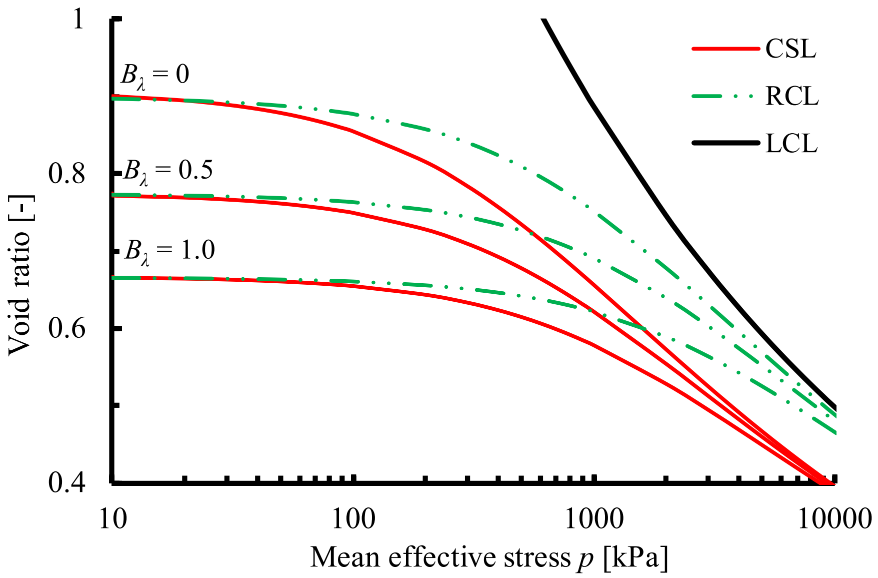

Figure 8.6: Evolution of the CSL, RCL, and LCL with increasing particle breakage

The evolution of the CSL, RCL, and LCL with increasing particle breakage are shown in Figure 8.6 for a granular soil with $N = 5$, $\lambda = 0.25$, $\Gamma = 4$, $e_{\mathrm{CS,ref}} = e_{\mathrm{CSL}} = 0.9$ at $p = 10$ kPa, $a = 0.3$. Substitution of Equation (8.17) into Equation (8.8) gives the modified state parameter with consideration of particle breakage

$$\Psi = e - N\Big/\left[p + \left(\frac{N}{e_{\mathrm{CS,ref}}\exp(-aB_\lambda)}\right)^{1/\lambda}\right]^{\lambda} \tag{8.18}$$

Based on Equation (8.18), a simple state-dependent constitutive model will be developed within the framework of Li & Dafalias (2000) in the following section.

8.5 Constitutive model

The total strain increment is calculated as the sum of the elastic strain increment and the plastic strain increment

$$d\varepsilon_{ij} = d\varepsilon_{ij}^{e} + d\varepsilon_{ij}^{p} \tag{8.19}$$

where the superscripts e and p represent the elastic and plastic, respectively.

8.5.1 Elastic strain increment

The elastic volumetric strain increment and the elastic deviatoric strain increment can be calculated as

$$\begin{cases} d\varepsilon_{\mathrm{v}}^{e} = \dfrac{dp}{K} \\ d\varepsilon_{\mathrm{s}}^{e} = \dfrac{dq}{3G} \end{cases} \tag{8.20}$$

where the subscripts v and s represent volumetric and deviatoric component, respectively; K and G are the elastic bulk modulus and the elastic shear modulus, respectively, and are dependent on mean effective stress and void ratio. The nonlinear hypoelastic relation proposed by Richart *et al.* (1970) is adopted for calculating G

$$G = G_0 \frac{(2.97 - e)^2}{(1 + e)} \sqrt{p \times p_{\mathrm{r}}} \tag{8.21}$$

where G_0 is a material constant. The elastic bulk modulus K can be determined by the Poisson's ratio μ

$$K = \frac{2(1 + \mu)}{3(1 - 2\mu)} G \tag{8.22}$$

8.5.2 Plastic strain increment

A simple yield surface that plastic deformation occurs whenever there is a change in stress ratio η (= q/p) proposed by Li & Dafalias (2000) for the triaxial compression is adopted

$$f = q - \eta p = 0 \tag{8.23}$$

The vector of the loading direction (n_{fv}, n_{fs}) is defined as

$$\begin{cases} n_{\text{fv}} = \dfrac{-\eta}{\sqrt{1+\eta^2}} \\ n_{\text{fs}} = \dfrac{1}{\sqrt{1+\eta^2}} \end{cases} \tag{8.24}$$

The plastic flow direction (n_{gv}, n_{gs}) is defined as

$$\begin{cases} n_{\text{gv}} = \dfrac{d_{\text{g}}}{\sqrt{1+d_{\text{g}}^{\ 2}}} \\ n_{\text{gs}} = \dfrac{1}{\sqrt{1+d_{\text{g}}^{\ 2}}} \end{cases} \tag{8.25}$$

where d_{g} is the state-dependent dilatancy equation, which is written as

$$d_{\text{g}} = \frac{\partial g}{\partial p} \Big/ \frac{\partial g}{\partial q} = d_0 \left(e^{m\Psi} - \frac{\eta}{M} \right) \tag{8.26}$$

in which g is the plastic potential function, d_0 and m are two positive material constants. Therefore, the non-associated flow rule is adopted in this paper. The plastic strain increment can be written as

$$\begin{cases} d\varepsilon_{\text{v}}^{p} = \dfrac{n_{\text{fv}} n_{\text{gv}}}{H_{\text{p}}} dp + \dfrac{n_{\text{fs}} n_{\text{gv}}}{H_{\text{p}}} dq \\ d\varepsilon_{\text{s}}^{p} = \dfrac{n_{\text{fv}} n_{\text{gs}}}{H_{\text{p}}} dp + \dfrac{n_{\text{fs}} n_{\text{gs}}}{H_{\text{p}}} dq \end{cases} \tag{8.27}$$

where H_{p} is the plastic modulus. The expression of H_{p} should satisfy the three conditions as suggested by Li & Dafalias (2000), i.e., (1) $H_{\text{p}} = +\infty$ at $\eta = 0$, (2) $H_{\text{p}} = 0$ at the critical state, and (3) $H_{\text{p}} = 0$ at the drained peak stress ratio. A simplified form of H_{p} as suggested by Liu & Gao (2016) is adopted in this paper.

$$H_{\text{p}} = H_0 G \frac{M_{\text{p}}^2 - \eta^2}{\eta} \tag{8.28}$$

where H_0 is a model constant; M_{p} is the virtual peak stress ratio, which is given as

$$M_{\text{p}} = M e^{[n\langle -\Psi \rangle]} \tag{8.29}$$

where n is a material constant. As indicated by Equation (8.29), when the sample is at a loose state ($-\Psi < 0$), we have $M_\mathrm{p} = M$; when the sample is in the dense state ($-\Psi > 0$), $M_\mathrm{p} > M$.

8.5.3 Stress-strain relationship

As can be obtained from Equation (8.20) and Equation (8.27), the stress-strain relations in the p - q space can be finally written as

$$\begin{pmatrix} d\varepsilon_\mathrm{v} \\ d\varepsilon_\mathrm{s} \end{pmatrix} = \begin{bmatrix} \dfrac{1}{K} + \dfrac{n_\mathrm{fv} n_\mathrm{gv}}{H_\mathrm{p}} & \dfrac{n_\mathrm{fs} n_\mathrm{gv}}{H_\mathrm{p}} \\ \dfrac{n_\mathrm{fv} n_\mathrm{gs}}{H_\mathrm{p}} & \dfrac{1}{3G} + \dfrac{n_\mathrm{fs} n_\mathrm{gs}}{H_\mathrm{p}} \end{bmatrix} \begin{pmatrix} dp \\ dq \end{pmatrix} \tag{8.30}$$

8.6 Model calibration and validation

8.6.1 Model calibration

The proposed model has 12 model parameters, which can be obtained by isotropic compression tests and conventional triaxial tests as described in the following:

(1) Four CSL, ICLs &LCL related parameters: M, N, λ, and $e_\mathrm{CS,ref}$.

These four parameters can be obtained by best fitting of the proposed equations of CSL, ICLs, and LCL with knowing experimental data of isotropic compression and triaxial tests. The critical state void ratio M can be measured as the slope of CSL in the p - q space by Equation (8.16), and parameter λ and $e_\mathrm{CS,ref}$ can be determined by Equation (8.5). The parameter N can be obtained by conducting one isotropic compression test at any initial void ratio via Equation (8.4).

(2) Two elastic parameters: G_0, and μ.

G_0 can be calculated from Equations (8.20) - (8.21) with ε_s - q plot, which can be rewritten as

$$G_0 = \frac{dq}{3d\varepsilon_\mathrm{s}^e} \frac{(1+e_0)}{(2.97-e_0)^2 \sqrt{p \times p_\mathrm{r}}} \tag{8.31}$$

where e_0 is the initial void ratio of sample, $\frac{dq}{d\varepsilon_{\mathrm{s}}^{e}}$ can be estimated by the slope of ε_{s} - q plot at small shear strain of approximately 1%. The Poisson's ratio μ can be obtained based on Equations (8.20) - (8.22) from ε_{s} - q plot and ε_{v} - p plot at initial stage

$$\mu = \left(9\frac{dp}{d\varepsilon_{\mathrm{v}}^{e}} - 2\frac{dq}{d\varepsilon_{\mathrm{s}}^{e}}\right) \Bigg/ \left(18\frac{dp}{d\varepsilon_{\mathrm{v}}^{e}} + 2\frac{dq}{d\varepsilon_{\mathrm{s}}^{e}}\right) \tag{8.32}$$

with $dp/d\varepsilon_{\mathrm{v}}^{e}$ estimated by the slope of ε_{v} - p plot at small volumetric strain of approximately 1%.

(3) Two particle breakage related parameters: a, and b.

The determination of the dynamic movement of CSL in the e - log (p) space is problematic. As proposed before, the critical state void ratio at low stress level e_{CS0} will change with various degree of particle breakage with evolution law by Equation (8.17). Thus, value of e_{CS0} of a given B_{λ} will be obtained by triaxial tests with low confining pressure, at which particle breakage is ignorable. The parameter b can be obtained by conducting a series of triaxial tests with different initial confining pressures. The input plastic work can be calculated by Equation(8.14), and the PSD at the end of each test can be determined by sieving test.

(4) Two dilatancy parameters: d_0, and m.

The parameter m can be determined when the sample is at phase transformation state where the dilatancy equation equals to zero. By setting d_{g} = 0 in Equation (8.26), parameter m can be expressed as

$$m = \frac{\ln\left(\frac{\eta_{\mathrm{PTS}}}{M}\right)}{\Psi_{\mathrm{PTS}}} \tag{8.33}$$

where η_{PTS} and Ψ_{PTS} are the stress ratio and modified state parameter at the phase transformation state. The parameter d_0 can be estimated by Equation (8.26) and ε_{s} - ε_{v} plot, where dilatancy equation d_{g} can be rewritten as

$$d_{\mathrm{g}} = d_0\left(e^{m\Psi} - \frac{\eta}{M}\right) = \frac{d\varepsilon_{\mathrm{v}}^{p}}{d\varepsilon_{\mathrm{s}}^{p}} \approx \frac{d\varepsilon_{\mathrm{v}}}{d\varepsilon_{\mathrm{s}}} \tag{8.34}$$

The parameter d_0 is determined by the slope of $\left(e^{m\Psi}-\dfrac{\eta}{M}\right)-\dfrac{d\varepsilon_{\mathrm{v}}}{d\varepsilon_{\mathrm{s}}}$ plot when the value of m is given.

(5) Two hardening parameters: H_0, and n.

The parameter n can be determined when the sample is at peak state by using Equation (8.29)

$$n=\frac{\ln\left(\dfrac{\eta_{\mathrm{PS}}}{M}\right)}{\langle\Psi_{\mathrm{PS}}\rangle} \tag{8.35}$$

where η_{PS} and Ψ_{PS} are the stress ratio and modified state parameter at the peak state. The parameter H_0 can determined by the drained triaxial test result based on Equations (8.21), and (8.24) - (8.29) with $dq = 3dp$, which can be expressed as

$$H_0=\frac{\dfrac{dq}{d\varepsilon_{\mathrm{s}}^{p}}(3-\eta)\eta}{3\sqrt{1+\eta^2}\sqrt{1+d_{\mathrm{g}}{}^2}G\left(M_{\mathrm{p}}{}^2-\eta^2\right)} \tag{8.36}$$

with $dq/d\varepsilon_{\mathrm{s}}^{p}\approx dq/d\varepsilon_{\mathrm{s}}$ by ignoring the small elastic deformations.

8.6.2 Model validation

To validate the proposed model, two sets of experimental data of drained and undrained triaxial tests on granular soils in the literature were adopted, i.e., the Cambria sand (Lade & Yamamuro, 1996; Yamamuro & Lade, 1996), and the Changhe rockfill (Liu *et al.*, 2011; Liu *et al.*, 2012). All model parameters are calibrated as discussed above and list in Table 8.1, and the computational steps for integration along imposed stress path for drained and undrained triaxial conditions are given in Appendix 8.1 and Appendix 8.2, respectively.

Table 8.1. Model parameters of the two granular soils

Soil name	Elastic parameters		CSL & ICL related parameters				Breakage parameters		Dilatancy parameters		Hardening parameters	
	G_0	μ	λ	M	N	$e_{\mathrm{CS,ref}}$	a	b	m	d_0	n	H_0
Cambria sand	350	0.25	1.12	1.35	96800	0.58	1.30	5408	0.50	2.50	0.60	0.45
Rockfill material	400	0.10	0.20	1.59	2.05	0.59	1.00	1055	0.30	1.50	1.0	0.35

8.6.2.1 Cambria sand

A series of drained and undrained triaxial tests on the Cambria sand were conducted by Lade and Yamamuro (Lade & Yamamuro, 1996; Yamamuro & Lade, 1996). The sand tested, which was composed of two main mineral constituents (i.e., 54% quartz, and 39% lithic) was uniformly graded with particle sizes between 0.83 and 2 mm. All the samples were prepared with initial void ratio of 0.52 before isotropic compression. The predicted CSL and ICL using Equations (8.4) - (8.5) are compared with the measured CSL and ICL in Figure 8.7. The RCL is then obtained by Equation (8.7) with known values of N, λ, and $e_{\mathrm{CS,ref}}$ (e_{CS0} at $B_{\lambda} = 0$). It is shown from Figure 8.7 that the proposed functions for CSL and ICL fit well with the measured results. Figure 8.8 shows the calibration of breakage parameters for the Cambria sand. The ultimate fractal dimension of the Cambria sand for calculating the relative PSD index B_{λ} is adopted as 2.6, which is assumed to be the same with the carbonate sand (Coop *et al.*, 2004; Xiao *et al.*, 2016c). It should be noted that it is not clear whether there is any impact of the ultimate fractal dimension on the final results, which is outside the scope of this study. A good agreement is obtained by using Equation (8.15) with material constant b = 5408 and Equation (8.17) with material constant a = 1.30. It should be noted that the values of e_{CS0} at various degrees of particle breakage are adopted from the back analysis conducted by Hu *et al.* (2018).

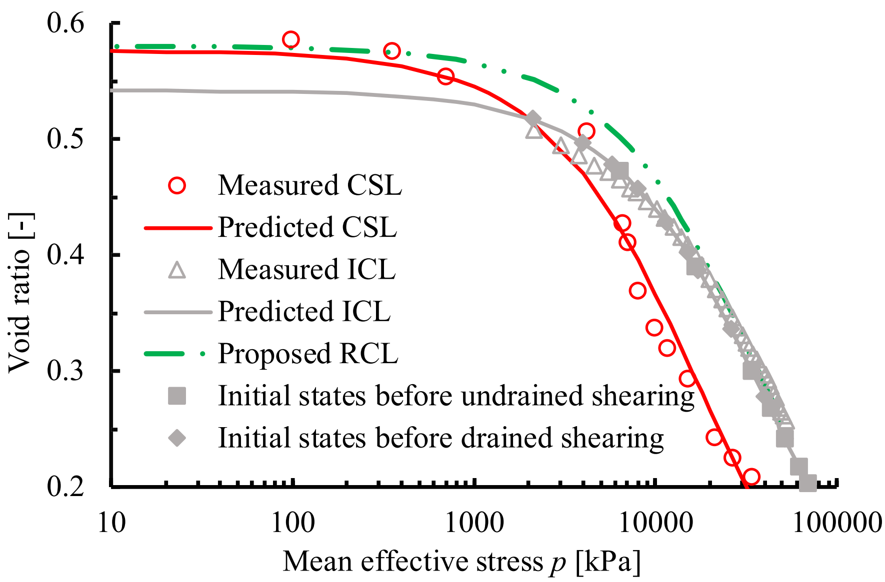

Figure 8.7: Measured and predicted CSL, ICL and proposed RCL of the Cambria sand. The square points represent the initial states of sample before undrained shearing (or,

after isotropic compression), the diamond points represent the initial states before drained shearing

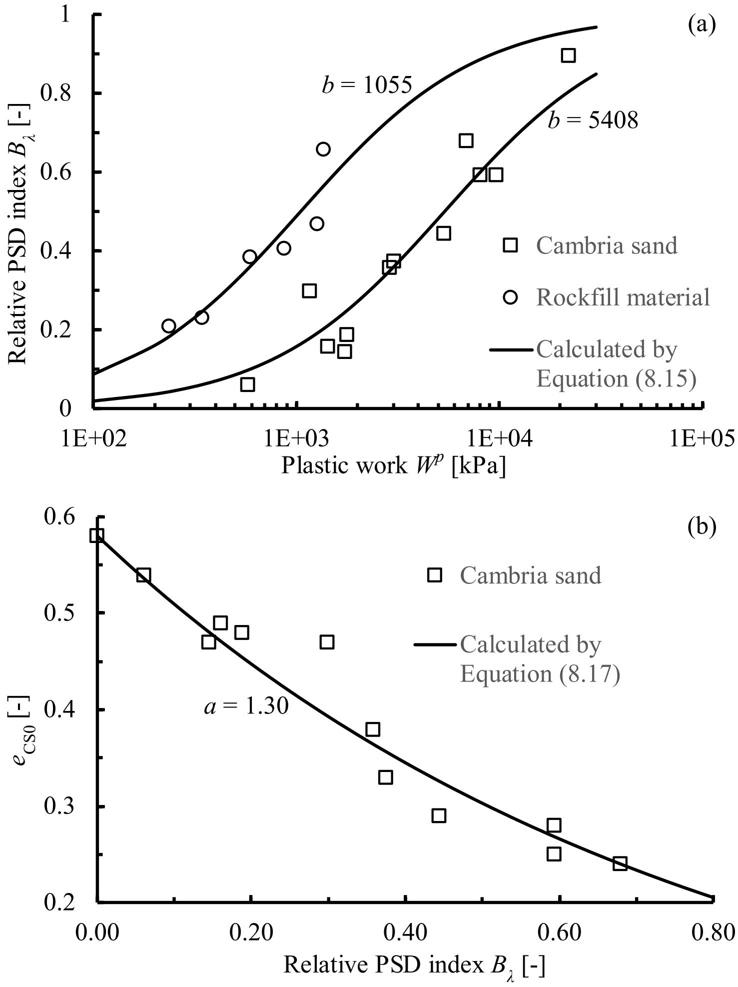

Figure 8.8: Calibration of breakage parameters: (a) relative PSD index B_λ versus plastic work, (b) e_{CS0} versus relative PSD index B_λ

Figure 8.9 and Figure 8.10 show the comparison between the measured and the predicted results of drained shearing tests with confining pressure varying between 2.1 MPa and 52.0 MPa, wherein the solid lines represent the predicted results and the dots the experimental results. The initial void ratios after isotropic compression at different confining pressures can be determined by the ICL (shown as the diamond points in Figure 8.7). As shown from the test results in Figure 8.9, the dilatant behaviour is observed with confining pressure of 2.1 MPa, and a transition from dilatant to contractive behaviour is also observed with increasing confining pressure. Such behaviour can be reasonably predicted by the proposed model although only a slight dilatancy is observed at the confining pressure of 2.1 MPa as shown in Figure 8.9. The volumetric strain, however, decreases with increasing confining pressure when it is larger than 17.2 MPa, as shown in Figure 8.10. Such behaviour is expected for crushable materials because more input work for the samples will be obtained after isotropic compression at larger confining pressure, which will lead to a larger breakage index (as indicated by Equation (8.15)) for the sample before shearing stage. As proposed before, a larger breakage index will also lead to a lower initial position of CSL and RCL in the e - ln(p) space, which means samples after isotropic compression at large confining pressure might be in a 'loose' state, while samples after isotropic compression at low confining pressure might be in a 'dense' state. The present model can describe such behaviour as shown in Figure 8.10 that less volumetric contraction during shearing for the sample after isotropic compression at 52 MPa is observed than that of 40 MPa. In general, the proposed model can describe the main response of drained tests within a wide range of confining pressures.

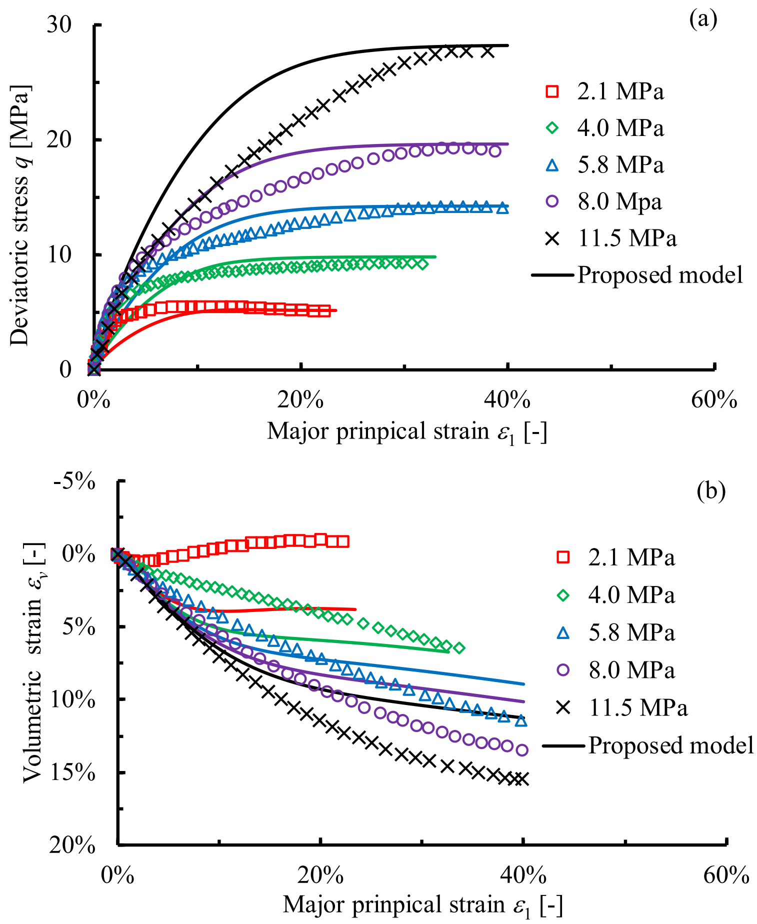

Figure 8.9: Measured and predicted drained shearing results of the Cambria sand with confining pressure varying between 2.1 MPa and 11.5 MPa (points: experimental data, lines: predicted results): (a) Deviatoric stress; and (b) volumetric strain relations

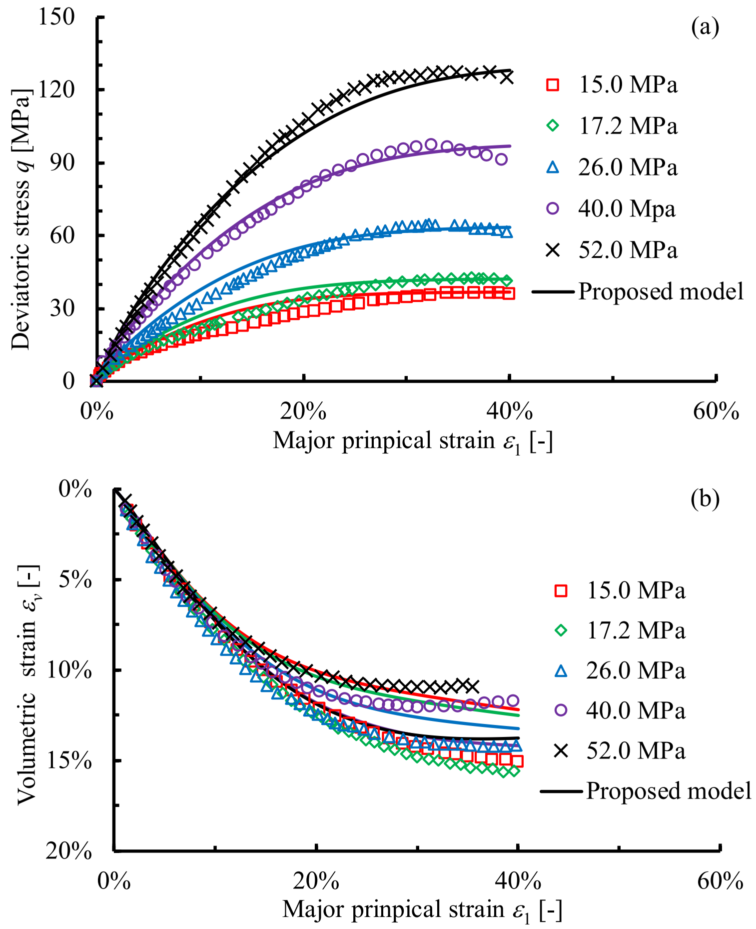

Figure 8.10: Measured and predicted drained shearing results of the Cambria sand with confining pressure varying between 15.0 MPa and 52.0 MPa: (a) Deviatoric stress; and (b) volumetric strain relations

Figure 8.11 shows the comparison between the measured and the predicted results of undrained shearing tests with confining pressure varying between 6.4 MPa and 68.9 MPa. Again, the initial void ratios after isotropic compression at different confining pressure can be determined by the ICL (shown as the square points in Figure 8.7). The proposed model can predict the stress-strain relations and pore water pressure relations of the Cambria sand during undrained shearing with satisfactory accuracy.

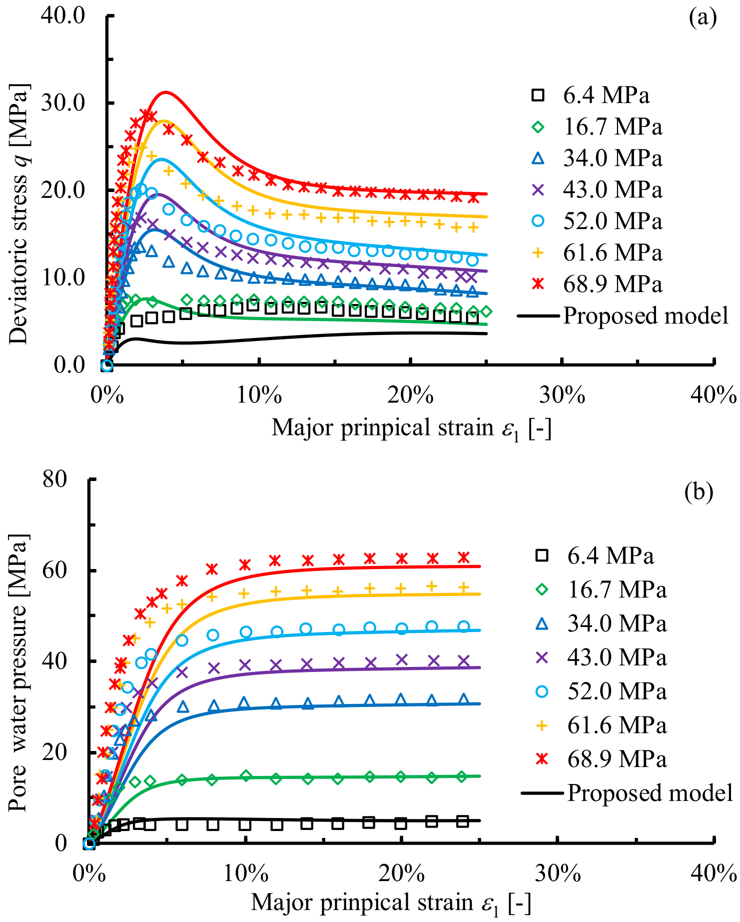

Figure 8.11: Measured and predicted undrained shearing results of the Cambria sand with confining pressure varying between 6.4 MPa and 68.9 MPa: (a) Deviatoric stress; and (b) pore water pressure relations

8.6.2.2 Changhe rockfill

Liu *et al.* (2011) and Liu *et al.* (2012) conducted a series of drained and undrained triaxial compression tests on a rockfill material from Changhe dam with confining pressure ranging from 400 kPa to 4000 kPa. The grains tested were hard diorite with maximum particle size of 60 mm. In Figure 8.12, Equation (8.4) is used to model the ICL and Equation (8.5) is used to model the CSL of the Changhe rockfill. The RCL is then determined with known parameters N, λ, and $e_{\mathrm{CS,ref}}$ (e_{CS0} at $B_\lambda = 0$) by using Equation (8.7). The agreement between the measured and the predicted results of ICL and CSL is relatively good. The ultimate fractal dimension of the Changhe rockfill is adopted as 2.7, in agreement with other studies on rockfill materials (Yin *et al.*, 2016; Xiao & Liu, 2017). The breakage parameter b = 1055 is adopted by using Equation (8.15) as presented in Figure 8.8. Another breakage parameter a, however, cannot be determined directly because of the insufficient experimental data. It can be obtained by best fitting of the stress and strain response under drained and undrained compression.

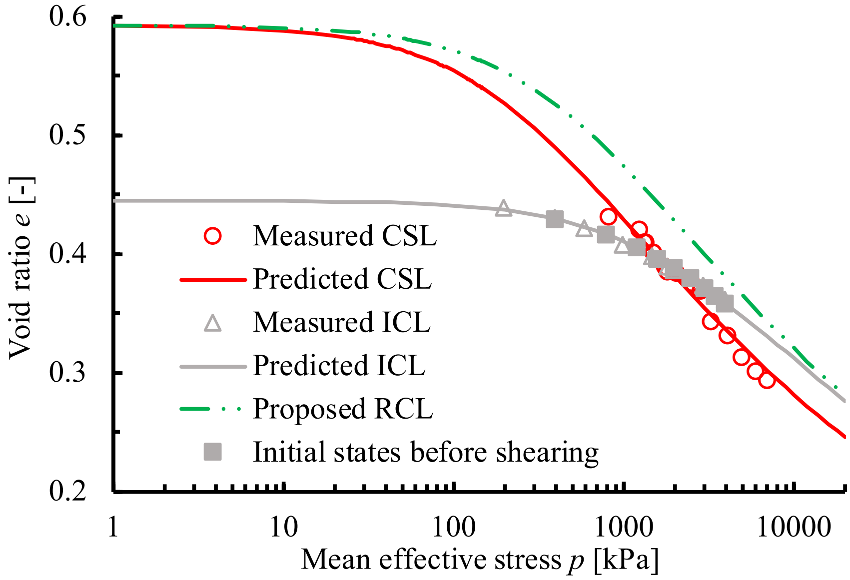

Figure 8.12: Measured and predicted CSL, ICL and proposed RCL of the Changhe rockfill

Figure 8.13 and Figure 8.14 show the comparison between the measured and the predicted results of drained and undrained triaxial compression with confining pressure varying between 400 kPa and 4000 kPa, respectively. It is observed in Figure 8.13 that the proposed model can well capture the stress and strain response of the Changhe rockfill subjected to drained shearing, i.e., the strain softening and dilatant behaviour are observed at a low confining pressure, while the strain hardening and volumetric contraction behaviour become more obvious as the confining pressure increases. Figure 8.14 shows the comparison between the measured and the predicted stress–strain and pore-pressure behaviour of the Changhe rockfill during undrained shearing. The proposed model predicts good values of deviatoric stress, especially when the confining pressure is high. The prediction of pore water pressure as shown in Figure 8.14(b) is better matched with the experimental results when the confining pressure is low. The pore water pressure is underestimated when the confining pressure is high, especially when the axial strain is less than 5%, and it can be better captured as the axial strain increases.

Overall, the proposed model seems to be able to capture the main features in granular soils behaviour during isotropic compression and drained and undrained shearing processes within a wide range of confining pressures.

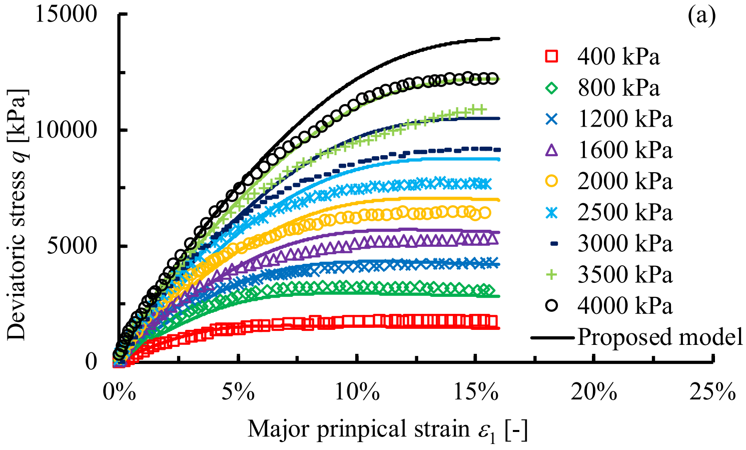

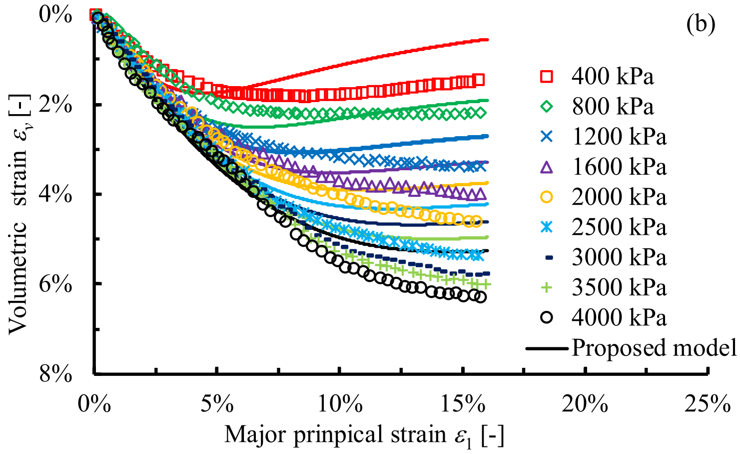

Figure 8.13: Measured and predicted drained shearing results of the Changhe rockfill with confining pressure varying between 400 kPa and 4000 kPa: (a) Deviatoric stress; and (b) volumetric strain relations

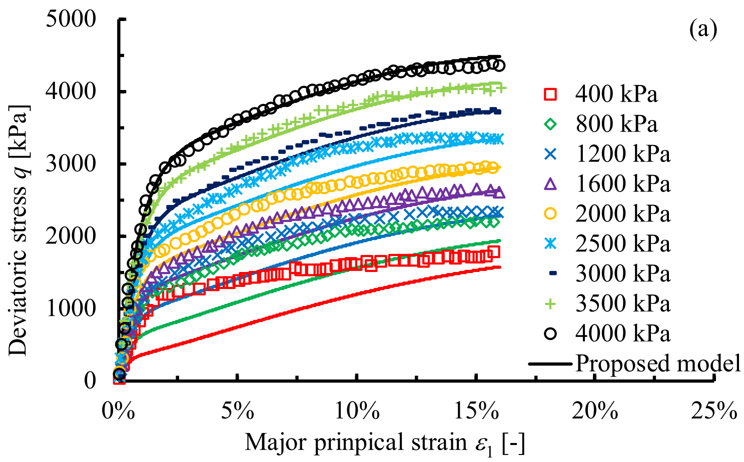

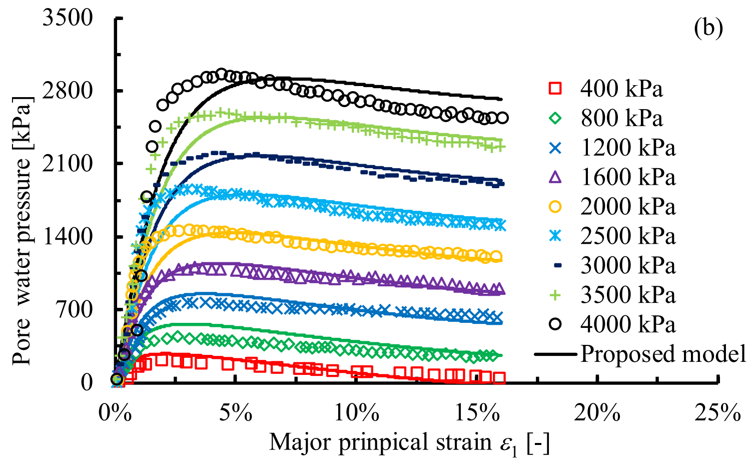

Figure 8.14: Measured and predicted undrained shearing results of Changhe rockfill with confining pressure varying between 400 kPa and 4000 kPa: (a) Deviatoric stress; and (b) pore water pressure relations

8.7 Conclusion marks

Traditional state-based constitutive models for granular soils use the state parameter proposed by Been & Jefferies (1985). The state parameter is defined as the difference between the current void ratio and the reference void ratio at critical state. However, it might not be appropriate when particle breakage is present, because the degree of particle breakage of the corresponding reference point is different with that of the current state point after shearing.

In this study, a simple constitutive model with consideration of the main properties of granular soils is present within the framework of Li & Dafalias (2000). These main properties include the nonlinear CSL and ICLs in the e - log (p) space, the state-dependent behaviour, and the particle breakage and its influence on the stress-strain behaviour. A double logarithmic approach for modelling the nonlinearity of the CSL, ICLs in the e - log (p) space is adopted, based on which, a new RCL intersect with the CSL at a very low stress level has been developed. The modified state parameter is defined as the difference between the current void ratio and void ratio on the RCL at the same mean effective stress.

A simple dynamic evolution law of the CSL, LCL, and RCL with increasing particle breakage is proposed. The relative PSD index B_λ is employed as a measurement of particle breakage, which can be calculated from the input plastic work. The initial position of CSL in the e - log(p) space moves downwards with increasing B_λ. However, it cannot be a parallel shift, and all the CSLs with various B_λ will eventually converge at high stresses, because particle breakage will complete and is no longer the main deformation mechanism of granular soils. The RCL evolves similarly with that of the CSL, i.e., shifts downwards from the initial position and converges eventually as particle breakage processes, while the LCL and the critical state stress ratio are independent of particle breakage. Such an evolution in the RCL has been incorporated into the proposed constitutive model by the concept of the proposed modified state parameter.

The proposed model was validated against experimental results of drained and undrained triaxial tests on the Cambria sand and Changhe rockfill. It has been shown that the proposed model is able to capture the nonlinear CSL and ICL in the e - log (p) space, and state-dependent behaviour of granular soils.

APPENDIX 8.A

8.A.1 Computational steps for integration under drained shearing

Step 1: The plastic work W_0^p before shearing (or, after isotropic compression) can be calculated as

$$W_0^p = \int_0^{\varepsilon_v^p} p \mathrm{d}\varepsilon_v^p \approx \int_{e_0}^{e_{s0}} \frac{p(e)}{1+e_0} \mathrm{d}e \tag{8.37}$$

where e_0 is the void ratio before isotropic compression, e_{s0} is the void ratio before shearing. For simplicity, the elastic volumetric strain is ignored since it is several orders of magnitude smaller than the plastic volumetric strain if the unloading stress path is not available.

Step 2: Setting the initial value of $p = p_{\mathrm{init}}$, $q_{\mathrm{init}} = 0$, $\eta_{\mathrm{init}} = (q_{\mathrm{init}}/p_{\mathrm{init}}) = 0$, calculating G_{init}, K_{init}, $B_{\lambda\mathrm{init}}$, Ψ_{init} based on Equations (8.21), (8.22), (8.15) & (8.37), and (8.18), respectively. Since $H_\mathrm{p} = +\infty$, when $\eta = 0$, a large value of H_{pinit} is adopted. Setting the increment of the axial strain $\Delta\varepsilon_1$.

Step 3: The increment of radial strain $\Delta\varepsilon_3$, and the increment of mean effective stress Δp can be determined by Equations (8.2), (8.30) with the stress path in drained condition, i.e., $\Delta q = 3\Delta p$

$$\begin{cases} \Delta\varepsilon_3 = \dfrac{2A+6B-3C-9D}{2A+6B+6C+18D}\Delta\varepsilon_1 \\ \Delta p = \dfrac{3}{A+3B+3C+9D}\Delta\varepsilon_1 \end{cases} \tag{8.38}$$

with

$$\begin{cases} A = \dfrac{1}{K} + \dfrac{n_{\mathrm{fv}} n_{\mathrm{gv}}}{H_{\mathrm{p}}}, B = \dfrac{n_{\mathrm{fs}} n_{\mathrm{gv}}}{H_{\mathrm{p}}} \\ C = \dfrac{n_{\mathrm{fv}} n_{\mathrm{gs}}}{H_{\mathrm{p}}}, D = \dfrac{1}{3G} + \dfrac{n_{\mathrm{fs}} n_{\mathrm{gs}}}{H_{\mathrm{p}}} \end{cases} \tag{8.39}$$

Step 4: Updating the state variables, stress and strain qualities: $p_{i+1} = p_i + \Delta p_i$, $q_{i+1} = q_i + 3\Delta p_i$, $\eta_{i+1} = q_{i+1} / p_{i+1}$, $\varepsilon_{\mathrm{v},i+1} = \varepsilon_{\mathrm{v},i} + \Delta\varepsilon_1 + 2\Delta\varepsilon_{3,i}, \varepsilon_{\mathrm{s},i+1} = \varepsilon_{\mathrm{s},i} + 2/3\left(\Delta\varepsilon_1 - 2\varepsilon_{3,i}\right)$, $W_{i+1}^p = W_i^p + \left\langle \Delta W_i^p \right\rangle, B_{\lambda,i+1} = f\left(W_{i+1}^p\right), \Psi_{i+1} = f\left(p_{i+1}, B_{\lambda,i+1}\right)$, $\Delta p_{i+1} / \Delta\varepsilon_{3,i+1} = f\left(K_{i+1}, G_{i+1}, \eta_{i+1}, \Psi_{i+1}\right)\Delta\varepsilon_1$.

Step 5: Starting a new step with constant $\Delta\varepsilon_1$.

8.A.2. Computational steps for integration under undrained shearing

Step 1: Calculating plastic work W_0^p before shearing from Equation (8.37).

Step 2: Setting the initial values with the same procedure with Step 2 in the drained stress path.

Step 3: Calculating the increment of radial strain $\Delta\varepsilon_3$, and the increment of mean effective stress Δp, the increment of mean effective stress Δq from Equations (8.2), (8.30) with the stress path in undrained condition, i.e., $\Delta\varepsilon_\mathrm{v} = 0$

$$\begin{cases} \Delta\varepsilon_3 = -\dfrac{1}{2}\Delta\varepsilon_1 \\ \Delta p = -\dfrac{B}{AD-BC}\Delta\varepsilon_1 \\ \Delta q = \dfrac{A}{AD-BC}\Delta\varepsilon_1 \end{cases} \tag{8.40}$$

Step 4: Updating the state variables, stress and strain qualities: $p_{i+1} = p_i + \Delta p_i$, $q_{i+1} = q_i + \Delta q_i$, $\eta_{i+1} = q_{i+1} / p_{i+1}$, $W_{i+1}^p = W_i^p + \left\langle \Delta W_i^p \right\rangle$, $B_{\lambda,i+1} = f\left(W_{i+1}^p\right), \Psi_{i+1} = f\left(p_{i+1}, B_{\lambda,i+1}\right)$,

$\Delta p_{i+1} / \Delta \varepsilon_{3,i+1} = f\left(K_{i+1}, G_{i+1}, \eta_{i+1}, \Psi_{i+1}\right) \Delta \varepsilon_1$, $p_{\mathrm{u},i+1} = p_0 + \frac{1}{3} q_{i+1} - p_{i+1}$ (where, p_{u} is the pore water pressure).

Step 5: Starting a new step with constant $\Delta \varepsilon_1$.

List of symbols

CSL	critical state line
ICL	isotropic compression line
LCL	limit compression line
CSSM	critical state soil mechanics
PSD	particle size distribution
RCL	reference compression line
e	void ratio
p	mean effective stress
q	shear stress
ε_s	deviatoric strain
ε_v	volumetric strain
p_r	the unit pressure (= 1 kPa)
e_{LCL}	void ratio on the LCL
N	void ratio on the LCL when p = 1kPa
λ	slope of LCL in the ln(e)-ln(p) space
e_{ICL}	void ratio on the ICLs
p_{ICL}	shifting stress controlling the curvature of the ICL
e_{CSL}	void ratio on the CSL
Γ	void ratio on the CSL when $p + p_{CSL} = 1$kPa
p_{CSL}	shifting stress controlling the curvature of the CSL
e_{CS0}	void ratio on the CSL when $p = 0$
Ψ	modified state parameter
ψ	state parameter
λ_p	parameter related to PSD
d_{max}	maximum particle size
$d_{63.2}$	particle diameter at which 63.2% of the sample by mass is smaller
B_λ	relative PSD index
W^p	plastic work
b	material constant controlling the evolution rate of PSD

M	critical state stress ratio
$e_{\mathrm{CS,ref}}$	intercept of CSL without particle breakage
a	material constant controlling the rate of CSL shifting caused by particle breakage
K, G	elastic bulk modulus and elastic shear modulus
G_0	material constant
μ	Poisson's ratio
η	stress ratio
f, g	yield surface function and plastic potential function
n_{fv} , n_{fs}	vector of the loading direction
n_{gv} , n_{gs}	vector of the plastic flow direction
d_{g}	dilatancy equation
d_0, m	positive material constants
H_{p}	plastic modulus
M_{p}	virtual peak stress ratio
H_0, n	model constants
η_{PTS}	stress ratio at the phase transformation state
Ψ_{PTS}	modified state parameter at the phase transformation state
η_{PS}	stress ratio at the peak state
Ψ_{PS}	modified state parameter at the peak state

Chapter 9 . Conclusions and future work

9.1 Conclusions

This thesis provides a systematic study on particle breakage of granular soils, from evolution laws to constitutive modelling. More specifically, the following key questions, as suggested by Muir Wood (Muir Wood, 2007; Muir Wood & Maeda, 2008), and Zhang *et al.* (2015) were discussed and as addressed in the form of six technical publications:

(1). How can the particle-size distribution (PSD) be reasonably represented by a simple variable that can be used in a constitutive model (PSD quantification)?

(2). How does this PSD variable evolve during the particle breakage (breakage evolution law)?

(3). How does this PSD variable influence the mechanical and deformational behaviour of the material (constitutive law)?

9.1.1 PSD quantification

(1). A simple and continuous PSD model with two parameters (λ_p and κ_p) for granular soils was proposed in Chapter 3. Such a mathematical model has several advantages. Firstly, the characteristics of the whole PSD curve can be obtained when the parameters of the model are known. Secondly, it is easier to correlate the entire PSD curve with other properties of the soil. Parameter λ_p is determined as a function of $d_{63.2}$, which represents the characteristic particle size of the soil sample, while κ_p is a shape parameter, which is closely correlated to the coefficient of uniformity (C_u) or the coefficient of curvature (C_c). The proposed PSD model can represent the main forms of continuous PSD curves and its performance was compared against other models in the literature by analysing 53 soil specimens with 154 PSD curves. It is shown that the proposed PSD model is superior to the other models in view of its better performance and fewer parameters used.

(2). A series of ring shear tests and one-dimensional compression tests were conducted on uniformly graded carbonate sand, in both dry and saturated conditions, and presented in Chapter 6. It was shown that λ_p was linearly related to Einav's breakage index B_r^* and the linear relationship was dependent on the initial PSD, but independent of testing conditions. Parameter κ_p was in a power relationship with Einav's breakage index B_r^*, and such a power relationship appeared to be independent of the initial grading and testing conditions.

(3). A series of one-dimensional compression tests were conducted on fractal-graded carbonate sands with different initial PSDs and initial densities as presented in Chapter 7. The PSDs after particle breakage tended to be fractal distributed. A breakage index B_D was defined in terms of the fractal dimension. The test results indicated that using B_D as the breakage index was able to highlight the importance of the initial PSD, while the effect of the initial PSD on particle breakage was not obvious when B_r^* was used.

9.1.2 Breakage evolution law

In order to tackle the second question, the evolution of particle breakage has been comprehensively studied from both mathematical modelling and experimental aspects.

(1). A breakage matrix model, which is widely used for modelling the intentional particle breakage in the field of the milling process, was introduced to describe the inadvertent degradation of PSD in geotechnical engineering in Chapter 4. The breakage matrix was determined by compressing the uniformly graded carbonate sands in a straightforward manner at a given vertical stress. The breakage matrix was applicable to predict the breakage of non-uniformly graded carbonate sands with different initial PSDs, subjected to the same vertical stress. Such an approach suffers from two main limitations: (1) the breakage matrix is not correlated properly with loading conditions, which makes the simulation more complicated and inapplicable when calculating the PSDs at varying loading conditions; (2) the effect of coordination number is not considered in the model, which results in an underestimation of the mass fraction of the coarsest particles.

(2). A stochastic approach, namely the Markov chain model, for predicting the evolution of PSDs of granular materials during one-dimensional compression tests considering the evolution of coordination number was developed in Chapter 5. Similar to the breakage matrix model introduced in Chapter 4, the proposed model also used a matrix to correlate the initial PSD with the PSD after the breakage. The survival probability of particles with different sizes in a particle assembly was captured by employing the Weibull distribution, wherein a trade-off between the effect of particle size and the effect of coordination number was considered.

(3). The two mathematical models presented in Chapters 4-5 can describe the evolution of the whole PSD accurately; however, they are difficult to consider in constitutive modelling. As indicated in Chapter 6, the input work per unit volume W_V was used as a mechanical parameter for correlating with λ_p and κ_p during the ring shear tests and the one-dimensional compression tests. The evolution law of λ_p is hyperbolically related to W_V and shows a high dependency on the initial grading. Parameter κ_p is in a power relation with W_V; however, this relationship is independent of the initial grading. Such a breakage evolution law is easy to incorporate into constitutive models.

9.1.3 Constitutive law

(1). As shown in Chapter 6, the stress-strain behaviour of uniformly-graded carbonate sand during both ring shear and one-dimensional compression tests was affected by the initial PSD. In one-dimensional compression tests, the yield stress first increased, and then decreased with increasing particle size. However, the compressibility (as defined by C_c) remained almost constant with different initial PSDs. In the ring shear test, the peak mobilised friction angle generally increased with increasing particle size, whereas the residual mobilised friction angle was independent of the initial PSD.

(2). As indicated in Chapter 7, the compression behaviour of non-uniformly graded carbonate sands was affected by the initial PSD, i.e., samples with wider-graded PSDs had larger values of tangent-constrained modulus M and smaller values of compression index C_c.

(3). A state-dependent constitutive model, considering the particle breakage was developed based on the critical state framework in Chapter 8. A double logarithmic approach for modelling the nonlinearity of the Critical State Line (CSL), Isotropic Compression Lines (ICLs) in the e - log (p) space was adopted, based on which, a new Reference Compression Line (RCL) intersecting with the CSL at a low stress level has been developed for defining the modified state parameter. The initial position of CSL was assumed to shift downwards with increasing particle breakage, while the CSLs with different particle breakage were assumed to converge to a steady state at a high stress level where particle breakage was completed and was no longer the main deformation mechanism of granular soils. Such an evolution has been incorporated into the proposed constitutive model by introducing a modified state parameter.

9.2 Future work

Although significant effort has been made on studying particle breakage of granular soils, further research is needed from the perspectives of breakage evolution law and constitutive modelling. The potential directions for further developments are suggested below.

(1). To improve our understanding of the particle breakage of granular soils, more attention should be paid to the breakage of a single particle. More specifically, comprehensive and quantitative studies are required to understand how the 'daughter' particles originating from a single particle are distributed in terms of particle size and particle shape. This is important for modelling particle breakage of a particle assembly and simulating the particle breakage via the Discrete Element Method (DEM).

(2). The effect of particle shape on the breakage evolution law should be investigated. The DEM as described in Chapter 5 were conducted on uncrushable and spherical particles to investigate the relations between the average coordination numbers, particle size, and loading conditions. However, most granular soils in engineering practice are irregular in shape. Therefore, the next phase of model development should focus on the coupling effect of the particle shape on the survival probability of particles in a particle assembly.

(3). The experimental tests reported in this thesis were limited to a few simple stress paths, such as one-dimensional compression tests and ring shear tests. Further studied are required to investigate the evolution of PSDs subjected to more advanced stress paths, for example triaxial tests.

(4). The influence of PSD on the stress-strain behaviour of granular soils needs to be further explored experimentally. In other words, more tests on granular soils with varying PSD parameters (i.e., λ_p and κ_p) should be carried out to develop an advanced constitutive model of granular soils that can describe the whole PSD. A unified constitutive model of soils with a wide range of initial PSDs can be developed if the PSD can be considered as a variable.

(5). The proposed breakage evolution law and the corresponding constitutive model can be extended to the problem of particle loss in granular soils, for example induced by internal erosion. The particle loss of granular soils, whose evolution is the opposite of the evolution of PSD as a result of particle breakage, can be described by the breakage matrix model or the Markov chain model.

Reference

Åberg, B. (1993). Washout of grains from filtered sand and gravel materials. *Journal of Geotechnical Engineering,* 119(1)**,** 36-53.

Afshar, T., Disfani, M. M., Arulrajah, A., Narsilio, G. A. and Emam, S. (2017). Impact of particle shape on breakage of recycled construction and demolition aggregates. *Powder Technology,* 308, 1-12.

Altuhafi, F. N. and Coop, M. R. (2011a). Changes to particle characteristics associated with the compression of sands. *Geotechnique,* 61(6)**,** 459-471.

Altuhafi, F. N. and Coop, M. R. (2011b). The effect of mode of loading on particle-scale damage. *Soils and Foundations,* 51(5)**,** 849-856.

Amirpour Harehdasht, S., Hussien, M. N., Karray, M., Roubtsova, V. and Chekired, M. (2019). Influence of particle size and gradation on shear strength–dilation relation of granular materials. *Canadian Geotechnical Journal,* 56(2)**,** 208-227.

Amirpour Harehdasht, S., Karray, M., Hussien, M. N. and Chekired, M. (2017). Influence of particle size and gradation on the stress-dilatancy behavior of granular materials during drained triaxial compression. *International Journal of Geomechanics,* 17(9)**,** 04017077.

Angemeer, J., Carlson, E. G. and Klick, J. H. Techniques and results of offshore pile load testing in calcareous soils. 5th Offshore Technology Conference, (1973), Houston, Texas. 677-692.

Austin, L., Shoji, K., Bhatia, V., Jindal, V., Savage, K. and Klimpel, R. (1976). Some results on the description of size reduction as a rate process in various mills. *Industrial & Engineering Chemistry Process Design and Development,* 15(1)**,** 187-196.

Bandini, V. and Coop, M. R. (2011). The influence of particle breakage on the location of the critical state line of sands. *Soils and Foundations,* 51(4)**,** 591-600.

Bard, E. (1993). *Comportement des matériaux granulaires secs et à liant hydrocarboné.* Châtenay-Malabry, Ecole centrale de Paris.

Bauer, E. (1996). Calibration of a comprehensive hypoplastic model for granular materials. *Soils and Foundations,* 36(1), 13-26.

Bayat, H., Rastgo, M., Zadeh, M. M. and Vereecken, H. (2015). Particle size distribution models, their characteristics and fitting capability. *Journal of Hydrology,* 529, 872-889.

Becker, D., Crooks, J., Been, K. and Jefferies, M. (1987). Work as a criterion for determining in situ and yield stresses in clays. *Canadian Geotechnical Journal,* 24(4), 549-564.

Been, K., Jefferies, M. and Hachey, J. (1991). Critical state of sands. *Geotechnique,* 41(3), 365-381.

Been, K. and Jefferies, M. G. (1985). A state parameter for sands. *Geotechnique,* 35(2), 99-112.

Belkhatir, M., Schanz, T., Arab, A., Della, N. and Kadri, A. (2014). Insight into the effects of gradation on the pore pressure generation of sand–silt mixtures. *Geotechnical testing journal,* 37(5), 922-931.

Ben-Nun, O. and Einav, I. (2010). The role of self-organization during confined comminution of granular materials. *Philosophical Transactions of the Royal Society of London A: Mathematical, Physical and Engineering Sciences,* 368(1910), 231-247.

Berthiaux, H. (2000). Analysis of grinding processes by Markov chains. *Chemical Engineering Science,* 55(19), 4117-4127.

Berthiaux, H. and Mizonov, V. (2004). Applications of Markov chains in particulate process engineering: a review. *The Canadian Journal of Chemical Engineering,* 82(6), 1143-1168.

Bolton, M. (1986). Strength and dilatancy of sands. *Geotechnique,* 36(1), 65-78.

Bolton, M., Nakata, Y. and Cheng, Y. (2008). Micro-and macro-mechanical behaviour of DEM crushable materials. *Géotechnique,* 58(6)**,** 471-480.

Bopp, P. A. and Lade, P. V. (2005). Relative density effects on undrained sand behavior at high pressures. *Soils and Foundations,* 45(1)**,** 15-26.

Broadbent, S. R. and Callcott, T. G. (1956). A matrix analysis of processes involving particle assemblies. *Philosophical Transactions of the Royal Society of London Series a-Mathematical and Physical Sciences,* 249(960)**,** 99-123.

Bromhead, E. (1979). A simple ring shear apparatus. *Ground Engineering,* 12(5)**,** 40,42,44.

Buchan, G. D. (1989). Applicability of the simple lognormal model to particle-size distribution in soils. *Soil Science,* 147(3)**,** 155-161.

Buchan, G. D., Grewal, K. and Robson, A. B. (1993). Improved models of particle-size distribution: An illustration of model comparison techniques. *Soil Science Society of America Journal,* 57(4)**,** 901-908.

Buscarnera, G. and Einav, I. (2012). The yielding of brittle unsaturated granular soils. *Geotechnique,* 62(2)**,** 147-160.

Butterfield, R. (1979). A natural compression law for soils (an advance on e–log p′). *Géotechnique,* 29(4)**,** 469-480.

Caicedo, B., Ocampo, M. and Vallejo, L. (2016). Modelling comminution of granular materials using a linear packing model and Markovian processes. *Computers and Geotechnics,* 80, 383-396.

Campbell, G. M., Bunn, P. J., Webb, C. and Hook, S. C. W. (2001). On predicting roller milling performance Part II. The breakage function. *Powder Technology,* 115(3)**,** 243-255.

Campbell, G. M. and Webb, C. (2001). On predicting roller milling performance Part I: the breakage equation. *Powder Technology,* 115(3)**,** 234-242.

Carrera, A., Coop, M. R. and Lancellotta, R. (2011). Influence of grading on the mechanical behaviour of Stava tailings. *Géotechnique,* 61(11)**,** 935-946.

Casini, F., Viggiani, G. M. B. and Springman, S. M. (2013). Breakage of an artificial crushable material under loading. *Granular Matter,* 15(5)**,** 661-673.

Cavarretta, I., Coop, M. R. and O'Sullivan, C. (2010). The influence of particle characteristics on the behaviour of coarse grained soils. *Geotechnique,* 60(6)**,** 413-423.

Chakraborty, T. and Salgado, R. (2010). Dilatancy and shear strength of sand at low confining pressures. *Journal of Geotechnical and Geoenvironmental Engineering,* 136(3)**,** 527-532.

Chen, Q., Indraratna, B., Carter, J. P. and Nimbalkar, S. (2016). Isotropic–kinematic hardening model for coarse granular soils capturing particle breakage and cyclic loading under triaxial stress space. *Canadian Geotechnical Journal,* 53(4)**,** 646-658.

Cheng, Y. P., Bolton, M. D. and Nakata, Y. (2004). Crushing and plastic deformation of soils simulated using DEM. *Geotechnique,* 54(2)**,** 131-141.

Cheng, Y. P., Nakata, Y. and Bolton, M. D. (2003). Discrete element simulation of crushable soil. *Geotechnique,* 53(7)**,** 633-641.

Cheng, Z. and Wang, J. (2018). Quantification of particle crushing in consideration of grading evolution of granular soils in biaxial shearing: A probability-based model. *International Journal for Numerical and Analytical Methods in Geomechanics,* 42(3)**,** 488-515.

Cho, G. C., Dodds, J. and Santamarina, J. C. (2006). Particle shape effects on packing density, stiffness, and strength: natural and crushed sands. *Journal of Geotechnical and Geoenvironmental Engineering,* 132(5)**,** 591-602.

Chuhan, F. A., Kjeldstad, A., Bjørlykke, K. and Høeg, K. (2002). Porosity loss in sand by grain crushing—Experimental evidence and relevance to reservoir quality. *Marine and Petroleum Geology,* 19(1)**,** 39-53.

Chuhan, F. A., Kjeldstad, A., Bjørlykke, K. and Høeg, K. (2003). Experimental compression of loose sands: relevance to porosity reduction during burial in sedimentary basins. *Canadian Geotechnical Journal,* 40(5)**,** 995-1011.

Ciantia, M. O., Arroyo, M., O'Sullivan, C. and Gens, A. (2019). Micromechanical inspection of incremental behaviour of crushable soils. *Acta Geotechnica***,** 14, 1337-1356.

Cohen, M. W. and Leslie, D. D. (1975). Shear Strength of Rockfill, Physical Properties. Engineering Study Number 526. Corps of Engineers Sausalito Calif South Pacific Div Lab.

Collins, I., Pender, M. and Yan, W. (1992). Cavity expansion in sands under drained loading conditions. *International Journal for Numerical and Analytical Methods in Geomechanics,* 16(1)**,** 3-23.

Coop, M. R. (1990). The mechanics of uncemented carbonate sands. *Géotechnique,* 40(4)**,** 607-626.

Coop, M. R. and Lee, I. (1993). The behaviour of granular soils at elevated stresses. *Predictive soil mechanics: Proceedings of the Wroth Memorial Symposium held at St Catherine's College, Oxford, 27-29 July 1992.* Thomas Telford Publishing.

Coop, M. R., Sorensen, K. K., Freitas, T. B. and Georgoutsos, G. (2004). Particle breakage during shearing of a carbonate sand. *Geotechnique,* 54(3)**,** 157-163.

Daouadji, A. and Hicher, P. Y. (2010). An enhanced constitutive model for crushable granular materials. *International Journal for Numerical and Analytical Methods in Geomechanics,* 34(6)**,** 555-580.

Daouadji, A., Hicher, P. Y. and Rahma, A. (2001). An elastoplastic model for granular materials taking into account grain breakage. *European Journal of Mechanics a-Solids,* 20(1)**,** 113-137.

de Bono, J. P. (2013). *Discrete element modeling of cemented sand and particle crushing at high pressures.* University of Nottingham.

de Bono, J. P. and McDowell, G. R. (2016). The fractal micro mechanics of normal compression. *Computers and Geotechnics,* 78, 11-24.

de Bono, J. P. and McDowell, G. R. (2018). On the micro mechanics of yielding and hardening of crushable granular soils. *Computers and Geotechnics,* 97, 167-188.

Einav, I. (2007a). Breakage mechanics—Part I: Theory. *Journal of the Mechanics and Physics of Solids,* 55(6), 1274-1297.

Einav, I. (2007b). Breakage mechanics—Part II: Modelling granular materials. *Journal of the Mechanics and Physics of Solids,* 55(6), 1298-1320.

El Mohtar, C. S., Yoon, J. and El-Khattab, M. (2015). Experimental study on penetration of bentonite grout through granular soils. *Canadian Geotechnical Journal,* 52(11), 1850-1860.

Ezaoui, A., Lecompte, T., Di Benedetto, H. and Garcia, E. (2011). Effects of various loading stress paths on the stress-strain properties and on crushability of an industrial soft granular material. *Granular Matter,* 13(4), 283-301.

Fredlund, M. D., Fredlund, D. and Wilson, G. W. (2000). An equation to represent grain-size distribution. *Canadian Geotechnical Journal,* 37(4), 817-827.

Fredlund, M. D., Wilson, G. W. and Fredlund, D. G. (2002). Use of the grain-size distribution for estimation of the soil-water characteristic curve. *Canadian Geotechnical Journal,* 39(5), 1103-1117.

Fuller, W. B. and Thompson, S. E. (1907). The laws of proportioning concrete. *Transactions, American Society of Civil Engineers,* 59, 67-143.

Gajo, A. and Muir Wood, D. (1999). Severn–Trent sand: a kinematic-hardening constitutive model: the q–p formulation. *Géotechnique,* 49(5), 595-614.

Gallage, C. P. K. and Uchimura, T. (2010). Effects of dry density and grain size distribution on soil-water characteristic curves of sandy soils. *Soils and Foundations,* 50(1), 161-172.

Gamboa, C. J. N. (2011). *Mechanical behavior of rockfill materials-Application to concrete face rockfill dams.* PhD, Ecole Centrale Paris.

Ghafghazi, M., Shuttle, D. and DeJong, J. (2014). Particle breakage and the critical state of sand. *Soils and Foundations,* 54(3), 451-461.

Gudehus, G. (1996). A comprehensive constitutive equation for granular materials. *Soils and Foundations,* 36(1), 1-12.

Gudehus, G. (1997). Attractors, percolation thresholds and phase limits of granular soils. *Powders and Grains,* 97, 169-183.

Guida, G., Casini, F., Viggiani, G., Ando, E. and Viggiani, G. (2018). Breakage mechanisms of highly porous particles in 1D compression revealed by X-ray tomography. *Géotechnique Letters,* 8(2), 155-160.

Guimaraes, M., Valdes, J., Palomino, A. and Santamarina, J. (2007). Aggregate production: fines generation during rock crushing. *International Journal of Mineral Processing,* 81(4), 237-247.

Gundepudi, M., Sankar, B., Mecholsky, J. and Clupper, D. (1997). Stress analysis of brittle spheres under multiaxial loading. *Powder Technology,* 94(2), 153-161.

Hagerty, M. M., Hite, D. R., Ullrich, C. R. and Hagerty, D. J. (1993). One-dimensional high-pressure compression of granular media. *Journal of Geotechnical Engineering,* 119(1), 1-18.

Ham, T. G., Nakata, Y., Orense, R. and Hyodo, M. (2010). Influence of water on the compression behavior of decomposed granite soil. *Journal of Geotechnical and Geoenvironmental Engineering,* 136(5), 697-705.

Hardin, B. O. (1985). Crushing of soil particles. *Journal of Geotechnical Engineering,* 111(10), 1177-1192.

Harris, C. (1968). The application of size distribution equations to multi-event comminution processes. *Trans. AIME,* 241, 343-358.

Hu, W., Yin, Z. Y., Scaringi, G., Dano, C. and Hicher, P. Y. (2018). Relating fragmentation, plastic work and critical state in crushable rock clasts. *Engineering Geology,* 246, 326-336.

Hu, W., Yin, Z. Y., Dano, C. and Hicher, P. Y. (2011). A constitutive model for granular materials considering grain breakage. *Science China-Technological Sciences,* 54(8)**,** 2188-2196.

Huang, J., Xu, S. and Hu, S. (2013). Effects of grain size and gradation on the dynamic responses of quartz sands. *International Journal of Impact Engineering,* 59, 1-10.

Hulburt, H. M. and Katz, S. (1964). Some problems in particle technology A statistical mechanical formulation. *Chemical Engineering Science,* 19(8)**,** 555-574.

Hwang, S. I. (2004). Effect of texture on the performance of soil particle-size distribution models. *Geoderma,* 123(3)**,** 363-371.

Hwang, S. I., Lee, K. P., Lee, D. S. and Powers, S. E. (2002). Models for estimating soil particle-size distributions. *Soil Science Society of America Journal,* 66(4)**,** 1143-1150.

Hyodo, M., Wu, Y., Aramaki, N. and Nakata, Y. (2017). Undrained monotonic and cyclic shear response and particle crushing of silica sand at low and high pressures. *Canadian Geotechnical Journal,* 54(2)**,** 207-218.

Indraratna, B., Ionescu, D., Christie, D. and Chowdhury, R. (1997). Compression and degradation of railway ballast under one-dimensional loading. *Australian Geomechanics Journal,* 12, 48–61.

Indraratna, B., Israr, J. and Rujikiatkamjorn, C. (2015). Geometrical method for evaluating the internal instability of granular filters based on constriction size distribution. *Journal of Geotechnical and Geoenvironmental Engineering,* 141(10)**,** 04015045.

Indraratna, B., Lackenby, J. and Christie, D. (2005). Effect of confining pressure on the degradation of ballast under cyclic loading. *Géotechnique,* 55(4)**,** 325-328.

Indraratna, B., Raut, A. K. and Khabbaz, H. (2007). Constriction-based retention criterion for granular filter design. *Journal of Geotechnical and Geoenvironmental Engineering,* 133(3)**,** 266-276.

Indraratna, B., Sun, Y. and Nimbalkar, S. (2016). Laboratory assessment of the role of particle size distribution on the deformation and degradation of ballast under cyclic loading. *Journal of Geotechnical and Geoenvironmental Engineering,* 142(7)**,** 04016016.

Ishihara, K. (1993). Liquefaction and flow failure during earthquakes. *Geotechnique,* 43(3)**,** 351-451.

Ishihara, K., Tatsuoka, F. and Yasuda, S. (1975). Undrained deformation and liquefaction of sand under cyclic stresses. *Soils and Foundations,* 15(1)**,** 29-44.

Jaeger, J. (1967). Failure of rocks under tensile conditions. *International Journal of Rock Mechanics and Mining Sciences & Geomechanics Abstracts.* Elsevier.

Jaky, J. *Soil mechanics,* Budapest, 1944.

Javanmardi, J., Imam, S., Pastor, M. A. and Manzanal, D. (2018). A reference state curve to define the state of soils over a wide range of pressures and densities. *Géotechnique,* 68(2)**,** 95–106.

Jefferies, M. (1993). Nor-Sand: a simle critical state model for sand. *Géotechnique,* 43(1)**,** 91-103.

Jekel, L. and Tam, E. (2007). Plastics waste processing: comminution size distribution and prediction. *Journal of Environmental Engineering,* 133(2)**,** 245-254.

Jiang, M., Yang, Z., Barreto, D. and Xie, Y. (2018). The influence of particle-size distribution on critical state behavior of spherical and non-spherical particle assemblies. *Granular Matter,* 20(4)**,** 80. doi:10.1007/s10035-018-0850-x.

Jin, Y. F., Wu, Z. X., Yin, Z. Y. and Shen, J. S. (2017). Estimation of critical state-related formula in advanced constitutive modeling of granular material. *Acta Geotechnica,* 12(6)**,** 1329-1351.

Kan, M. E. and Taiebat, H. A. (2014). A bounding surface plasticity model for highly crushable granular materials. *Soils and Foundations,* 54(6)**,** 1188-1201.

Karol, R. H. *Chemical grouting*, Marcel Dekker, 1990.

Kelly, R. B. and Airey, D. W. (2005). A large diameter ring shear apparatus and the effects of long distance shearing on interface friction angles and grain crushing. *Australian Geomechanics Journal,* 40(2)**,** 65-74.

Kenney, T. and Lau, D. (1985). Internal stability of granular filters. *Canadian geotechnical journal,* 22(2)**,** 215-225.

Kenney, T. and Lau, D. (1986). Internal stability of granular filters: Reply. *Canadian Geotechnical Journal,* 23(3)**,** 420-423.

Kikumoto, M., Wood, D. M. and Russell, A. (2010). Particle crushing and deformation behaviour. *Soils and Foundations,* 50(4)**,** 547-563.

Konrad, J. M. and Salami, Y. (2018). Particle breakage in granular materials—a conceptual framework. *Canadian Geotechnical Journal,* 55(5)**,** 710-719.

Kwa, K. and Airey, D. (2016). Critical state interpretation of effects of fines in silty sands. *Geotechnique Letters,* 6(1)**,** 100-105.

Ladd, R. (1978). Preparing test specimens using undercompaction. *Geotechnical Testing Journal,* 1(1)**,** 16-23.

Lade, P. V. and Yamamuro, J. A. (1996). Undrained sand behavior in axisymmetric tests at high pressures. *Journal of Geotechnical Engineering,* 122(2)**,** 120-129.

Lade, P. V., Yamamuro, J. A. and Bopp, P. A. (1996). Significance of particle crushing in granular materials. *Journal of Geotechnical Engineering,* 122(4)**,** 309-316.

Lashkari, A. (2009). On the modeling of the state dependency of granular soils. *Computers and Geotechnics,* 36(7)**,** 1237-1245.

Lassabatere, L., Angulo-Jaramillo, R., Soria Ugalde, J., Cuenca, R., Braud, I. and Haverkamp, R. (2006). Beerkan estimation of soil transfer parameters through infiltration experiments—BEST. *Soil Science Society of America Journal,* 70(2), 521-532.

Lee, K. L. and Farhoomand, I. (1967). Compressibility and crushing of granular soil in anisotropic triaxial compression. *Canadian Geotechnical Journal,* 4(1), 68-86.

Lee, K. L. and Seed, H. B. (1967). Drained strength characteristics of sands. *Journal of Soil Mechanics & Foundations Div,* 93(6), 117-141.

Leslie, D. (1963). Large scale triaxial tests on gravelly soils. *Proc. of the 2nd Pan-American Conf. on SMFE, Brazil.*

Li, G., Liu, Y. J., Dano, C. and Hicher, P. Y. (2014). Grading-dependent behavior of granular materials: from discrete to continuous modeling. *Journal of Engineering Mechanics,* 141(6), 04014172.

Li, M., Zhang, J., Zhou, N. and Huang, Y. (2017). Effect of particle size on the energy evolution of crushed waste rock in coal mines. *Rock Mechanics and Rock Engineering,* 50(5), 1347-1354.

Li, X. S., Dafalias, Y. F. and Wang, Z. L. (1999). State-dependant dilatancy in critical-state constitutive modelling of sand. *Canadian Geotechnical Journal,* 36(4), 599-611.

Li, X. and Dafalias, Y. F. (2000). Dilatancy for cohesionless soils. *Geotechnique,* 50(4), 449-460.

Li, X. S. and Wang, Y. (1998). Linear representation of steady-state line for sand. *Journal of Geotechnical and Geoenvironmental Engineering,* 124(12), 1215-1217.

Liu, E. L., Tan, Y. L., Chen, S. S. and Li, G. Y. (2012). Investigation on critical state of rockfill materials. *Journal of Hydraulic Engineering,* 43(5), 505-511,519.

Liu, E. L., Chen, S. S., Li, G. Y. and Zhong, Q. (2011). Critical state of rockfill materials and a constitutive model considering grain crushing. *Rock and Soil Mechanics,* 32(2), 148-154.

Liu, H. and Ling, H. I. (2008). Constitutive description of interface behavior including cyclic loading and particle breakage within the framework of critical state soil mechanics. *International Journal for Numerical and Analytical Methods in Geomechanics,* 32(12), 1495-1514.

Liu, H. and Zou, D. (2013). Associated generalized plasticity framework for modeling gravelly soils considering particle breakage. *Journal of Engineering Mechanics,* 139(5), 606-615.

Liu, M. and Gao, Y. (2016). Constitutive modeling of coarse-grained materials incorporating the effect of particle breakage on critical state behavior in a framework of generalized plasticity. *International Journal of Geomechanics,* 17(5), 04016113.

Liu, M., Gao, Y. and Liu, H. (2014a). An elastoplastic constitutive model for rockfills incorporating energy dissipation of nonlinear friction and particle breakage. *International Journal for Numerical and Analytical Methods in Geomechanics,* 38(9), 935-960.

Liu, Y. J., Li, G., Yin, Z. Y., Dano, C., Hicher, P. Y., Xia, X. H. and Wang, J. H. (2014b). Influence of grading on the undrained behavior of granular materials. *Comptes Rendus Mécanique,* 342(2), 85-95.

Lobo-Guerrero, S. and Vallejo, L. E. (2006). Application of Weibull statistics to the tensile strength of rock aggregates. *Journal of Geotechnical and Geoenvironmental Engineering,* 132(6), 786-790.

Lőrincz, J., Imre, E., Gálos, M., Trang, Q., Rajkai, K., Fityus, S. and Telekes, G. (2005). Grading entropy variation due to soil crushing. *International Journal of Geomechanics,* 5(4), 311-319.

Lu, P., Jefferson, I., Rosenbaum, M. and Smalley, I. (2003). Fractal characteristics of loess formation: evidence from laboratory experiments. *Engineering Geology,* 69(3), 287-293.

Luo, H. Y., Cooper, W. L. and Lu, H. B. (2014). Effects of particle size and moisture on the compressive behavior of dense Eglin sand under confinement at high strain rates. *International Journal of Impact Engineering,* 65, 40-55.

Luzzani, L. and Coop, M. R. (2002). On the relationship between particle breakage and the critical state of sands. *Soils and Foundations,* 42(2), 71-82.

Manzari, M. T. and Dafalias, Y. F. (1997). A critical state two-surface plasticity model for sands. *Geotechnique,* 47(2), 255-272.

Marketos, G. and Bolton, M. D. (2007). Quantifying the extent of crushing in granular materials: a probability-based predictive method. *Journal of the Mechanics and Physics of Solids,* 55(10), 2142-2156.

Marsal, R. J. (1967). Large-scale testing of rockfill materials. *Journal of the Soil Mechanics and Foundations Division,* 93(2), 27-43.

Mayoraz, F., Vulliet, L. and Laloui, L. (2006). Attrition and particle breakage under monotonic and cyclic loading. *Comptes Rendus Mécanique,* 334(1), 1-7.

McDowell, G. (2005). A physical justification for log e–log σ based on fractal crushing and particle kinematics. *Géotechnique,* 55(9), 697-698.

McDowell, G. and Amon, A. (2000). The application of Weibull statistics to the fracture of soil particles. *Soils and Foundations,* 40(5), 133-141.

McDowell, G. and Bolton, M. D. (1998). On the micromechanics of crushable aggregates. *Geotechnique,* 48(5), 667-679.

McDowell, G., Bolton, M. D. and Robertson, D. (1996). The fractal crushing of granular materials. *Journal of the Mechanics and Physics of Solids,* 44(12), 2079-2101.

McDowell, G. and Harireche, O. (2002). Discrete element modelling of yielding and normal compression of sand. *Géotechnique,* 52(4), 299-304.

McDowell, G. and Humphreys, A. (2002). Yielding of granular materials. *Granular Matter,* 4(1), 1-8.

McDowell, G. R. (2002). On the yielding and plastic compression of sand. *Soils and Foundations,* 42(1)**,** 139-145.

Merkus, H. G. Particle size measurements: fundamentals, practice, quality. Springer Science & Business Media, 2009.

Mesri, G. and Vardhanabhuti, B. (2009). Compression of granular materials. *Canadian Geotechnical Journal,* 46(4)**,** 369-392.

Miao, G. and Airey, D. (2013). Breakage and ultimate states for a carbonate sand. *Geotechnique,* 63(14)**,** 1221-1229.

Minh, N. H. and Cheng, Y. P. (2013). A DEM investigation of the effect of particle-size distribution on one-dimensional compression. *Geotechnique,* 63(1)**,** 44-53.

Mishra, S., Parker, J. and Singhal, N. (1989). Estimation of soil hydraulic properties and their uncertainty from particle size distribution data. *Journal of Hydrology,* 108, 1-18.

Miura, N. and O'Hara, S. (1979). Particle-crushing of a decomposed granite soil under shear stresses. *Soils and Foundations,* 19(3)**,** 1-14.

Miura, N. and Yamanouchi, T. (1975). Effect of water on the behavior of a quartz-rich sand under high stresses. *Soils and Foundations,* 15(4)**,** 23-34.

Moraci, N., Mandaglio, M. and Ielo, D. (2014). Analysis of the internal stability of granular soils using different methods. *Canadian Geotechnical Journal,* 51(9)**,** 1063-1072.

Moraci, N., Mandaglio, M. and Ielo, D. (2015). Reply to the discussion by Ni et al. on “Analysis of the internal stability of granular soils using different methods”. *Canadian Geotechnical Journal,* 52(3)**,** 385-391.

Muir Wood, D. Soil behaviour and critical state soil mechanics, Cambridge University Press, 1990.

Muir Wood, D. (2007). The magic of sands - The 20th Bjerrum Lecture presented in Oslo, 25 No. *Canadian Geotechnical Journal,* 44(11)**,** 1329-1350.

Muir Wood, D. and Maeda, K. (2008). Changing grading of soil: effect on critical states. *Acta Geotechnica,* 3(1)**,** 3-14.

Muir Wood, D., Maeda, K. and Nukudani, E. (2010). Modelling mechanical consequences of erosion. *Geotechnique,* 60(6)**,** 447-457.

Murff, J. D. (1987). Pile capacity in calcareous sands: State of the art. *Journal of Geotechnical Engineering,* 113(5)**,** 490-507.

Murthy, T., Loukidis, D., Carraro, J., Prezzi, M. and Salgado, R. (2007). Undrained monotonic response of clean and silty sands. *Géotechnique,* 57(3)**,** 273-288.

Nakata, A., Hyde, M., Hyodo, H. and Murata. (1999). A probabilistic approach to sand particle crushing in the triaxial test. *Geotechnique,* 49(5)**,** 567-583.

Nakata, Y., Hyodo, M., Hyde, A. F. L., Kato, Y. and Murata, H. (2001a). Microscopic particle crushing of sand subjected to high pressure one-dimensional compression. *Soils and Foundations,* 41(1)**,** 69-82.

Nakata, Y., Kato, Y., Hyodo, M., HYDE, A. F. and Murata, H. (2001b). One-dimensional compression behaviour of uniformly graded sand related to single particle crushing strength. *Soils and Foundations,* 41(2)**,** 39-51.

Nanda, S., Sivakumar, V., Donohue, S. and Graham, S. (2018). Small-strain behaviour and crushability of Ballyconnelly carbonate sand under monotonic and cyclic loading. *Canadian Geotechnical Journal,* 55(7)**,** 979-987.

Nguyen, D. H., Azéma, E., Sornay, P. and Radjai, F. (2015). Effects of shape and size polydispersity on strength properties of granular materials. *Physical Review E,* 91(3)**,** 032203.

Nimbalkar, S., Indraratna, B., Dash, S. K. and Christie, D. (2012). Improved performance of railway ballast under impact loads using shock mats. *Journal of Geotechnical and Geoenvironmental Engineering,* 138(3)**,** 281-294.

Okada, Y., Sassa, K. and Fukuoka, H. (2004). Excess pore pressure and grain crushing of sands by means of undrained and naturally drained ring-shear tests. *Engineering Geology,* 75(3-4)**,** 325-343.

Oldecop, L. and Alonso, E. (2007). Theoretical investigation of the time-dependent behaviour of rockfill. *Géotechnique,* 57(3)**,** 289-301.

Ouyang, M. and Takahashi, A. (2016). Influence of initial fines content on fabric of soils subjected to internal erosion. *Canadian Geotechnical Journal,* 53(2)**,** 299-313.

Ovalle, C. (2018). Role of particle breakage in primary and secondary compression of wet and dry sand. *Géotechnique Letters,* 8(2)**,** 161-164.

Ovalle, C., Dano, C., Hicher, P. Y. and Cisternas, M. (2015). Experimental framework for evaluating the mechanical behavior of dry and wet crushable granular materials based on the particle breakage ratio. *Canadian Geotechnical Journal,* 52(5)**,** 587-598.

Ovalle, C., Frossard, E., Dano, C., Hu, W., Maiolino, S. and Hicher, P. Y. (2014). The effect of size on the strength of coarse rock aggregates and large rockfill samples through experimental data. *Acta Mechanica,* 225(8)**,** 2199-2216.

Ovalle, C., Voivret, C., Dano, C. and Hicher, P. Y. (2016). Population balance in confined comminution using a physically based probabilistic approach for polydisperse granular materials. *International Journal for Numerical and Analytical Methods in Geomechanics,* 40(17)**,** 2383-2397.

Ozkan, G. and Ortoleva, P. (2000). Evolution of the gouge particle size distribution: A Markov model. *Pure & Applied Geophysics,* 157(3)**,** 449-468.

Pasikatan, M., Steele, J., Milliken, G., Spillman, C. and Haque, E. (1999). Particle size distribution and sieving characteristics of first-break ground wheat. *American Society of Agricultural Engineers. ASAE. S,* 319, 1-11.

Pestana, J. M. and Whittle, A. (1995). Compression model for cohesionless soils. *Géotechnique,* 45(4)**,** 611-631.

Pino, L. F. M. and Baudet, B. A. (2015). The effect of the particle size distribution on the mechanics of fibre-reinforced sands under one-dimensional compression. *Geotextiles and Geomembranes,* 43(3)**,** 250-258.

Poulos, H. (1980). A review of the behaviour and engineering properties of carbonate soils. *NASA STI/Recon Technical Report N.*

Ramkrishna, D. Population balances: Theory and applications to particulate systems in engineering. Elsevier, 2000.

Richart, F. E., Hall, J. R. and Woods, R. D. Vibrations of soils and foundations. International Series in Theoretical and Applied Mechanics, (1970) Englewood Cliffs, NJ. Prentice-Hall.

Roscoe, K. H., Schofield, A. and Wroth, C. (1958). On the yielding of soils. *Geotechnique,* 8(1)**,** 22-53.

Rosin, P. and Rammler, E. (1933). The Laws Governing the Fineness of Powdered Coal. *J.inst.fuel,* 7, 29-36.

Rowe, P. W. (1962). The stress-dilatancy relation for static equilibrium of an assembly of particles in contact. *Proceedings of the Royal Society of London. Series A. Mathematical and Physical Sciences,* 269(1339)**,** 500-527.

Russell, A. R. (2011). A compression line for soils with evolving particle and pore size distributions due to particle crushing. *Geotechnique Letters,* 1(1)**,** 5-9.

Russell, A. R. and Khalili, N. (2004). A bounding surface plasticity model for sands exhibiting particle crushing. *Canadian Geotechnical Journal,* 41(6)**,** 1179-1192.

Sadrekarimi, A. and Olson, S. M. (2010). Particle damage observed in ring shear tests on sands. *Canadian Geotechnical Journal,* 47(5)**,** 497-515.

Salami, Y., Dano, C. and Hicher, P. Y. (2017). An experimental study on the influence of the coordination number on grain crushing. *European Journal of Environmental and Civil Engineering,* 23(3)**,** 1-17.

Salami, Y., Dano, C., Hicher, P., Colombo, G. and Denain, P. (2015). The effects of the coordination on the fragmentation of a single grain. *IOP conference series: earth and environmental science.* IOP Publishing.

Salim, W. and Indraratna, B. (2004). A new elastoplastic constitutive model for coarse granular aggregates incorporating particle breakage. *Canadian Geotechnical Journal,* 41(4)**,** 657-671.

Sammis, C., King, G. and Biegel, R. (1987). The kinematics of gouge deformation. *Pure and Applied Geophysics,* 125(5)**,** 777-812.

Sanvitale, N. and Bowman, E. T. (2017). Visualization of dominant stress-transfer mechanisms in experimental debris flows of different particle-size distribution. *Canadian Geotechnical Journal,* 54(2)**,** 258-269.

Schofield, A. and Wroth, P. *Critical state soil mechanics*, McGraw-Hill London, 1968.

Schuhmann, R. (1940). Principles of comminution, I-size distribution and surface calculations. *Am. Inst. Min. Met. Eng., Tech. Pub.,* 1189, 1-11.

Shahnazari, H. and Rezvani, R. (2013). Effective parameters for the particle breakage of calcareous sands: An experimental study. *Engineering Geology,* 159, 98-105.

Shen, C., Liu, S. and Wang, Y. (2017). Microscopic interpretation of one-dimensional compressibility of granular materials. *Computers and Geotechnics,* 91, 161-168.

Sheng, D. C., Yao, Y. P. and Carter, J. P. (2008). A volume–stress model for sands under isotropic and critical stress states. *Canadian Geotechnical Journal,* 45(11)**,** 1639-1645.

Shipton, B. and Coop, M. (2015). Transitional behaviour in sands with plastic and non-plastic fines. *Soils and Foundations,* 55(1)**,** 1-16.

Shipton, B. and Coop, M. R. (2012). On the compression behaviour of reconstituted soils. *Soils and Foundations,* 52(4)**,** 668-681.

Sitharam, T. and Nimbkar, M. (2000). Micromechanical modelling of granular materials: effect of particle size and gradation. *Geotechnical & Geological Engineering,* 18(2)**,** 91-117.

Skempton, A. and Brogan, J. (1994). Experiments on piping in sandy gravels. *Geotechnique,* 44(3)**,** 449-460.

Smettem, K., Bristow, K. L., Ross, P., Haverkamp, R., Cook, S. and Johnson, A. (1994). Trends in water balance modelling at field scale using Richard's equation. *Trends Hydrol,* 1, 383–402.

Steacy, S. J. and Sammis, C. G. (1991). An automaton for fractal patterns of fragmentation. *Nature,* 353(6341)**,** 250.

Sukumaran, B., Einav, I. and Dyskin, A. (2006). Qualitative assessment of the influence of coordination number on crushing strength using DEM. *AIChE Annual Meeting, Conference Proceedings.*

Sun, D. A., Huang, W. X., Sheng, D. C. and Yamamoto, H. (2007). An elastoplastic model for granular materials exhibiting particle crushing. *Key Engineering Materials,* 1273-1278, Trans Tech Publ.

Sun, Q., Indraratna, B. and Nimbalkar, S. (2014a). Effect of cyclic loading frequency on the permanent deformation and degradation of railway ballast. *Géotechnique,* 64(9)**,** 746-751.

Sun, Y., Xiao, Y. and Ju, W. (2014b). Bounding surface model for ballast with additional attention on the evolution of particle size distribution. *Science China Technological Sciences,* 57(7)**,** 1352-1360.

Takei, M., Kusakabe, O. and Hayashi, T. (2001). Time-dependent behavior of crushable materials in one-dimensional compression tests. *Soils and Foundations,* 41(1)**,** 97-121.

Talbot, A. N. and Richart, F. E. (1923). The strength of concrete, its relation to the cement aggregates and water. University of Illinois at Urbana Champaign, College of Engineering. Engineering Experiment Station.

Tapias, M., Alonso, E. and Gili, J. (2015). A particle model for rockfill behaviour. *Géotechnique,* 65(12)**,** 975-994.

Todisco, M., Wang, W., Coop, M. and Senetakis, K. (2017). Multiple contact compression tests on sand particles. *Soils and Foundations,* 57(1)**,** 126-140.

Tong, C. X., Burton, G. J., Zhang, S. and Sheng, D. (2018a). A simple particle-size distribution model for granular materials. *Canadian Geotechnical Journal,* 55(2)**,** 246-257.

Tong, C. X., Burton, G. J., Zhang, S. and Sheng, D. (2019a). Particle breakage of uniformly graded carbonate sands in dry/wet condition subjected to compression/shear tests. *Acta Geotechnica*. doi.org/10.1007/s11440-020-00931-x.

Tong, C. X., Zhang, K. F., Zhang, S. and Sheng, D. (2019b). A stochastic particle breakage model for granular soils subjected to one-dimensional compression with emphasis on the evolution of coordination number. *Computers and Geotechnics,* 112, 72-80.

Tong, C. X., Zhang, S., Li, X. and Sheng, D. (2015). Evolution of geotechnical materials based on Markov chain considering particle crushing. *Chinese J. Geotech. Engng,* 37(5)**,** 870-877.

Tong, C. X., Zhang, S. and Sheng, D. (2018b). A Breakage Matrix Model for Calcareous Sands Subjected to One-Dimensional Compression. *GeoShanghai International Conference,* 17-24, Springer.

Turcotte, D. (1986). Fractals and fragmentation. *Journal of Geophysical Research: Solid Earth,* 91(B2)**,** 1921-1926.

Tyler, S. W. and Wheatcraft, S. W. (1989). Application of fractal mathematics to soil water retention estimation. *Soil Science Society of America Journal,* 53(4)**,** 987-996.

Tyler, S. W. and Wheatcraft, S. W. (1992). Fractal Scaling of Soil Particle-Size Distributions: Analysis and Limitations. *Soil Science Society of America Journal,* 56(2)**,** 362-369.

Ueng, T. S. and Chen, T. J. (2000). Energy aspects of particle breakage in drained shear of sands. *Geotechnique,* 50(1)**,** 65-72.

Verdugo, R. and Ishihara, K. (1996). The steady state of sandy soils. *Soils and Foundations,* 36(2)**,** 81-91.

Vipulanandan, C. and Ozgurel, H. G. (2009). Simplified relationships for particle-size distribution and permeation groutability limits for soils. *Journal of Geotechnical and Geoenvironmental Engineering,* 135(9)**,** 1190-1197.

Wan, C. F. and Fell, R. (2008). Assessing the potential of internal instability and suffusion in embankment dams and their foundations. *Journal of Geotechnical and Geoenvironmental Engineering,* 134(3)**,** 401-407.

Wan, R. and Guo, P. (1998). A simple constitutive model for granular soils: modified stress-dilatancy approach. *Computers and Geotechnics,* 22(2)**,** 109-133.

Wan, R. and Guo, P. (2001). Effect of microstructure on undrained behaviour of sands. *Canadian Geotechnical Journal,* 38(1)**,** 16-28.

Wan, R. G. and Guo, P. J. (2004). Stress dilatancy and fabric dependencies on sand behavior. *Journal of Engineering Mechanics,* 130(6)**,** 635-645.

Wang, P. and Arson, C. (2018). Energy distribution during the quasi-static confined comminution of granular materials. *Acta Geotechnica,* 13(5)**,** 1075-1083.

Wang, W. and Coop, M. R. (2016). An investigation of breakage behaviour of single sand particles using a high-speed microscope camera. *Géotechnique,* 66(12)**,** 984-998.

Wang, W. and Coop, M. R. (2018). Breakage behaviour of sand particles in point-load compression. *Géotechnique Letters,* 8(1)**,** 61-65.

Wang, Z. L., Dafalias, Y. F., Li, X. S. and Makdisi, F. I. (2002). State pressure index for modeling sand behavior. *Journal of Geotechnical and Geoenvironmental Engineering,* 128(6)**,** 511-519.

Wei, H., Zhao, T., He, J., Meng, Q. and Wang, X. (2018). Evolution of particle breakage for calcareous sands during ring shear tests. *International Journal of Geomechanics,* 18(2)**,** 04017153.

Weibull, W. (1951). A Statistical Distribution Function of Wide Applicability. *Journal of Applied Mechanics,* 13(2)**,** 293-297.

Xiao, Y., Coop, M. R., Liu, H., Liu, H. L. and Jiang, J. S. (2016a). Transitional behaviors in well-graded coarse granular soils. *Journal of Geotechnical and Geoenvironmental Engineering,* 142(12)**,** 06016018.

Xiao, Y. and Liu, H. (2017). Elastoplastic constitutive model for rockfill materials considering particle breakage. *International Journal of Geomechanics,* 17(1)**,** 04016041.

Xiao, Y., Liu, H., Chen, Q., Ma, Q., Xiang, Y. and Zheng, Y. (2017). Particle breakage and deformation of carbonate sands with wide range of densities during compression loading process. *Acta Geotechnica,* 12(5)**,** 1177-1184.

Xiao, Y., Liu, H., Chen, Y. and Jiang, J. (2014a). Bounding surface model for rockfill materials dependent on density and pressure under triaxial stress conditions. *Journal of Engineering Mechanics,* 140(4)**,** 04014002.

Xiao, Y., Liu, H., Chen, Y. and Jiang, J. (2014b). Strength and deformation of rockfill material based on large-scale triaxial compression tests. II: Influence of particle breakage. *Journal of Geotechnical and Geoenvironmental Engineering,* 140(12)**,** 04014071.

Xiao, Y., Liu, H., Chen, Y., Jiang, J. and Zhang, W. (2014c). Testing and modeling of the state-dependent behaviors of rockfill material. *Computers and Geotechnics,* 61, 153-165.

Xiao, Y., Liu, H., Ding, X., Chen, Y., Jiang, J. and Zhang, W. (2016b). Influence of particle breakage on critical state line of rockfill material. *International Journal of Geomechanics,* 16(1)**,** 04015031.

Xiao, Y., Liu, H., Xiao, P. and Xiang, J. (2016c). Fractal crushing of carbonate sands under impact loading. *Geotechnique Letters,* 6(3)**,** 199-204.

Xiao, Y., Liu, H., Yang, G., Chen, Y. and Jiang, J. (2014d). A constitutive model for the state-dependent behaviors of rockfill material considering particle breakage. *Science China Technological Sciences,* 57(8)**,** 1636-1646.

Xiao, Y., Long, L., Matthew Evans, T., Zhou, H., Liu, H. and Stuedlein, A. W. (2018a). Effect of particle shape on stress-dilatancy responses of medium-dense sands. *Journal of Geotechnical and Geoenvironmental Engineering,* 145(2)**,** 04018105.

Xiao, Y., Meng, M., Daouadji, A., Chen, Q., Wu, Z. and Jiang, X. (2018b). Effects of particle size on crushing and deformation behaviors of rockfill materials. *Geoscience Frontiers*. doi.org/10.1016/j.gsf.2018.10.010.

Xiao, Y., Sun, Y. and Hanif, K. F. (2015). A particle-breakage critical state model for rockfill material. *Science China Technological Sciences,* 58(7)**,** 1125-1136.

Xiao, Y., Sun, Z., Stuedlein, A. W., Wang, C., Wu, Z. and Zhang, Z. (2019a). Bounding surface plasticity model for stress-strain and grain-crushing behaviors of rockfill materials. *Geoscience Frontiers*. doi.org/10.1016/j.gsf.2019.06.010.

Xiao, Y., Yuan, Z., Chu, J., Liu, H., Huang, J., Luo, S., Wang, S. and Lin, J. (2019b). Particle breakage and energy dissipation of carbonate sands under quasi-static and dynamic compression. *Acta Geotechnica***,** 14, 1741-1755.

Xiao, Y., Yuan, Z., Lin, J., Ran, J., Dai, B., Chu, J. and Liu, H. (2019c). Effect of particle shape of glass beads on the strength and deformation of cemented sands. *Acta Geotechnica,* 14(6)**,** 2123-2131.

Xu, M., Hong, J. and Song, E. (2017). DEM study on the effect of particle breakage on the macro-and micro-behavior of rockfill sheared along different stress paths. *Computers and Geotechnics,* 89, 113-127.

Yamamuro, J. A. and Lade, P. V. (1996). Drained sand behavior in axisymmetric tests at high pressures. *Journal of Geotechnical Engineering,* 122(2)**,** 109-119.

Yan, W. and Dong, J. (2011). Effect of particle grading on the response of an idealized granular assemblage. *International Journal of Geomechanics,* 11(4)**,** 276-285.

Yan, W. M. and Shi, Y. (2014). Evolution of grain grading and characteristics in repeatedly reconstituted assemblages subject to one-dimensional compression. *Geotechnique Letters,* 4(3)**,** 223-229.

Yao, Y. P., Liu, L., Luo, T., Tian, Y. and Zhang, J. M. (2019). Unified hardening (UH) model for clays and sands. *Computers and Geotechnics,* 110, 326-343.

Yao, Y. P., Yamamoto, H. and Wang, N. D. (2008). Constitutive model considering sand crushing. *Soils and Foundations,* 48(4)**,** 603-608.

Yao, Y. P., Liu, L. and Luo, T. (2018). A constitutive model for granular soils. *Science China Technological Sciences,* 61(10)**,** 1546-1555.

Yin, Z. Y., Hicher, P. Y., Dano, C. and Jin, Y. F. (2016). Modeling mechanical behavior of very coarse granular materials. *Journal of Engineering Mechanics,* 143(1)**,** C4016006.

Yin, Z. Y., Xu, Q. and Hu, W. (2012). Constitutive relations for granular materials considering particle crushing: Review and development. *Chinese Journal of Geotechnical Engineering,* 34(12)**,** 2170-2180.

Yu, F. (2017a). Characteristics of particle breakage of sand in triaxial shear. *Powder Technology,* 320, 656-667.

Yu, F. (2017b). Particle breakage and the drained shear behavior of sands. *International Journal of Geomechanics,* 17(8)**,** 04017041.

Yu, F. (2018a). Particle Breakage and the Undrained Shear Behavior of Sands. *International Journal of Geomechanics,* 18(7)**,** 04018079.

Yu, F. (2018b). Particle breakage in triaxial shear of a coral sand. *Soils and Foundations,* 58(4)**,** 866-880.

Yu, F. W. (2017c). Particle breakage and the critical state of sands. *Geotechnique,* 67(8)**,** 713-719.

Zhang, J., Li, M., Liu, Z. and Zhou, N. (2017). Fractal characteristics of crushed particles of coal gangue under compaction. *Powder Technology,* 305, 12-18.

Zhang, S., Tong, C. X., Li, X. and Sheng, D. (2015). A new method for studying the evolution of particle breakage. *Géotechnique,* 65(11)**,** 911-922.

Zhang, X. and Baudet, B. A. (2013). Particle breakage in gap-graded soil. *Geotechnique Letters,* 3(2)**,** 72-77.

Zhao, B., Wang, J., Andò, E., Viggiani, G. and Coop, M. (2019). An Investigation of Particle Breakage under One-Dimensional Compression of Sand Using X-ray Micro-Tomography. *Canadian Geotechnical Journal*. doi.org/10.1139/cgj-2018-0548.

Zhao, B., Wang, J., Coop, M. R., Viggiani, G. and Jiang, M. (2015). An investigation of single sand particle fracture using X-ray micro-tomography. *Geotechnique,* 65(8)**,** 625-641.

Zheng, W. and Tannant, D. (2016). Frac sand crushing characteristics and morphology changes under high compressive stress and implications for sand pack permeability. *Canadian Geotechnical Journal,* 53(9)**,** 1412-1423.

Zheng, W. and Tannant, D. D. (2018). Grain breakage criteria for discrete element models of sand crushing under one-dimensional compression. *Computers and Geotechnics,* 95, 231-239.

Zhou, B., Wang, J. F. and Wang, H. B. (2014). A new probabilistic approach for predicting particle crushing in one-dimensional compression of granular soil. *Soils and Foundations,* 54(4)**,** 833-844.

Zhou, Z. Q., Ranjith, P. G. and Li, S. C. (2016). Optimal model for particle size distribution of granular soil. *Proceedings of the Institution of Civil Engineers-Geotechnical Engineering,* 169(1)**,** 73-82.

Zhu, J. G., Guo, W. L., Wang, Y. L. and Wen, Y. F. (2015). Equation for soil gradation curve and its applicability. *Chinese Journal of Geotechnical Engineering,* 37(10)**,** 1931-1936.

Zhuang, J., Jin, Y. and Miyazaki, T. (2001). Estimating water retention characteristic from soil particle-size distribution using a non-similar media concept. *Soil Science,* 166(5)**,** 308-321.